MONASH University

The role of PPARγ mediated regulation of peroxisomal phospholipid metabolism in tumour lipidomic reprogramming and chemoresistance

By Spencer Greatorex

Bachelor of Science (Honours in Biochemistry)

A thesis submitted for the degree of *Doctor of Philosophy* at

Monash University in 2019

Monash Biomedical Discovery Institute

Monash University, Clayton

Faculty of Medicine, Nursing & Health Sciences

Copyright notice

Contents

Declaration

I hereby declare that this thesis contains no material which has been accepted for the award of any other degree or diploma at any university or equivalent institution and that, to the best of my knowledge and belief, this thesis contains no material previously published or written by another person, except where due reference is made in the text of the thesis.

Signature: 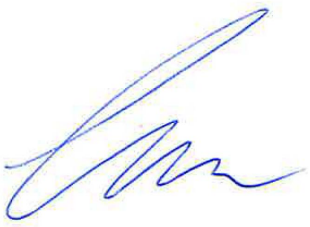

Print Name: Spencer Greatorex

Date: 3/12/2019

List of Abbreviations

5FU	5-Fluorouracil
AA	Amino Acid
ACC	Acetyl-CoA Carboxylase
ACL	ATP-citrate Synthetase
ADP	Adenosine Diphosphate
AMP	Adenosine Monophosphate
AMPK	AMP-activated Protein Kinase
APC	Adenomatous Polyposis Coli
BMP	Bismonoacylglycerophosphate
BRAF	v-Raf Murine Sarcoma Viral Oncogene B
CCLE	Cancer Cell Line Encyclopedia
CE	Cholesterol Ester
Cer	Ceramide
CK1α	Casein Kinase 1α
CSC	Cancer Stem Cell
cSRC	Chicken SRC
DAG	Diglyceride
DHAP	Dihydroxyacetone Phosphate
DHRS7B	Dehydrogenase/Reductase Family Member 7B
DNA	Deoxyribonucleic Acid
DR	Direct Repeat
DVL	Dishevelled
EMT	Epithelial to Mesenchymal Transition
ER	Endoplasmic Reticulum
FA	Fatty Acid
FAHFA	Fatty Acid Ester of Hydroxyl Fatty Acid

FASN	Fatty Acid Synthetase
FOX	5-Fluorouracil & Oxaliplatin
FZD	Frizzled
GM3	Ganglioside GM3
GPCR	G-protein Coupled Receptor
GRB2	Growth Factor Receptor-binding protein 2
GSEA	Geneset Enrichment Analysis
GSK3β	Glycogen Synthetase Kinase 3β
HBMP	Hemibismonoacylglycerophosphate
HexCer	Hexosylceramide
HIF1A	Hypoxia Inducible Factor 1 Alpha
HMGCR	HMG-CoA Reductase
HMGCS	HMG-CoA Synthase
KRAS	Kristen Rat Sarcoma
LDH	Lactate Dehydrogenase
LPC	Lysophosphocholine
LPE	Lysophosphoethanolamine
LPI	Lysophosphoinositol
LPL	Lysophospholipid
LXRA	Liver X Receptor Alpha
MS	Mass Spectrometry
mTOR	Mammalian Target of Rapamycin
NKκB	Nuclear Factor Kappa-light-chain-enhancer of Activated B-cells
NES	Normalised Enrichment Score
NGS	Next Generation Sequencing
Oxa	Oxaliplatin
OxPHOS	Oxidative Phosphorylation
PA	Phosphatidic Acid
PAK	p21-activated Protein Kinase

PC	Phosphocholine
PE	Phosphoethanolamine
PI	Phosphoinositol
PL	Phospholipid
PPARα	Peroxisomal Proliferator-activated Receptor Alpha
PPARδ	Peroxisomal Proliferator-activated Receptor Delta
PPARγ	Peroxisomal Proliferator-activated Receptor Gamma
PPL	Peroxisomal Phospholipid
PPRE	Peroxisomal Proliferator-activated Receptor Response Element
PS	Phosphoserine
PUFA	Polyunsaturated Fatty Acid
PUPL	Polyunsaturated Phospholipid
RNA	Ribonucleic Acid
RNAseq	Ribonucleic Acid Sequencing
Ros	Rosiglitazone
RTK	Receptor Tyrosine Kinase
SCAP	SREBP Cleavage Activating Protein
SFA	Saturated Fatty Acid
SM	Sphingomyelin
SOS	Son of Sevenless
SPL	Saturated Phospholipid
SRE	Sterol Response Element
SREBF1	Sterol Regulatory Element-binding Protein 1
SREBF2	Sterol Regulatory Element-binding Protein 2
TAG	Triglyceride
TCGA	The Cancer Genome Atlas
Vem	Vemurafenib
vSRC	Viral SRC

Publications

Bird A.D, **Greatorex S***, Reser R, Lavery G.G & Cole T. J., Hydroxysteroid Dehydrogenase HSD1L is localised to the pituitary-gonadal axis of primates. Endocrine Connections, 2017. 6(7): p. 489-499. Doi: 10.1530/EC-17-0119

* A. D Bird and S. Greatorex contributed equally

Acknowledgements

I would like to take the time to thank the great support base that I have had the privilege of working alongside in the last three years. To my supervisor, Assoc. Prof. Tim Cole, thank you for your open-door policy and the time you take out of your day to always make you feel welcome with something as simple as a good morning or a quick chat about the weekends footy news. To Kelly Short and Bennet Seow, thank you for morning coffee runs and the casual light-hearted joking around that made the long strange working hours barrable. To Judy Ng, thank you for your kind heart and your eagerness to help your fellow lab members. Without all of your daily input I have no doubt my experiences would have been all the worse for it.

To my panel members, Assoc. Prof. Jackie, Dr Morag, Dr Lisa Ooms and my co-supervisor Pro. Peter Fuller, thank you for taking time out of your busy work schedules to meet with me at my yearly reviews. You feedback was helpful, and your expertise has helped develop me into the scientist I am today. To Dr Birunthi Niranjan, thank you for all your help and expertise you helped pass onto me in the art of cell culture. Even though I was not in your lab and you always had so many people at the will of your knowledge, you were always willing to help me when I needed. To Dr. Chris Barlow, thank you for taking me through the complicated field of lipidomics, without your input and guidance on some of my experiments they would never have been finished and I may not have been her writing my acknowledgments.

Finally, I would like to thank my friends and family. Without your undivided support over the last three years this would not have been possible. To my girlfriend Kye Li, I want to especially thank you for your support and patients over the last three years without you and our Sunday morning brunches I probably would have lost my mind or had done nothing but work 7 days a week. I am looking forward to the future and what it might hold and hope to repay my gratitude in whatever way necessary.

Thesis Preface

The work presented in this thesis contains writings based on original work in requirement of the degree of the Doctor of Philosophy. Chapter 1 contains a current literature review relevant to the findings and topic of this thesis. Chapter 2 contains materials and methods for the experiments performed and discussed in this thesis. Chapters 3-5 contain writings based on the original work that was prepared as required for the degree of the Doctor of Philosophy. Chapter 5 is a general discussion and overview of the results presented in this thesis detailed relevant conclusion and future directions of this work. This thesis if fewer than 100, 000 words in length, exclusive of tables, figures, bibliography and appendices.

Abstract

Human tumours undergo a variety of metabolic transformations that regulate many aspects of tumour biology including survival, proliferation and stress responses. Metabolic reprogramming has been one of the key targets of oncology research in recent decades while altered cellular energetics has been identified as one of the key new additions to the hallmarks of cancer. The mechanism that drive tumour metabolism are vast and varied while understanding how tumours manipulate metabolism to gain survival advantages is still unclear. Mutation dependent metabolic reprogramming has been identified in many human tumours while common changes in key lipogenic transcriptional regulatory pathways have been extensively associated with human tumours, disease progression and patient survival outcomes. .

In this study, a systematic approach targeting tumour metabolic rewiring was investigated using high-throughput transcriptomic datasets such as the The Cancer Genome Atlas (TCGA). Transcriptome analysis of metabolic associated genesets utilising frequency distribution data normalisation methods showed an altered tumour landscape compared to conventional Geneset Enrichment Analysis (GSEA) methods. Furthermore, metabolic mapping of human colorectal cancer transcriptomes showed the existence of two distinct metabolic colorectal tumour subtypes based on HIF1A signatures while two key lipogenic transcription factors were also shown to harbour key differences within the two tumour subtypes. Significant changes in key transcriptional regulators of fatty acid metabolism were shown through upregulation of SREBF1 pathway while this coincided with downregulation of PPARγ signatures. Loss of PPARγ signalling was shown to be associated with increased tumour mutation burden and more specifically $BRAF^{V600E}$ oncogenic mutations. Further investigations utilising cell culture models of $BRAF^{V600E}$ driven tumours confirmed loss of PPARγ signalling leading to hyperlipidemic phenotype driven through loss of associated Peroxisomal Phospholipid (PPL) metabolic pathways allowing for sustained SREBF1 transcriptional activity. CRISPR/Cas9 mediated PPL biosynthesis knockout models through loss of the terminal enzyme DHRS7B was shown to mimic $BRAF^{V600E}$ tumours, primarily through loss of efficient AMPK signal transduction through decreased

polyunsaturated phospholipid biosynthesis. Lipid based metabolic tumour associated perturbations, a high fidelity lipidome was generated targeting 22 lipid classes across 15 human cancer cell lines. The tumour lipidome showed significant correlation based on lipid saturation while associations between lipidomic readouts was shown to be independent of tissue of origin, cell growth and mutation landscape. Finally, high throughput mass spectrometry analysis of human tumour cells revealed characteristic changes in polyunsaturated phospholipid ratios in many tumour cell lines. This ratio was associated with resistance to 5-FU mediated by protection of cells to pro-apoptotic signalling via hyperactivation of ER stress responses.

The implications of tumour metabolism in recent years have been highlighted as a key area of interest in oncology. The associations between changes in metabolism and pro-oncogenic outcomes is of concern, while our understanding of these pathways remains poor. This study provides a systematic approach to targeting PPARγ signalling in the context of tumour phospholipid metabolism. Our findings suggest that PPARγ plays a key role in tumour differentiation through regulation of phospholipid composition mediated through regulation of peroxisomal lipid metabolism. Furthermore, utilising well characterised PPARγ agonists in addition to Cas9 mediated targeting of peroxisomal phospholipid biosynthesis pathways provide an interesting clinical target for regulation of chemoresistance in drug resistant human tumours. Targeting peroxisomal phospholipid metabolism as a potential tumour theraputic is an interesting aspect that requires further *in vivo* analysis for better understanding of how this signalling pathway operates in more complex biological systems.

List of Figures and Tables

Chapter 4

Chapter 5

Chapter 1 – Introduction

1.1. Cancer as a genetic disease: The genetic revolution

Cancer at its most simplistic level is a genetic disease. The discovery of the DNA code in the 1960's gave insight into the cellular mechanisms of hereditary information. Studies leading to the discovery of the first oncogenes including viral SRC (vSRC) played pivotal roles in the notion of cancer as a genetic disease. One of the first such experiments showed that through the use of radiolabelled probes researchers could show the presence of the SRC gene in both Rous sarcoma virus infected cells and non-infected cells. Despite the presence of SRC in both infected and non-infected cells only infected cells exhibited oncogenic transformation, while unknown at the time there were some small differences between the vSRC and chicken SRC (cSRC), and these differences were enough to transform virally infected cells into oncogenic cells while the presence of cSRC in normal cells was not sufficient for tumour transformation. The idea of a protooncogene was formed and to this day is defined as the key transformation required in oncogenesis and tumour formation [1]. Further observations in later years consolidated the idea that the potential of normal cells to be transformed into tumorigenic cells lay within the cells own genetic code [2, 3]. In the same decade studies using the Harvey and Kirsten sarcoma viruses were isolated as potent oncogenic inducing retrovirus in the 1960's [4, 5]. These studies eventually led to the discovery of the protooncogene RAS. .

However, it wasn't until the early 1980's that these virally transformed genes were identified through, at the time, novel DNA sequencing techniques [6, 7]. Opposing oncogenes at the other end of the spectrum are the tumour suppressors. The most commonly mutated tumour suppressor gene and probably most well characterised is TP53, otherwise known as the 'guardian of the genome'. Loss of TP53 results in ineffective DNA repair mechanisms leading to an accelerated accumulation of tumorigenic mutations [8]. Tumours derived from mutant forms of tumour suppressor genes have been described in the literature as early as the 1800's. TP53 and another tumour suppressor gene RB were

both initially brought to researchers' attention in the 1970's. However, like RAS and SRC, they were not identified until the early 1980's and in subsequent years finally cloned and characterised [9, 10]. We now know the existence of dozens of protooncogenes, including MYC [11] and ERBB [12] in addition to many other tumour suppressors including PTEN [13]and APC [14]. The availability of large scale high-throughput DNA sequencing methods has allowed us to dive deeply into the genetic basis of tumour biology. Common cellular mutations can be found in many key cellular regulators in every tumour and this is fundamentally required for oncogenic transformation.

1.2. The role of β-catenin and RAS/RAF in epithelial derived cancers

Epithelial derived tumours account for most solid tumours in humans, and their cancer genetics are extremely complex and diverse depending on tumour subtype and tissue of origin. However, similarities can be derived, and common to many solid tumours is dysregulation of key pro-survival signalling pathways such as WNT/β-catenin and RAS mediated regulation of MAPK signalling. β-catenin driven tumours are the most common oncogenic perturbation found in colorectal cancer but somatic mutations affecting the status of β-catenin signalling has been observed in many other tumours including hepatocellular carcinoma and ovarian cancers [15, 16]. Furthermore, dysregulated MAPK signalling can be considered among the most commonly observed altered signalling pathway together with loss of TP53 signalling. Dysregulation of MAPK signalling through genetic changes in the RAS/RAF GTPases/kinases has been shown to be a key driver in the dysregulation of growth, survival and proliferation of colorectal cancers, melanomas, lung adenomas and thyroid cancers [17, 18].

1.2.1. The oncogenic β-Catenin signalling pathway

Wnt/β-catenin signalling in cells is crucial for many normal developmental processes. For example, it has been identified as a key regulator of stem cell maintenance in the colon epithelial crypt. Furthermore, dysregulation of β-catenin signalling accounts for as much as 80% of human intestinal

tumours [19]. Under normal physiological conditions β-catenin activity is primarily controlled by the biological activity of a family of 19 secreted glycoproteins, the WNT protein family [20]. WNT proteins illicit a range of physiological responses including proliferation, growth and chemotaxis, and do so through actions between mature circulating WNT proteins acting through a group of 10 G-protein couple receptors (GPCR), the Frizzled (FZD) GPCR family. In the absence of WNT ligand, the β-catenin destruction complex composed of adenomatous polyposis coli (APC), AXIN, casein kinase 1α (CK1α) and glycogen synthase kinase 3β (GSK3β) are able to form a stable complex with cytoplasmic β-catenin leading to sequential phosphorylation of β-catenin at Ser45 by CK1α. Further phosphorylation events at Thr41, Ser37 and Ser33 mediated by GSK3β are important in the regulation and recruitment of ubiquitin ligase complexes allowing for polyubiquitination of β-catenin and proteasomal-mediated degradation. The presence of WNT alone is insufficient for complete and robust β-catenin activation, and cell surface interaction between FZD, WNT and LRP-5/6 is required for cell surface localisation of Dishevelled (DVL) to the FZD receptor which is phosphorylated by CK2 [21, 22]. Activation and localisation of DVL leads to inhibition of GSK3β leading to accumulation of unphosphorylated stabilised forms of β-catenin. Accumulation of β-catenin allows for nuclear translocation and interactions with transcription factors such as members of the TCF/LEF family. This process is crucial in the stem cell zone of the gastrointestinal tract where high levels of WNT ligands secreted by localised crypt Paneth cells leads to high levels of β-catenin activity and generation of key regulators of proliferation and cell stemness including, c-MYC, c-JUN, CD44, LGR5 and CCND1 **(Fig. 1.1)**.

As mentioned previously alterations in WNT/β-catenin are observed in many solid tumours, and colorectal and gastrointestinal tumours account for most β-catenin driven tumours. By far the most common alteration associated with dysregulated β-catenin is truncation of APC, and is the major cause of hereditary forms of colorectal cancer but also accounts for a large proportion of sporadic colon tumours [23]. APC truncation, most commonly formed through nonsense and frameshift mutations, aberrates the biological function and formation of the β-catenin destruction complex. Loss of wild type APC is closely associated with accumulation of nuclear β-catenin, driving proliferation, growth and survival in early colorectal adenomas. Furthermore, mutations to β-catenin itself accounts for fewer solid tumours, approximately 5% in colorectal cancers and is significantly more common in liver and

ovarian tumours [23-25]. However, the phenotypic readout is much the same. Mutations to GSK3β and CK1α phosphorylation sites such as at Ser33 and Ser45 led to inefficient ubiquitin-mediated proteasomal degradation of β-catenin, allowing increased nuclear accumulation of β-catenin, while APC and β-catenin mutations account for most β-catenin driven solid tumours, recent development of deep genomic sequencing techniques has allowed researchers to carefully probe the very heterogenous tumour biological landscape. Other key genes including TCF7L2, a key transcription factor involved in β-catenin mediated transcription, have shown to be mutated in a low percentage of colorectal tumours. VTI1A-TCF7L2 fusions account for a small cohort of 3% of colorectal tumours sequenced, however the biological consequence of this mutation remains unclear, while some recent research has shown that it can act in a dominant negative fashion, inhibiting WNT mediated transcription while transcriptionally allowing for genetic regulation by CDX2 [26, 27].

1.2.2 Oncogenic RAS/RAF and dysregulation of MAPK signalling pathways

The MAPK signalling pathway forms an incredibly versatile and diverse family of kinases responsible for transcriptional regulation of many key transcription factors that include cMYC and cJUN. The upstream regulation of MAPK signalling is strict and crucial for maintenance of homeostatic cellular behaviour. Most commonly, MAPK signalling cascades are downstream of growth factor dependent receptor tyrosine kinases (RTKs). For example, EGF and in turn subfamilies including the VEGF and FGF families of secreted growth factors bind to their respective RTK's. Upon growth factor binding, RTK's dimerise leading to autophosphorylation of key Tyr residues and conformational changes allowing for protein-protein interactions mediated through SH2 domains that allow for binding of adaptor proteins, including growth factor receptor-binding protein 2 (GRB2). GRB2 further interacts with Son of Sevenless (SOS) which is a guanine nucleotide exchange factor allowing the generation of the active form of RAS^{GTP} [28, 29]. The Human genome encodes three RAS family members, KRAS, HRAS and NRAS all of which are implicated in tumorigenesis **(Fig. 1.2)**.

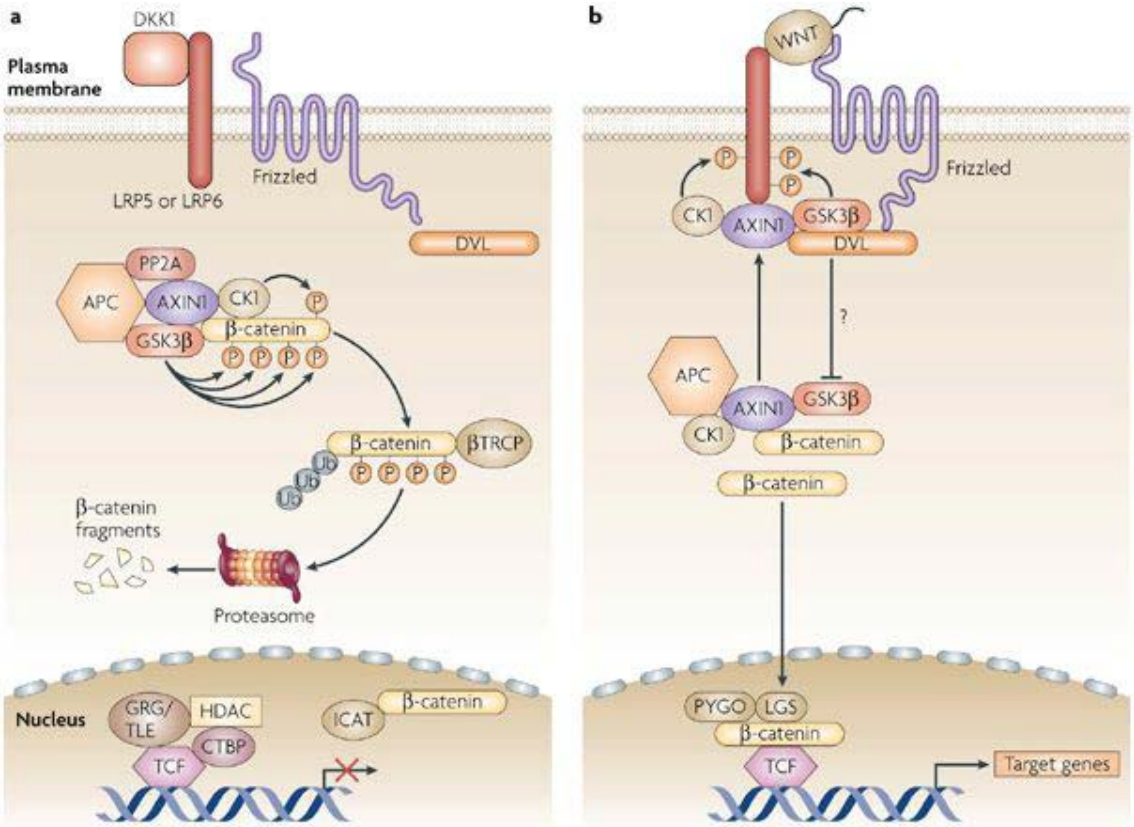

Figure 1.1. The WNT/β-catenin signalling pathway. ***(a)*** In the absence of WNT ligand, Levels of active nuclear and cytoplasmic β-catenin remain low due to phosphorylation of key regulatory residues on β-catenin mediated by GSK3β and CK1 kinase subunits forming the destruction complex along with scaffold subunits APC and AXIN1 responsible for protein-protein interactions. ***(b)*** Binding of WNT ligand to its receptor Frizzled, LRP5/6 forms a complex and recruits the destruction complex to the plasma membrane. DVL interacts with GSK3β and inhibits kinase activity allowing for unphosphorylated β-catenin to accumulate leading to nuclear translocation and transcriptional regulation through members of the TCF family of transcription factors. Adopted from [30].

Downstream to RAS GTPases is the family of RAF kinases. RAF kinases directly target MAPK activation through phosphorylation cascades. Again, three family members of RAF kinases are encoded in the human genome, where cRAF is the best understood family member. Phosphorylation of two crucial residues, Thr491 and Ser 494, are key to downstream activation of cRAF [31]. Phosphorylation events are key to activation it seems that protein localisation plays at least some part in the regulation of RAF. The RAF kinase bound to RAS^{GTP} is required for full RAF activation leading to phosphorylation at Ser338 of cRAF and the priming of RAF for heterodimerisation [32]. Furthermore, signal crosstalk mediated through key signalling transducers from converging pathways have been shown to be involved in RAF activation that include p21-activated protein kinase (PAK) and

SRC kinase, that target cRAF at Ser338 and Tyr341 respectively [33, 34]. BRAF phosphorylation at Ser364, Ser428 and Thr439 have all been shown to be crucial in BRAF activation while BRAF specific phosphorylation of residues Ser428 and Thr439 have been shown to negatively regulate BRAF activity [35]. Furthermore, phosphorylation of cRAF by AKT and AMPK have been shown to inhibit 14-3-3 binding leading to protein stabilisation and these residues have been shown to be conserved across all RAF members [36]. Activation of RAF kinases are crucial for further downstream MAPK signalling mediated through MEK1/2 which further phosphorylate and activate ERK1/2. ERK1/2 is the key member involved in biological and phenotypic alterations in response to activation of the MAPK pathway. ERK1/2 has a diverse array of protein targets and can regulate transcriptional activity through phosphorylation dependent regulation of transcription factors such as cFOS and cMYC, or inhibition through phosphorylation of the pro-apoptotic transducer proteins MCL1 and BIM, that can inhibit apoptotic signalling.

The roles that RAS and RAF family members play in tumorigenesis are relatively straight forward. Key mutations are crucial for RAS/RAF driven tumours. The $KRAS^{G12D}$ mutation is commonly found in colorectal, breast and lung adenomas accounting for approximately 20-30% of tumours, while in pancreatic cancers this accounts for upwards of 40% of tumours [37-39]. The $KRAS^{G12D}$ mutant leads to ineffective GTP to GDP exchange allowing for KRAS signalling to remain stronger and sustained for longer periods of time. The G12 residue is highly conserved across all family members with the same mutations observed in other RAS family members. Both HRAS and NRAS have been shown to exhibit G12X mutations, many of which are phenotypically identical. Mutations of HRAS have been shown to be sporadic in many bladder cancers while further attributing to Costello Syndrome [40]. NRAS is far less commonly mutated and is significant in only a few human solid tumours including oral cavity tumours and hepatocellular carcinomas. The $BRAF^{V600E}$ mutation, similar to RAS mutants, leads to ineffective downregulation of BRAF mediated signalling allowing for constitutive BRAF-mediated phosphorylation of MEK1/2 and subsequent downstream pro-survival signalling [41]. ARAF and cRAF on the other hand are rarely mutated in human tumours. Some mutations were identified in the Depmap project however the phenotypic consequence of these mutations is largely unknown. Recently, the cRAF R391W mutation was described as an oncogenic driver gene in a small population

of melanomas while a large proportion of melanomas were BRAF driven. CRAF R391W overexpression was shown to increase soft agar colony formation while knockdown of mutant CRAF was shown to be important for the M375 mutant melanoma cell line but had limited effects on $cRAF^{WT}$.

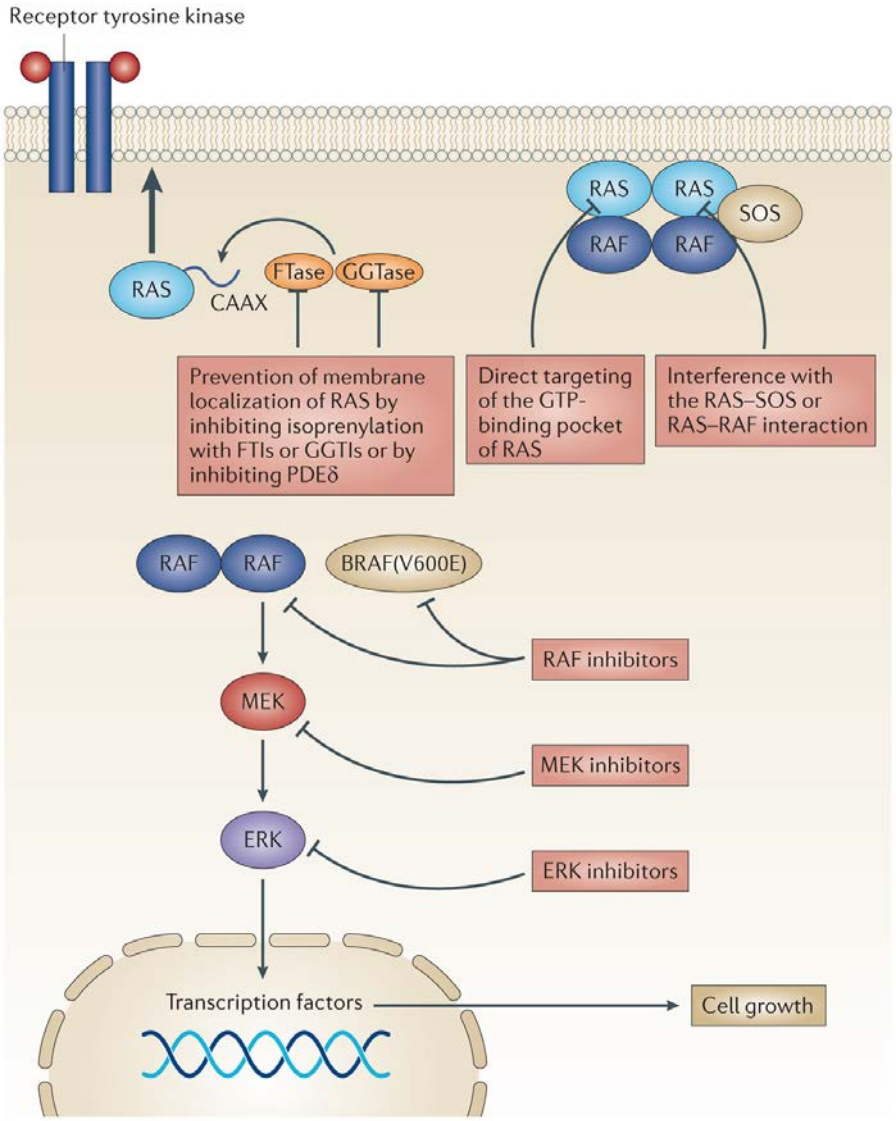

Figure 1.2. The oncogenic RAS-RAF-ERK signalling pathway. The RAS-RAF-ERK signalling pathway acks downstream to mediated extracellular signals from RTK's. RAS is a GTPase that regulates RAF activity while RAF kinases regulate ERK activity through direct phosphorylation. Several well characterised oncogenic mutations occur that leads to hyperactivation of the RAS-RAF-ERK pathway. BRAF V600E mutations shown here led to hyperactive mutant forms of BRAF and increased ERK signalling while similar mutations are found in RAS family members such as the G12X KRAS mutations leading to ineffective GTP:GDP cycling and increase KRAS activity. Many drugs have been developed to target this pathway and are currently used to treat human tumours such as melanomas. Adopted from [18].

1.2.3. Molecular interactions between RAS and β-catenin driven tumours

While mutations play integral roles in the initiation of tumour formation many years of research has highlighted the importance of a multi-hit mutation hypothesis. In most cases single mutations alone are insufficient to induce complete malignant tumour transformation. Early studies looking at the functions of RAS/β-catenin showed that sporadic tumour formation in $APC^{MIN/+}$ mice was increased in mice that also had hyperactive oncogenic RAS signalling [42]. Furthermore, hepatocellular carcinoma models using a floxed β-catenin exon 3 which was permissive to form a stabilised mutant form of β-catenin was shown to form sporadic tumours at 100% penetrance when coupled with HRAS mutations, while β-catenin or HRAS alone was insufficient for tumour formation [43]. Direct molecular interactions between MAPK and WNT/β-catenin have been observed and there seems to be significant levels of cross talk between the MAPK and β-catenin signalling pathways. For example, WNT3A stimulation of NIH3T3 cells was shown to increase levels of ERK1/2 activation while siRNA knockdown of EGFR inhibited this mechanism, and led to decreased proliferation rates indicating that both MAPK and WNT signalling were somewhat dependent on one another [44]. Furthermore, APC knockout mouse embryonic fibroblasts have been shown to have increased levels of ERK activity while further analysis into β-catenin involvement using siRNA knockout showed that this mechanism was β-catenin dependent. In addition, they also showed that activation of ERK was critical for the prevention of the formation of a dominant negative form of TCF4 [45]. Other groups in the context of developmental biology have brought further attention to possible cooperative signalling between RAS/RAF and β-catenin. EGF signalling was shown to maintain and regulate proliferation of intestinal stem cells in Drosophila while immunofluorescence has shown that phosphorylated ERK1/2 is confined to the intestinal stem cell and proliferating compartment of the intestinal crypt [46, 47]. Furthermore, analysis of both RAS and β-catenin protein stability showed that RAS interacted with β-catenin at the GSK3β phosphorylation interface while GSK3β inhibition and targeting of β-catenin for proteasomal degradation was crucial for RAS co-degradation [48].

In melanomas, BRAF has also been shown to work in opposing directions through inhibition of WNT/β-catenin signalling. $BRAF^{V600E}$ melanoma mutants were shown to have low β-catenin activity, while reactivation of β-catenin was required for the BRAF inhibitor PLX4720 to induced apoptosis. Β-catenin has also been shown to be a good prognosis marker of melanoma [49]. Furthermore, $BRAF^{V600E}$ in mouse intestinal models was shown to induce intestinal differentiation and loss of stemness indicating opposing actions to β-catenin, while BRAF appears to play roles in negative regulation of β-catenin it should be noted that $BRAF^{V600E}$ alone was insufficient to induce sporadic tumours in the mouse intestine [50]. Clearly the roles of RAS/RAF and β-catenin crosstalk are seemingly isoform dependent with BRAF largely associated with inhibition of β-catenin while others upstream of RAF, KRAS and HRAS both have been shown to amplify oncogenic behaviour of β-catenin. This could be through alternative divergent pathways. However, this does not explain the observations of seemingly synergistic signalling observed in intestinal stem cells clearly indicating that further research is required to identify a robust molecular mechanism.

1.3. Metabolic regulation of tumorigenesis: The metabolic hallmark of cancer

Metabolic rewiring is undoubtedly an important cancer hallmark and a rate limiting step involved in tumorigenesis. The vast divergent mechanisms that tumours can employ to manipulate cellular energetics in order to sustain prolonged periods of cellular growth, proliferation and ultimately metastasis border on the unsurmountable. One of the first key associations between cancer genetics and tumour metabolic reprogramming was the identification of cMYC-mediated regulation of lactate dehydrogenase (LDH) activity. Activation of increased LDH expression and activity resulted in increased lactate production leading to what is now known as the Warburg effect (discussed in detail in the next section) [51, 52]. Further studies revealed that TP53, one of the most mutated genes in cancer also played a pivotal role in the regulation of glycolysis.

From this point forward, the race to understand tumour metabolism led to decades of astonishing discoveries that provided an alternative angle to study tumour progression. Previously well characterised and understood signalling pathway were once again suddenly under careful observation, this time looking for genetic changes to cellular metabolism. PI3K/AKT signalling was shown to somewhat dependent on lipid reprogramming in order to illicit key changes in cellular energetics while PTEN mutations were seen to have similar metabolic phenotypes [53-55]. Furthermore, key studies into PI3K/AKT signalling revealed that successful signalling was completely dependent on secondary lipid mediators including diglycerides and phosphatidic acid generation through enzymatic modification of phosphatidylinositol [56]. In recent decades, our understanding of metabolic reprogramming in cancer has increased dramatically and advanced well past the early observations of Warburg. It has become increasingly obvious that almost all major genetic changes that are crucial for tumorigeneses have in some way been associated with major changes in cellular energetics through either direct or indirect mechanisms. A key question to ask is whether tumours arise from loss of regulation of the classic hallmarks including proliferation and uncontrollable growth or is the key player a dysregulation of cellular metabolism and then consequential dysregulation of cellular proliferation and growth.

1.4. Tumour metabolic reprogramming

Tumour metabolism is a complex and multistep process that in its most fundamental state drives tumour progression and all the key hallmarks of cancer. The ability of tumours to override the normal control of metabolic wiring within the cell is important for every aspect of tumour biology. Key genetic mutations have been associated with diverse and adverse changes in metabolism while several key regulators of important metabolic pathways including HIF1A have been shown to be key pathways that tumours hijack in order to drive processes such as neo-angiogenesis and metastasis.

1.4.1. Alterations in glycolysis in cancer: The Warburg effect

Under normal physiological conditions in most tissues glucose in the presence of oxygen undergoes aerobic respiration to produce pyruvate and then further enter the mitochondria to drive adenosine triphosphate (ATP) production. However, mammalian tissues do have cellular machinery that allows anaerobic respiration in which pyruvate undergoes fermentation to produce lactate and ethanol as a by-product in a much less energy efficient process. Lactate can be used to synthesize glucose in the liver through the enzymatic actions of lactate dehydrogenase but requires ATP input further increasing the discrepancies of the energy efficiency between aerobic and anaerobic respiration. Despite the energy efficiency of aerobic respiration, as opposed to anaerobic respiration, the later has been shown to be the primary pathway utilised in tumours. This is a well understood metabolic alteration in cancer and is known as the Warburg effect [57]. Logically, mitochondrial defects were initially thought to explain this outcome, however further research has shown fully functional aerobic respiratory systems are in place across many tumour samples indicating that alternative mechanisms are responsible.

Although the exact mechanism that underpins this phenomenon is unknown possible explanations have been suggested in recent years. For example, tumours favouring anaerobic respiration result in a far less proportion of the tumour tissue suffering from anoxic environments causing a considerable decrease in necrotic tissue. By reducing the oxygen consumption by cells near blood vessels, increased oxygen penetration is achieved in the tumour reducing the proportion of cells suffering from hypoxia. Another explanation may reside in the hostility of the tumour microenvironment where carbon sources are scarce and deviations towards anerobic respiration may provide a survival advantage. However, given that rapidly dividing cells also demonstrate this behaviour in energy rich environments this is unlikely to be a major reason [51]. The consequences of elevated oxidative phosphorylation result in increased levels of reactive oxygen species and perturbations in the ATP: adenosine diphosphate (ADP) ratios. Elevated ATP levels have been shown to negatively affect cell growth and survival with aerobic cells showing high ATP:ADP ratios while perturbations in these ratios can led to cell cycle arrest and elevated levels of catabolic metabolism [58, 59]. Furthermore, adenylated kinase proteins are associated with poor

prognosis while being shown to increase growth, metastatic behaviour and drug sensitivity [60-62]. Increased expression of adenylate kinases results in a survival advantage in cancer cells circumventing negative growth aspects when ATP levels reach critical levels in which normal tissues will undergo apoptosis. Similar mechanisms are in place for skewed ADP levels in ATP:ADP ratios. LKB1 is a known tumour suppressor gene responsible for cellular responses to elevated levels of ADP. Elevated levels of ADP activate members of the AMP-activated protein kinases leading to activation of LKB1 which leads to phosphorylation and activation of protein targets involved in energy exchange. Loss of ADP sensory mechanisms and ADP induced cell cycle arrest and apoptosis would allow cancer cells to survive in harsh competitive environments such as the tumour microenvironment allowing cancer cells to thrive where normal tissue would die out [63].

1.4.2. Alterations in glutamine metabolism in cancer

Another key alteration observed in tumours is changes associated with glutamine metabolism. Fatty acid (FA) synthesis is dependent on citrate input generated primarily through glycolysis in normal cells. Glutamine provides an alternative method for citrate production and is associated with increased FA biosynthesis. Mammals can produce a large repertoire of FA derivatives with varied roles in many cellular processes. However, *de novo* synthesis of FAs is highly dependent on acetyl-CoA synthesis via conversion of citrate by ATP-citrate lyase (ACL). Logically, due to the association with the Warburg effect and oncogenesis, one might think that in cancer FA pools would decrease because of these metabolic alterations. However observations have shown the opposite is true with tumours harbouring large FA pools and elevated levels of FA-derived growth factors [64]. Furthermore, the highly specific and ordered synthesis of FA derivatives in normal tissues are tissue specific while FA derivatives involved in signalling act as endocrine hormones as opposed to an autocrine or paracrine action. Exogenous sources of FA however are limited and furthermore many types of cancer show elevated expression levels of important metabolic enzymes involved in FA synthesis pathways including FASN, indicating that FA synthesis is a local process and produced endogenously [65, 66]. Alterations in glucose metabolism opposes this theory given

that the skew towards anaerobic respiration does not produce citrate that is vital for *de novo* FA synthesis.

Glutamine metabolism is a major energy source in mammals, feeding into the TCA cycle producing the products that include citrate. An elevation in glutamine metabolism is commonly observed in cancer and provides an alternative route in which cancer cells can synthesize FA derivatives critical to tumour progression. Increased levels of glutamine metabolism led to an increase in citrate levels that are then used to generate acetyl-CoA and chain elongation in FA synthesis. Again, these features align with observations seen in normal rapidly dividing cells however in the case of cancer, somatic evolutionary processes and the accumulation of somatic mutations results in a failure to employ proper regulatory mechanism to regulate changes in metabolism leading to an uncontrollable positive feedback loop resulting in pro-survival and growth outcomes. Increased glutamine metabolism could explain how cancer cells survive by altering their carbon source. Glutamine catabolism however requires oxygen, much the same as aerobic respiration, with elevated levels of glutamine metabolism most likely feeding into FA synthesis. Observations including elevated levels of citrate/isocitrate carrier protein have been observed in many forms of cancer while possibly being linked as a transcriptional target of mutated p53 support these claims [67, 68]. Furthermore, loss of citrate/isocitrate carrier protein expression results in inhibition of tumour growth and progression further stimulating the idea that endogenous FA production and their downstream pathways are crucial for later stages of tumour development [68].

1.4.3. Alterations in lipid metabolism in cancer

Alterations in glucose and glutamine metabolism are often observed in many types of cancer. The alterations in normal metabolic processes can partially explain the changes of cellular FA pools and the key metabolic pathways utilised and manipulated in many tumours. Citrate is a key molecule that feeds through the TCA cycle driving oxidative phosphorylation in the lumen of the mitochondria. In normal cellular metabolism citrate is primarily used for oxidative phosphorylation however under the guidance of the correct cellular signals mitochondrial citrate/isocitrate carrier proteins shuttle citrate from the

mitochondrial lumen to the cytoplasm. In the cytoplasm citrate undergoes a different process and is the primary input in the FA synthesis pathway. In addition, in cancer alterations in citrate metabolism coincides with an upregulation of many key metabolic enzymes involved in FA synthesis resulting in elevated levels of *de novo* FA synthesis that is key to tumour progression. **ATP citrate lyase (ACL)** forms the earliest step in FA synthesis converting citrate to oxaloacetate and acetyl-CoA in a reversible enzymatic reaction. ACL is extensively upregulated in many cancers while knockdown of ACL has been shown to inhibit tumour growth *in vitro* and inhibit tumour grafts in xenograft mouse models [69-71]. Furthermore, high levels of ACL expression have been shown to have a negative correlation with survival rates in advance stage tumours [77].

Acetyl-CoA carboxylase (ACC) 1 and 2 are responsible for the synthesis of malonyl-CoA and marks the commitment of acetyl-CoA to FA synthesis. ACC is positively regulated by citrate and glutamate through AMP-activated kinase signalling pathways. Normally expression of ACC is typically restricted to specialised tissues such as adipose where ACC1 is highly expressed, while ACC2 is important in high energy demanding tissues such as skeletal muscle. In cancer, both ACC 1 and 2 have both been shown to be upregulated in prostate, breast and colon tumours. Furthermore, knockdown of ACC in several types of cancer showed increased levels of apoptosis while soraphen-mediated inhibition showed similar outcomes [73-75]. Malonyl-CoA decarboxylase is essential in driving the reverse reaction of ACC reverting malonyl-CoA to acetyl-CoA. Interestingly, knockdown of MCD showed similar results leading to increased levels of apoptosis in breast cancer [76]. Bioactive FAs further undergo modifications by members of the **acetyl-CoA synthetase (ACS) and Fatty acid synthase (FASN)** families. Several isoforms of ACS including ACLS4 has been shown to be upregulated in breast, prostate and colorectal cancer, promoting cell survival by the attenuation of lipid driven apoptotic signals while in breast and prostate cancer it was shown to be correlated with castration of sex steroids [77, 78]. Chemical inhibition of ACSL1, 2 and 4 has been shown to increase apoptosis in lung, breast and CRC [79]. **FASN** is important in the generation of the cellular pool of FA. C16 chain FAs generated from acetyl-CoA and malonyl-CoA are further converted to palmitic acid which forms the major cellular and circulating pools of FAs in mammals. FASN dysregulation has been shown to be crucial for cancer progression, driving tumour survival with FASN overexpression highly correlated

with a poor prognosis and decreased patient survival rates [80, 81]. Furthermore, chemically induced suppression of FASN in CRC HT29 and LoVo cell lines showed decreased malignancy through down regulation of mTOR signalling pathways while other groups have shown similar results in tumour xenograft models via attenuation of CD44 associated signalling pathways [82, 83]. Furthermore, FASN has been shown to promote angiogenesis through activation of VEGF-A and downregulation of metalloproteinase 9 in CRC associated endothelial cells [84]. **HMG-CoA synthase (HMGCS)** and the highly conserved cousin **HMG-CoA reductase (HMGCR)** form one of the earliest steps in cholesterol synthesis from acetyl-CoA. c-MYC driven cancers have been shown to have downregulated levels of HMGCS2 [85]. Furthermore, HMGCS2 has been shown to be a rate limiting step involved in the formation of ketone bodies providing alternative energy sources in CRC and increased cell survival and growth rates [86]. HMGCR has been shown to be differentially regulated in CRC. In a study performing immunostaining of 535 colon cancer tumours, positive staining of HMGCR showed a strong correlation with non-metastatic disease and an overall improved outcome [87]. Conversely, detrimental consequences of elevated expression and mutated variants of HMGCR in HepG2 cells led to an increase in cell growth rates and colony formation [88]. The **CYP family members** form a group of enzymes responsible for many of the synthesis steps in sterol/steroid formation from cholesterol precursors. Expression of CYP family members are primarily restricted to endocrine tissues including the adrenal gland and gonads, however expression and polymorphisms of CYP1A2, CYP1B1, CYP11A1, CYP3A4/5 and CYP19A1 have all been associated with endometrial and CRC [89, 90]. Furthermore, knockdown of the intracellular nuclear receptor LRH-1 has been shown to regulate proliferative rates in CRC through downregulation of CYP family members CYP11A1 and CYP11B1 [91].

1.5. Transcriptional regulation of lipogenic pathways

Lipid metabolism is a complex and multi-faceted process. Regulation of lipogenic pathways is incredibly diverse and tissue specific, leading to the tissue and indeed tumour specific utilisation of lipids. Transcriptional regulation is key to regulating lipid utilisation and is controlled by two crucial transcriptional regulators of lipogenic pathways, the PPAR subfamily of intracellular nuclear receptors and the sterol regulatory element-binding proteins (SREBF). Both respond to the presence of specific lipid biproducts through divergent mechanisms allowing for the transcriptional control of key metabolic enzymes and pathways that in turn dictate the outcome of how lipids are metabolised, stored and utilised.

1.5.1. Signalling through the PPAR subfamily of nuclear receptors

The PPAR receptors are a subfamily of three (PPARα (NR1C1), PPARβ/δ (NR1C2) & PPARγ (NR1C3)) highly conserved ligand dependent intracellular nuclear receptors which form a much larger family of predominantly ligand dependent transcription factors. Other examples include the retinoic acid receptors and steroid hormone receptors that include the androgen and estrogen receptors. All nuclear receptors and in turn PPAR's are characterised by a modular structure defined by five major protein domains. The N-terminal A/B domain consists of the AF-1 or ligand independent region, a C-terminal AF-2 or ligand dependent region, a central DNA binding domain, a ligand binding domain and finally a D domain or hinge region. All these protein domains are critical for correct receptor function and play integral roles in the regulation of PPAR-mediated transcription. PPARα was originally cloned from cDNA libraries of mouse liver in the early 1990's and identified as a nuclear receptor family member responsible for biological responses to a series of hepatocarcinogens [92]. Since then great advances in PPAR research has revealed a lot of the biological roles and mechanism that PPAR's are responsible for. All three members of the PPAR's, in addition to several other nuclear receptor members, are known as RXR dependent heterodimers. Like other nuclear receptors, in the absence of ligand the PPAR's can form protein complexes with heat shock proteins

which function to limit availability to nuclear localisation signals and regulate PPAR protein levels through proteasome regulation [93]. In response to ligand such as unsaturated fatty acids and prostaglandins, PPAR's form obligate heterodimers with RXR nuclear receptors in response to their biological relevant ligand 9-*cis*-retinoic acid. Ligand binding allows for appropriate protein conformational changes allowing for access of importins to the conserved nuclear localisation signals found in the hinge region and AF-1 domains [94]. On translocation to the nucleus PPAR/RXR heterodimers bind to directly repeated DNA sequences (AGGTCA) known as the peroxisome proliferator response element (PPRE), or the direct repeat (DR1/2) sites. The hinge region forms key interactions with other regulatory DNA sequences further upstream [95]. Nuclear protein interactions between the active PPAR/RXR heterodimer are immensely complex and varied. Inactive PPAR/RXR heterodimers in the nucleus are most commonly found in complex with the nuclear receptor corepressor complex through direct protein-protein interactions with both SMRT and NCoR [96]. SMRT and other corepressor complex proteins such as NRIP1, recruit and form further protein complexes with histone deacetylases blocking access to gene promoter elements. Upon ligand binding recruitment of the coactivator complex replaces the corepressor complex leading the acetylation and transcriptional activation of PPAR regulated target genes. The coactivator complex is much more complex than the corepressor complex and includes the histone acetyltransferases SRC-1/2, coactivators such as PPARGC1A/B [97, 98]. .

In addition to complex protein-protein interactions, PPAR's can be post-transcriptionally modulated through the actions of several kinases and acetylases. Key phosphorylation sites found predominantly in the AF-1 domain are key to kinase mediated regulation. P38-MAPK has been shown to phosphorylate PPARα at Ser6, 12 and 20 and is thought to enhance activity by priming protein complex formation with coactivators such as PPARGC1A [99]. Furthermore, p38-MAPK has been shown to have similar responses in the regulation of PPARγ transcriptional activity [100]. Similarly, ERK activity has been shown to directly phosphorylate PPARα at Ser12/20 and again was responsible for an increase in transcriptional activity [101, 102]. ERK can also phosphorylate PPARγ at Ser112 however unlike PPARα this is known to regulate PPAR protein stability, while it has been shown that this phosphorylation site is key to regulation of PPARγ that is mediated by other protein kinases including

JNK1 [103-105]. Furthermore, mutational studies have shown that this residue is key to the repressive action of MAPK dependent growth factor signalling pathways that include PDGF, while PPARγ activation is also known to negatively regulate MAPK signalling [106, 107]. PKA has also been shown to phosphorylate all members of the PPAR family. PPARδ is phosphorylated by PKA, while the exact function of this remains elusive, it is believed to regulate the protein complex formation between NCoR and SMRT [108, 109]. Phosphorylation has been shown to regulate PPAR's in both positive and negative feedback loops. Furthermore, other forms of post transcriptional modification have also been shown to regulate PPAR activity. Acetylation of PPARγ by sirtuin-1 at Lys268/293 has been shown to be crucial for regulation of PPARγ activity through forcing PPAR into a repressor state through increased affinity of PPARγ with corepressor proteins NCoR and SMRT [110, 111]. Furthermore, ligand dependent regulation of PPARγ protein levels have also been observed [112]. NEDD4 and TRIM25 have been identified as a E3 ubiquitin ligases that regulate PPARγ stability in a concentration dependent mechanism, while ligase dependent regulation of PPARγ activity through regulation of protein stability and proteasomal degradation has been observed in several other biological systems [113 - 116] **(Fig. 1.3)**.

1.5.2. The canonical/non-canonical SREBF1 pathways

SREBF proteins form a second major transcription regulator of FA biosynthesis. SREBF transcription factors in an inactive state are resident heterodimeric membrane bound endoplasmic reticulum proteins that form dimers with SREBP cleavage activating protein (SCAP) through a C-terminal cytoplasmic WD40 repeat domain. In response to low lipid levels, including low membrane cholesterol concentrations, the SREBF/SCAP heterodimer shuttles into the Golgi apparatus leading to SREBF protein cleavage/maturation. Cleaved/mature SREBF can shuttle to the nucleus and form transcriptional complexes at sterol-response elements (SRE) found near the promoter regions of certain genes. The function of SCAP is crucial at the activation loop of SREBF. SCAP plays roles in both protein stability

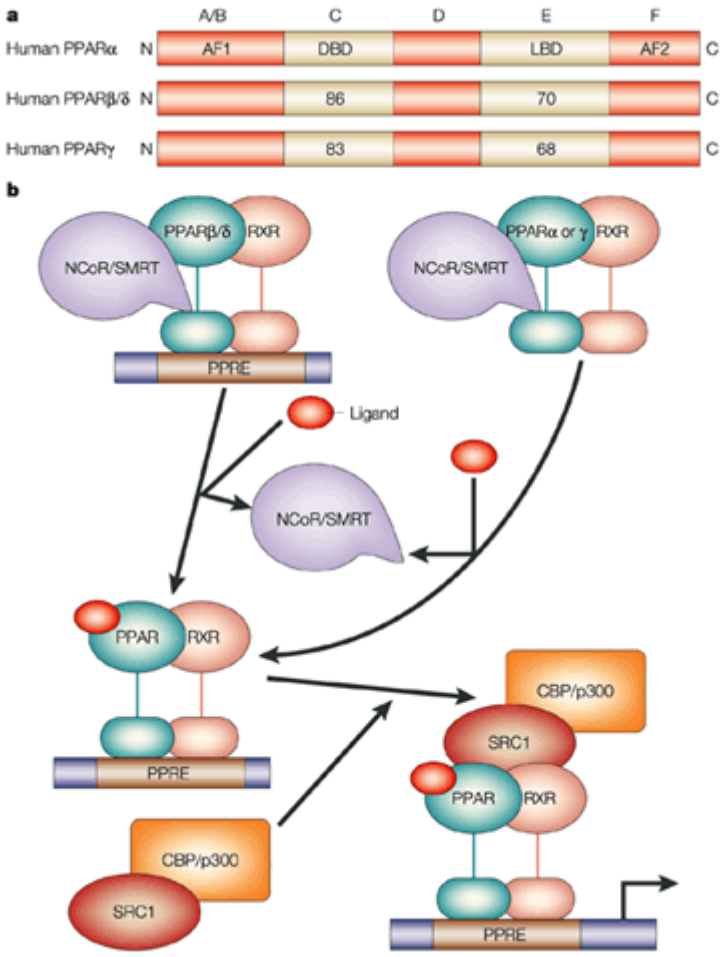

Figure 1.3. PPAR structure and ligand induced transcriptional complex formation. **A.** The human PPAR family of ligand activated transcriptional factors contains three members each consisting of 5 conserved protein domains. The most conserved domains are the C and E domain consisting of the DNA-binding domain and the ligand binding domains. The AF1, N-terminal domains is largely responsible for post transcriptional modifications of PPAR's regulating transcriptional activity. The AF2 domain forms an evolutionarily divergent area of PPAR's while D domain contains the hinge region responsible for protein conformational changes allowing for nuclear transport and activator/repressor complex formation. **B.** PPAR's are responsive to a number of both synthetic and natural ligands such as prostaglandins of unsaturated FA's. Ligand activation is a series of response that occur after ligand bind in the LBD region of a PPAR. Under ligand starvation PPAR's are often found in complexes with co-repressor proteins such as NCoR/SMRT which inhibits formation of further complexes with activators and transcriptional machinery. Upon ligand binding conformations changes allow for PPAR's to disassociated with co-repressor complex and form complex with co-activators such as SRC1 and CBP/p300 which allows for further formation of transcriptional complexes leading to changes in PPAR regulated gene expression. Adopted from [117]

and in ER to Golgi transport. SCAP knockout studies have revealed that induced monomeric forms of SREBF led to rapid degradation and reduction in transcription of SREBF target genes [118]. Furthermore, this mechanism of protein stability was recently identified as a HSP90 dependent process. HSP90 inhibition led to decreased SCAP/SREBF protein stability while HSP90 was shown to directly interact with SCAP through C-terminal protein-protein interactions [119]. SREBF transport into the Golgi is required and again is mediated through a SCAP dependent mechanism. Interactions between a SCAP hexapeptide (MELADL) sequence was found to be crucial for SCAP mediated SREBF Golgi transport via direct interaction with COPII-coated transport vesicles [120]. In a low cholesterol environment conformation changes led to interactions between large ER luminal loop regions and allow for SCAP/COPPII interactions [121]. Furthermore, N-glycosylation of SCAP appears to play an important role in the regulation of SCAP-mediated SREBF transport [122]. Two additional ER resident proteins INSIG1/2 are crucial for inhibition of SREBF Golgi transport. INSIG1 binds to SCAP at the sterol sensing domain in a complex with oxysterols and inhibits the conformation required for SCAP to interact with COPII vesicles. High cholesterol levels led to stabilisation of INSIG while cholesterol depletion inhibits this interaction, and therefore allows for COPII mediated Golgi transport [123-125]. Furthermore, INSIG1 can play roles in the regulation of SREBF1 protein stability through recruitment of multiple E3 ligases, such as GP78 and TRC8, while other groups have described a PKA dependent phosphorylation of RNF20 that is important for decreased SREBF1 protein stability [126-128]. Under low cholesterol conditions as discussed previously, INSIG1 is destabilised leading to conformational changes through inhibition of INSIG/SCAP protein-protein interactions. SCAP/SREBF1 complexes are then allowed to interact with COPII coated vesicles allowing for SREBF1 Golgi transport. Once in the Golgi, SREBF1 cytoplasmic loops are cleaved by S1P and again this has been demonstrated to be a SCAP dependent mechanism through C-terminal protein-protein interactions [129, 130]. S1P mediated cleavage released a protein product roughly half the size of the full length SREBF1. Further cleavage mediated post transcriptional regulation of mature SREBF1 is mediated by a close relative to S1P, called S2P. Structural analysis has hypothesised that S1P cleavage is required for conformational changes that are required for access to the S2P enzyme however, this has remained elusive and needs to be experimentally confirmed. As mentioned previously cholesterol levels

are a key regulator of SREBF1-mediated protein trafficking and post transcriptional processing. Furthermore, recent evidence suggests the existence of a non-canonical activation pathway of SREBF1. Polyunsaturated fatty acids (PUFA) and phosphocholines have in recent years been highlighted as key regulators of SREBF1 activation and transcription. Although the primary mechanism for PUFA mediated SREBF1 regulation appears to be a mechanism at the transcriptional levels, other groups have shown alterations in protein localisation and cleavage products. PUFA acting through the PUFA sensory protein UBXD8, act to inhibit UBXD8/INSIG protein-protein interactions leading to ER membrane stabilised INSIG1 and decreased ubiquitylation dependent proteasomal degradation, therefore inhibiting SREBF1 mediated transport to the Golgi [131, 132] **(Fig. 1.4)**.

1.5.3. PPAR and SREBF1 signalling in tumour progression and metabolism

Lipids acting as endocrine hormones are crucial for regulation of cellular metabolism. The transcriptional networks that regulated intracellular stores of lipid mediators are complex and deeply interwoven. This statement holds consistent in both normal untransformed cells in addition to neoplastic tissue. The roles of SREBF1 and the PPAR's in human cancers are well documented and add weight to the notion of tumour metabolic centric models showing that they not only regulate tumour metabolism, but this extends to virtually all facets of tumour biology. PPARα is associated with poor prognosis in breast while use of synthetic ligands targeting PPARα including fenofibrates have been explored to supress cellular proliferation and inhibiting pro-oncogenic NFκB signalling [133-135]. PPARδ plays roles in regulation and maintenance of stemness across a variety of tissue types [136]. In the colon PPARδ plays roles in cooperation with WNT/β-catenin signalling maintaining crypt stem cells [137, 138]. Despite this several researchers have shown the PPARδ is a negative regulator of colon carcinogenesis. $APC^{MIN/+}$ mice, a common mouse model of sporadic colorectal tumour formation showed that $PPAR\delta^{-/-}$:$APC^{MIC/+}$ mice led to an increase in colon polyp formation [139, 140]. Conversely, other groups have shown the exact opposite where PPARδ cooperation with WNT/β-catenin signalling led to an increase in carcinogenesis, while PPARδ is known to be an APC

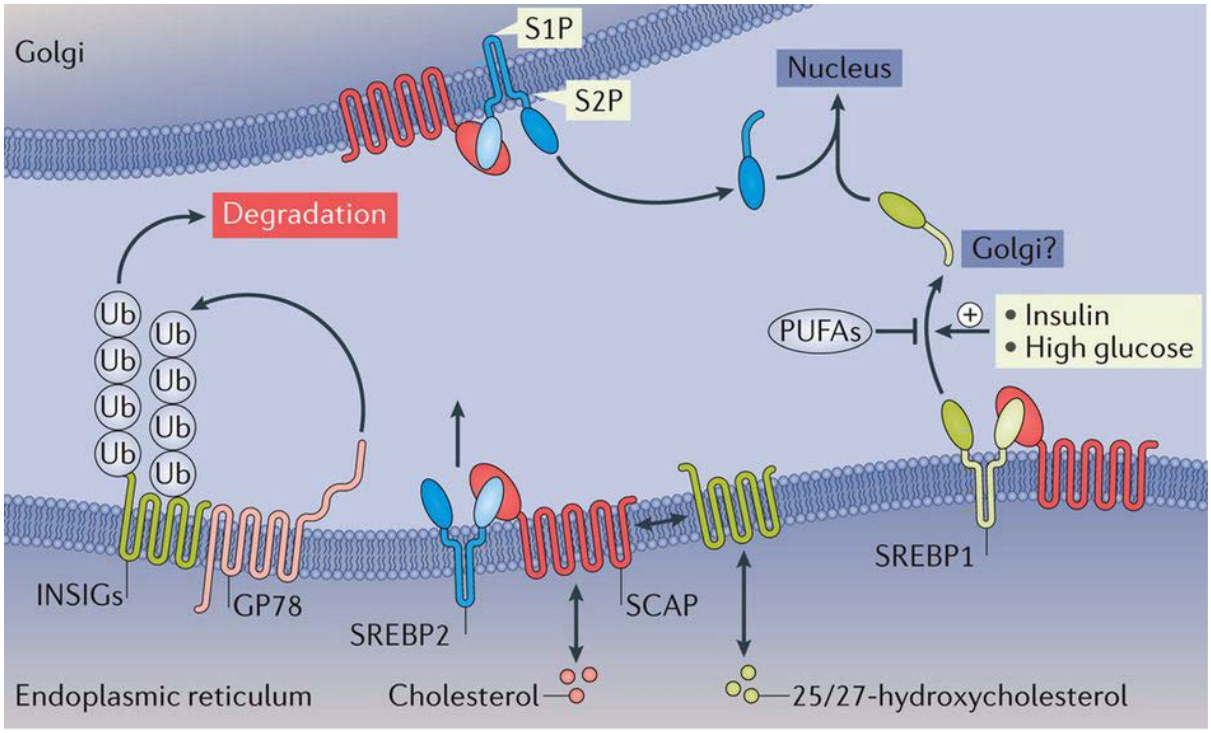

Figure 1.4. SREBP regulatory protein modification and processing pathway. SREBP proteins in the presence of high membrane associated cholesterol, SCAP/SREBP complex is stabilised in the ER. Ubiquitylation of INSIG in response to low cholesterol levels led to rapid degradation of INSIG allowing for protein translocation of the SCAP/SREBP complex to the golgi apparatus. Resident proteases, S1P/S2P in the golgi led to protein modification of SREBP forming membrane associated SREBP fragment and a N-terminal mSREBP fragment. SREBP2 is strongly sterol regulated while ratios of PUPL are also thought to regulate SREBF1. mSREBP is able to shuttle into the nucleus and form transcriptional complexes targeting target genes such as FASN or SCD1. Adopted from [142].

regulated target and is degraded in a similar manner to excess β-catenin levels in the colon epithelia while PPARδ overexpression correlates with β-catenin overexpression in colorectal cancer [141, 143]. The relationship of PPARγ with human tumours is much the same as PPARδ, convoluted and inconclusive. Some groups have described potentiation of PPARγ signalling using $APC^{MIN/+}$ mouse models [144]. Overexpression of PPARγ correlated with increase β-catenin while increased β-catenin levels were also observed in HT-29 cells treated with a PPARγ agonist [145]. PPARγ is a known target of β-catenin transcriptional activity so it is possible that PPARγ expression is increased due to an over expression of β-catenin while this research did not show a functional relationship [146]. In addition, PPARγ has been shown to induce β-catenin proteasomal degradation in a similar manner as to APC [147]. Furthermore, as discussed earlier PPARγ agonist in HT-29 cells showed increase β-catenin

protein stability. The clinical relevance of these findings are questionable given that HT-29 is largely a BRAF-ERK driven tumour cell, known to be a driver of poor differentiation while β-catenin driven tumours largely represent colon stem cell like phenotypes [148, 149]. Several researchers have also shown an opposing result regarding PPARγ and colon polyp formation. PPARγ activity was shown to negatively regulate TCF/LEF transcriptional activity and inhibit tumour growth [150].Similar observations have been made regarding tumour inflammation. PPARγ agonism was shown to negatively regulate tumour growth and survival through inhibition of NFκB signalling, while clinical associations show that PPARγ expression is associated with favourable clinical outcomes. [151, 152]. On the other end of the spectrum, SREBF1 is associated with many tumours subtypes and generally associated with pro-oncogenic processes. PPARγ and SREBF1 have known interplay with one another with SREBF1 mediated lipogenesis associated with increased PPARγ activity through generation of known PPAR ligands while this action has been shown to negatively regulate SREBF1 transcriptional activity [153, 154]. Despite this most of the relevant data suggests SREBF1 as a potential metabolic oncogene. Downregulation of SREBF1 in colorectal cancer has been demonstrated to negatively regulate tumour progression and cell proliferation [155] While several observation have been made regarding SREBF1 activity and its implication in drug resistance to a variety of cytotoxic antitumour drugs. Sustained SREBF1 transcriptional activity was shown to drive BRAF targeted therapeutic resistance in melanomas [156]. In addition, SREBF1 transcription regulation of lipogenesis is commonly associated with late stage metastatic skin cancer [157]. Similar observations were made in colorectal cancer where SREBF1 was associated with increased MMP7 expression due to amplification of the NFκB signalling pathway [158]. In addition, a second group observed similar results with EMT induction mediated through cooperation of SREBF1 with cMYC, while keratin remodelling in invasive breast cancers were also shown to be dependent on SREBF1 activity [159, 160]. Furthermore, several studies have shown sustained lipogenesis mediated through SREBF1 transcriptional activity to be a key feature in rapidly growing energy dense tumours in a variety of models including liver, glioblastoma and melanomas [54, 157, 161, 162].

1.6. Regulation of lipogenesis by the AMPK/mTOR (energy sensory) signalling pathways

Maintenance of cellular energetics is a crucial process that falls primarily to the responses of two major energy sensory protein kinases, mTOR and AMPK. Both of which play pivotal roles in metabolic feedback of key cellular survival and proliferative mechanisms. AMPK primarily responds to cellular energetically induced stress such as low ADP:ATP ratios and is primarily responsible for fine tuning mitochondrial metabolism to maintain or restore metabolic homeostasis. mTOR can be considered a beneficiary of AMPKs hard work, relaying pro-survival and growth signalling into the cell nucleus in response to energetically favourable conditions.

1.6.1. The AMPK complex: The guardian of cellular energetics

Like many protein kinases, AMPK consists of a heterotrimeric protein complex containing a catalytic subunit (α-subunit) and two additional regulatory subunits (β & γ subunits). The α subunit contains the catalytic kinase domain and kinase function is regulated by a series of phosphorylation events **(Fig. 1.5)**. The Thr172 site is considered to the be the crucial phosphorylation event for AMPK activation and is required for AMPK kinase activity. Thr172 is often used to measure AMPK activity within a cellular system however it is not always a reliable method. Two additional phosphorylation sites in the α-subunit have been described and form the catalytic triad that are crucial for full AMPK activation [163]. The regulatory domains form a structural based inhibitory mechanism through the implementation of highly conserved protein domains. The β-subunit contains a carbohydrate-binding module allowing for glycogen sensing whiles a secondary C-terminal domain facilitates trimer formation and is the interface for direct protein-protein interactions between the α/γ subunits [164]. The second regulatory subunit, the γ-subunit has a series of cystathionine β-synthase repeats, all of which play a role in binding to ATP, ADP and AMP in a competitive manner allowing for competitive modulation of AMPK activity. The activation loop sites at this interface generate proximal localisation

of key activating phosphorylation groups and nucleotide binding allowing for rapid and responsive protein conformational changes. One of the key roles of AMPK is the sensing of AMP:ADP:ATP ratios. High AMP:ATP ratios is often a sign of metabolic stress while competitive binding of AMP/ADP to the γ-subunit is an important mechanism of AMPK phosphorylation at Thr172 downstream by either LKB1 or CAMKKβ. Furthermore, important conformational changes in response to AMP/ADP binding allows for protective protein conformations leading to sustained AMPK activity. Without binding of AMP/ADP, phosphorylated AMPK Thr172 is quickly dephosphorylated. LKB1 functions similarly to AMPK, as a trimeric protein complex between LKB1, STRAD and M025, while both STRAD and M025 play important roles in protein-protein interactions with the AMPK complex, LKB1 is considered to be the catalytic activator, directly phosphorylating AMPK at Thr172 with knockout studies showing the importance of LKB1 in response to mitochondrial dysfunction or poorly energetically favourable conditions [58, 165, 166]. Furthermore, CAMKK2 is a Ca2+ activated protein kinase and is generally responsive to intracellular levels of Ca2+ released from the endoplasmic reticulum in response to DAG-mediated protein signalling events. Studies have also revealed that CAMKK2 is an important regulator of AMPK activity while also phosphorylating AMPK at Thr172 [167].

1.6.2. AMPK mediated regulation of lipogenesis

In response to energetic crisis, AMPK is activated through mechanisms that we described in detail in the previous section. Active AMPK has many downstream targets, all of which in some facet regulate metabolism. Both ACC1/2, responsible for *de novo* acetyl-CoA biosynthesis, were identified originally as key direct targets of AMPK [168]. Both ACC1/2 have three major phosphorylation sites all of which play roles in the regulation of enzymatic activity. Phosphorylation of ACC at Ser79 by AMPK leads to enzymatic inhibition of *de novo* lipogenesis [169, 170]. PKA has also shown to phosphorylate ACC at Ser1200 however, further studies have shown that only one phosphorylation is required to effectively regulate *de novo* lipogenesis [171]. Furthermore, other observations have shown that AMPK can regulate later stages of *de novo* lipogenesis through inhibition of the key regulatory enzymes responsible

for generation of cholesterol esters. Phosphorylation of HMG-CoA reductase, responsible for the rate limiting step in cholesterol biosynthesis, leads similarly to ACC, enzymatic inhibition [172]. Complementary to the inhibition of key regulatory enzymes involved in *de novo* lipogenesis, AMPK can also target lipogenesis at the transcriptional level through regulation of SREBF1-mediated transcriptional pathways. Phosphorylation of SREBF1 leads to destabilisation of mature SREBF1 and proteasomal degradation resulting in the reduction of the levels of key lipogenesis enzymes. Phosphorylation of SREBF1 at Ser372 has been shown to inhibit Golgi translocation and lipid depleted dependent SREBF1 cleavage also leading to inhibition of lipogenic transcriptional activity [173]. Well characterised gene targets of SREBF1 including FASN, ACC, ACLY and HMGCR have all been shown to be downregulated as a result of AMPK while converse to this, inhibition of mTOR has been shown to inhibit SREBF1 nuclear translocation [174]. Furthermore, AMPK was recently shown to regulate a close relative to SREBF1, ChREBP. S568D ChREBP mutants mimicking the phosphorylated state of ChREBP showed reduced lipid sensing dependent DNA binding while phosphor-deficient mutants showed the converse outcome. This corresponded with overexpression of active forms of AMPK inhibiting lipid dependent DNA binding of ChREBP [175]. AMPK can directly alter circadian rhythms of energy homeostasis via phosphorylation of the circadian transcription factor CRY1. Phosphorylation of CRY1 at Ser71 leads to protein destabilisation through ubiquitin-mediated proteasomal degradation thereby decreasing circadian transcriptional activity of several metabolic pathways including lipogenic pathways [176]. Similar observations have also been shown for other metabolic transcriptional regulators including HNF4A and TR4-mediated SCD1 transcription [177, 178]. Finally, AMPK has been shown to induce mitochondrial respiration. PPARGC1A, a key regulator of mitochondrial biosynthesis and fatty acid oxidation has been identified as a direct target of AMPK and showed that PPARGC1A activation and transcriptional regulation of mitochondrial activity is dependent of AMPK activity [179]. Furthermore, AMPK has recently been highlighted a key regulator of adipose browning and thermogenesis. Both processes are highlighted by increased fatty acid oxidation and increased mitochondrial turn-over and PPARGC1A transcriptional activity [180].

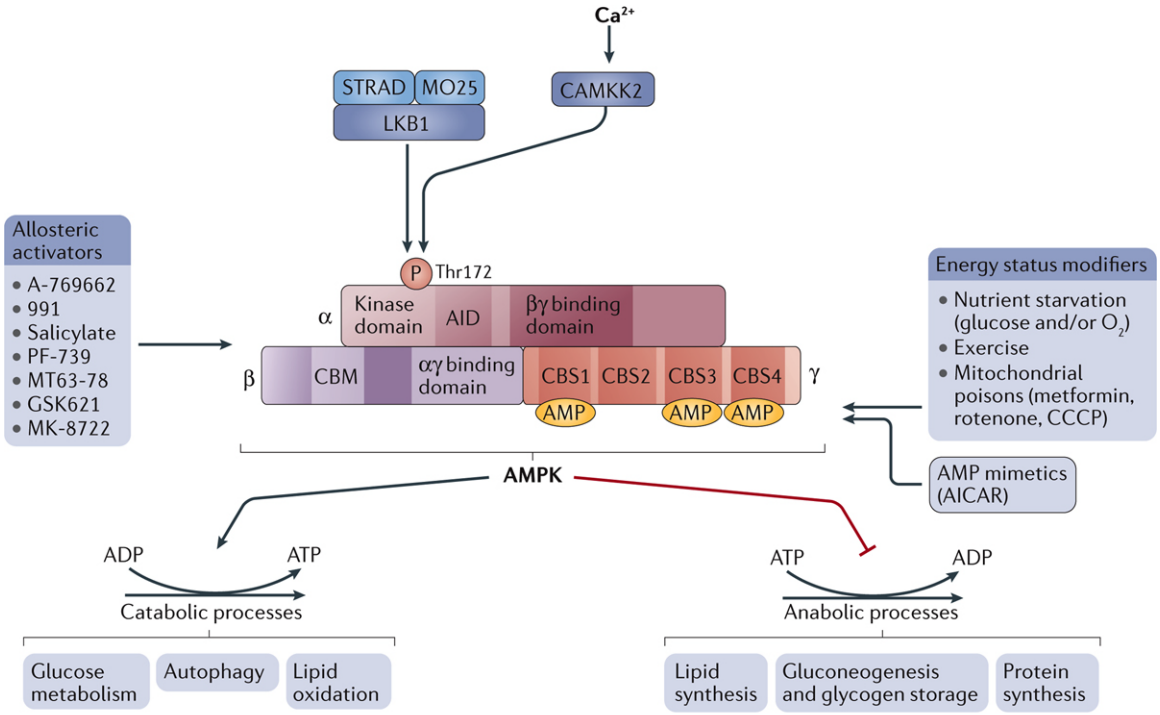

Figure 1.5. Regulation of trimeric AMPK through chemical and cellular processes. AMPK is a trimeric protein complex consisting of three AMPK subunits, α, β and γ. The primary roles of AMPK are regulation of cellular energetic through AMP binding events targeted to the regulatory γ subunit. Binding of AMP is required for AMPK activation while several AMP mimetics drugs and allosteric activators are also used for AMPK activation. AMPK targets a variety of downstream pathways including Autophagy stimulation, glycolysis, β-oxidation and FA biosynthesis inhibition all with the primary goal to regulate cellular energetics towards homeostatic behaviour. Adopted from [181].

1.6.3. AMPK and mTOR crosstalk, autophagy and cancer

Another crucial regulatory network involved in energy sensing mechanisms is the mammalian target of rapamycin (mTOR) kinase complex. Phosphorylation is crucial for activation of mTOR signalling and is primarily mediated through activation of the PI3K/AKT signalling pathway. The mTOR kinase complex consisting of RPTOR, DEPTOR, mLST8 and PRAS40 functions as an ATP/amino acid sensor responsive to conditions where energetics is favourable. Phosphorylation of mTOR at Ser2448 seems to be the crucial regulatory residue leading to downstream activation of key protein complexes such as the S6 kinase, a key regulator of protein translation, inhibition of the translational repressor 4E-BP1 and activation of SREBF-mediated lipogenic pathways, while the mechanisms discussed previously highlighted AMPK as the key regulator of low energy cellular states, mTOR and AMPK work together in order to orchestrate short term signal transduction responsible for energetic

homeostasis. One of the key pathways co-regulated by both MTOR and AMPK are the catabolic autophagy pathways in response to poor energetic cellular conditions. AMPK is the guardian of pro-autophagic processes, mTOR works against AMPK in energetic rich conditions to inhibit autophagy. Here we focus only on AMPK/mTOR mediated autophagy stimulation of ULK1. A complete review of autophagy stimulation, nucleation and clearance can be found here [182]. Although the large majority of downstream phosphorylation targets of AMPK and mTOR differ there are a few key targets that converge. The critical autophagy activating kinase ULK1 is one these crucial targets. mTOR-mediated phosphorylation of ULK1 at Ser757 is responsible for post transcriptional negative regulation of autophagy initiation. Phosphorylation of ULK at Ser757 leads to destabilisation of AMPK/ULK1 complex leading to ineffective AMPK-mediated stimulation of autophagy [183]. In response to low energy environments, phosphatases dephosphorylate ULK1, while decreased levels of PI3K/AKT-mediated phosphorylation of mTOR, due to lack of upstream growth signalling, leads to proteasomal degradation of the mTOR signalling complex. Consequently, converse accumulation of active forms of AMPK leads to increased ULK1/AMPK stable complexes and subsequent phosphorylation of ULK1 at Ser555, which is a crucial phosphorylation event for ULK1 activation and kinase activity. Furthermore, activation of AMPK can also directly inhibit mTOR activity through direct phosphorylation of the critical mTOR regulator RPTOR at Ser792 leading to ubiquitylation and proteasomal degradation [184, 185]. Finally, phosphorylation and activation of TSC2 at Ser1387 by AMPK inhibits GTPase mediated mTOR activation by RheB [186]. As mentioned previously, under sufficient nutrient conditions mTOR interacts with and phosphorylates ULK1, disrupting complex formation with AMPK. In nutrient poor conditions AMPK/ULK1 protein complexes are stabilized while AMPK mediated phosphorylation of ULK1 on Ser555 primes ULK1 for kinase activity. The active form of ULK1 can target several downstream protein targets, many of which are directly involved in autophagosome nucleation. Actively phosphorylated ULK1 forms a protein complex with ATG13, ATG101 and FIP200 with both ATG13 and FIP200 being directly phosphorylated by ULK1. Both ATG13 and FIP200 are essential for ULK1-mediated autophagy however research shows that they can act in the absence of ULK1 but ULK1 cannot act without ATG13 or FIP200, indicating that phosphorylation by ULK1 is not essential [187]. However, formation of ULK1 complex with heatshock proteins showed that phosphorylated ATG13

and FIP200 were required for complete autophagosome clearance in the context of stress induced mitophagy [188]. Other crucial targets of ULK1 include BECLIN1 and ATG14 both of which form an additional pro-autophagosome forming class III PI3K complex together with two addition proteins VPS34 and VPS15 [182, 189, 190]. Phosphorylation of BECLIN1 is essential for activation of the VPS34 lipid kinase activity responsible for local accumulation of phospholipids required for autophagosome formation [191]. Furthermore, phosphorylation of ATG14 by ULK1 has similar effects responsible for activation of the PI3K complex leading to autophagosome formation and nucleation [191, 192].

1.7. Lipogenesis and the hallmarks of cancer

Originally defined as a set of six key characteristics of tumorigenesis, the hallmarks of cancer define the major cellular process that are dysregulated in aggressive forms of human tumours [193]. Originally the focus was mainly on proliferation and evasion of apoptosis while in recent years the focus has broadened the hallmarks to include features such as immune evasion and dysregulation of cellular energetics [194]. While a mutational centric model has led to many cancer discoveries, a large amount research is currently taking a different approach and considering the effects of metabolism as a direct mediator of the effects on cancer cellular growth. While changes in metabolism have been shown to regulate all hallmarks, I will primarily focus on two key features, the regulation of cancer stem cells (CSC) through metabolic alterations and how these metabolic alterations provide survival advantages in harsh cellular environments including responses to cytotoxic drugs.

1.7.1. Lipogenic reprogramming & cancer stem cells

The identification of niche populations of cells that were responsible for tumour regeneration has been relatively recent. In the late 1990's, identification of a distinct tumour cell type CD34+/ CD38- tumour cells were shown to be required for tumour initiation in leukemia immunodeficient mouse models and

brought forward the idea of a progenitor stem-like cell responsible for tumour formation [195]. Since then CSC have been identified in many solid tumours including CD44+/CD24- in breast, CD44+/ EpCam+/CD166+ in colon and CD44+/EPCAM+/CD24+ in pancreatic tumours [196, 197]. The original static tumour-based model describing a mutational based hypothesis stating tumour behaving as monoclonal populations of cells brought about by key oncogenic mutations was breaking *in vivo. In vivo* analysis of multiple genetic induced tumours in addition to xenograft tumour models showed the tendency of tumour cells to undergo levels of differentiation as normal tissue would. Changes in the metabolic landscape of CSC compared to the majority of the tumour population has also been observed. Despite a large body of research in this field in recent years there is still conjecture over what the metabolic state of these cells are. As discussed previously a key genetic feature of tumour cells is apparent switching of aerobic respiration to the energetically unfavourable anerobic respiration. Induced or pluripotent stem cells, primarily utilise anerobic respiration much alike what is observed in tumours cell exhibiting features of the Warburg effect [198]. On the other hand, terminally differentiated cells rely heavily on oxidative phosphorylation for ATP production, and CSC have been shown to be similar in nature. Loss of FBP1 in breast CSC-like cells was shown to regulate glycolysis while inhibiting oxygen consumption through suppression of mitochondrial complex I, thereby pushing the cells towards anerobic respiration [199]. Similar observations can be seen in other CSC populations from colon, ovarian cancer and glioblastoma [200-202]. cMYC has been identified as a critical regulator of this process while in normal stem cells again similar observations have been observed [203, 204]. Interestingly, and in contrast, the exact opposite has been defined for many CSC populations showing a complete dependence on oxidative phosphorylation. Oxidative phosphorylation dependent lung tumours, glioblastoma and leukemic cells have all been identified and described [205-208]. Lipogenesis is another key metabolic pathway that has been highlighted as a key pathway dysregulated in human cancer. In line with glycolysis and OxPHOS, lipid reprogramming has also been associated with a CSC phenotype. Interactions between PML and PPARδ in hematopoietic stem cells was shown to drive mitochondrial fatty acid oxidation while loss of either PML or PPARδ led to differentiation and loss of stemness [136]. Chemo-resistant Leukemic stem cells were shown to be dependent on lipolysis

and fatty acid oxidation. Oxidative cells were significantly more chemoresistant, through upregulation of CD36 provided increase lipid efflux into the cell [209]. Furthermore, NANOG-induced inhibition of OxPHOS in hepatocellular carcinoma CSC showing increased levels of fatty acid oxidation driving ATP production while colon CD133+ CSC's sorted for high/low lipid content showed that high lipid content cells were more effective in tumour formation [210, 211]. The key lipogenic gene SCD, responsible for production of PUFA and a key target of SREBF1, was shown to regulate lung cancer stemness through stabilisation of nuclear YAP/TAZ complexes [212, 213]. In colorectal cancer COX2 a key regulator of the actions of highly PUFAs including arachidonic acid showed transcriptional repression of FOXP3 leading to a reduced CSC phenotype [214]. Tumour-associated adipocytes have been shown to be important for tumour maintenance and metabolic reprogramming allowing for rapid tumour growth and development [215]. In addition, PUFA have also been highlighted as important stress regulatory endocrine hormones playing roles in many aspect of tumour progression [216]. Lipid desaturases in ovarian cancer spheroids was shown to regulate formation of ovarian spheroids, while loss of lipid desaturases inhibited CSC formation through downregulation of NFkB signalling [217]. Furthermore, divergent lipogenic biosynthetic pathways including mevalonate metabolism and cholesterol biosynthesis have also been associated with a CSC phenotype. c-MYC-dependent regulation of HMGCOA in brain tumour initiator cells was shown to be crucial for maintenance of a CSC like phenotype through attenuation of RAS/ERK signal transduction [218]. The same pathway has also been shown to regulate YAP/TAZ signalling in a similar mechanism as PUFA, with loss of HMGCOA mediated biosynthetic pathways leading to reduction and destabilisation of nuclear YAP/TAZ [219].

1.7.2. Lipogenic reprogramming and drug resistance

Tumour metabolism is a complex process that leads to fundamental changes in the way tumours behave biologically. One of the key aspects of tumour metabolism and particular tumour lipid metabolism is the associated made the association between lipid metabolic reprogramming and cytotoxic drug resistance. Many groups have highlighted the importance of metabolic changes in

gaining mutation independent resistance to commonly prescribed cytotoxic drugs. Focus on manipulation of tumour metabolic pathways has been under dissection as a possible interventional method for regulated drug resistance responses in tumours.

Fatty acid oxidation is one of the key changes observed in tumour metabolism. Changes in key regulatory genes has been shown in many tumours including PPARGC1A as discussed previously. Knockdown of an enzymatic regulator of mitochondrial fatty acid oxidation, CPT2 was shown to induce cisplatin resistance in hepatocellular carcinoma cells. Furthermore, it was shown that reduction of mitochondrial fatty acid oxidation led to increased levels of PUFA through increased expression of SCD [220]. Downregulation of CPT2 was also shown to induce a hyperlipidemic cellular environment in both wild type and HCC tissues in mice models [221]. While high levels of mitochondrial cholesterol has been shown to induce chemoresistance through inhibition of mitochondrial permeabilization and resistant cytochrome c release, also in HCC models [222]. Interestingly, CPT1, a homologue of CPT2, was shown to have contrasting results where knockdown led to a severe reduction in cell proliferation and altered mitochondrial morphology, however it was revealed that this mechanism was independent of fatty acid oxidation [223]. Furthermore, tumours grown in adipocyte positive tumour microenvironments have shown to be resistant to anti-angiogenic drugs. These drugs were shown to induce hypoxic responses while tumours in high fat content environments were able to rewire to FAO and remained viable [224]. There is a clear gap in our knowledge regarding fatty acid oxidation and its effects on tumour growth and promotion where it appears to be entirely contextual. Lipid rich environments have been shown to induce drug resistance in many other solid tumours. HIF2A in renal cancer was shown to induce *de novo* fatty acid biosynthesis, correlating with high levels of PLIN2 expression. Furthermore, HIF2A associated lipogenesis was associated with ER homeostasis and ER stress resistance [225]. Tumours cells with high levels of *de novo* fatty acid biosynthesis were also shown to have reduced adverse effects from free radicals and was shown to drive resistance to doxorubicin [226]. Other research looking at commonly prescribed chemotherapeutics including 5-fluorouracil and oxaliplatin showed that chemo-induced lipogenesis was associated with chemoresistance

while inhibition of a key lipogenic enzyme LPCAT2 sensitized cells to chemo-induced cell death through inhibition of lipid droplet accumulation [227]. A recent paper focusing of Vemurafenib resistant melanomas showed that pooling of lipids was due to sustained lipogenesis mediated through increase SREBF1 transcriptional activity [156]. .

Targeting lipogenesis in the treatment of cancer has been explored too. COX2 inhibitors are probably the earliest examples of targeting lipogenesis to treat tumours through downregulation of VEGF signalling pathways. The COX2 inhibitor, Celecoxib is currently used as an anti-metastatic inhibitor in colorectal, prostate, bladder, [228]head-neck and breast cancers [229-231]. The FASN inhibitor Orlistat, currently under investigation in clinical trials, has shown promise in regulating tumour growth. FASN was identified as a key regulation of tumour growth in many topological tumours including colorectal and breast tumours [81, 232]. Similarly, ACLY inhibitors including SB-204990 have shown novel promise in treatment of lung cancers with antiproliferative effects, while several synthesis inhibitors such as hydroxycitrate has been shown to inhibit cholesterol biosynthesis in HEPG2 cells [233]. Inhibition of the SREBF maturation proteases S1P and S2P through treatment with Nelfinavir showed decreased levels of cellular fatty acids leading to ER stress associated apoptosis in both liposarcoma and prostate cancer cells and is currently in clinical trials for myeloma, glioblastoma, pancreatic and lung cancers [234-236].

1.8. Mass-spectrometry, CRISPR/Cas9 and next-generation sequencing as tools to dissect the metabolic genome

Alterations in lipid metabolism is commonly observed in many solid tumours. This leads to the possibility of utilising the tumour metabolic landscape as an exploitable means for developing tumour therapeutics and use for prognosis/biomarkers. The invention of modern-day chromatographic methodology has further developed metabolomics as a useful tool for diagnostic purposes. Current modern high throughput high performance mass-spectrometry and gas chromatography mass-spectrometry allow researchers to identify and quantify thousands of metabolic molecules within a single biological system.

1.8.1. HPLC and high throughput untargeted lipidomics

Predictions place the diversity of lipid species in biological systems from anywhere between ten to hundreds of thousands distinct molecular species. We can define this accumulation of total lipids found within a biological sample as the 'lipidome'. Analytical methods to measure lipids within biological samples in previous decades relied on time-consuming biochemical techniques through the use of exploitable lipid-specific chemical traits. For example, exploiting the process of lipolysis through conversion of glycerolipids to free fatty acids and using the fact that they react with free oxidised glycerol allowed researchers to measure triglyceride levels through colourimetric methods. However, the limitations of these applications became obvious in response to the implementation of high-throughput mass spectrometry in order to quantify and identify lipid species. In addition, to being time consuming and expensive research has highlighted the diversity of lipid storage in many different cell types. Furthermore, the inability to distinguish between similar lipid groups including phospholipids and triglycerides gives the inability to accurately measure any given lipid species in a biological system. Early methodology to measure lipids using MS techniques dates to the early 1990's using electron spray ionisation in order to measure phospholipid composition of human erythrocytes [237]. Although pivotal to modern day methodologies, throughput in early applications were relativity low due to mainly instrument sensitivity and limited mass spectrum of known lipid species. High throughput lipidomic methodology was further developed in the early 2000's applying MS techniques to identify and quantify lipid species in biological samples while the some of the first cases of using lipidomic analysis to identify biological markers for human disease were implemented [238-240]. The principles of LCMS are relatively straight forward. Large complex pools of biomolecules can be sorted based on biochemical principles such as pH and hydrophobicity prior MS analysis while identification of biomolecules through MS can be made based on two major properties, their ionisation state and molecular mass.

1.8.2. CRISPR/Cas9, pooled screening and next-generation sequencing

Prior to next-generation sequencing techniques, DNA sequencing was achieved primarily though Sangar and pyrosequencing methods. While, advancement in implementation of capillary separation and modern-day microscopy methods have vastly increased the accuracy and throughput of such methods, they still lacked the throughput of current modern NGS technologies. Introduction of truly next-generation platforms in the mid 2000's has led to increasingly dramatic reduction in sequencing costs while further increasing the throughput through implementation of barcoding libraries allowing for multiplexing. These days it is very much possible to sequence the human genome for as little as $1000 USD while multiplexing allows generated readouts of global gene expression for the same price as qPCR experiments. Illumina is by far the most popular platform and dominates the next generation sequencing world. Fluorescently labeled nucleotides are used to generate short DNA reads of between 50-150bp while super high-resolution digital images of the fluorescent probes are used to image the DNA fragments and image analysis tools can be used to automatically make base calls based on fluorescent properties. Further advancements in DNA sequencing led to the use of paired end sequencing techniques. While previous iterations of Illumina based sequencing used single end reads, paired end reads as predicted given the name, makes reads from both ends of the DNA strands. This provides increased sensitivity through production of overlapping reading frames, increasing fidelity and allowing for longer read length. A more recent development in the world of genomics was the implementation of bacterial based DNA editing enzymes, Cas proteins. The most common form is known as the Cas9 system and using biologically active RNA molecules containing a scaffold RNA sequence and a ~20nt gRNA, clustered regularly interspaced short palindromic repeats (CRISPR) allows biologists to make DNA indels with incredible efficiency and accuracy. RNA interference was previously used in order to alter gene expression of specific genes however this was not without its limitations.

Given the editing is post transcriptional this means that the effects are short lived. Furthermore, protein stability can greatly alter the effectiveness of RNAi as a genomic tool as this method targets the RNA and not the proteins directly. While DNA transfection methods can greatly affect the efficiency of RNA knockdown. This was somewhat rectified through use of lentiviral technology allowing for constitutive expression of siRNA fragments however, many biological systems can silence vector-based expression systems providing another hurdle to overcome. CRISPR/Cas9 has the advantage of targeting DNA and therefor creating hereditary changes while incredible versatility regarding the applications of the CRISPR/Cas9 system allow this method to be useful in almost all biological contexts. By far most commonly adopted protocols for CRISPR/Cas9 is lentiviral mediated overexpression of the Cas9 protein. Antibiotic selection markers can be used to overcome gene silencing and remove non-Cas9 expressing cells. However, the Cas9 system is not without its flaws. Different gRNA can be shown to have varied genome editing efficiency supporting the need for monoclonal populations to generate true knockout models, which can be both a lengthy and often impossible task depending on the model system. Since the first initial implementation of the Cas9 system, many great strides have been made including introduction of nuclease deficient Cas9 (KRABCas9). This defective Cas9 allows for siRNA like uses. gRNA targeting specific genes can be used to disrupt gene expression while further implementation of techniques such as doxycycline inducible expression can allow for RNA mediated editing with great control and efficiency. Furthermore, other Cas9 variants including Cas9-VPS34 or otherwise known as CRISPRa has provided a more biologically relevant tool for analysis of gene overexpression. Conventional gene overexpression techniques often place genes downstream of a constitutive gene promoter often leading to vastly biologically irrelevant expression levels. CRISPRa has been shown to allow for gene overexpression however in a more biological relevant context with overexpression raising to the 5-10-fold compared to potentially more than 100 fold increases in expression. In conjunction with both NGS and Cas9 implementation was the implementation of pooled screening methods. Large pools targeting in many cases genome-wide pools of gRNA can be used to answer many biological questions. For example, one of the first paper describing such techniques looked at targeting drug

resistence to a commonly prescribed BRAF inhibitor Vemurafenib [241]. NGS sequencing techniques targeted to lentiviral elements in cells transduced with pooled lentivirus gRNA libraries allowed for positive selection methods based on the assumption that genes with negative effects towards in this case drug resistance, would be enriched when pressure was applied, while negative screening assumption including genes that were required for drug resistance would either be depleted or lowly expressed. Multiplexing gRNA targeting the same gene allows for high confidence readouts of genes associated with many biological questions and pooled screens are currently being ever increasingly used to answer biological questions with similar approaches being used for CRISPRi and CRISPRa libraries.

1.9. Hypothesis and Aims

Metabolic rewiring in human tumours allows for the manipulation of metabolic pathways to generate survival advantages in otherwise harsh and adverse cellular environments. The PPAR family of transcription factors are relatively well characterised in normal metabolic homeostasis. The role that PPARγ plays as a lipid regulator in tumours is relatively uncharacterised where the primary focus has been on the function of PPARγ in regulation of proliferation and apoptosis. The transcriptional pathways that regulate metabolic processes such as PPARγ are still poorly uncharacterised and are central to many tumours. I hypothesise that regulation of tumour progression through metabolism is in part mediated by PPARγ signalling roles in regulation of the tumour lipidomic landscape.

To address this hypothesis, this study is aimed to:

1 – Explore the metabolic landscape of human tumour biology through transcriptomic analysis of tumours based on changes observed between normal:tumour samples and high:low survival patient samples utilising novel bioinformatic analysis of 50 manually curated metabolic pathways.

2 – Investigation of the associations between $BRAF^{V600E}$ driven tumours and the loss of PPARγ signalling and ether lipid metabolism in colorectal cancer.

3 – Investigate the human lipidome utilising high-throughput mass spectrometry approaches to identify risk factors associated with transcriptional regulation of lipid metabolism in solid human tumours.

Chapter 2 – Materials & Methods

2.1. Bioinformatic analysis of the TCGA & Depmap datasets

2.1.1. Data normalisation and acquisition

Raw mapped mRNA reads from 18 tumours subtypes defined by tissue of origin with normal patient tissue samples were downloaded from The Cancer Genome Atlas (TCGA) data portal (https://portal.gdc.cancer.gov/projects). For the metabolic pathway analysis raw datasets were trimmed down to a small subset of 3,033 metabolic associated genes. For differential expression analysis data was normalised using DESeq2 and was performed on complete datasets consisting of 56, 318 mapped RNA transcripts [242]. All data analysis was performed using MATLAB R2019a (https:// au.mathworks.com/downloads/). The subset of 3,065 metabolic related genes were further trimmed to 2,065 genes that were constitutively expressed across all topological tumour subtypes corresponding to an average raw read count of greater than 5. CCLE metabolomics and transcriptome RNAseq datasets were downloaded from the DepMAP data portal (https://depmap.org/portal/download/). Metabolomic dataset was not subjected to further data manipulation [243]. The cancer cell line encyclopedia (CCLE) dataset looking at the mRNA expression levels across 1271 human cancer cell lines through NGS based RNAseq was used as described previously utilizing the TCGA RNAseq dataset.

2.1.2. Geneset enrichment and determination of metabolic signature

Gene set enrichment analysis was used to analyse the changes in tumour metabolic pathways through the analysis of gene pathway enrichment scoring of differentially expressed genes from both the TCGA and CCLE datasets. GSEA software was obtained from the GSEA webserver (http:// software.broadinstitute.org/gsea/downloads.jsp). GSEA was either run using tumour versus normal samples or high verse low survival tumour groups using ranked t-statistics and modified versions of the KEGG and Reactome to incorporate positive/negative pathway regulation (http:// software.broadinstitute.org/gsea/)) datasets [249, 394].

.

Metabolic pathway enrichment for each tumour types were averaged to look for commonly enriched genesets above threshold and FDR parameters. Genescoring and pathway enrichment was performed looking at the normalised gene t-scores derived from the following four equations to look at ranked gene enrichment of each molecular pathway:

$$\mu = \frac{\sum_{i=1}^{N} x_i}{N}$$

Equation 1.1 represents μ as the sum of all elements of x divided by the number of elements in x (population mean, deviation of gene expression across each tumour subtype).

$$\bar{x} = \frac{\sum_{i=1}^{n} x_i}{n}$$

Equation 1.2 represents as the sum of all elements of x divided by the number of elements in x (Sample mean, deviation or ranked expression levels of each gene in a given sample (frequency distribution)).

$$s = \frac{1}{n-1} \sum_{i=1}^{n} (x_i - \bar{x})$$

Equation 1.3 represents the sum of the sample mean minus each element of x divided by the number of elements in the set x minus 1 (Standard deviation). Therefore the equation for t s statistics becomes:

$$t_i = \frac{\mu - \bar{x}}{s}$$

Equation 1.4. represents the t score of each gene represented in the element of each patient sample. We can further transform this into normalised values looking at the impact of ranked gene expression of each gene on the expression of all genes within a set defined by biological function:

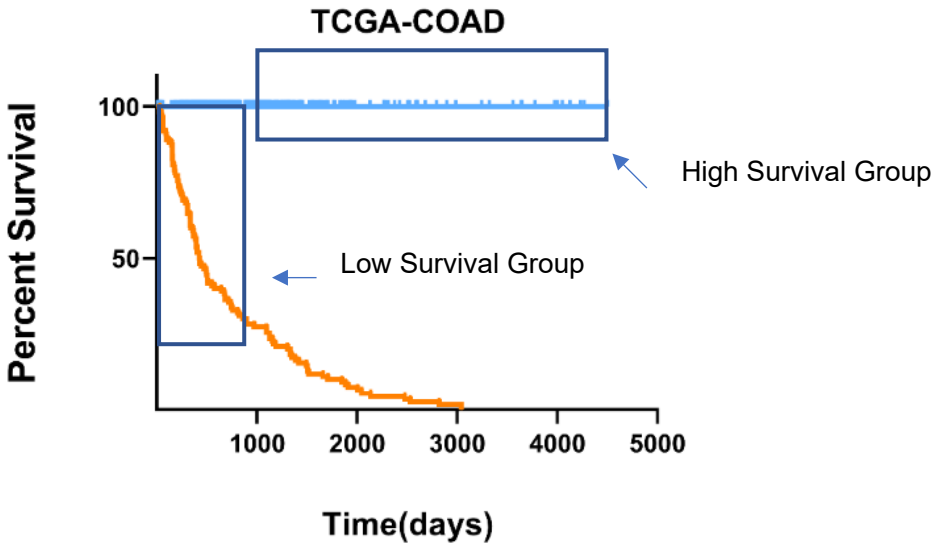

Figure 2.1. Example of the survival-based patient grouping using colorectal adenoma TCGA dataset. *The 75th percentile of both patient groups corresponding to patient with longest measure survival rates in days compared to the patients with the lowest survival rates were subdivided as indicated above.*

$$t_M = \frac{\sum_{i=1} e_i}{n}$$

Equation 1.5 describing t_M is the result of equation 1.4, where t_M the sum of each element represented by a pathway defined by the KEGG/Reactome datasets, divided by the number of the elements in each set.

2.1.4. Correlation analysis

All correlation analysis was performed using either-Pearson's ranked correlation for parametric normally distributed data while for non-parametric skewed data, Spearman ranked correlation was used. Statistical significance was measured using a standard student's two-tailed t-test. Correlation between molecular signatures generated and explained in the previous section were used to generate a ranked correlation matrix defining metabolic signatures and tumour metabolic subtypes represented by equation 2.5 below:

$$\rho(x,y) = \frac{\sum_{i=1}^{n}(x_i - \bar{x})(y_i - \bar{y})}{\sqrt{\sum_{i=1}^{n}(x_i - \bar{x})^2}\sqrt{\sum_{i=1}^{n}(y_i - \bar{y})^2}}$$

Equation 1.6

Both $\bar{x}\ and\ \bar{y}$ are represented in equation 1.2 but are either projected in the x or y direction where y represents the sample correlation and x represents the Pearson's correlation. For Spearman ranked correlation analysis the following equation 1.7 was used:

$$\rho\ (x,y) = \frac{\frac{1}{n}\sum_{i=1}^{n}(x_i - \bar{x})(y_i - \bar{y})}{\sqrt{(\frac{1}{n}\sum_{i=1}^{n}(x_i - \bar{x})^2)(\frac{1}{n}\sum_{i=1}^{n}(y_i - \bar{y})^2)}}$$

2.1.5. Survival analysis

To investigate the links between molecular signatures and tumour metabolic subtypes survival analysis was integrated into the data analysis pipeline. Based on overall survival rates the top 75th percentile of both high and low survival was taken as per figure 2.2. Patients with survival time of less than or equal to 0 were ignored. Downstream data analysis was as per previous described in the previous sections. Differential expression analysis and GSEA was used to identified enriched molecular pathways based on ranked t-statistic methodology using manually curated datasets generated through differential analysis of high and low survival groups represented in each topological tumour normalised as per previously discussed to normal tissue mRNA expression levels.

Table 2.1 | Cell lines, associated mutations and culture methods

Cell Line	Tissue	Disease	Culture Method	Notable Mutations
U2OS	Bone	Osteosarcoma	McCoy's 5a, 10% FBS	NA
HS578T	Breast	Carcinoma	DMEM, 10% FBS, 2mM L-glutamate	TP53-V157F, CDKN2A-Del, HRAS-G12N
MDAMB231	Breast	Metastatic Adenocarcinoma	RPMI-1640, 10% FBS, 2mM L-glutamate	TP53-R280K, KRAS-G13N, CDKN2A-Del
MDAMB468	Breast	Metastatic Adenocarcinoma	DMEM, 10% FBS, 2mM L-glutamate	TP53-R273H
ZR-75-1	Breast	Metastatic Ductal Carcinoma	RPMI-1640, 10% FBS, 2mM L-glutamate	PTEN-L108R
HT-29	Colon	Adenocarcinoma	RPMI-1640, 10% FBS, 2mM L-glutamate	APC-E853*, TP53-R273H, BRAF-V600E
LIM1215	Colon	Adenocarcinoma	RPMI-1640, 10% FBS, 2mM L-glutamate	CTNNB1-T41A, AVCR2A-K437fs*5
LIM2405	Colon	Adenocarcinoma	RPMI-1640, 10% FBS, 2mM L-glutamate	APC-2194fs*5, BRAF-V600E, PTEN-V290fs*5
RKO	Colon	Carcinoma	RPMI-1640, 10% FBS, 2mM L-glutamate	BRAF-V600E, ACVR2A-K437fs819
SW480	Colon	Adenocarcinoma	RPMI-1640, 10% FBS, 2mM L-glutamate	APC-Q1338*, TP53-R273H, KRAS-G12V
SW620	Colon	Metastatic Adenocarcinoma	RPMI-1640, 10% FBS, 2mM L-glutamate	APC-Q1338*, TP53-R273H, KRAS-G12V
A549	Lung	Carcinoma	DMEM, 10% FBS, 2mM L-glutamate	KRAS-G12S, STK11-Q37*
THP-1	Myeloid	Monocytic Leukemia	RPMI-1640, 10% FBS, 0.5mM BME	NRAS-G12D
COV434	Ovary	Granulosa Tumour	DMEM, 10% FBS, 2mM L-glutamate	NA
PC3	Prostate	Metastatic Adenocarcinoma	RPMI-1640, 10% FBS, 2mM L-glutamate	TP53-K139fs*31

2.2. Cell culture

2.2.1. Passaging and experimental cell models

Most cells were maintained in either Roswell Park Memorial Institute (RPMI)-1640 medium or Dulbecco's modified Eagles (DMEM) medium. L-glutamine was added to a final concentration of 4mM along with 5-10% fetal bovine serum (FBS) and either with/without 10U/mL of Penicillin-Streptomycin. All cells were maintained at 37°C and 5% CO_2. Media was changed every 3-4 days and passaging was performed using TrypLE (Life Technologies cat. no. 12563-011), detached cells were centrifuged at 500xg, resuspended in appropriate media and plated at 10% confluency as required (Table 2.1). All experiments were performed during passages 10-20.

Table 2.2| List of drug treatments and concentrations used.

Drug ID	Source	Identifier	Stock Conc.	Treatment Conc.
Rosiglitazone	Chem Supply	R0106-500mg	10mM	1-5uM
Vemurafenib	Cell Signaling	17531S	10mM	0.5-5uM
GW-9662	Med Chem Express	HY-16578	10mM	5uM
3-Methyadenin	Sigma Aldrich	M9281-100MG	10mM	5uM
Chloroquine Phosphate	Sigma Aldrich	PHR1258-1G	10mM	5uM
5-Fluorouracil	Sigma Aldrich	F6627-1G	10mM	1-5uM
Oxaplatinin	Sigma Aldrich	Q9512-5MG	10mM	1-5uM
GW-501516	Med Chem Express	HY-10838	10mM	5uM

2.2.2. Drug treatments

All drug treatments were performed 16 hours post cell seeding in all experiments presented in the thesis and treatment time is stated in the appropriate figure legends. All treatments were performed at 5µM unless otherwise stated in the figure legend as with co-treatment groups (See figure legend for detailed description of all drug concentrations). All treatment groups were compared to a control using a equvilant base solvent as control. All drugs stock solutions were made up in dimethyl sulfoxide (DMSO) except for 3-methyadenine and Chloroquine that were dissolved in H_2O. The table above contains the list of drugs, the most commonly used concentration and manufacturer information:

2.3. Lentiviral generation and transduction

2.3.1. Vectors/Plasmids

Lentiviral packaging vectors pMD2.G and psPAX2 were a gift from Didier Trono (Addgene cat. no. 12259 & 12260). lentiCRISPR-V2-Blast was a gift from Mohan Babu (Addgene cat. no. 83480) [244]. dsDNA fragments corresponding to gRNA sequences were cloned into plentiCRISPR using the BsmBI restriction site. 1ug of lentiCRISPR-V2-Blast was incubated at 37°C for 1hour with BsmBI and cut fragments were run on a 2% agarose gel. The required fragment corresponding to ~12.7kb was excised from the gel and isolated using the QIAquick gel extraction kit (Qiagen, USA). DNA primers corresponding to the gRNA fragment with required 5'-CACC overhang for sequence complementarity were incubated with complimentary DNA primer and phosphorylated using T4 polynucleotide kinase (NEB, USA) at 37°C for 30 minutes followed by incubation at 95°C for 5 minutes for enzyme inactivation and then temperatures were ramped down to room temperature at 1°C per minute for DNA annealing. For DHRS7B-mCherry or DHRS7B-T2A-eGFP vectors dsDNA gene fragments corresponding to either mCherry or T2A-eGFP (idtDNA, gBlock gene fragments) were cloned into pcDNA3.1(+)-Neomycin using EcoRI/XbaI cloning sites starting with 1ug of plasmid. Digested pcDNA3.1(+) plasmid was isolated as per the protocol used for lentiCRISPR-V2-Bst. Full length human DHRS7B was PCR amplified from wild type human colon RNA samples using primers corresponding to human DHRS7B (Forward 5' – TCGTTGGATCCGCCACCATGGTCTCTCCGGCTACCAG, reverse 5' – CTGCCGAATTCGGAG TTCTTGGATTTTCCGC) and cloned into either pcDNA3.1(+) using BamHI/EcoRI restriction sites. All ligation reactions were performed at 4°C for 16 hours using T4 DNA ligase (NEB, Cat. # M020) and transformed into alpha select chemically competent ***E.coli*** (Bioline, USA) and were selected using agar plates at 37°C for 16hours using the appropriate selection antibiotic. Luciferase Dual reporter pGreenFire lentiviral system (System Biology Cat. #. TR101PA-P) was used to measure transcription activity of PPARγ and PPARδ

2.3.2. Lentiviral generation, transduction & stable cell generation

Lentiviral particles were generated using the second-generation packaging plasmids pMD2.G and psPAX2 as described in the previous section. plentiCRISPR-V2-Blast transfer plasmid was used to generate Cas9 stable cells and was used to deliver gRNA, and pGreenFire-PPRE ORE vectors were used to measure transcriptional activity. Packaging plasmids and the appropriate transfer plasmid were transfected into 293T cells seeded onto 10cm cell culture dishes at ~50% and left to adhere overnight. The following day 293T cells were washed twice with PBS and replenished with 4mL of DMEM (10% FBS, 4mM L-glutamine) and 2mL transfection buffer (Opti-MEM (Gibco cat. no. 31985-070) up to 2mL, 24µL of Lipofectamine 2000 (Invitrogen cat. no. 11668030) 1.3pmol psPAX2, 0.72pmol pMD2.G & 1.64pmol of transfer plasmid) and left for a further 24 hours. H293T cells were transferred into standard DMEM with no penicillin/streptomycin and media was collected every 24 hours for 96 hours. Media containing virus was spun down at 500xg for 5 minutes to remove cellular debris and passed through a 0.2µm PES filter (Sigma Aldrich cat. no.GPWP047). To generate stable cells, the cell line of interest was seeded at 40% confluency in a 10cm dish and left to adhere overnight. The following day media was replaced with 1:1 ratio of viral supernatant and standard culture media without penicillin/streptomycin and 10µg/mL of polybrene (Merck cat. no. H9268-5G). Cells were selected with 1-2µg for most cell types of puromycin or blasticidin (Sapphire Biosciences cat. no. 13884 & 14499) for 72-96 hours and between 500-1500µg/mL of Geneticin (Life Technologies cat. no. 10131035) for 7-10 days. Stable cells were maintained on 50% of the selection antibiotic required for successful selection for all downstream applications i.e. growth assays, cells were taken off selection media for the length of the subsequent experiments.

2.4. CRISPR/Cas9 knockout cell generation

Constitutive Cas9 overexpressing cells were used to generate knockout cell lines. lentiCRISPR-V2-Bst with the appropriate gRNA cloned were used to generate lentiviral particles as described in the previous

section. lentiCRISPR-V2-Bst package lentiviral particles were used to infect cell line of interest at a MOI of less than 1. Successfully transduced cells were selected using blasticidin at 1-2ug/mL for most cell lines and were either used as polyclonal populations or serially diluted to generate monoclonal null cell lines. All CRISPR/Cas9 cell lines were validated through western blot analysis targeted towards protein of interest.

2.5. Western Blot Analysis

Total protein was extracted using a modified RIPA buffer (150mM sodium chloride, 1% Triton x-100, 0.5% cholic acid, 0.1% sodium dodecyl sulfate & 50mM Tris pH 8.8) at 4°C for 2hrs with gentle agitation. One tablet of Complete mini protease inhibitor cocktail (Roche cat. No. 11836170001) and PhosSTOP phosphatase inhibitor cocktail (Roche cat. No. 4906845001) were added per 15mL of RIPA buffer. Protein was heated to 95°C for 5 min in the presence of 1x sample buffer (416.7mM Tris-HCl, pH 6.8, 66.6% glycerol (v/v) 6.6% sodium dodecyl sulphate 0.03% bromophenol blue). Protein loading was first normalised to total protein colorimetrically using TGX Fast-Cast stain-free gel system (Bio-Rad cat. no. 1610173). Protein was then further normalised to total levels of beta-actin. For non-normalising gels standard polyacrylamide was used at between 7.5-15% (Bio-Rad cat. no. 1610146) and run using Tris-glycine running buffer (25mM Tris, 192mM glycine & 0.1% sodium dodecyl sulfate pH 8.5) at 100V for 2 hours. Protein was transferred from polyacrylamide gels onto either 0.44µm Immobilon-P (Sigma-Aldrich cat. no. P2938-1ROL) or 0.2um (Bio-Rad cat. no. 1620177) PVDF membrane using Tris-glycine transfer buffer (25mM Tris, 192mM glycine & 10% methanol) at 30V for 16 hours at 4°C. Membranes were blocked using 5% bovine serum albumin (Sigma Aldrich cat. no. A9648-50G) dilluted in 1xTBST for 30 min at room temperature. All primary antibodies were diluted in block buffer at 1:1000 dilution and incubated for 16 hours at 4°C. A list of antibodies used can be found in Table 2.3. Primary antibody was washed away in five changes of 1x TBST. Secondary antibody incubation was performed at room temperature for 1 hour using either anti-rabbit IgG (Cell Signalling, cat. no. 7074) or anti-mouse IgG(Invitrogen cat. no. 31430) horse radish peroxidase conjugated antibodies diluted in block buffer at

1:10000 dilution. All western blots were developed using x-ray film methodology (Fujifilm cat. no. 497690). Developed X-ray film was scanned into digital files and images were produced using Image J software (https:// imagej.net/Fiji/Downloads).

2.8. Immunohistochemistry/Immunofluorescence

All mouse tissue was fixed overnight at room temperature in 4% paraformaldehyde (PFA) dissolved in ddH_2O and washed three times in 1xPBS and a further three times in 70% ethanol. Tissue was infused and embedded in paraffin. Tissue sections were cut and prepared at 4µm. Cells were seeded into either 24/48 well dishes or chamber slides at the appropriated confluency. Tissue sections were dewaxed in three changes of xylene for three minutes and then hydrated in five graded ethanol washes followed by two final washes in dH_2O for three minutes each. Antigen retrieval was performed using 1mM EDTA, pH8.0 antigen retrieval buffer and brought to boil in a microwave oven, and then left to boil for a further 20 minutes. Sections/cells were blocked and permeabilised in immuno block buffer (5% bovine serum & 0.1% tween 20, dilluted in 1xPBS) for 30 minutes at room temperature. Rabbit anti-DHRS7B was used at 1:200, Goat anti-Rabbit IgG-Biotin (Invitro, Cat # 31820) and Streptavoden-HRP (Thermo Scientific, Cat. #N100) were both used at 1:1000 all were diluted in immuno blockbuffer. Primary antibodies were incubated overnight at 4C while secondary antibodies were incubated at room temperature for 1h. For immunohistochemistry, slides were developed using chromogenic methods (Dako cat. no. GV82511-2) and counter stained using haematoxylin and coverslips were mounted using DPX. DAPI dilluted in 1xPBS 1:10000 from a 5mg/mL stock was used as a counter-stain for immunofluerescence (Molecular Probes cat. no D1306) and mounted using ProLong Gold mountant (Molecular Probes cat. no. P36934). All imaging was performed using the Olympus IX71 coupled with the camera system. Image analysis was performed using Fiji image analysis software [398].

Table 2.3 | List of primary antibodies used for western blotting

Target	Source	Manufacturer	Identifier
Anti-phospho p44/42 MAPK ERK1/2 (Thr202/Tyr204)	Rabbit polyclonal	Cell Signaling	Cat. # 8544
Anti-p44/42 MAPK ERK1/2	Rabbit polyclonal	Cell Signaling	Cat. # 9102
Anti-phospho AMPK (Thr 172)	Rabbit monoclonal	Cell Signaling	Cat. # 2535
Anti-AMPKa	Rabbit monoclonal	Cell Signaling	Cat. # 5832
Anti-phospho RPTOR (Ser792)	Rabbit polyclonal	Cell Signaling	Cat. # 2083
Anti-RPTOR	Rabbit monoclonal	Cell Signaling	Cat. # 2280
Anti-phospho ULK1 (Ser555)	Rabbit monoclonal	Cell Signaling	Cat. # 5869
Anti-phospho ULK1 (Ser757)	Rabbit polyclonal	Cell Signaling	Cat. # 6888
Anti-ULK1	Rabbit monoclonal	Cell Signaling	Cat. # 8054
Anti-phospho MAPKAPK2 (Thr334)	Rabbit monoclonal	Cell Signaling	Cat. # 3007
Anti-phospho SAPK/JNK *(Thr183/Tyr185)	Rabbit monoclonal	Cell Signaling	Cat. # 4668
Anti-JNK1	Mouse monoclonal	Cell Signaling	Cat. # 3708
Anti-phospho cJUN (Ser73)	Rabbit monoclonal	Cell Signaling	Cat. # 3270
Anti-cleaved Caspase 3 (Asp175)	Rabbit monoclonal	Cell Signaling	Cat. # 9664
Anti-phospho p38 MAPK (Thr180/Tyr182)	Rabbit monoclonal	Cell Signaling	Cat. # 4511
Anti-cleaved PARP (Asp214)	Rabbit monoclonal	Cell Signaling	Cat. # 5625
Anti-BiP	Rabbit monoclonal	Cell Signaling	Cat. # 3177
Anti-phospho eIF2a (Ser51)	Rabbit monoclonal	Cell Signaling	Cat. # 3398
Anti-eIF2a	Rabbit monoclonal	Cell Signaling	Cat. # 5324
Anti-ATG12	Rabbit monoclonal	Cell Signaling	Cat. # 4180
Anti-Beclin1	Rabbit monoclonal	Cell Signaling	Cat. # 3495
Anti-FASN	Rabbit monoclonal	Cell Signaling	Cat. # 3180
Anti-LC3A/B	Rabbit monoclonal	Cell Signaling	Cat. # 12741
Anti-SREBF1 (2A4)	Mouse monoclonal	Santa Cruz Biotech	Cat. # sc-13551
Anti-DHRS7B	Rabbit polyclonal	Atlas Antibodies	Cat. # HPA012132

2.9. Cell growth and cytotoxic assays

For Brd-U incorperation assay, cells were plated into 24 well plates at approximately $1x10^5$ cells/ well and left to adhere overnight. Post treatment cells were incubated in the presence of 10uM BrdU for 2h and fixed in 2% PFA for 20 min at 4°C. Cells were incubated with anti-BrdU antibody dilluted in immuno block buffer 1:1000 (Abcam, Cat. # ab8955) overnight at 4°C and a donkey anti-mouse IgG Alexa 488 secondary antibody (Invitro, Cat. # R37114) at RT for 1h and then counterstained with DAPI for 5 min. Blocking was performed using adult bovine serum and all antibody staining was performed in the presence block buffer. 5 FOV per well were collected with all treatments performed in triplicates from three indipendent experiments .

and the average was taken relative to DAPI positive cells. MTT based or luciferase RealTime-Glo (Promega, cat. # G9711, G3582) assay was performed as per manufacturer's instructions over a period of 72 hours. Approximately 1,000 cells were plated into 96 well luminescent white TC treated plates and left to adhere overnight. Nanoluc luminescence was measured using a Clariostar spectrophotometer at 480nm.

2.10. Lipid droplet analysis

Cells were seeded into either 48 well dishes at 20% confluency. After the appropriate treatments were performed cells were incubated in 250µM Nile Red (Sigma Aldrich cat. no. N3013-100MG) for 10 minutes diluted in 1xPBS, washed three times and then fixed using 2% PFA diluted in growth media for 20 minutes in the dark at 4°C. Cells were counter stained with DAPI (Molecular Probes cat. no D1306) and mounted using ProLong Gold mountant reagent (Molecular Probes cat. no. P36934). All imaging was performed using the Olympus IX71 microscope coupled with a camera system. 6-8 fields of view were taken, and 300 cells were counted per replicate. Analysis was repeated three separate times and all image analysis was performed using Fiji image analysis software.

2.11. Cell based promoter assay

Cells were seeded in 96 well plates at 20, 000 cells per well and left to adhere overnight. Cells were transferred into 5% serum media with the appropriate treatments and left for a further 24 hours. Cells were lysed using 60µL of 1x passive lysis buffer (Promega cat. no. E1941) for 20 minutes at 4°C with gentle agitation. 20µL of lysate was transferred onto luminescent plates (Thermo Scientific cat. no. 136101) and luminescence was measure using the Firefly luciferase assay system (Promega cat. no. E1501). 5µL of protein lysate was used to measure total protein concentration using the detergent compatible protein quantification kit (Bio-Rad cat. no. 5000111) and luminescence was normalised to total protein.

2.12. Fluorescence associated cell sorting (FACS)

Cells were seeded at the appropriate confluency and left to adhere overnight. After appropriate treatments cells were washed three times with PBS and detached using TrypLE (Gibco cat. no. 12563-011). Cells were spun down at 200xg for 5 minutes and resuspended into RPMI-1640 (no phenol red, 10% FBS & 100mM EDTA) at between 5-10 x 10^6 cells/ml. Cells were sorted for either eGFP or mCherry into fresh standard growth media or for RNA collection directly into RNA*later* stabilisation buffer (Invitrogen cat. no. AM7020). Propidium iodine (PI) was used as a viability dye at 1µg/mL (Molecular Probes cat. no. P3566).

2.14. Quantitative PCR, Nanostring analysis and RNAseq analysis

Total RNA was extracted using either TriZol reagent (Life Technologies cat. no. 15596-026) or the RNeasy mini kit (Qiagen cat. no. 74104) following manufacturer's instructions. 1µg of total RNA was reverse transcribed to cDNA using the QuantiTect reverse transcriptase kit (Qiagen cat. no. 205311) as per manufacturer's instructions and dilluted 1:20 with RNAse free H_2O, and Realtime qPCR was performed using the QuantiNova SYBR qPCR master mix (Qiagen cat. no. 208252). All primers used for qPCR analysis were ordered through Sigma Aldrich and were used at a final concentration of 250nM. 1ug of cDNA was used per reaction assuming a 1:1 RNA:cDNA and all reactions were performed in triplicates with between three to six biological replicates. Thermal cycling was performed using the CFX384 Realtime thermal cycler (Bio-Rad) and data analysis was performed using the $\Delta\Delta^{Ct}$ method using either RPS29 or GAPDH as a housekeeping gene [397]. The sequences of all primers used in this study can be found in Table 2.3 below. For Nanostring analysis, 120ng of total unamplified RNA was used. RNA was mixed with hybridisation/codeset master mix (3µL reporter codeset, 5µL hybridisation buffer, 2µL capture probe & 120ng of RNA made into 5µL of ddH_2O). Hybridisation was performed at 65°C for 16 hours and then ramped down to 4°C at 1°C per/ minute. 15µL of hybridized probes and RNA mixture was loaded into a Nanostring cartridge and run on the Nanostring SPRINT system. All data analysis was performed using Nanostring in house software

nSolver (https://www.nanostring.com/products/analysis-software/nsolver). For DHRS7B overexpressing GFP sorted cell lines, the PanCancer progression panel was used and for the LIM1215/2405 DHRS7B knockout cells lines the PanCancer pathways panel was used. For RNAsequencing, standard polyA library preparation was used and sequencing was performed on an illumina platform. Short read alignment was performed using Hisat2 [399]. Differential expression analysis was performed using DeSeq2 using raw read counts obtained from previous step.

2.15. Mass spectrometry

Cells were seeded into a 60mm TC treated cell culture dish. Post appropriate treatment cells were washed three times in ice cold 1xTBS and then disassociated using TrypLE as per section 2.2.1. Cells were spun down at 500xg for 5min and then resuspended into ~500uL of ice-cold TBS and counted using trypan blue. Approximately $2.5x10^6$ cells were transferred to a sterile 2ml Eppendorf tube spun down again at 500xg for 5min and supernatant was removed and snap frozen. For lipid extraction cell pellet was thawed on ice and resuspended in 125uL of TBS, 25uL of cell suspension was transferred for protein quantification and refrozen while 100uL (~$2x10^6$ cells) was used for non-polar lipid extraction. Cell suspension was sonicated for 5 seconds and repeated three times and then transferred into a 4mL glass vial and 2mL of chloroform:methanol 2:1 (v/v) was added. Samples were agitated for 10min and then left to stand for a further 50min. 0.4mL of LCMS grade water was added and samples were agitated for 10min and left to stand for a further 1hour. The lower hydrophobic phase was transferred into clean 2mL glass vials and chloroform was evaporated under nitrogen gas and resuspended into 160uL of chloroform:methanol and transferred into a 200uL glass insert and dried down again. Upon mass spectrometry samples were resuspended into 1:1 butanol:methanol and 10uL of each sample was used as a pooled QC sample. Samples were separated on a C8, 100 x 2.1mm, 1.8um particles (Agilent 858750-906, USA) using a Dionex Ultimate 3000 Rapid seperation liquid chromotography system and mass spectrometry was performed using QExactive system (Thermo Scientific, USA). Lipid identification was performed using a concentrated pooled QC sample using the LipidBlast v10 dataset and normalised to internal SPLASH MS lipid class standards (Avanti Polar Lipids, USA). For saturation index, each lipid species

Table 2.4 | List of DNA primer sequences used for RT qPCR

Gene ID	Forward Primer 5′	Reverse Primer 5′
AACS	CGTGTGTATGATGAGGTTGTGG	TCCTCTTTGCCTTCCCTTGC
ACACA	CCATGTGGGCTTTAGGGGAT	TCCACACGAAGACCACTGC
ADIPOQ	TGTATGGGGAAGGAGAGCGT	GCCTGTGAAGGTGGAGTCAT
AGPAT3	CTGTACCAGGAGAAGGACGC	GCCCAGGACAGGAAGTTCAG
ATG10	TCAAAGGACTGTTCTGATGGCT	AATCACTTCGGACGCTGCT
ATG12	CTTTGCTCCTTCCCCAGACC	CCATCACTGCCAAAACACTCATAG
ATG16L1	TCTTTGGGAGACGCTCTGT	CAGCGTTGACTTCCCCATCA
ATG5	CACAAGCAACTCTGGATGGGA	AGCCACAGGACGAAACAGC
ATG7	AGTGCCTTGGATGTTGGGTT	CCCAGCAGAGTCACCATTGT
BENC1	CCCCTGAAACTGGACACGAG	CTGCGAGAGACACCATCCTG
BNIP3	TGAGGAACACGAGCGTCATG	CTGGTGGAGGTTGTCAGACG
CD36	TGTCCTGGCTGTGTTTGGAG	TTGGCTAGAAAACGAACTCTGT
CHPT1	ATCTCCTACTGTCCCACGGC	GCTCCCACTGCCATAAATACTGT
CPT1A	GCCTTTCAGTTCACGGTCAC	AGTGATGATGCCGTTCTTGAATC
DGAT1	GGAAGAGGAGGTGCGGGA	TCAGCATCACCACACACCAG
DGAT2	TTCCTTGTACTGGGAGTGGC	GGTCAGCAGGTTGTGTGTCT
DHRS7B	AGGGCTGGGCAAAGAATGTG	CCACAGAGCACCAGTTTAGCA
FASN	CTGGAAGGCGGGGCTCTA	CCAGTGTGTGTTCCTCGGAG
GAPDH	AATCCCATCACCATCTTCCAGG	TGGACTCCACGACGTACTCA
GPAT3	GCCAGACAGCAGCCTCAAAA	ATTCCCATCAAGCCGCCATG
HADHB	CCTGAACCTTGCTCCGAGAG	GAACACCATCCACCACCACA
LIPC	CGGCGTGCTAGAAAACTGGA	GATGGTGTAGTGGTCGTGGG
LIPE	CTTCCAGTTCACGCCTGCC	CGTTTGTAGTGCTCCCCGAA
LPCAT3	AACCAGCTCTACCACTCCCT	TCAACAGCCAAACCAATCAGC
LPIN1	TCAGCAAGTCCACGGAAAGG	GCTCAATGGGCTGGACTCTT
LPL	CCGCCGACCAAAGAAGAGAT	GGGAATGAGGTGGCAAGTGT
MGLL	GCAGACGGACAGTACCTCTTC	ATCCTCTCCCCTTCGCTCTG
MTOR	TCCGAGAGATGAGTCAAGAGGA	CAACTGGGTCATTGGAGGGG
PLIN2	GGGTAGAGTGGAAAAGGAGCA	CGTGACTCAATGTGCTCAGC
PLIN3	CCACCTGCCCCTTACGGATG	GCCTTGCTTGACAGTTTCCATCAG
PNPLA2	TCACCAACACCAGCATCCAG	CATCTCTCGCAGCACCAGG
PPARA	CAAGTGCCTTTCTGTCGGGA	ACAAAAGGTGGATTGTTACTGGC
PPARD	GCATGTCACACAACGCTATCC	CTGTGGGTTGTACTGGCTCC
PPARG	GGTTGACACAGAGATGCCATTC	GCAGGCTCCACTTTGATTGC
PPARGC1A	GACCCTCCTCACACCAAACC	TGGTTTGGCTTGTAAGTGTTGTG
PPLP1	AGTTAAGGAAGGCAGGTTGTCC	CCAGTCAACACATCGCTCCA
PRDM16	ACAGACTTCGGATGGGAGCAAA	GCTCCTCACCTGGCTCAATGT
PRKAA1	CGGAGCCTTGATGTGGTAGG	TCATCCAGCCTTCCATTCTTACAG
RPS29	GGTTCTCGCTCTTGTCGTGT	GTGCCAAGGAAGACAGCTCA
RXRA	CCTATGAACCCCGTCAGCAG	CCATAGTGCTTGCCTGAGGA
RXRB	GAAGCCACCAGTCTTAGGGG	CCCCGTAGTGTTTGCCTGAG
RXRG	GAACTACCCATCCACCAGCC	CCCCGTAGTGCTTTCCTGAG
SCD	ACCACCACCACCATTACAGC	TCCAAGTAGAGGGGCATCGT
SIRT1	AACAGGTTGCGGGAATCCAA	TGCAAAGGAACCATGACACTG
SREBF1	CTTTGCCGACCCTGGTGAG	CCACCACCAGATCCTTGAGC
tPPARG	GGGCGATCTTGACAGGAAAG	AGACAGCAGAAGAGAACTAACTG
ULK1	AACATCCTGCTGTCCAACCC	GAAGCCGAAGTCAGCGATCT

associated with a lipid class were grouped based on total number of unsaturated carbon atoms across all lipid chains. Each lipid species was used to generate an average species fold change across the geometric mean of the individual lipid species (average fold change according to row geomean) (equation 2.8 below).

$$L_M = Log_2\left(\frac{x_i}{\bar{x}}\right)$$

Where $\bar{x}$ represents the geometric means of each row vector represented by a finite n x n matrix where each row in the n x n matrix represents a mass spectrometry read out of individual lipid species in each sample.

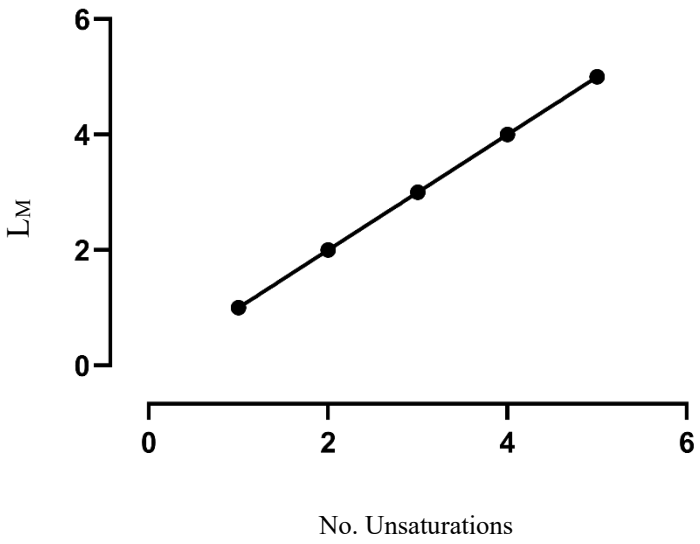

Figure 2.2. Linear regression model of membrane associated lipid unsaturation patterns. Idealised xy plot of linear regression model of the saturation index based on the ratio of unsaturated lipid species in a sample.

Xy plot of the average lipid fold change as per equation 2.6 is plotted against the number of unsaturations in each lipid species. Saturation index is calculated by (equation 2.9 below).

$$SI = M * r$$

Where r is represented by the Pearson's coefficient (equation 2.10, below) and M is the slope of the line of best fit.

Chapter 3 - Linear Predictive Metabolic Mapping define PPARγ and SREBF1 Signatures Associated with Colorectal Tumours

3.1 Introduction

Metabolic rewiring of cancer cells is a crucial process highlighted by early landmark studies looking at changes in anerobic/aerobic metabolism in tumours known as the Warburg effect [245]. Despite the importance of such research and the ever-increasing interest in tumour metabolism as a potential therapeutic target, much is still unknown about tumour metabolism. The classical genetic centric model of tumour progression is slowly starting to incorporate a metabolic centric model of tumorigenesis. This is not surprising when you consider the interest in tumour metabolism has shed light on metabolic mediated regulation of all the tumorigenic hallmarks. Meta-analysis of large cohort datasets looking at metabolism based on transcriptome analysis has been used to identify many important aspects of tumour metabolism. For example, Negative bilinear gene expression models based on the TCGA dataset showed downregulation of oxidative phosphorylation as a key metabolic change in both metastatic melanomas but was also associated with patients exhibiting poor clinical prognosis correlating with increase epithelial to mesenchymal transition (EMT) potential [246]. .

One of the problems with modelling of phenotypic outcomes in tumour metabolism is if the association defined by genomic analysis correlates to metabolic output. For example, targeted analysis of microarray mRNA expression profiles of human tumour colorectal tumours compared to normal untransformed tissue samples showed dysregulation of glycolysis. Further analysis utilising modern high-throughput mass spectrometry analysis was implemented for pathway validation and correlated with transcriptome analysis [247]. One of the major difficulties when utilising transcriptomic data to investigate associations with defined signalling pathways or metabolism is deciding how to approach gene expression as a geneset rather than an individual gene expression change. Geneset Enrichment Analysis (GSEA), originally developed by a group working at the broad institute has been extensively utilised across many fields including oncology [248, 249]. GSEA ranks genes based usually on fold change or pvalue in order to address gene enrichments associated with a predicted phenotype by scoring enriched genesets based on two major factors. The enrichment scores are based upon a random walk algorithm. Significant results indicate overrepresentations associated with the edges of the data

distribution. A second metric, the leading edge represents the directionality of the data and is simply a measurement of the distance from the beginning of the random walk to reach its maximum height. A short leading edge represents a positive enrichment score where the majority of genes associated within any given set are enriched at the far left of the ranked gene list while a long leading edge represents a negative enrichment score with the majority of associated genes with a geneset found at the far right of the ranked gene list assuming high to low ranking based on expression. Data representation and analysis is often complicated and required large volumes of computing power and expertise. Differential expression based models have been developed for RNAseq technologies and provide an effective computational method to identify differentially expressed genes when using well defined controls [250]. However, it was not ideally developed for looking at complex transcriptomes such as the varied and distorted transcriptomes found in human tumours. These models have been utilised to performed large scale pan cancer pathway enrichment analysis [246]. Other normalisation and data analysis methods have been employed to look complex disordered tumour samples such as transcripts per million (TPM) or RPKM (Reads Per Kilobase Million) [242, 251, 252].

In this chapter I look at the tumour metabolic transcriptome of a subgroup of 2,065 constitutively expressed metabolic associated genes from an original pool of 3,033 genes. T-statistical (read count frequency distribution model) ranked transcriptomics normalisation methods were used in place of negative binomial differential expression models normalised to normal tissue sample. Pathway analysis of 50 modified metabolic genesets were considered and were corrected for promiscuous genes across 18 tumour subtypes and 8036 tumour samples. Finally, machine learning methods were implemented to investigate metabolic patterns associated with tumorigenesis. Tumour metabolic pathways showed either well defined metabolic associated signatures based on tissue of origin or poorly defined metabolic tumours subtypes that were largely independent of tumour tissue of origin. Further analysis of gastrointestinal tumours revealed two major colorectal cancer associated metabolic clusters associated with HIF1A signatures while further analysis revealed two similar transcription factors responsible for the regulation of FA metabolism, SREBF1 and PPARγ led to drastically different transcriptomic analysis regulating crucial pathways associated with tumour immunity and EMT.

3.2 Metabolic mapping in human tumours

3.2.1 Data analysis and processing

Transcriptomic based metabolic mapping in human cancer was performed on 18 solid human tumour subtypes. Raw RNA sequencing data from the TCGA data portal was used to generate a sub-pool of 3,033 metabolic enriched genes defined by genes associated with enzymativ activity, solute transporters and transcriptional regulation of metabolic enzynmes across 8038 tumour samples normalised to tissue of origin with 762 normal tissue samples **(Table 3.1)** [395]. For differential expression analysis and data normalisation, DeSeq2 algorithm was used while all data processing was performed using the MATLAB 2019a software suite [250]. The dataset was further curated by removing tissue specifically expressed genes or genes with a geometric mean read count of less than 5 across all tumour samples giving a sub-pool of 2,065 constitutively expressed metabolic associated genes. A t-statistical model based on gene read count frequency distribution across a set of samples was used with preference over the raw read counts and DEseq2 based differential expression analysis. This methodology allows for identification of genes based on percentile distribution across samples comparing frequency distribution as opposed to average fold change and minimizing the effects that processes such as library size and distribution have on other bilinear based normalisation models [253, 254]. T-statistics or z-scores were based and normalised to normal tissue gene distribution with 2,065 genes across 8038 tumour samples generating a ranked order read distribution dataset **(Fig. 3.1)**.

Table 3.1 | Tumour and normal sample information

Cancer Subtype	Abbreviation	Tumour Sample (n)	Normal Sample (n)
Bladder Urothelial Carcinoma	BLCA	408	19
Breast Invasive Carcinoma	BRCA	1100	112
Colonrectal Adenocarcinoma	COADREAD	626	51
Esophageal Carcinoma	ESCA	185	11
Glioblastoma Multiforme	GBM	166	5
Head and Neck Squamous Cell Carcinoma	HNSC	522	44
Kidney Chromophobe	KICH	66	25
Kidney Renal Clear Cell Carcinoma	KIRC	534	72
Kidney Renal Papillary Cell Carcinoma	KIPC	291	32
Liver Hepatocellular Carcinoma	LIHC	373	50
Lung Adenocarcinoma	LUAD	517	59
Lung Squamous Cell Carcinoma	LUSC	501	51
Pancreatic Adenocarcinoma	PAAD	179	4
Prostate Adenocarcinoma	PRAD	498	52
Stomach Adenocarcinoma	STAD	415	35
Stomach and Esophageal Carcinoma	STEC	600	46
Thyroid Carcinoma	THCA	509	59
Uterine Corpus Endometrial Carcinoma	UCEC	546	35
Subtotal			762

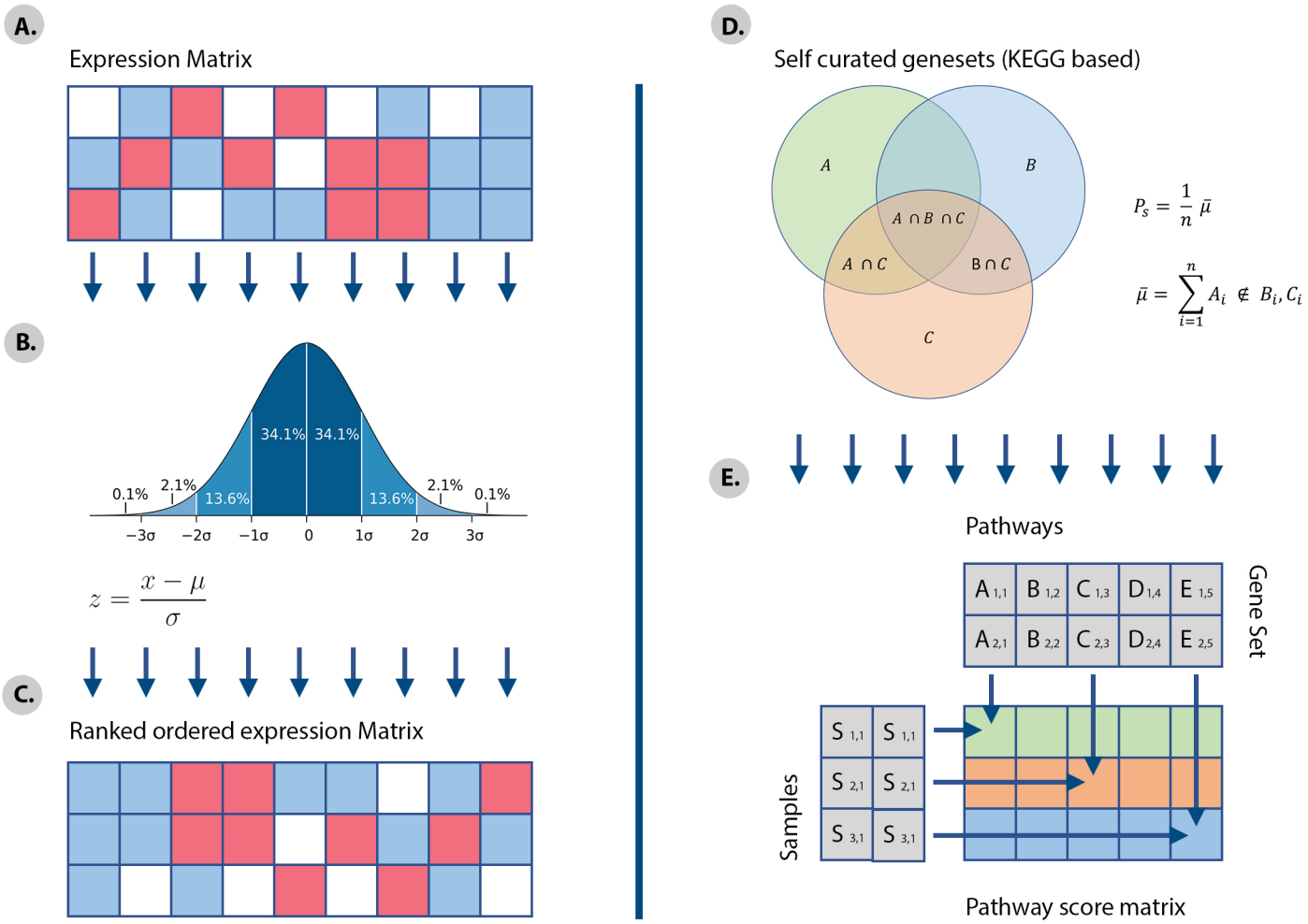

Figure 3.1. Data pipeline for linear based transcriptome-based z-score metabolic pathway analysis. A. Raw RNA mapped reads can be used in further analysis based on t-statistical population distribution model. **B.** Raw RNA reads are used to generate a z-score (z) corresponding to a ranked order distribution of RNA transcripts in any given sample based on frequency distribution and standard deviations generated through control population samples refer to methods section 2.1. **C.** Ranked order gene expression models can be used to look at pattern of percentile genes rather than Raw or normalised read counts. **D.** Geneset analysis is performed by looking at a group of gene sets with associated phenotypes while only concentrating on genesets associated with single phenotypes (gene promiscuity correction). E. gene set scores corresponding to the sum of all z-score of associated gene set A that does not correspond to genes associated with gene set b or c. Downstream data analysis pipelines such as linear statistical models and machine learning can be applied to identify patterned clusters based on metabolic genetic signatures. Refer to methods section 2.1.

3.2.2. Geneset Enrichment Analysis of human tumours based on differential gene expression

In order to generate a base line for the analysis used, whole transcriptome differential expression analysis was used using a standard Deseq2 based differential expression model. GSEA was performed on differentially expressed normalised transcriptomic data using two commonly implemented gene set datasets, KEGG and REACTOME. Datasets were limited to characterised signalling pathways and metabolic pathways. A heatmap representing the 18 tumour subtypes analysed showing statistically downregulated pathways in blue, statistically significant upregulated pathways in red and either none enriched or not significant pathways in white. Pearson's-based hierarchical clustering was performed showing three major metabolic cancer subtypes based signatures associated with 50 metabolic pathways with closely related tumour subtypes including colorectal and colon adenomas showing similar metabolic outputs **(Fig. 3.2A)**. To get a better understanding of dysregulated pathways across multiple tumours a volcano plot was generated using the average pathway enrichment score compared to the average p-value, based on both KEGG and REACTOME genesets. KEGG based genesets showed only two upregulated pathways across all tumour subtypes being involved in nucleotide metabolism, while nitric oxide response, DAG/IP_3 signalling and phospholipase C cascades were shown to be downregulated across most tumour subtypes **(Fig. 3.2B)**. The REACTOME dataset showed significant differences in dysregulated pathways. Additional dysregulated pathways were observed to be associated with AA metabolism, and ether lipid metabolism was shown to be downregulated, while tyrosine metabolism, VEGF signalling and WNT/β-catenin signalling was all significantly upregulated **(Fig. 3.2C)**.

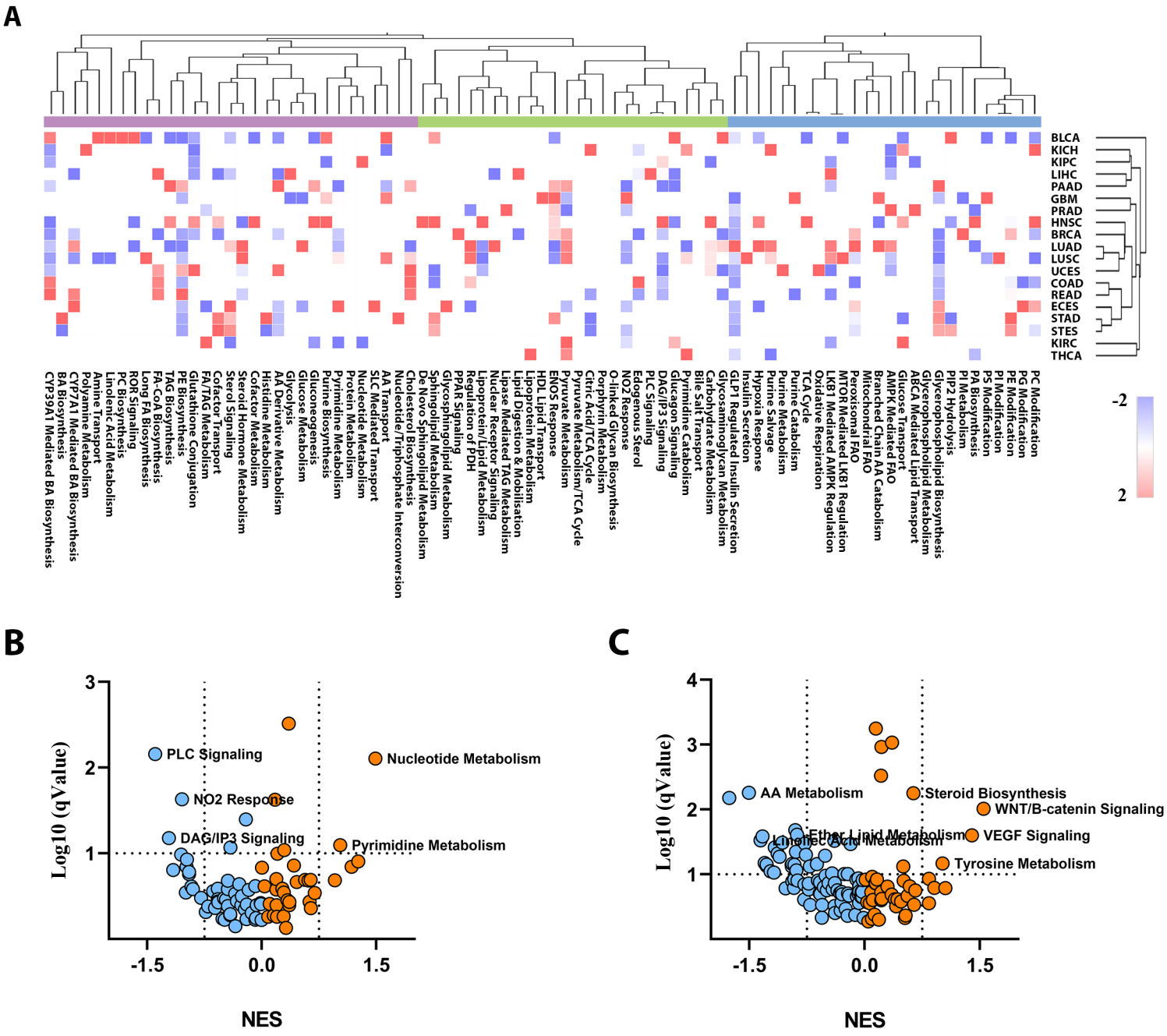

Figure 3.2. Genesets Enrichment analysis of 18 human cancers subtypes based on whole transcriptome sequencing. A. Heat map representation of significantly differentially expressed pathways utilising differential expression analysis based on normal tissue normalised tumour samples. Red corresponds to upregulated enriched pathways; blue cells correspond to downregulated enriched pathways and white cells correspond to undetected enrichment or no statistical significance. **B.** Volcano plot representation of the average enrichment score of each pathway represented in the KEGG dataset against -log10 (FDR) and **C.** same but using the REACTOME dataset. All differential expression analysis was done using the DeSeq2 algorithm and data analysis was performed using Matlab 2019a. Raw RNAseq read counts for 18 human tumour subtypes were downloaded from the TCGA data portal (See materials and methods).

3.2.3. The impacts of T-statistic based normalisation on GSEA

One common problem associated with GSEA based approaches is association of several genes with multiple genesets (gene promiscuity). The KEGG and REACTOME datasets are not immune to this problem, with many genes associated with multiple pathways while the literature does not always back up this association [246]. Furthermore, lowly expressed genes can also play a role to heavily skew data analysis. To tackle these issues and gather a better understanding of metabolic dysregulation in human tumours a smaller curated dataset of 2,065 constitutively expressed metabolically associated genes was generated as described earlier. Manually curated genesets associated with cellular metabolism were generated based on the KEGG dataset, while genes that were associated with multiple pathways were removed to limit the impact of gene promiscuity. Analysis of 50 KEGG based curated gene sets across 18 human cancer subtypes showed significant alterations compared to standard KEGG-based GSEA approaches described in the previous section. Looking at the average z-scores of genes associated with various metabolic pathways showed most genes were associated with a slightly positive or negative skew, while several genes had consistently higher t-scores indicating that they existed in the top percentiles across most tumour samples **(Fig. 3.3A)**. I then performed the same data analysis this time comparing genesets based on patient survival rates. The bottom 75th percentile of high survival groups was compared to the top 75th percentile of low survival patient groups while patients with clinical survival data indicating survival of either zero or below zero were removed and not further addressed in the analysis **(Fig. 2.1)**. The average pathway z-score was compared to the average p-value across 18 tumour subtypes. Among the top upregulated pathways associated with poor prognosis was the metastatic associated HIF1A signature. Furthermore, closely associated pathways including glycolysis were also upregulate in poor survival tumours. Conversely, FA-CoA biosynthesis and sterol biosynthesis were among the most commonly dysregulated pathways associated with high survival patient groups **(Fig. 3.3B)**. To validate the transcriptomic based model, I looked at using the Depmap dataset looking at 888 human cancer cell lines with matched metabolic mass spectrometry data [255, 256]. The same data pipeline was applied to the Depmap dataset looking at the same 2,065

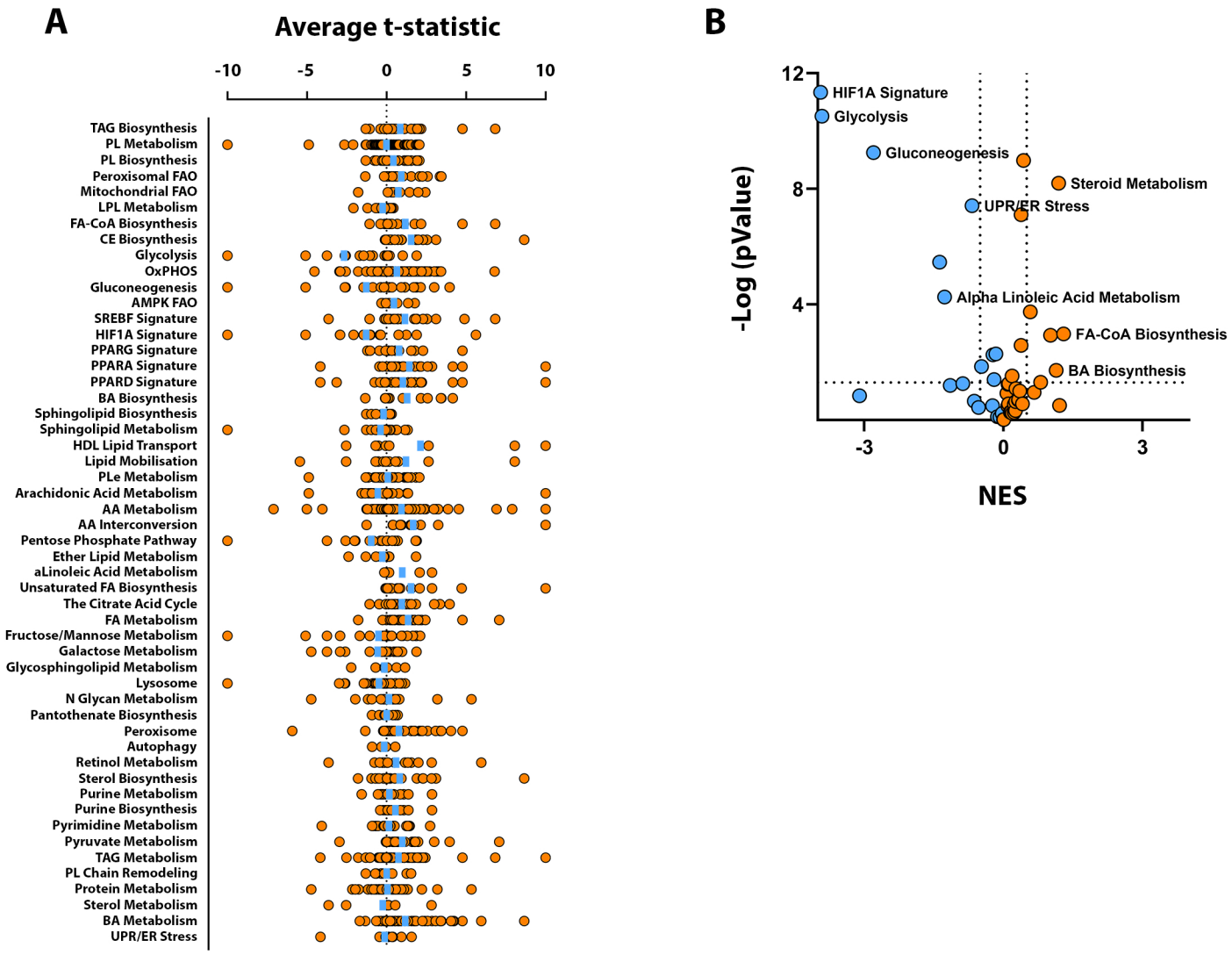

Figure 3.3. Generation of manually curated KEGG based Genesets for dissection of tumour metabolic reprogramming. A. Aligned dot plot representing the average t-score of each gene associated with 50 designated metabolic pathways across 18 human cancer subtypes with the median represented by a blue line. **B.** Volcano plot representation of the average pathway score of 50 manually curated genesets of normal tissue normalised samples looking at the changes of pathway score associated with poor prognosis. All data analysis was performed using Matlab 2019a. Raw RNAseq read counts for 18 human tumour subtypes were downloaded from the TCGA data portal (See materials and methods).

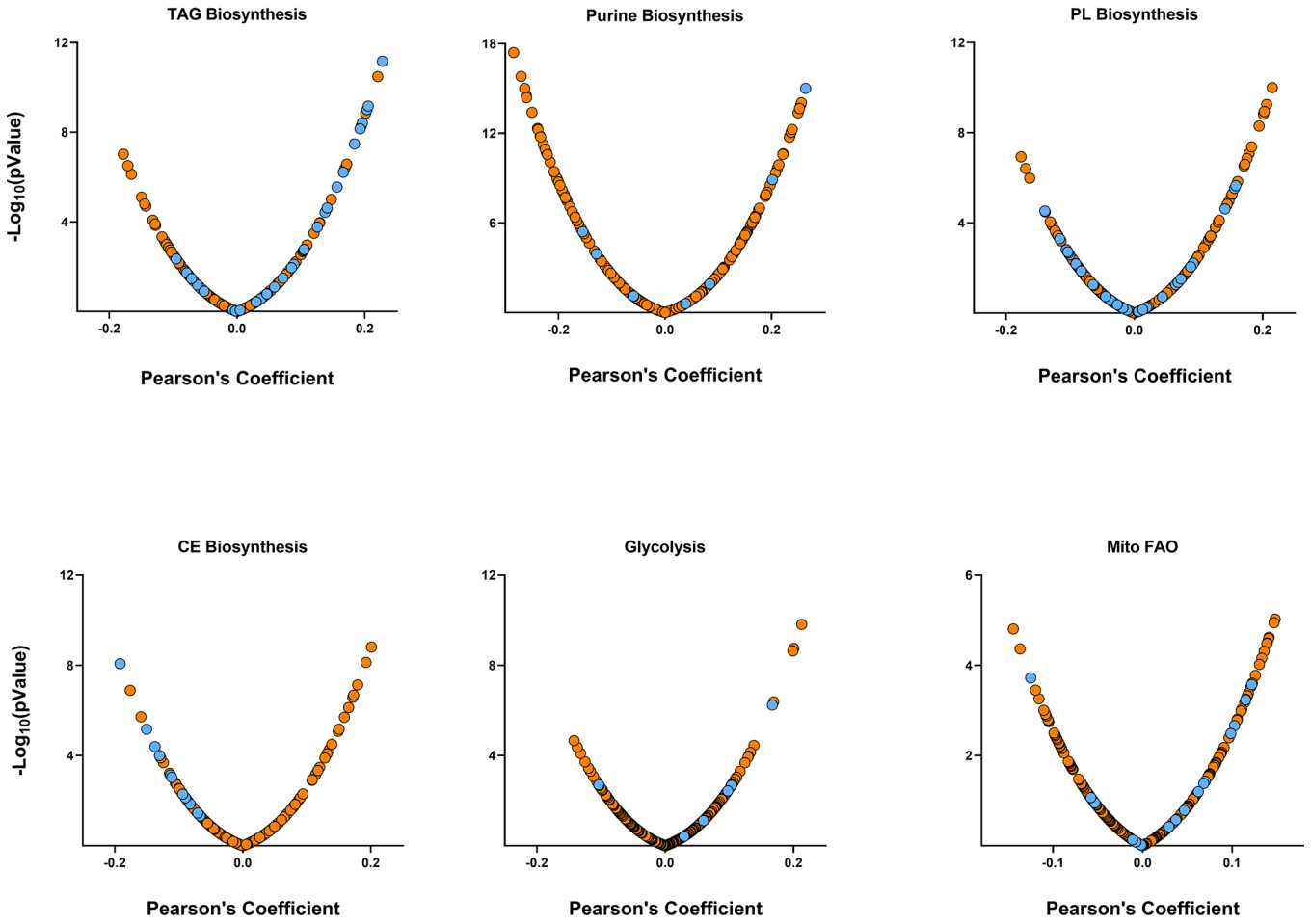

Figure 3.4. Metabolic association of predicted pathway score using the CCLE dataset. The CCLE metabolomics dataset was used in conjunction with match RNA transcriptomic datasets. Pathway analysis using manually curated metabolic associated pathways were used to generate pathway scores in 888 human cancer cell lines. Pearson's correlation was used to assess the correlation by means of Pearson's correlation coefficient value and was plotted as a U-plot against -log10 (pValue). Blue dots represent metabolites associated with the metabolic pathway, while orange dots represent metabolites not associated. This was performed for pathways with measure metabolite levels, triacylglycerides, purines, phospholipids, cholesterol esters, metabolites associated with glycolysis and FA derivates derived from fatty acid oxidation. All data was downloaded from the Depmap data portal (See materials and methods). All data analysis was performed using Matlab 2019a and as described with the TCGA dataset.

constitutively expressed metabolically associated genes. In order to gain an insight of the associations between the pathways and their associated metabolic phenotype, spearman ranked correlation coefficients were calculated between each metabolic pathway and each of the 231 metabolites that were identified across all 888 cell lines in the Depmap metabolomic dataset. I focused primarily on lipids, nucleotides and glycolysis associated genesets. Purine, TAG biosynthesis and glycolysis were shown to be on average positively associated with metabolites associated with those pathways. CE biosynthesis pathway was negatively correlated with CE metabolites, while mitochondrial FAO showed an overall positively correlated with pathway associated metabolites **(Fig. 3.4)**.

3.3 Identification of metabolically distinct subtypes of colorectal tumours

Unsupervised clustering methods for analysis of tumour transcriptomes has been commonly used to look at patterns in tumour gene expression. Tumours largely cluster based on tissue of origin due to the commonality of tissue types in relation to epigenetics and active cell signalling pathways. To better understand how human tumours, regulate metabolism I applied modern unsupervised clustering methodologies using the pathway enrichment scores calculated in Section 3.1. Spearman ranked correlation of metabolic pathways were calculated and used to generate a correlation matrix. Metabolic pathways generate three related metabolic clusters. Close associations between CE, TAG biosynthesis and SREBF1 signature genesets were identified in cluster 1. A larger second cluster showed more divergence in the similarities between metabolic pathways with pathways such as HIF1A signature, and glycolysis the most closely related with the third cluster was largely associated with PL metabolism, biosynthesis and more exotic lipid metabolism **(Fig. 3.5A)**.

T-distributed stochastic neighbourhood joining (t-SNE) is an unsupervised clustering method based on the principles of machine learning [257]. t-SNE was used to generate clustering based on pathway signature scores and was colour coded according to tumour tissue of origin. seven major clusters were identified using this method with tumours isolated from liver, kidney, breast and prostate showing significant divergence in their relationship between other tumour types indicating they are metabolically

distinct **(Fig 3.5B)**. Other tumour types such as lung and gastric tumours were primarily found in a much larger central cluster showing small signatures based on tissue of origin, and these tumour samples were associated with mostly similar metabolic phenotypes. One exception was observed in this second larger cluster **(Fig. 3.5B)**. Analysis of the standard deviation of pathways associated in colorectal cancers compared to all other tumours showed that colorectal tumours had significant divergence in pathways associated with oxidative phosphorylation, PPARγ signalling and AMPK-mediated fatty acid oxidation. The highest divergent pathways associated with non-colorectal tumours were AA interconversion, and pathways associated with HDL and lipid mobilisation **(Fig. 3.5C).** Looking at the clustering of just gastrointestinal cancers showed three major patient associated clusters. Gastric and oesophageal tumours showed to largely cluster into one group while several metabolically divergent samples were also observed and did show correlation with most samples. Interestingly, colorectal tumours were shown to cluster into two major patient associated clusters **(Fig. 3.5D, left panel)**. Finally, to determine the pathways that were responsible for these two distinct colorectal tumours subtypes the average fold change of the geneset scores were determined across the two patient clusters. HIF1A signalling together with glycolysis were shown to be primarily responsible for this metabolic signature where the upper cluster was associated with high HIF1A signature compared to the lower cluster which was associated with low HIF1A signatures **(Fig. 3.5D, right panel)**. As discussed previously, among the most divergent metabolic pathway associated with colorectal cancer was PPARγ-mediated signalling. To further address the roles of PPARγ signalling and closely related signalling pathways in the context of the two identified colorectal cancer subtypes we looked to measure PPARy signatures utilising our previously defined methodology. As mentioned previously, I showed that these two clusters were largely divergent based on a HIF1A signature. Given the close relationship between lipid metabolic transcription factors such as PPARγ and SREBF1, the associations between the two related signalling pathways was assessed. Analysis of the top 10^{th} and 90^{th} percentile of PPARγ and SREBF1 signature scores for human colorectal cancers showed that high SREBF1 tumours were largely associated with the HIF1A active top colorectal signature, while the opposite was true for PPARγ showing mainly more upregulation in the lower larger metabolic cluster **(Fig. 3.6B)**. Analysis of the association between the PPARγ and SREBF1 signature indicated that

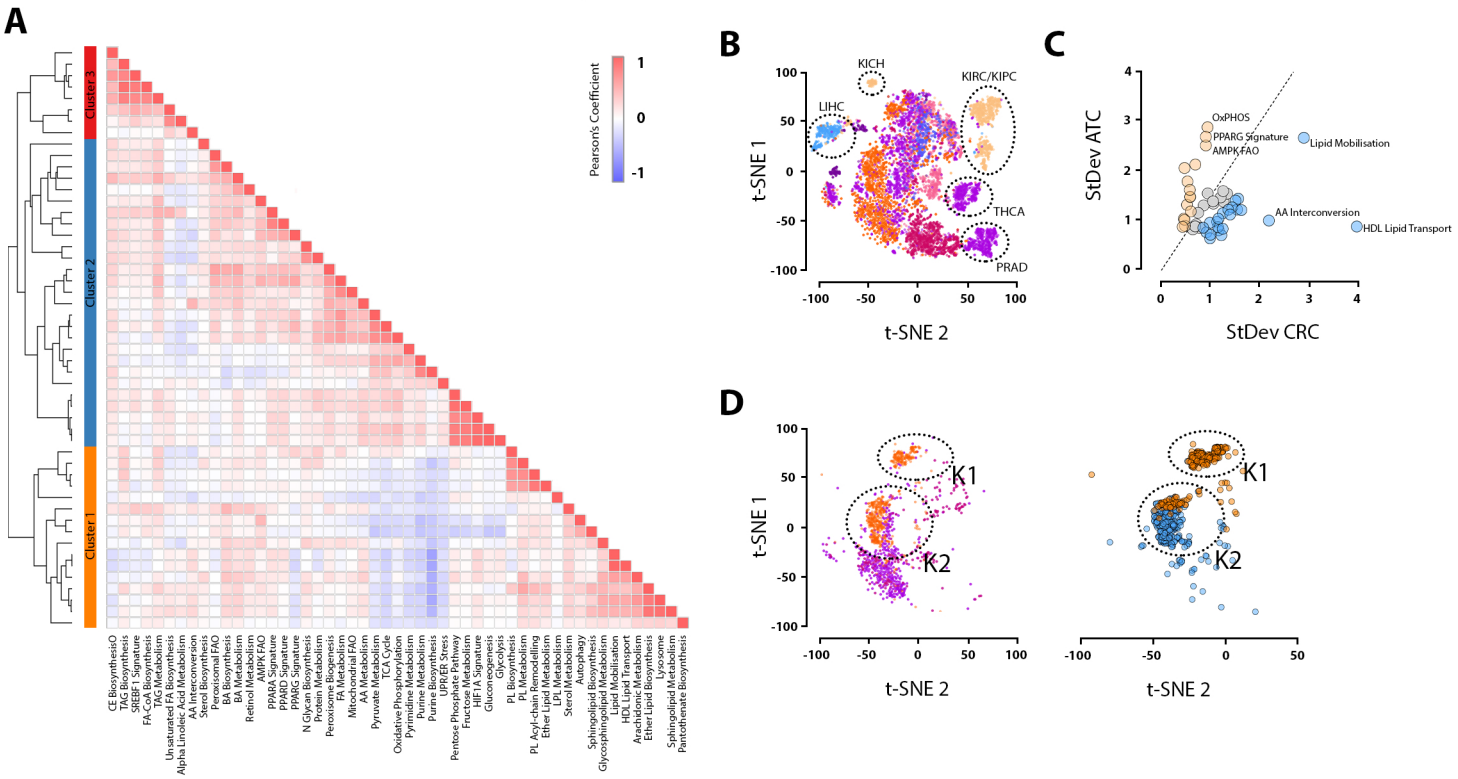

Figure 3.5. Machine learning based on metabolic pathway enrichment of human tumour samples reveal two metabolic subtypes of colorectal cancer. A. Spearman ranked correlation analysis of 50 manually curated genesets in 8034 human tumour samples based on 18 different tumour subtypes. Correlation matrix was performed assessing the dependency relation of metabolic pathway in human cancer. **B**. T distributed stochastic neighbourhood joining based clustering methods were used to generate unsupervised clusters of human tumour relationships based on metabolic pathway enrichment scores. **C.** x, y plot of the standard deviation of each of the 50 metabolic pathways in colorectal cancer plotted against the standard deviation of metabolic pathways in all tumour subtypes. **D, left panel.** Same as **B** but only looking at gastric intestinal tumours, with two distinct gastrointestinal cancer subtypes highlighted as K1 and K2 **right panel,** Same **D left panel** but only looking at colorectal tumours colour coordinated based on tumour sample HIF1A signature scores. All data analysis was performed using Matlab 2019a. Raw RNAseq read counts for 18 human

.

the two pathways were co-regulated in the lower cluster however, this relationship was not present in the upper cluster. Differential gene expression analysis of the two metabolic tumour subtypes showed significant changes in gene expression associated with not surprisingly HIF1A signalling, but also showed upregulation of FA metabolism and oxidative phosphorylation. Finally, gene sets associated with the larger bottom cluster showed upregulation of WNT signalling and interestingly EMT associated genes **(Fig. 3.6D & E)**.

3.4 HIF1A associated colorectal metabolic tumours are associated with low PPARγ signatures and high SREBF1 signatures

In the previous section a close relationship was described between PPARγ and SREBF1 signalling in colorectal cancer patient data sets. Colorectal tumours were broadly defined into two clusters and a lower cluster with strong correlation between a SREBF1 and PPARγ signature. While a second cluster that contained with a HIF1A signature was more associated with a high SREBF1 signature but a low PPARγ signature. Given the controversial role that PPARγ may play in negative regulation of colorectal tumorigenesis I investigated the transcriptome of these two distinct tumour classes. I analysed four tumour subclasses based on the predicted PPARγ and SREBF2 signatures (Class 1; High SREBF1/Low PPARγ, Class 2; High PPARγ/Low SREBF1, Class 3; Low PPARγ/low SREBF1 & Class 4; High PPARγ/high SREBF1) **(Fig. 3.7A, bottom panel)**. Mutational analysis of the 10th percentile of patients associated with each group showed that Class 1, associated with both high SREBF1 and PPARγ, was also associated with the lowest mutational load while the highest mutational load on average was associated with the low PPARγ signature and high SREBF1 signature **(Fig. 3.7A, top panel)**. APC mutants were relatively consistent across clusters 2-4 while only three patients were associated with APC truncation mutations in class 1 **(Fig. 3.7B)**. Oncogenic BRAF mutations were also observed in a higher frequency in patients associated with low PPARγ signatures **(Fig. 3.7B)**. Differential expression analysis of the four clusters based on SREBF1 and PPARγ signatures showed significant divergence in expression patterns **(Fig. 3.7C)**. GSEA analysis of the different clusters showed differential expression of several oncogenic associated genetic pathways. Class 1, associated

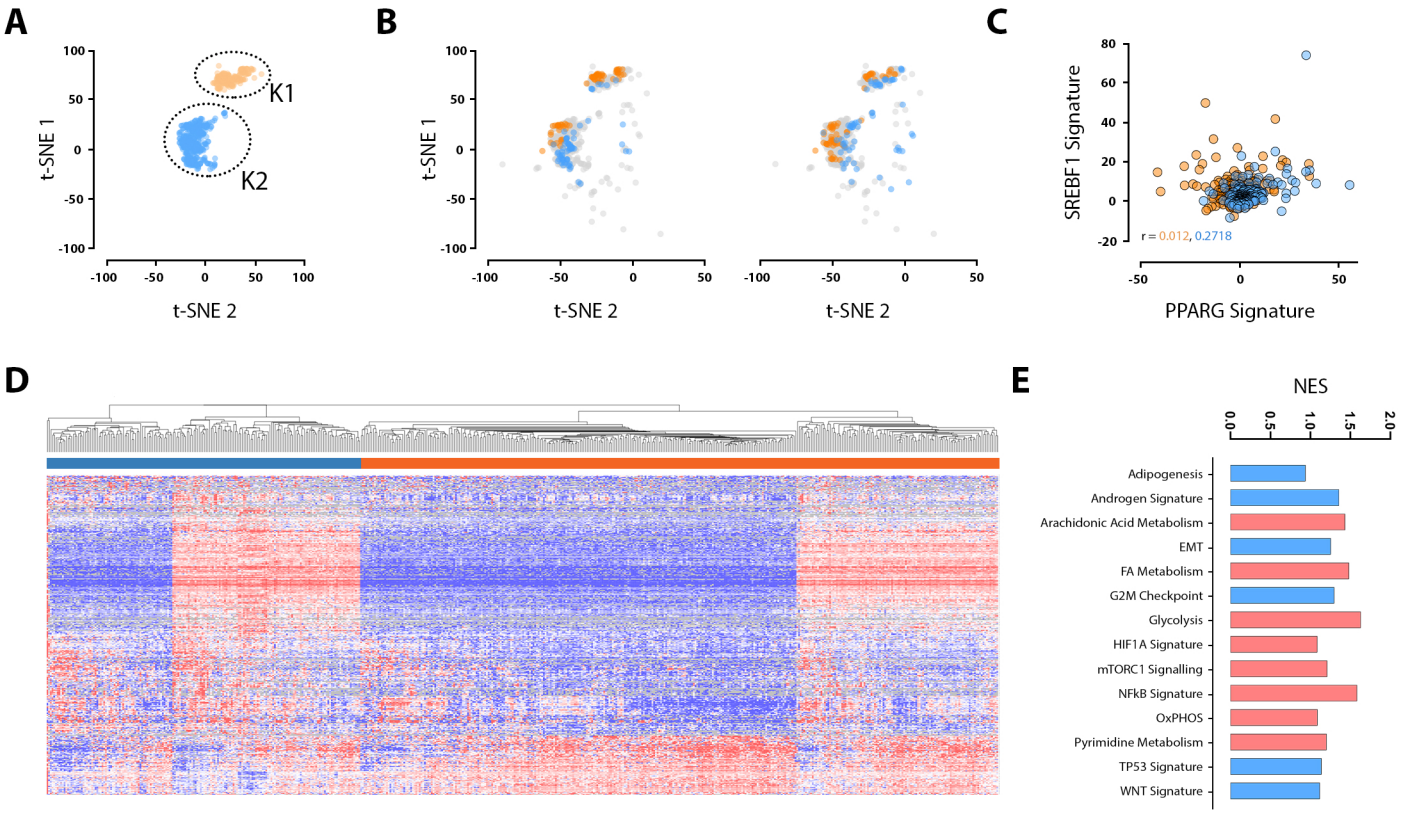

Figure 3.6. SREBF1 and PPARγ are differentially regulated in HIF1A active colorectal tumours. A. t-SNE analysis of human colorectal tumour clusters based on 50 metabolic pathway signatures showing the existences of two distinct tumour metabolic cluster types. High HIF1A signature shown in orange and Low HIF1A signature shown in blue **B.** same as A but colour according to SREBF1 signature scores. Up/ downregulated SREBF1 signatures are based on the 10th and 90th percentile groups (left panel), and same but for PPARG signature scores (right panel). **C.** x, y plot of PPARG signature scores plotted against SREBF1 signature scores across the two colorectal metabolic clusters and their corresponding Pearson's correlation coefficient value. **D.** Heat map representation of the top 500 differential expression genes in the two distinct colorectal tumour subtypes. **E.** GSEA analysis performed using KEGG and Hallmarks datasets using differential expression analysis from panel D. All differential expression analysis was performed using the DeSeq2 algorithm and data analysis was performed using Matlab 2019a. Raw RNAseq read counts for human colorectal tumours were downloaded from the TCGA data portal (See materials and methods).

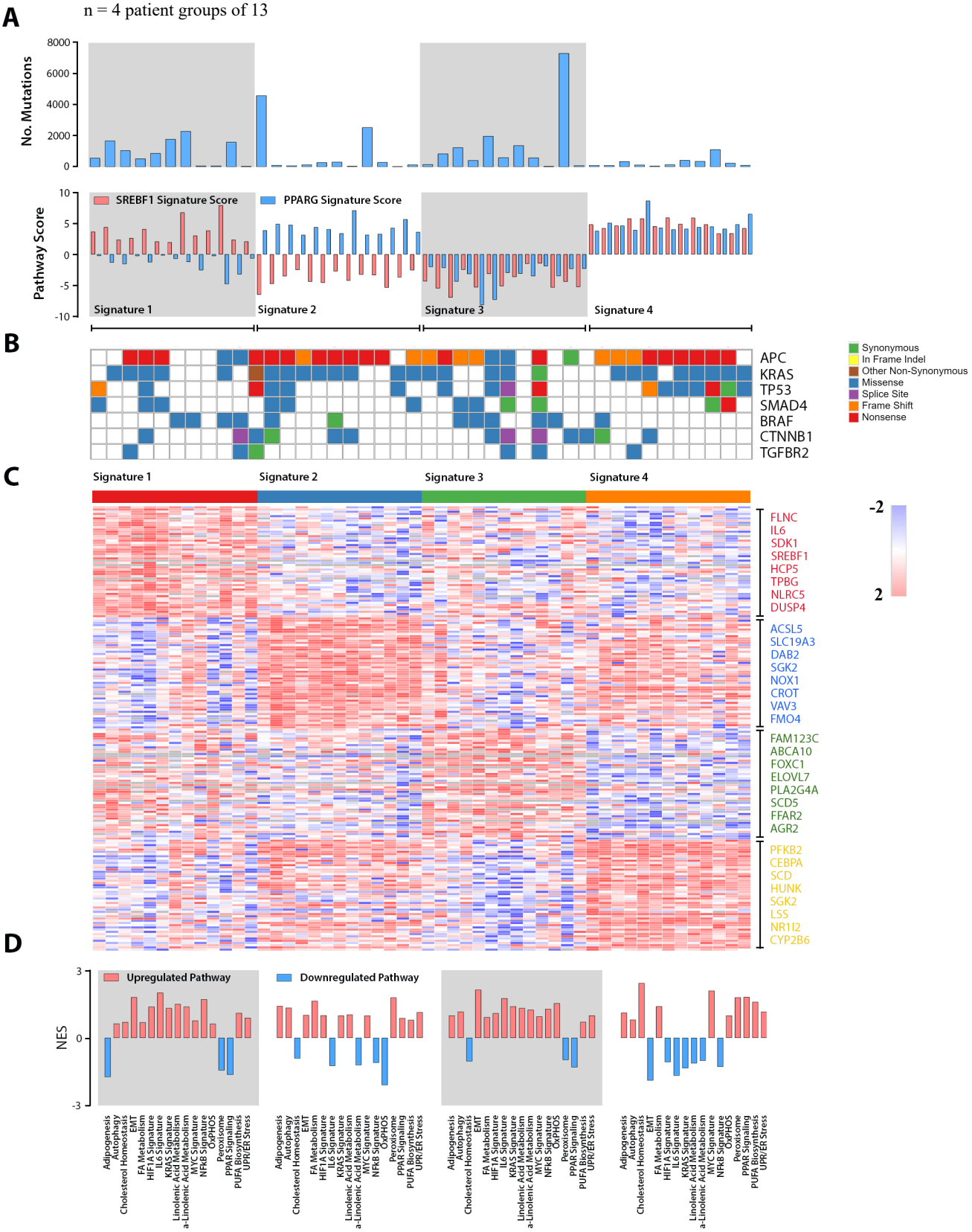

Figure 3.7. Pathway analysis of PPARγ and SREBF1 associated tumour phenotypes in colorectal cancer. A. Average mutation frequency calculated in each of the patient samples defined by PPARG and SREBF1 signature scores **(Top panel)**. and PPARG and SREBF1 signature scores of each of the four identified clusters **(Bottom panel)**. **B.** Mutation analysis of commonly mutated genes involved with colorectal cancer progression. **C.** Heatmap representation of the top 50 upregulated genes associated with each of the four clusters derived from PPARG and SREBF signatures. **D.** GSEA analysis of each of the four identified clusters looking at 18 different oncogenic associated pathways using RNAseq data from 52 colorectal cancer patients and grouped into 4 signatures defined by PPARG and SREBF1 signature scores. All differential expression analysis was performed using the DeSeq2 algorithm and data analysis was performed using Matlab 2019a. Raw RNAseq read counts for colorectal tumours were obtained from the TCGA dataportal.

with high SREBF1 signatures but low PPARγ signatures, showed downregulation of peroxisomal genes in addition to PPAR signalling and adipogenesis associated genes, while the highest upregulated pathways were EMT, IL6 & NFkB signalling. Class 3, the second cluster associated with low PPARγ signalling, showed similar results with downregulation of PPAR signalling and peroxisomal associated pathways while cholesterol homeostasis was downregulated in class 3 but upregulated in class 1 which was expected given the loss of the SREBF1 signature in class 3. EMT and IL6 signalling associated pathways were again among the most upregulated pathways. Class 2 and 4, that were associated with low SREBF1 signatures and were somewhat more divergent. High PPARγ signatures and low SREBF1 signatures were associated with low cholesterol homeostasis, oxidative phosphorylation and immune associated signalling pathways, while increased levels of peroxisomal associated pathways and FA metabolism were among the most upregulated pathways. Class 4, associated with upregulation of both PPARγ and SREBF1, again was associated with immune associated signalling pathways in addition to well characterised SREBF1 targets including SCD1, while low levels of HIF1A signalling was also observed, while interestingly cholesterol homeostasis and c-MYC targets were observed to be the most upregulated pathways **(Fig. 3.7C & D)**.

As discussed previously, one of the major oncogenic mutations associated with a low PPARγ signature was oncogenic BRAF mutations. BRAF missense mutations were associated with both class 1 and 3 that were both associated with low PPARγ signatures **(Fig. 3.7B)**. To further investigate this finding, without the limitations and interference of SREBF1 signatures scores, looking at the top and bottom 50 patient samples based on PPARγ signature score I investigated the simple average mutation frequency in colorectal tumours **(3.8A, top panel)**. PPARγ high signatures was associated with an overall lower mutation load while the opposite was true for the PPARγ low signature tumours. Interestingly, this frequency was not observed in the most commonly mutated genes in colorectal cancers. While this did confirm that low PPARγ signatures were associated with high frequencies of oncogenic BRAF mutations, this also coincided with decreased APC truncation mutations but increased frame shift mutations **(Fig. 3.8A, bottom panel)**. Finally, I classified the metabolic pathways associated with the most commonly mutated oncogenes associated with colorectal tumorigenesis. Analysis of the manually curated metabolic associated

genesets (characterised earlier in this chapter) was calculated on the average genesets score while patient samples were distributed according to genes associated with oncogenic mutations. BRAF mutants were classified as either oncogenic $BRAF^{V600E}$ mutants or uncharacterised BRAF mutants and I also looked at the pathway enrichment in BRAF wild type tumours. APC mutants were either characterised by truncation or wild type and CTNNB1 were either S33, S37, T41 or S45X mutants corresponding to proteasomal resistant oncogenic CTNNB1 mutations. KRAS was defined either as G12X or wild type while SMAD4 and PIK3CA were defined as either wild type or missense mutants. Spearman ranked hierarchical clustering was performed on the 8 different mutation signatures and 50 metabolically associate gene sets. CTNNB1, KRAS, SMAD4 and PIK3CA showed a largely similar metabolic phenotype with decreased AMPK DAO and associated PL biosynthesis pathways while showed increase PPAR signatures and associated peroxisomal FAO and unsaturated FA biosynthesis. $BRAF^{V600E}$ tumours were largely metabolically divergent to other tumour subtypes. Importanately, PPAR associated signatures were downregulated while this also correlated with decreased TAG biosynthesis and was also associated with increased AMPK FAO, PL metabolism and autophagy associated pathways **(Fig. 3.8B)**.

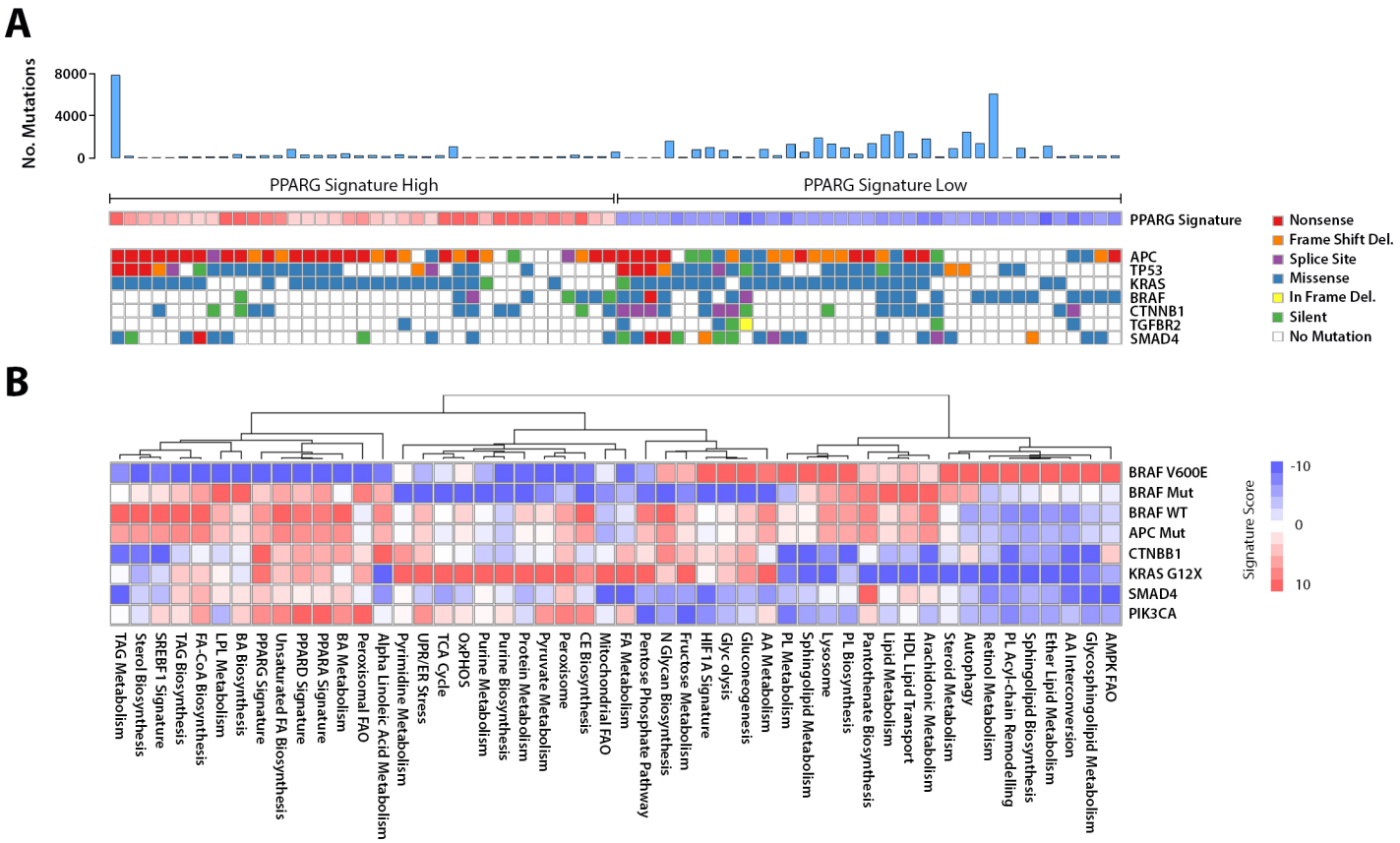

Figure 3.8. A Low PPARG signature is associated with oncogenic BRAF mutilations in colorectal cancer. A. Mutational frequency in the 10th and 90th percentile of patient samples associated with the PPARG signature (top panel). Mutation analysis of the same tumour samples based on PPARG signature (bottom panel). **B.** Heatmap representation of 50 manually curated metabolic associated pathway scores across patient samples associated with the most commonly mutated genes associated with colorectal cancer. All differential expression analysis was performed using the DeSeq2 algorithm and data analysis was performed using Matlab 2019a. Raw RNAseq read counts for 18 human tumour subtypes were downloaded from the TCGA data portal (See materials and methods).

3.5 Discussion

This Chapter has presented a systematic approach towards data normalisation and the identification of dysregulated metabolic and signalling pathways utilising complex and large-scale clinical tumour datasets from the TCGA and DepMAP patient tumour databases. Analysis of 18 human tumour subtypes revealed two major forms of cancers. Epithelial derived tumours metabolically were relatively similar while analysis of kidney, pancreatic and liver tumours were shown to be metabolically distinct. Metabolic associated transcriptome changes have been analysed and found to be strongly associated with tumour progression. Analysis of 22 human tumour types showed frequent upregulation of pathways that included glycolysis and nucleotide biosynthesis, while changes associated with the OxPHOS pathway was more tumour specific. Furthermore, reports were also made showing the importance of overexpression of glycolytic enzymes were able to mimic the effects of metabolic mutations such IDH1/2 [247]. Other groups have described the importance of changes in metabolic pathways such as downregulation of OxPHOS and its association with metastatic disease [246]. This was in line with observations I made regarding associations between HIF1A signalling and closely associated glycolysis pathways. Identified differences in colorectal metabolism revealed two major metabolic subtypes of colorectal cancer based on HIF1A activity and glycolysis. In addition, co-expression analysis associated with metastatic tumour samples showed consistent dysregulation of known HNF4A target genes in clear cell kidney tumours while further analysis across other tumour types showed this process to be importance in regulation of mitochondrial dysfunction in advance tumour progression [258]. Other groups back up claims with varied biological responses shown to be responsible, including epigenetic changes in alcohol dehydrogenases [259]. Mass spectrometry approaches in targeting tumour metabolism looking matched normal and tumour samples from 8 tissues of origin have also showed gross metabolic alterations in tumour tissue. Breast cancer samples were shown to upregulate almost all metabolites investigates while several lipid species were also shown to be high upregulated across multi tumour types including breast, bladder and prostate [260]. Furthermore, mass spec analysis of

2181 metabolites in 54 human cancer cell lines looking at transcriptional responses associated with transcription factor activity profiles based on transcriptomic readouts revealed a highly interconnect transcriptomics and transcriptional associations with metabolic readouts [255]. One of the key findings in this chapter was the identification of two distinct metabolic colorectal tumour subtypes. The major discerning factor associated with these two colorectal tumour subtypes was the level of HIF1A activity. Other groups have shown a close association of HIF1A with metabolic pathways including glycolysis [396]. Recent research outlined the importance of HIF1A in regulation of glycolysis driven migration while also outlined an important role in OxPHOS associated immunosuppressive functions in glioblastomas [261]. Similar observations regarding HIF1A mediated control of glycolytic processes have been observed in several other tumour types including cutaneous squamous cell carcinoma, pancreatic, invasive breast and hepatocellular carcinomas [262-264]. Other groups have also recently associated HIF1A in tumour metabolism regarding the Warburg effect [265]. One of the major dysregulated pathways associated with human tumours are aberrant changes in lipid metabolism. Recent dissection of 32 human cancer subtypes showed the significance of lipid metabolism in tumorigenesis. Lipid metabolism was shown to be the top dysregulated associated pathway across many of the 32 human tumour types. Interestingly, this correlates with glycolysis associated processing and amino acid metabolism. Tumours with perturbations associated with metabolic genes were also shown to be associated with tumour aggressiveness [266]. One of the key changes among the HIF1A associated colorectal cancer subgroup was changes in lipid transcriptional regulatory networks. PPARγ, largely considered tumour suppressive in colorectal cancers was largely shown to be inactive in this metabolic cluster. A second major player in transcriptional regulation of cellular lipid metabolism, SREBF1, was shown to oppose this notion where high SREBF1 tumour cells were largely associated with a HIF1A driven tumour metabolic phenotype. Pathway cross talk associated with HIF1A and PPARγ are well characterised in the context of cellular metabolism in normal tissues and with immune responses. However, this is poorly characterised in the context of tumour metabolism. The PPARγ/HIF1A axis has been described as a key regulator of glycolysis and lipid anabolism in a largely cooperative manner leading to increase lipid uptake and generation of glycerolipids [267]. Furthermore, PPARγ has been demonstrated to be a key hypoxia-associated HIF1A target gene in

HepG2 cells [268]. Conversely, HIF1A has also been shown to negatively regulate PPARγ activity in adipogenesis, inhibiting PPARγ activity in response to hypoxic conditions [269]. SREBF1 has also shown to work in synergy with HIF1A. Both SREBF1 transcriptional regulation of lipogenesis and HIF1A activity has been shown to act downstream of active mTOR [270]. While upregulation of FASN, a well characterised SREBF1 target gene, in response to AKT-mediated activation of SREBF1, has also be observed to be dependent on hypoxic conditions in mouse xenograft tumour models and in human mesenchymal stem cells [271, 272]. Conversely, opposing responses to HIF1A signalling have been observed in alcoholic fatty liver disease models where HIF1A induced activity led to suppression of excessive lipid accumulation. SREBF1 and subsequent target genes were shown to negatively correlate with HIF1A activity [273]. The interplay between SREBF1 and PPARγ is also convoluted and relatively poorly characterised. SREBF1 mediated lipogenesis has been shown to be a key process involved in PPARγ stimulation and adipogenesis [153]. While both PPARα and PPARγ have been shown to inhibition SREBF1 promoter activity induced by LXR [274]. Similar observations were shown in rat hepatoma cells with activation of PPARα and PPARγ leading to reduced TAG biosynthesis through reduction of nuclear mSREBF1 [154]. Associations between low and high PPARγ signature tumours reveals that PPARγ low tumours were associated with increased immunogenic associated signalling such as the pro-oncogenic IL6 responses. Furthermore, low PPARγ signatures were associated with poorly differentiated tumours and particularly with $BRAF^{V600E}$ tumours. PPARγ is a known phosphorylation target of MEK/ERK1 leading to PPARγ mediated proteasomal degradation [275]. Both ERK1/MEK1 are downstream of BRAF and are associated clinically with BRAF mutant tumours [276]. Conversely, SREBF1 has been shown to be important in therapy resistant $BRAF^{V600E}$ melanomas leading to sustained lipogenesis and PUPL mediated Vemurafenib resistance [156]. Furthermore, inhibition of SCD1 has been shown to reduce cancer stem cell associated therapeutic resistance in oncogenic driven BRAF melanomas [277]. This is interesting given that SCD1 is a well characterised target gene of SREBF1. Furthermore, I showed that SCD1 was one of the most significant upregulated genes associated with both high PPARγ and high SREBF1 transcriptional activity in colorectal cancer. In addition, HMGCA1 and HMGCL again both well characterised target gene of SREBF1 has also been shown to have genetic

dependencies in $BRAF^{V600E}$ tumours [278, 279]. Oncogenic BRAF inhibition has also been shown to increase OxPHOS gene expression and mitochondrial biogenesis mediated through MITF regulation of PPARGC1A [280]. I also looked at the general overview of common mutation associated with colorectal cancers including APC, CTNNB1, KRAS and BRAF. Colorectal cancers were largely metabolically associated with one another. Overall pathway regulation clustered consistently with one another except for BRAF mutant tumours. They formed a metabolically distinct tumour that was opposed to other colorectal tumours. Loss of PPARγ signalling was further associated with upregulation of several lipid metabolic pathways including PL and ether linked phospholipid metabolism, glycolysis, Autophagy and AMPK mediated FAO. This was opposed to other lipid associated metabolic pathways including peroxisomal machinery and peroxisomal FAO. While as discussed above, there is significant evidence to suggest that oncogenic BRAF is a key regulator of cellular energetic process it is limited. Further research is required to investigate the association between dysregulation of key lipogenic pathway signatures and the apparent loss of a PAPRG signature which has been associated with poor clinical outcomes across many colorectal cancer patient datasets [152].

Chapter 4 - PPARγ-dependent lipid reprogramming by peroxisomal lipids in $BRAF^{V600E}$ colon tumours

4.1 Introduction

One of the major findings from Chapter 3 was the association with a loss of PPARγ signatures in human tumours containing oncogenic BRAF mutations. PPARγ signalling in many tumour subtypes is complex and a clear consensus on the role of PPARγ in tumorigenesis is still unclear. Investigation in the use of PPARγ agonists as potential cancer therapeutics has been extensively studied despite the controversial and contradicting research. Furthermore, given the roles that PPARγ plays as a regulator of differentiation, proliferation and apoptosis in addition to the vast roles PPARγ plays in the regulation of lipid metabolism I looked to further investigate the roles of PPARγ in colorectal cancer tumour metabolic reprogramming. Furthermore, I looked to validate the findings from chapter 3 and further investigate the roles that oncogenic BRAF mutations might play in downregulation of PPARγ signalling pathways and the consequences associated with loss of PPARγ signatures.

Oncogenic RAS mutations account for approximately 30-40% of colorectal tumours. Downstream to RAS kinases is the RAF kinase superfamily [281, 282]. More commonly mutated in thyroid and melanomas they account for approximately 10-15% of colorectal cancers and often represent a particularly fast growing and aggressive tumour [18]. Recent advances in BRAF targeted therapy has led to significant increases in patient survival rates. However, like many tumours drug resistance has become a challenging obstacle and can render high effective and specific target therapeutics ineffective. The roles of BRAF in tumour metabolic reprogramming have primarily focused on oxidative phosphorylation and glycolysis, however recent research has shown that gross lipogenic changes are associated with progressive disease in chemotherapy resistant tumours [156, 280, 283]. Interestingly, little research is available looking at metabolic alterations to lipogenic pathways despite known links between PPAR signalling and downstream MAPK cascades. PPARγ is a known target of ERK1/MEK and is directly downstream of BRAF and indeed all RAF kinases. Furthermore, direct phosphorylation of PPARγ by ERK1/MEK has been shown to inhibit PPARγ transcriptional activity and drive proteasomal degradation [105, 269, 275]. While PPARγ is thought to be an important negative regulator of β-catenin and PPARδ mediated stemness in the intestinal crypt and thus is thought to drive terminal

differentiation and intestinal epithelial turn-over [150, 284, 285]. Mutations in the PPARγ gene are rare, however loss of PPARγ mRNA/protein expression is a common alteration in human tumours while PPARγ expression is associated with poor clinical outcome many tumour types including colorectal cancer. Many groups have associated these alterations of PPARγ expression to epigenetic changes but little research has focused on the oncogenic mutations that drive loss of PPARγ expression [286, 287]. In this chapter I have investigated the effects of oncogenic BRAF mutations and $BRAF^{V600E}$ targeted therapy through the use of the mutant specific BRAF inhibitor Vemurafenib (Vem) on PPARγ signaling. Furthermore, given the known roles of PPARγ in lipid regulation, I investigated the effects of PPARγ activation through use of the PPARγ agonist, Rosiglitazone and compared this the lipidomic readout associated with BRAF inhibition. Both BRAF targeted therapy and PPARγ agonists showed similar whole-cell lipidomic readouts. Furthermore, downregulation of peroxisomal phospholipid (PPL) biosynthetic pathways was identified as a key change in $BRAF^{V600E}$ mutant cells. The PPL biosynthesis pathway was shown to be a key regulator of unsaturated phospholipid biosynthesis and targeting the PPL biosynthesis pathway was shown to be a useful cell model mimicking oncogenic BRAF alteration in lipogenic pathways. In addition, the roles that loss of PPL biosynthesis played in $BRAF^{V600E}$ driven metabolic reprogramming was more that superficial. Identification of a complex multimeric signaling axis involving sustained SREBF1 transcriptional activity. Loss of polyunsaturated PL species through CRISPR/Caas9 PPL knockout models targeting the terminal enzyme, DHRS7B was shown to be required for effective AMPK pro-autophagy signaling in response to Rosiglitazone and serum starvation. Downregulation of PPL biosynthesis pathway drives sustained SREBF1 activity through loss of AMPK signaling which is a known negative regulator of SREBF1 transcriptional activity leading to uncontrolled hyperlipidemic phenotype driven by $BRAF^{V600E}$ oncogenic mutations [173].

4.2. $BRAF^{V600E}$ driven tumours display lipogenic reprogramming through suppression of PPARγ signalling networks

To investigate the role that PPARγ dysregulation plays in colorectal cancers we used a custom TCGA-COADREAD dataset looking at the mRNA expression levels of 4034 potentially PPARγ regulated target genes identified by high throughput ChIPseq analysis (CHEA). K-means clustering was used to identify genetic signatures across a cohort of 601 tumour and 51 normal mucosa tissue samples. We identified 5 subgroups based on PPARγ target genes expression analysis while one cluster corresponded to normal colon mucosa samples while a further four clusters were associated with tumour samples **(Fig. 4.1A & B)**. Mutational analysis across the four tumour related subgroups showed high levels of TP53 mutations associated with subgroup 1 and 4 while subgroup 2 was shown to be associated BRAF mutations **(Fig. 4.1A)**. Survival analysis of tumours expressing high verse low PPARγ mRNA levels showed that low PPARγ expression was associated with a poor prognosis, while analysis of patient survival rate clustering patterns, identified by K-means clustering, showed that clusters 1 and 2 were associated with poor survival rates compared to clusters 3 and 4 **(Fig. 4.1C & D)**. Furthermore, looking at PPARγ mRNA expression levels across the four subgroups compared to normal mucosa controls showed that PPARγ was significantly downregulated in cluster 2 ($BRAF^{Mut}$ cluster) compared to other subgroups and normal mucosa, while this expression pattern was identical when assessing $BRAF^{V600E}$ verse $BRAF^{WT}$ tumours and validated previous associations made looking at PPARγ predicted genetic signatures in colorectal tumours **(Fig. 4.1E & F)**. Furthermore, well characterized PPARγ target genes LPL, HMGCS2, ACSL5, PCK1 and CEBPA were all significantly downregulated in $BRAF^{V600E}$ tumours **(Fig. 4.1F)**.

To further investigate the association of PPARγ expression in $BRAF^{V600E}$ tumours I assessed colorectal cancer cells that were either wild type for BRAF or heterozygous for the $BRAF^{V600E}$ mutation. Cells were assessed for cytotoxicity in response to the PPARγ agonist Rosiglitazone. $BRAF^{V600E}$ tumours cells were found to be ten-fold more resistant compared to $BRAF^{WT}$ cells to Rosiglitazone mediated cellular cytotoxicity **(Fig. 4.2A)**. Co-treatment of $BRAF^{V600E}$ mutants with 0.5 μM Vemurafenib and

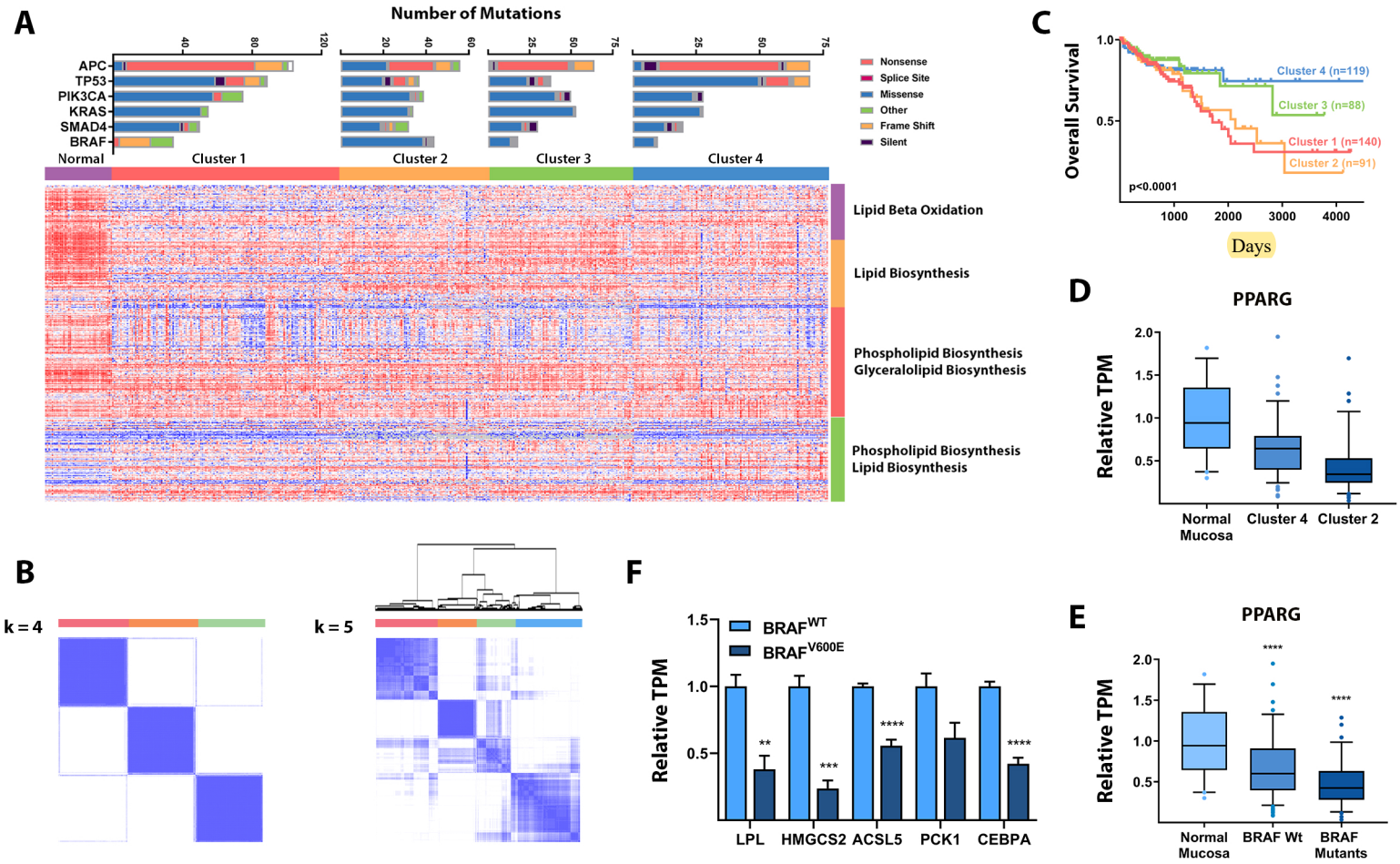

Figure 4.1. BRAFV600E mutation downregulates PPARGγ RNA and transcriptional networks. A. Heatmap representation of TCGA-COADREAD RNAseq data of CHIPseq identified PPARγ target genes associated with lipid metabolism clustered base on supervised K means clustering. **B.** Similarity matrix of K means clustering. **C.** Kaplan meier survival curve of patients based on K means supervised clustering. **D.** PPARγ mRNA expression levels in transcripts per million (TPM) across K means supervised clustering compared to normal mucosa adjacent controls. **E.** PPARγ mRNA expression levels across normal mucosa controls compared to BRAFMut and BRAFWt tumour samples. **F.** Expression of well characterized PPARγ transcriptional target genes in BRAFWt and BRAFV600E tumour samples. All experiments were performed at n=3 regardless if biological replicates were used. All error bars represent S.E.M and two tailed students t-test was used to test for statistical significance (*p < 0.05, **p < 0.01, ***p < 0.001 & ****p< 0.0001). K means were validated looking at iteration stabilization and validation of centroids and distance to centroids. All analysis was performed using Matlab 2019b.

increasing concentrations of Rosiglitazone led to a ten-fold increase in Rosiglitazone sensitivity returning to levels comparable to $BRAF^{WT}$ cells **(Fig. 4.2B)**. Luciferase based real time cell growth monitoring showed that $BRAF^{WT}$ cells were significantly more sensitive to Rosiglitazone mediated cellular growth arrest compared to $BRAF^{V600E}$ tumour cells which showed only a small but non-significant change in cell growth **(Fig. 4.2C)**. Furthermore, I also performed the assay as per previous discussed co-treating LIM2405 $BRAF^{V600E}$ colorectal tumour cells with Rosiglitazone in conjunction with 0.5µM of Vemurafenib. Again, Rosiglitazone showed little response across all four time points in $BRAF^{V600E}$ tumours cells with non-significant small decreases in cell growth while $BRAF^{WT}$ cells showed approximately 2 fold decrease in cell growth. Vemurafenib alone showed a one-fold reduction in cell growth in $BRAF^{V600E}$ cells while co-treatment with Rosiglitazone showed a ten-fold decrease in cell growth in $BRAF^{V600E}$ colorectal cancer cells **(Fig. 4.2D).** To further address the association of Rosiglitazone on cell proliferation and growth I performed a similar experiment using BrdU incorporation. The changes observed in cellular growth were shown to be cell proliferation dependent. $BRAF^{WT}$ tumour cells showed an approximated ~2-fold decrease in cellular proliferation. $BRAF^{WT}$ cells were unresponsive to Vemurafenib with no significant change in proliferation with Vemurafenib alone while co-treatment groups showed no change compared to Rosiglitazone alone. $BRAF^{V600E}$ tumour cells showed the exact opposite in single treatment groups with little response to Rosiglitazone alone, an approximately 2-fold decrease in cellular proliferation with Vemurafenib alone and an approximately 2-fold further decrease to cellular proliferation when treated with both Rosiglitazone and Vemurafenib **(Fig. 4.2E).** We further investigated cell growth signals and stress mediated pathways associated with apoptosis in response to Rosiglitazone, Vemurafenib or co-treatment of cells. Phospho-ERK/MEK was used as a marker for BRAF activity and was shown to be significantly decreased in $BRAF^{V600E}$ mutants but not $BRAF^{WT}$ cells in response to Vemurafenib treatment. Co-treatment of Rosiglitazone and Vemurafenib in $BRAF^{V600E}$ cells showed an increase in phosphorylation in stress activated MAPK p38 pathway and downstream targets MAPKAPK2 and JNK correlating with the late stage apoptosis marker, cleaved PARP in comparison to Rosiglitazone and Vemurafenib treatments on their own **(Fig. 4.2F)**. PPARγ transcriptional activity was measured using a luciferase reporter under the control of a consensus PPRE promoter. $BRAF^{V600E}$ RKO and

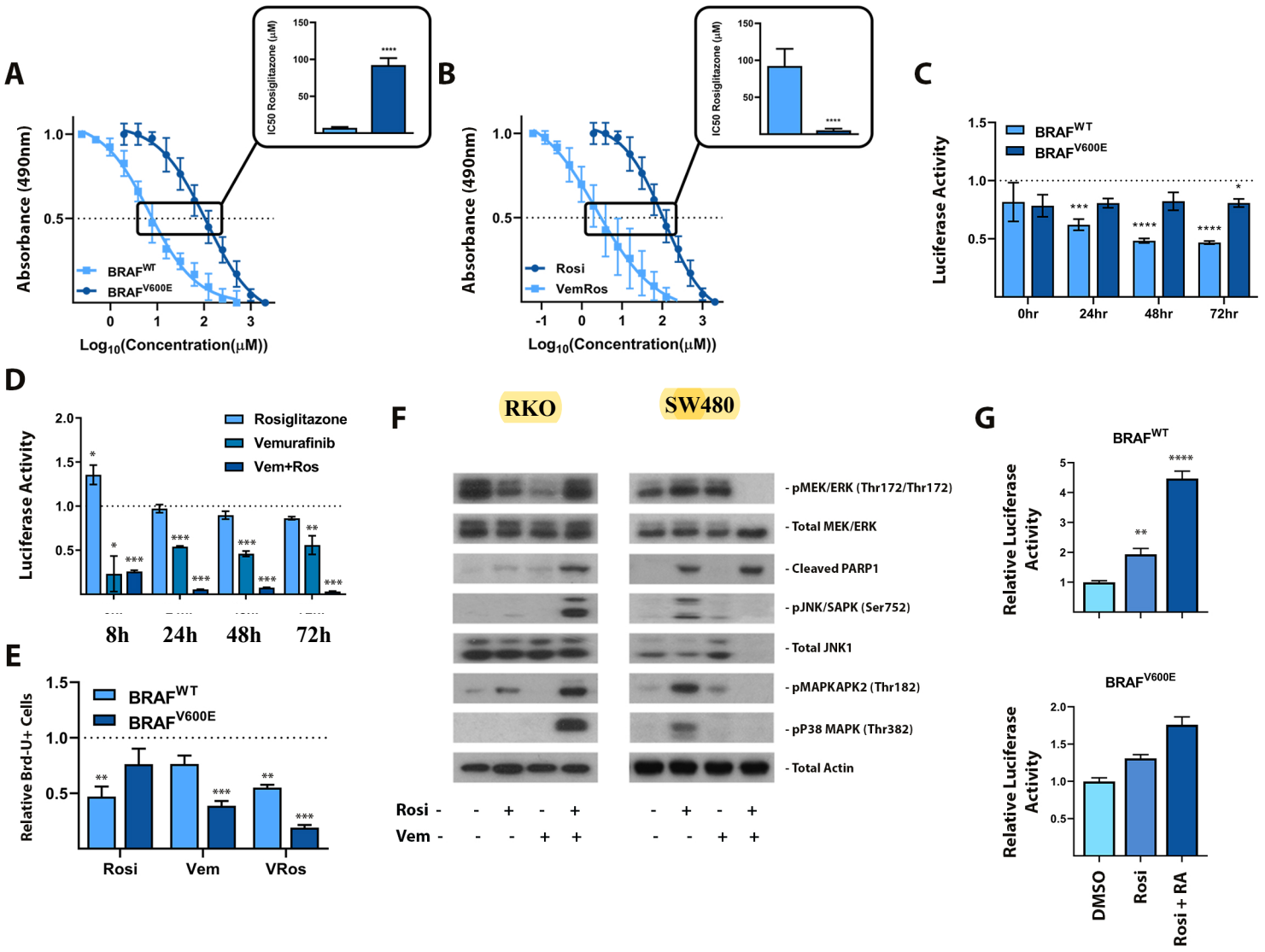

Figure 4.2. BRAFV600E mutants are resistant to Rosiglitazone mediated cellular cytotoxicity. A. IC50 determination of 3 BRAFWT (LIM1215, SW620 & SW480) and 3 BRAFV600E (RKO, LIM2405 & HT-29) cell cytotoxicity in response to Rosiglitazone. **B.** IC50 determination of BRAFWT and BRAFV600E cells in response to Rosiglitazone in the presence of 0.5μM of Vemurafenib measured 48hrs post treatment. **C.** Luciferase based proliferation/viability assay of BRAFWT and BRAFV600E cells in response to Rosiglitazone alone or **D**. BRAFV600E (RKO,LIM2405 & HT-29) in the presence of 0.5μM of Vemurafenib. **E.** BrdU incorporation assay of BRAFWT and BRAFV600E cells in response to either Rosiglitazone or Vemurafenib alone, or treated with both Rosiglitazone and Vemurafenib. **F.** Western blot analysis of key cell stress and apoptotic markers in response to either Rosiglitazone or Vemurafenib alone, or Rosiglitazone and Vemurafenib, 48hrs post treatment. **G.** PPRE-luc X4 reporter assay of BRAFWT and BRAFV600E cells treated with either DMSO, Rosiglitazone or Rosiglitazone and Retinoic acid. All experiments were performed as n=3 regardless if biological replicates were used or not. Vemurafenib treatments were performed at 0.5uM while all other treatments were performed at 5uM unless otherwise stated. All error bars represent S.E.M and two tailed students t-test was used to test for statistical significance except for D, E & G where a oneway ANOVA was performed (*p < 0.05, **p < 0.01, ***p < 0.001 & ****p< 0.0001). Each experiment was repeated 3 times and averages were taken of each replicate .

$BRAF^{WT}$ LIM1215 cells were transduced with a lentivirus containing a PPRE-eGFP-Luciferase reporter construct. The cells were selected for 96hours with puromycin, while the remaining stable cells were counted and transferred into luminescent tissue culture plates at ~20, 000 cells per well. Treatment with either DMSO, Rosiglitazone alone or in conjunction with retinoic acid (RA) was shown to induce a strong transcriptional response in $BRAF^{WT}$ LIM1215 cells **(Fig. 4.2G, top panel).** While RKO $BRAF^{V600E}$ cell showed no significant induction of PPARγ transcriptional activity in response to either Rosiglitazone alone or co-treated with both Rosiglitazone and RA **(Fig. 4.2G, bottom panel)**.

4.3. $BRAF^{V600E}$ drives a hyperlipidemic phenotype through suppression of PPARγ

Given the roles of PPARγ in lipid metabolism I was interested to investigate the alterations in lipid metabolic pathways in $BRAF^{V600E}$ driven cancers. Untargeted high throughput lipidomic/mass spectrometry approach was used to analyse the lipidomic profile of lipids across 22 lipid classes. $BRAF^{V600E}$ colorectal tumour cells were shown to have increased levels of almost all major lipid storage forms except for TAG's which remained unchanged and ether linked PL's which were downregulated. **(Fig. 4.3A & F)**. Analysis of lipid partitioning and storage through immunofluorescent analysis of lipid bodies showed a similar result with $BRAF^{V600E}$ cell lines having an increase in total lipid droplet levels measure per cell while this was negatively correlated with PPARγ mRNA expression levels across six human colorectal cancer cell lines **(Fig. 4.3B & C)**. Total lipid levels showed a consistent change with an overall increased level of total lipids **(Fig. 4.3E)**. Changes in phospholipid composition in general followed this same trend with overall increases in most phospholipid classes except for ether-linked phospholipids (PLe) indicating potential changes in peroxisomal lipid metabolism **(Fig. 4.3D)**. Analysis of the profile of phospholipid levels when separated by number of unsaturation in fatty acid chains showed an interesting pattern. $BRAF^{WT}$ cells showed a lower average level of saturated and monounsaturated PL levels while the opposite was true for $BRAF^{V600E}$ mutant cells **(Fig. 4.3G)**. Furthermore, a similar pattern was observed for ether linked PL's with the number of unsaturation's

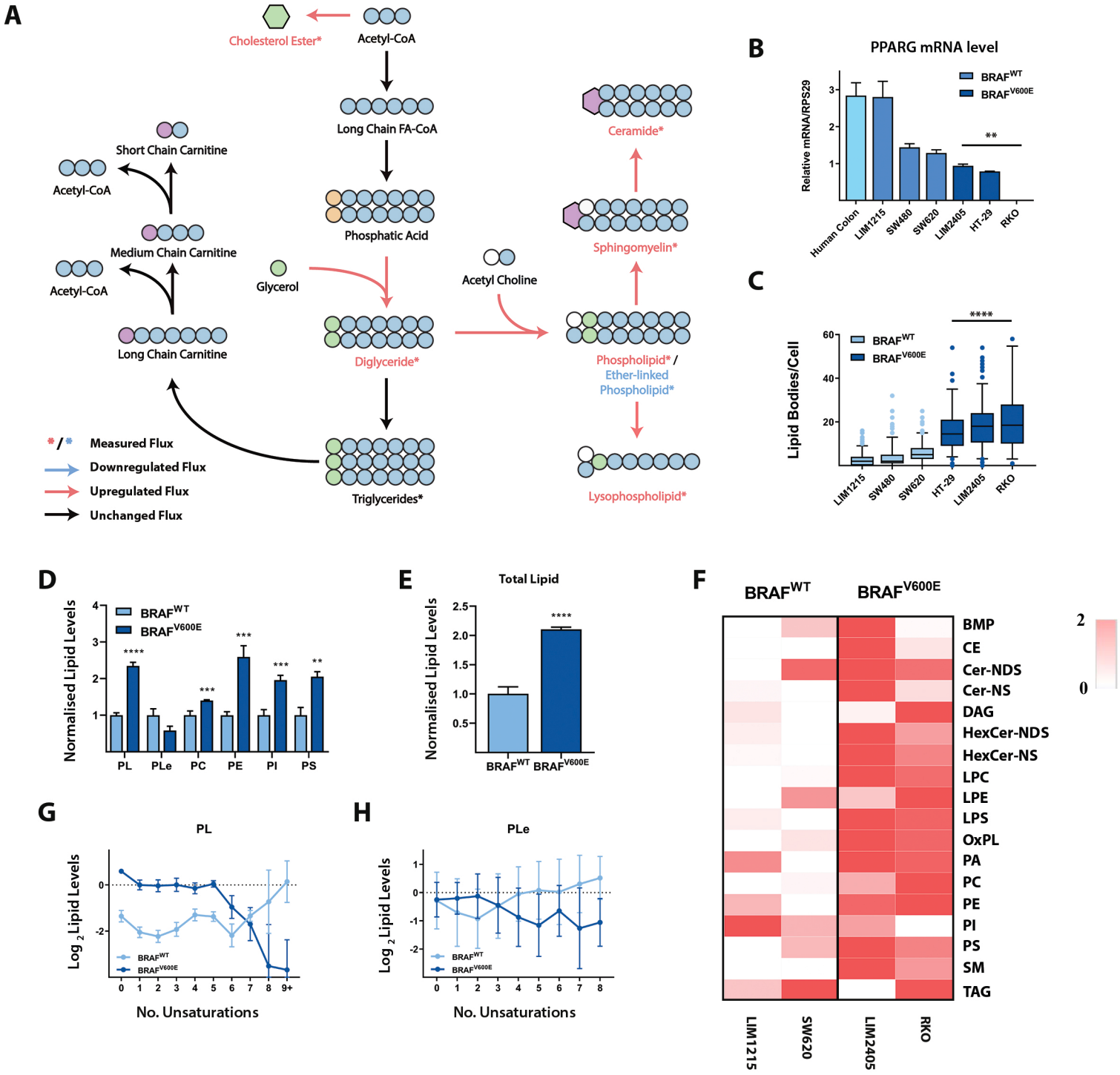

Figure 4.3. The BRAF V600E mutation drives a hyperlipidemic phenotype and is negatively correlated with PPARγ expression. A. Schematic representation of lipid species changes between BRAFV600E and BRAFWT cell lines; measured changes are represented with * and their direction of change is indicated by colors (Red, upregulated) and (Blue, Downregulated). **B.** PPARγ mRNA levels measured in 6 human colorectal cancer cell lines and normal colon mucosa by qPCR using RPS29 as a reference gene. **C.** Quantification of Nile Red positive vesicles per cell for 6 colorectal cancer cell lines. **D.** Relative lipid levels normalized to BRAFWT cells measuring total changes of phospholipid levels in cells dependent on their BRAF gene status measure by mass spectrometry. **E.** Mass spectrometry measurement of total lipid levels according to cells BRAF gene status **F.** heatmap representation of total lipid levels of 22 different lipid species in the four cell lines measured. **G.** Mass spectrometry measured average non-ether-linked phospholipid level separated by number of unsaturation's found in the phospholipid fatty acid chain. **H.** Mass spectrometry measured average ether-linked phospholipid level separated by number of unsaturation's found in the phospholipid fatty acid chain. All experiments were performed at n=3. Vemurafenib treatments were performed at 0.5uM while all other treatments were performed at 5uM unless otherwise stated. All error bars represent S.E.M, except for G & H where they represent SD and two tailed students t-test was used to test for statistical significance (*$p < 0.05$, **$p < 0.01$, ***$p < 0.001$ & ****$p < 0.0001$). For lipid droplet counts 300 individual cells were counted and the experiment was repeated 3 times and averages were taken of each replicate.

showing a positive slope with high levels of PUPL's and lower levels of SPL's or MUPL's in $BRAF^{WT}$ cells while the opposite help true in $BRAF^{V600E}$ colorectal cancer cells **(Fig. 4.3H)**. To investigate the effects of PPARγ chemical activation and $BRAF^{V600E}$ selective inhibition on intracellular lipid profiles untargeted high throughput mass spectrometry was used to measure the changes of total lipid levels for 22 individual lipid classes in response to either Rosiglitazone or Vemurafenib treatment for 24hours. Total lipid levels were unchanged in response to Rosiglitazone in both $BRAF^{WT}$ and $BRAF^{V600E}$ cells **(Fig. 4.4A).** Interestingly, analysis of lipid droplet levels showed a significant change in lipid partitioning despite no loss of total lipids. Rosiglitazone led to a decrease in total lipid droplet number in both $BRAF^{WT}$ and $BRAF^{V600E}$ cells, while inhibition of PPARγ with the antagonist, GW9669 showed the reverse effect, increasing total lipid droplet numbers per cell **(Fig. 4.4B)**. It is worth noting that in conjunction with the previous data regarding $BRAF^{V600E}$ induced resistance to Rosiglitazone, $BRAF^{V600E}$ cells showed significantly reduced responses to Rosiglitazone and GW9669 compared to $BRAF^{WT}$ cells. Changes in lipid droplet levels, but not total intracellular lipid levels, indicate there are changes in lipid mobilisation and metabolism rather than lipid degradation. Realtime qPCR analysis was used to look at several key lipogenic regulators involved with *de novo* lipid metabolism at various metabolic checkpoints. Expression changes resulting from both Vemurafenib and Rosiglitazone are coloured coded (Red for an increase in expression, blue for a decrease in expression and black indicating opposing changes in expression). Several genes were significantly changed in response to both Rosiglitazone and Vemurafenib including DGAT1, involved in TAG biosynthesis, while the TAG lipolysis enzyme LIPC was downregulated. Furthermore, upregulation of key enzymes involved in FA-CoA biosynthesis including FASN and GPAT were both upregulated, and increased expression levels of genes involved in beta-oxidation were also upregulated in response to both Vemurafenib and Rosiglitazone **(Fig. 4.4C & D).** Analysis of the major lipid storage forms by lipidomic mass spectrometry showed that both Rosiglitazone in $BRAF^{WT}$ cells and Vemurafenib in $BRAF^{V600E}$ cells had a significant effect on TAG biosynthesis and this confirmed the observed changes in key TAG biosynthesis enzyme levels in addition to enzymes involved in DAG metabolism **(Fig. 4.4E-G)**. The overall response to Rosiglitazone in $BRAF^{V600E}$ cells again showed a similar result however the increase in TAG levels was significantly attenuated **(Fig. 4.4h)**. The top

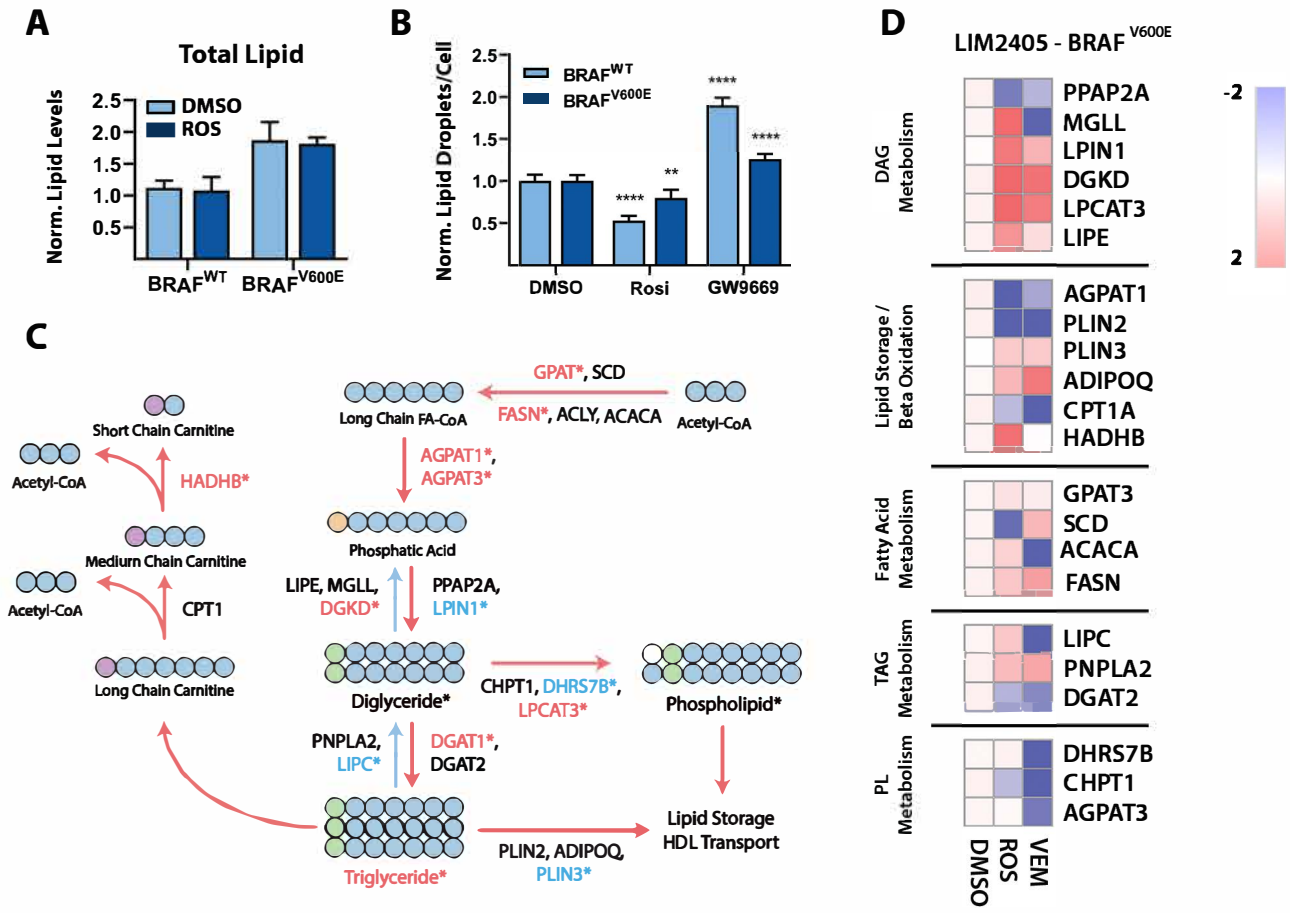
A
Total Lipid
Norm. Lipid Levels
DMSO
ROS
BRAFWT
BRAFV600E
B
Norm. Lipid Droplets/Cell
BRAFWT
BRAFV600E
DMSO
Rosi
GW9669
C
Short Chain Carnitine
Acetyl-CoA
HADHB*
Medium Chain Carnitine
CPT1
Long Chain Carnitine
Long Chain FA-CoA
GPAT*, SCD
FASN*, ACLY, ACACA
Acetyl-CoA
AGPAT1*, AGPAT3*
Phosphatic Acid
LIPE, MGLL, DGKD*
PPAP2A, LPIN1*
Diglyceride*
CHPT1, DHRS7B*, LPCAT3*
Phospholipid*
PNPLA2, LIPC*
DGAT1*, DGAT2
Triglyceride*
PLIN2, ADIPOQ, PLIN3*
Lipid Storage HDL Transport
D
LIM2405 - BRAFV600E
DAG Metabolism
PPAP2A
MGLL
LPIN1
DGKD
LPCAT3
LIPE
Lipid Storage / Beta Oxidation
AGPAT1
PLIN2
PLIN3
ADIPOQ
CPT1A
HADHB
Fatty Acid Metabolism
GPAT3
SCD
ACACA
FASN
TAG Metabolism
LIPC
PNPLA2
DGAT2
PL Metabolism
DHRS7B
CHPT1
AGPAT3
DMSO
ROS
VEM

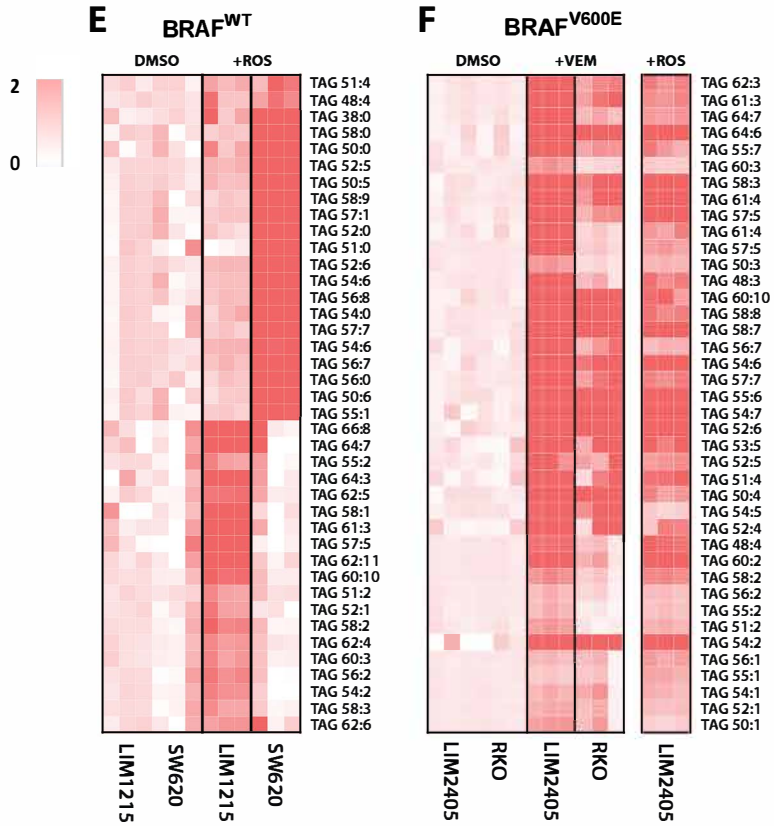
E
BRAFWT
DMSO
+ROS
TAG 51:4
TAG 48:4
TAG 38:0
TAG 58:0
TAG 50:0
TAG 52:5
TAG 50:5
TAG 58:9
TAG 57:1
TAG 52:0
TAG 51:0
TAG 52:6
TAG 54:6
TAG 56:8
TAG 54:0
TAG 57:7
TAG 54:6
TAG 56:7
TAG 56:0
TAG 50:6
TAG 55:1
TAG 66:8
TAG 64:7
TAG 55:2
TAG 64:3
TAG 62:5
TAG 58:1
TAG 61:3
TAG 57:5
TAG 62:11
TAG 60:10
TAG 51:2
TAG 52:1
TAG 58:2
TAG 62:4
TAG 60:3
TAG 56:2
TAG 54:2
TAG 58:3
TAG 62:6
LIM1215
SW620
LIM1215
SW620
F
BRAFV600E
DMSO
+VEM
+ROS
TAG 62:3
TAG 61:3
TAG 64:7
TAG 64:6
TAG 55:7
TAG 60:3
TAG 58:3
TAG 61:4
TAG 57:5
TAG 61:4
TAG 57:5
TAG 50:3
TAG 48:3
TAG 60:10
TAG 58:8
TAG 58:7
TAG 56:7
TAG 54:6
TAG 57:7
TAG 55:6
TAG 54:7
TAG 52:6
TAG 53:5
TAG 52:5
TAG 51:4
TAG 50:4
TAG 54:5
TAG 52:4
TAG 48:4
TAG 60:2
TAG 58:2
TAG 56:2
TAG 55:2
TAG 51:2
TAG 54:2
TAG 56:1
TAG 55:1
TAG 54:1
TAG 52:1
TAG 50:1
LIM2405
RKO
LIM2405
RKO
LIM2405
G
Normalised Lipid Levels
VEM
ROS
CE
DAG
TAG
PL
H
Normalised Lipid Levels
VEM
ROS
CE
DAG
TAG
PL

Figure 4.4: Vemurafenib inhibition of BRAF drives reactivation of PPARγ signalling converging on TAG metabolism. A. Total lipid levels measured through mass spectrometry of $BRAF^{WT}$ (SW620 & LIM1215) and $BRAF^{V600E}$ (LIM2405 & RKO) cell lines treated with either DMSO or Rosiglitazone. **B.** Quantification of Nile Red positive vesicles using 6 cell lines ($BRAF^{WT}$ (SW620, SW480 & LIM1215) and $BRAF^{V600E}$ (LIM2405, HT29 & RKO). separated according to their BRAF gene mutation status in response to either DMSO, Rosiglitazone or GW9669. Graphs are representative of group mean and SEM. **C.** Schematic representation of total lipid metabolic changes and the key regulatory enzymes involved in lipid metabolism between $BRAF^{V600E}$ treated cells with either Vemurafenib or Rosiglitazone compared to a DMSO control. Measured changes are represented with * and their direction of change is indicated by colours (Red, upregulated) and (Blue, Downregulated). **D.** Heatmap representation of qPCR analysis of LIM2405 cells treated with either DMSO, Rosiglitazone or Vemurafenib and measurement of key lipid regulatory enzyme genes involved in lipid metabolism at various stages. **E.** Mass spectrometry measurement of TAG's (as a heatmap) in response to Rosiglitazone in SW620 and LIM1215 $BRAF^{WT}$ cell lines, & **F.** RKO cells in response to Vemurafenib and LIM2405 $BRAF^{V600E}$ cells in response to either Rosiglitazone or Vemurafenib. **G.** Mass spectrometry measurement of average levels of major lipid storage forms in response to Rosiglitazone in $BRAF^{WT}$ cells and Vemurafenib in $BRAF^{V600E}$ cells. **H.** LIM2405 ($BRAF^{V600E}$) cells treated with either Rosiglitazone or Vemurafenib. All experiments were performed as n=3. Vemurafenib treatments were performed at 0.5uM while all other treatments were performed at 5uM unless otherwise stated. All error bars represent S.E.M and two tailed students t-test was used to test for statistical significance. For lipid droplet counts 300 individual cells were counted and the experiment was repeated 3 times and averages were taken of each replicate.

upregulated TAG lipid species are shown in a heatmap and both Rosiglitazone and Vemurafenib showed no specificity for unsaturation levels or fatty acid chain length **(Fig. 4.4E & F)**.

4.4. Downregulation of peroxisomal phospholipid metabolism drives $BRAF^{V600E}$ dependent lipid reprogramming

Increased levels of almost all major lipid classes were observed in the lipidomic profile of $BRAF^{V600E}$ driven tumours. with the exception of two major lipid classes, TAGs and ether-linked phospholipids. PPARγ has well established roles in TAG metabolism while the result shown in Section 4.3 validated this with the majority of lipidomic changes associated with Rosiglitazone treatments were shown to be TAG species while a significant level of overlap was seen in Vemurafenib treated cells to. A second major difference was downregulation of ether-linked phospholipid. Ether linked phospholipids are primarily produced through the PPL biosynthesis pathway or the DHAP pathway. The PPL biosynthesis pathway can be used to generate ether linked PL or can be sent through the ER for salvage to generate non-ether linked phospholipid **(Fig. 4.5C)** [288]. Furthermore, ether linked lipids have been shown to be a ligand for the PPAR family [289]. We therefore investigated peroxisomal PL pathways in $BRAF^{V600E}$ tumour cells. We first measured mRNA expression levels of various peroxisomal lipogenic pathways using RNAseq data of 6 $BRAF^{V600E}$, 12 $KRAS^{G12X}$ and 18 $BRAF^{WT}$ derived colorectal cell lines. Four major peroxisomal lipogenic pathways were investigated. Peroxisomal lipid metabolism and

the PPL biosynthesis pathways were both downregulated in $BRAF^{V600E}$ derived tumour while FA transport and oxidation remained unchanged **(Fig. 4.5A)**. To further validate this observation, I looked key enzymes involved in lipid metabolism in both $BRAF^{V600E}$ tumour cells compared to $BRAF^{WT}$ and further addressed this observation in the closely related oncogenic KRAS cells. As with the pathway enrichment analysis, significant changes were observed in several peroxisomal associated lipogenic enzymes. The lipid transporter ABCD1 and 4 were upregulated in both $BRAF^{V600E}$ and oncogenic KRAS mutant colorectal cancer cell lines while several enzymes associated with peroxisomal lipid metabolism was differentially expressed with ACAA1, downregulated in both oncogenic BRAF and KRAS while ALDH3A1 and 2 were downregulated in BRAFV600E cells but upregulated in oncogenic KRAS cell lines. Furthermore, key enzymes involved in the PPL biosynthesis pathway, DHRS7B and FAR2 were shown to be downregulated in BRAFV600E tumour cells and correlated with the previous observation that ether linked PL were downregulated in BRAFV600E tumour cells (Fig. 4.5B). To address the effects of Vemurafenib and Rosiglitazone treatment on PLe biosynthesis I again looked to investigate cellular lipid profiles through use of high-throughput untargeted mass spectrometry. Total PL levels were shown to be unchanged in response to both Vemurafenib and Rosiglitazone, sorting PL by class showed that both Rosiglitazone and Vemurafenib treatments led to marked increases in the levels of both ether-linked PC and PE phospholipids (Fig. 4.5D & E). Another major change observed between BRAFV600E and BRAFWT cell lipid profiles was the ratio between saturated/monounsaturated PLs compared to polyunsaturated PL levels. BRAFV600E tumour cells had high levels of saturated/monounsaturated PL but low levels of high order polyunsaturated PL giving an overall negative slope, while the opposite was true for BRAFWT tumour cells (Fig. 45F &G). Interestingly, both Vemurafenib and Rosiglitazone treatment of BRAFV600E cells induced major changes in the PL profile when assessing the number of unsaturation's per lipid class leading to a reversion of this negative slope to give a positive slope similar to BRAFWT cells. Furthermore, this coincided with an increase in peroxisomal PL biosynthesis indicating a role for BRAF signalling in the regulation of peroxisomal lipogenic pathways and membrane saturation (Fig 4.5F & G). Furthermore, the same held true with ether-linked lipid species showing a similar profile in response to both Rosiglitazone and Vemurafenib **(Fig. 4.5H & I).**

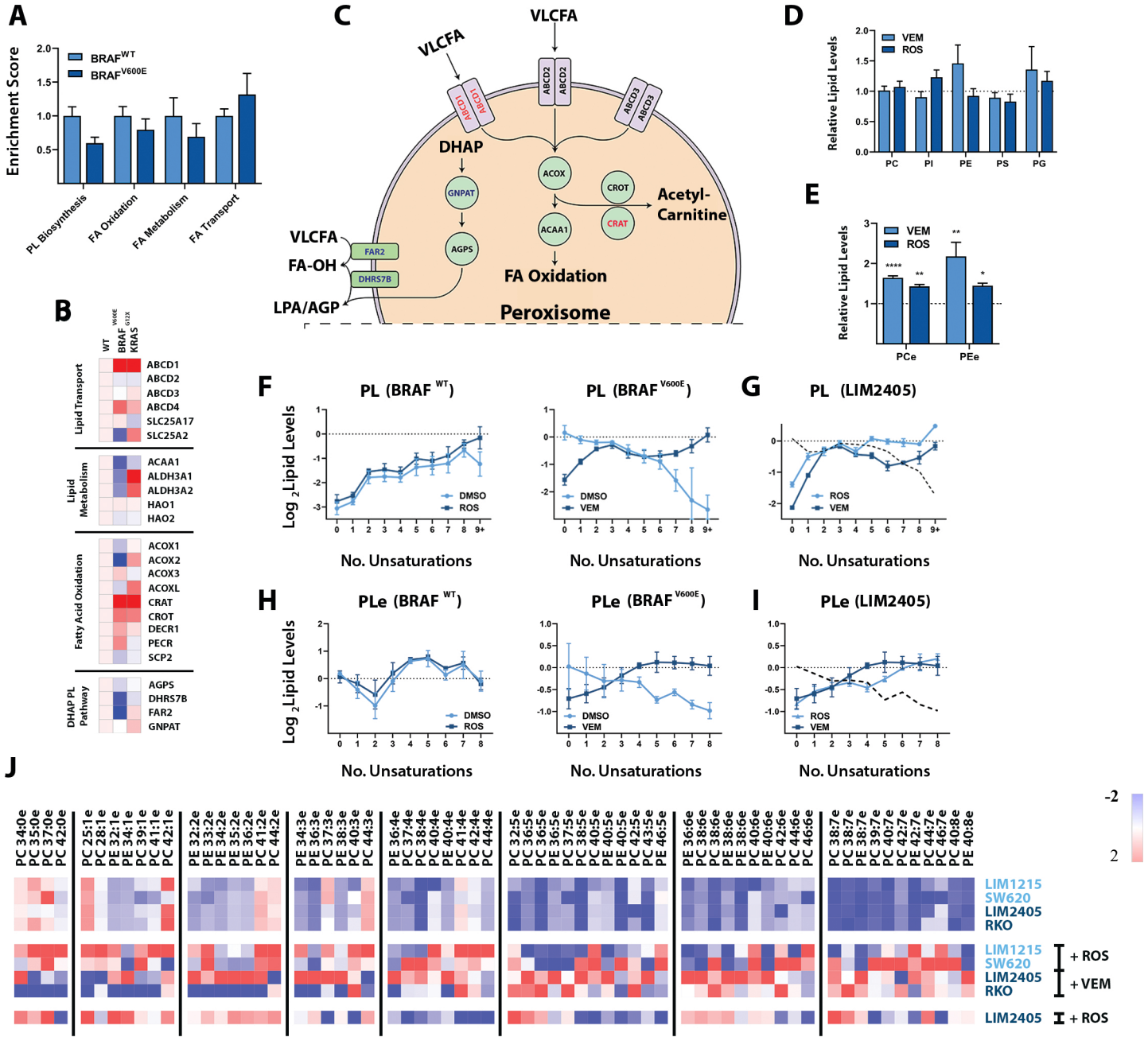

Figure 4.5. The BRAFV600E mutation downregulates peroxisomal phospholipid biosynthesis pathways. A. Gene signature scores of different peroxisomal lipid metabolic pathways based on gene signature of cell lines partitions based on BRAF gene mutation status **B.** heatmap representation of the average gene expression of key regulatory genes in different peroxisomal lipogenic pathways of cell lines either with wild type BRAF and KRAS mutation or KRASG12X and BRAFV600E cell lines **C.** Schematic representation of key lipogenic pathways utilized by the peroxisome in cells with gene expression changes indicated by colours (Red, upregulated) and (Blue, Downregulated) and are shown for BRAFV600E mutant cells compared to BRAFWT/KRASWT colorectal cancer cells. **D.** Total levels of non-ether linked phospholipid levels in BRAFWT cells treated with Rosiglitazone and BRAFV600E cells treated with Vemurafenib normalized to a DMSO control, and measured using mass spectrometry & **E.** the same for ether-linked phospholipid levels. **F.** Non ether-linked phospholipid levels separated by number of unsaturation's with BRAFWT cells treated with Rosiglitazone (Left panel) and BRAFV600E cells treated with Vemurafenib (Right panel) compared to a DMSO control & **G.** LIM2405 cells treated with either Vemurafenib or Rosiglitazone compared to DMSO control represented by a doted line. **H.** Ether-linked phospholipid levels separated by number of unsaturation's from BRAFWT cells treated with Rosiglitazone (Left panel) and BRAFFV600E cells treated with Vemurafenib (Right panel) compared to DMSO control & **I.** LIM2405 cells treated with either Vemurafenib or Rosiglitazone compared to DMSO control represented by a dotted line. **J.** Heatmap representation of the top upregulated ether-linked phospholipids in response to either Rosiglitazone or Vemurafenib compared to a DMSO control. All experiments were performed as n=3. Vemurafenib treatments were performed at 0.5uM while all other treatments were performed at 5uM unless otherwise stated. All error bars represent S.E.M and two tailed students t-test was used to test for statistical significance (*p < 0.05, **p < 0.01, ***p < 0.001 & ****p< 0.0001).

In addition, looking at the effects of Rosiglitazone and Vemurafenib on ether linked phospholipid species showed that the majority of significantly upregulated ether linked PL's in $BRAF^{V600E}$ colorectal tumour cells were polyunsaturated species while the monounsaturated/saturated ether linked PL levels were largely downregulated, while this was more obvious in RKO cell compared to LIM2405 **(Fig.4.5J)**. $BRAF^{WT}$ cells as discussed previously showed little change in polyunsaturated PL levels with the average level remaining unchanged. Looking at individual ether linked PL species did show alterations in the content of individual ether linked species however this was largely monounsaturated and saturated PL species. Interestingly, LIM1215 cells were largely unresponsive in the PL content in response to Rosiglitazone, while the $KRAS^{G12V}$ mutant, SW620 cells did show a significant change in some ether linked PUPL levels, however this was not further addressed **(Fig. 4.5J)**.

To further investigate the roles that PPL biosynthesis plays in regulation of tumour lipidomic reprogramming a null cell line was generated using CRISPR/CAS9 gene-editing targeting the terminal metabolic enzyme in the peroxisomal PL pathway, DHRS7B (DH7B) in both LIM1215 ($BRAF^{WT}$) and LIM2405 ($BRAF^{V600E}$) colorectal tumour cells [290]. Clonal populations were generated and expanded from stable cells overexpressing gRNA's targeting DHRS7B and Cas9 while knockout clones were validated through western blot analysis **(Fig. 4.6A)** Nanostring gene expression arrays were used to investigate cellular mRNA changes between $BRAF^{V600E}$ LIM2405 cells, and $LIM1215^{WT/DH7B\text{-}KO}$ cells. $BRAF^{V600E}$ cells showed 278 dysregulated genes >1.5-fold change with primarily EMT-associated genes upregulated and cancer stem-cell/β-catenin target genes downregulated. This was consistent with the genomics of the cell lines used with LIM1215 cells high in β-catenin activity mediated through a β-catenin ^{S49A} mutation leading to a proteasomal resistant β-catenin mutant. Furthermore, loss of DHRS7B in LIM1215 cells showed 306 dysregulated genes, 144 of which overlapped with the dysregulated genes associated with LIM2405 $BRAF^{V600E}$ cell line **(Fig. 4.6B)**. The top 25 up/downregulated genes based on pValue and log2 fold change are shown as a heatmap representation **(Fig. 4.6C)**. Analysis of lipid levels through quantification of lipid droplets per cell showed again that loss of DHRS7B led to a $BRAF^{V600E}$ like phenotype with a 3-fold increase in lipid droplets per cell, while no change was observed in the LIM2405 DHRS7B null cell lines **(Fig. 4.6D)**. High-throughput untargeted mass

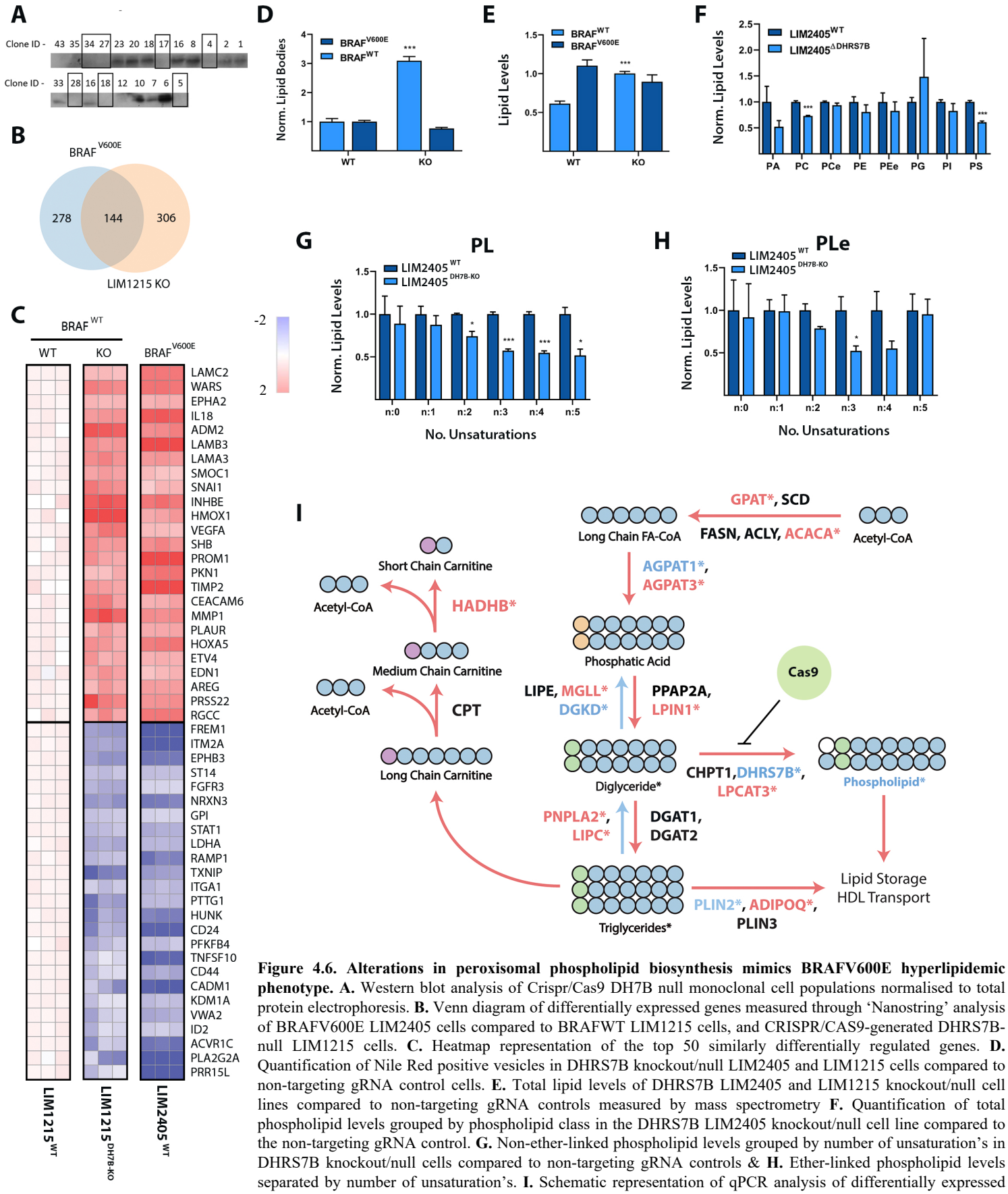

Figure 4.6. Alterations in peroxisomal phospholipid biosynthesis mimics BRAFV600E hyperlipidemic phenotype. A. Western blot analysis of Crispr/Cas9 DH7B null monoclonal cell populations normalised to total protein electrophoresis. **B.** Venn diagram of differentially expressed genes measured through 'Nanostring' analysis of BRAFV600E LIM2405 cells compared to BRAFWT LIM1215 cells, and CRISPR/CAS9-generated DHRS7B-null LIM1215 cells. **C.** Heatmap representation of the top 50 similarly differentially regulated genes. **D.** Quantification of Nile Red positive vesicles in DHRS7B knockout/null LIM2405 and LIM1215 cells compared to non-targeting gRNA control cells. **E.** Total lipid levels of DHRS7B LIM2405 and LIM1215 knockout/null cell lines compared to non-targeting gRNA controls measured by mass spectrometry **F.** Quantification of total phospholipid levels grouped by phospholipid class in the DHRS7B LIM2405 knockout/null cell line compared to the non-targeting gRNA control. **G.** Non-ether-linked phospholipid levels grouped by number of unsaturation's in DHRS7B knockout/null cells compared to non-targeting gRNA controls & **H.** Ether-linked phospholipid levels separated by number of unsaturation's. **I.** Schematic representation of qPCR analysis of differentially expressed lipogenic enzyme genes in LIM2405 WT compared to DHRS7B knockout/null LIM2405 cells. All experiments were performed as n=3. All error bars represent S.E.M and two tailed students t-test was used to test for statistical significance (*$p < 0.05$, **$p < 0.01$, ***$p < 0.001$ & ****$p < 0.0001$).

spectrometry approaches showed similar results with a 1-fold increase in total lipid levels associated with DH7B null LIM1215 cells while no change was observed in DH7B null LIM2405 cells **(Fig. 4.6E)**. The total levels of PLs in DHRS7B null cells showed a small decrease in most PL subclasses while PC and PS levels were significantly reduced **(Fig. 4.6F)**. Analysis of the levels of PLs when they were separated according to number of unsaturation's showed again a strikingly similar phenotype compared to the $BRAF^{V600E}$ cells, with large reductions in polyunsaturated fatty acid-containing PLs, which was observed in both ether linked and non-ether linked PLs **(Fig. 4.6G & H)**. Finally, analysis of the changes for all lipids and changes in the major lipogenic pathways showed an increased activity of lipogenic pathways and *de novo* lipogenesis **(Fig. 4.6I)**. This is likely due to blocking PL synthesis (by loss of DHRS7B) and with an emphasis on polyunsaturated PL levels leading to the cell attempting to remodel lipogenic pathways to increase PL biosynthesis.

4.5. Peroxisomal phospholipid biosynthesis is critical for membrane fluidity and controls a complex PPARγ-SREBF1-AMPK signalling axis

As previously discussed, loss of PPL through Cas9 mediated DH7B knockout cell lines was a useful cell model to investigate the lipidomic changes seen in $BRAF^{V600E}$ tumour cells. Genomic downregulation of key members of the PPL pathway was a key attribute leading to a hyperlipidemic phenotype. Therefore I was interested in the changes associated with Rosiglitazone treatment in DH7B null lines. Realtime qPCR analysis of key lipogenic genes in response to Rosiglitazone in LIM2405 wild type and DH7B null cell lines was used to measure the changes in response to Rosiglitazone. Interestingly, the DHRS7B-null DMSO control mirrored many of the responses that wild type cells had towards Rosiglitazone, except for SCD and DGAT2, while furthermore, the responses of DHRS7B loss to Rosiglitazone led to a large array of unresponsive lipogenic genes where both Rosiglitazone and DMSO treated DH7B null cells lines largely mimicked the effects of Rosiglitazone of LIM2405 wild type cells treated with Rosiglitazone **(Fig. 4.7A)**. Nile red immunofluorescence was used to measure cellular levels of lipid droplets in DH7B null cell lines in response to Rosiglitazone. As discussed in section 4.6, DH7B null LIM1215 $BRAF^{WT}$ cells showed a 2-fold increase in lipid droplets, this was

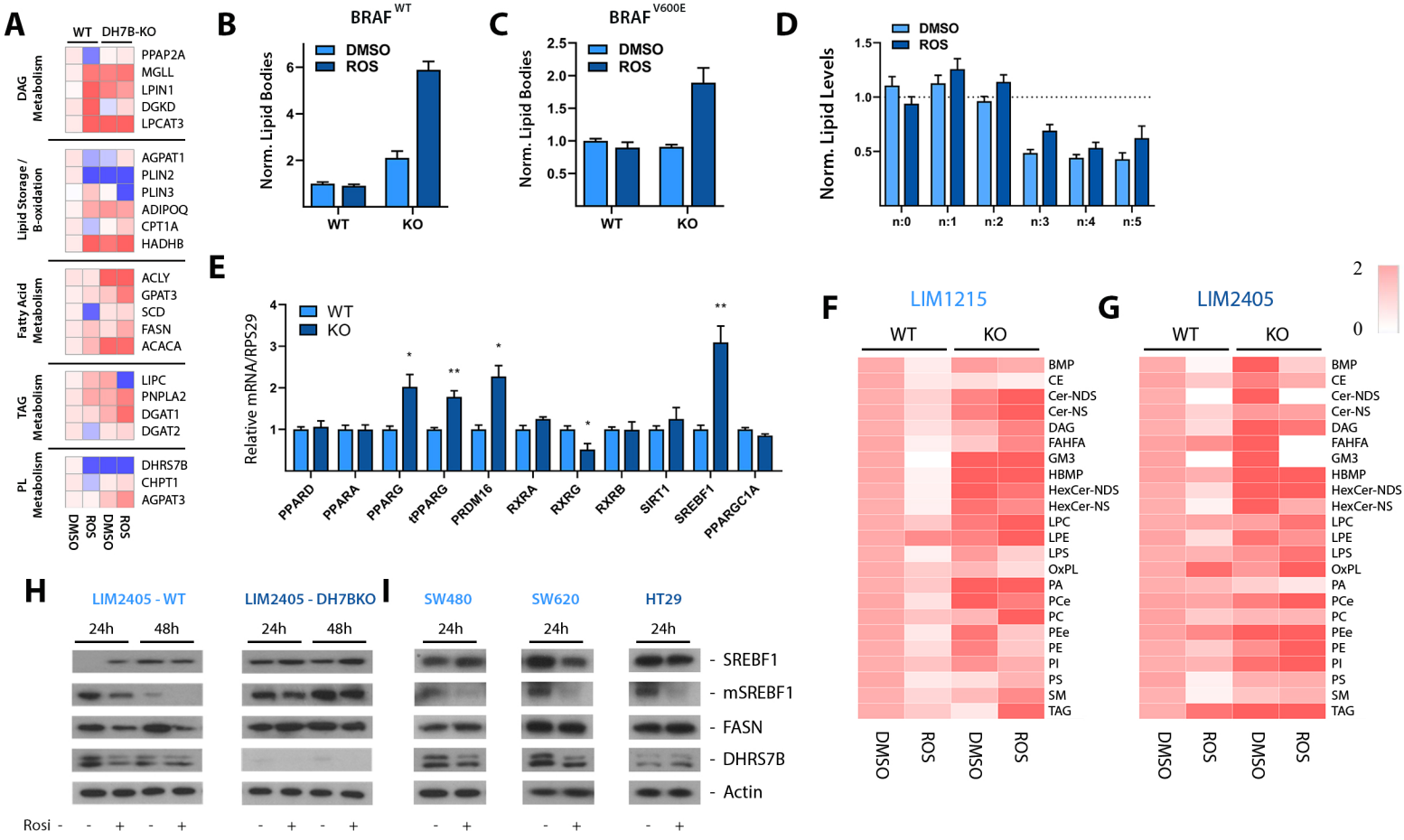

Figure 4.7. Altered peroxisomal phospholipid biosynthesis mimics a BRAFV600E hyperlipidemic phenotype. A. Heatmap representation of DHRS7B-null LIM2405 cells or LIM2405 WT cell in response to Rosiglitazone for 6 hours. **B.** Quantification of Nile Red positive vesicles in DHRS7B null LIM1215 cells compared to non-targeting gRNA controls in response to Rosiglitazone compared to a DMSO control & **C.** LIM2405 DHRS7B null and WT cells (Right). **D.** Non-ether linked phospholipid levels separated by number of unsaturations in response to Rosiglitazone in DHRS7B null LIM2405 cells. **E.** qPCR analysis of lipogenic pathway transcriptional regulators in DHRS7B null LIM2405 cells compared to WT control. **F.** Total lipid levels of 22 lipid species in response to Rosiglitazone treatment compared to DMSO control in LIM1215 WT and DHRS7B null cells & **G.** LIM2405 WT and DHRS7B null cells. **H.** Western blot analysis of genes associated with SREBF1 transcriptional activity in LIM2405 WT and LIM2405 DHRS7B null cells. **I.** Western blot analysis of genes associated with SREBF1 transcriptional activity in three additional colon cancer cell lines. All experiments were performed as n=3 regardless if biological replicates were used or not. All treatments were performed at 5uM unless otherwise stated. All error bars represent S.E.M and two tailed students t-test was used to test for statistical significance. For lipid droplet counts 300 individual cells were counted and the experiment was repeated 3 times and averages were taken of each replicate. .

further shown to increase in response to Rosiglitazone treatment **(Fig. 4.7B)**. Furthermore, $BRAF^{V600E}$ LIM2405 cells had little or no change in total lipid droplet number in DH7B null cells compared to wild type cells while a 1-fold increase in total lipid droplet numbers was observed in response to Rosiglitazone **(Fig. 4.7C**). This is an important distinction between what was addressed earlier in section 4.3 where Rosiglitazone was shown to decrease the lipid droplet levels in wild type cells. Furthermore, both Vemurafenib and Rosiglitazone were shown to target several PUPL species leading to an increase in the ratio of unsaturated to saturated PL's through actions mediated by PPARγ. Furthermore, in the previous section I showed that DH7B null cells were almost identical in lipidomic profile with the exception of higher order PUPL species. I was interested in the response in PUPL levels in DH7B null cells. Untargeted mass spectrometry was used to measure lipid levels in DH7B null and wild LIM2405 cells in response to Rosiglitazone treatment. DH7B null cells were unable to pool PUPL level in response Rosiglitazone **(Fig. 4.7D)**. Furthermore, loss of DHRS7B led to a large increase in almost all lipid classes measured in response to Rosiglitazone, again opposing what we previously showed where rosiglitazone had little effect on total lipid levels, but changed the dynamics of lipid present in the cell leading to mobilization of lipid droplets and cellular lipid reshuffling **(Fig. 4.7F & G)**. To further understand the changes in PPARγ-mediated cross talk we analysed the expression of several crucial lipid pathway transcriptional regulators in response to loss DHRS7B in cells. The total mRNA levels of full length and truncated forms of PPARγ were increased in DHRS7B null cells while a key transcriptional dimer partner of PPARγ, RXRG was downregulated. Furthermore, an important key regulator of lipogenic pathways, SREBF1 was upregulated significantly while mRNA levels of all other transcriptional regulators were unchanged **(Fig. 4.7E)**. Changes in the SREBF1 pathway was then assessed by western blot analysis of LIM2405 cells treated with Rosiglitazone. In wild type cells Rosiglitazone was shown to negatively regulate SREBF1 expression, with both 24hr and 48hr responses to Rosiglitazone leading to a loss of mSREBF1 (its transcriptionally active form). Furthermore, Rosiglitazone led to a slight change in both isoforms of DHRS7B protein levels (and a significant reduction in key targets of SREBF1 including FASN. This was reversed in DHRS7B null cells leading to sustained mSREBF1 levels in both DMSO and

Rosiglitazone treatment groups, while FASN protein levels were increased in response to Rosiglitazone in DHRS7B null cells indicating increased capacity for *de novo* fatty acid synthesis **(Fig. 4.7H)**. We further verified these results in three additional cell lines with all three showing similar responses indicating a broad level of redundancy, while interestingly as predicted $BRAF^{V600E}$ cells showed reduced protein levels of DHRS7B **(Fig. 4.7I)**.

Identification of sustained SREBF1 mediated transcriptional activity was shown to be responsible for PPARγ mediated regulation of lipid homeostasis while it is known that in addition to cholesterol a non-canonical PUFA PL regulated SREBF1 pathway is active in mammals. We hypothesise that upregulation of lipolysis genes in response to Rosiglitazone is only partially responsible for the observed PPARγ dependent reduction in total lipid levels. Furthermore, we attributed the PPARγ mediated regulation of lipid compartmentalisation was largely regulated through key autophagy pathways. To investigate the association of PPARγ mediated lipolysis of intracellular lipid droplets I looked at the response of LIM2405 cells treated with either Rosiglitazone alone as previously described or with 3methyadenine (3MA) (Autophagosome formation inhibitor). Nile red analysis of lipid body formation in response to Rosiglitazone led to a reduction in total lipid droplet numbers per cell as previous shown while 3MA alone was shown to led to an increase in lipid droplet levels. Co-treatment of Rosiglitazone with 3MA led to a similar increase in lipid droplet numbers indicating that Autophagy was a key regulator of lipid droplet levels **(Fig. 4.8B)**. To investigate Rosiglitazone/ PPARγ mediated regulation of lipophagy we analysed major autophagy initiator pathways focusing primarily on AMPK due to its relationship with the regulation of lipogenesis **(Fig. 4.8A)**. Rosiglitazone was shown to increase levels of phospho-AMPK between 8-24hours post treatment while direct AMPK targets, including phospho ULK1 (Ser555), correlated with the increase in phospho-AMPK levels **(Fig. 4.8D)**. Again, we further confirmed these observations in three additional cancer cell lines looking at the active form of AMPK and well characterised targets of AMPK signalling 16hrs post treatment. A similar response to Rosiglitazone mediated AMPK activation was observed with increased levels of active phospho-AMPK (Thr172) and increased levels of its downstream targets including phospho-PRTOR (Ser792) and phospho-ULK1 (Ser555) while reduction in the levels of the inhibitory phosphor-ULK (Ser757) form were observed (a known

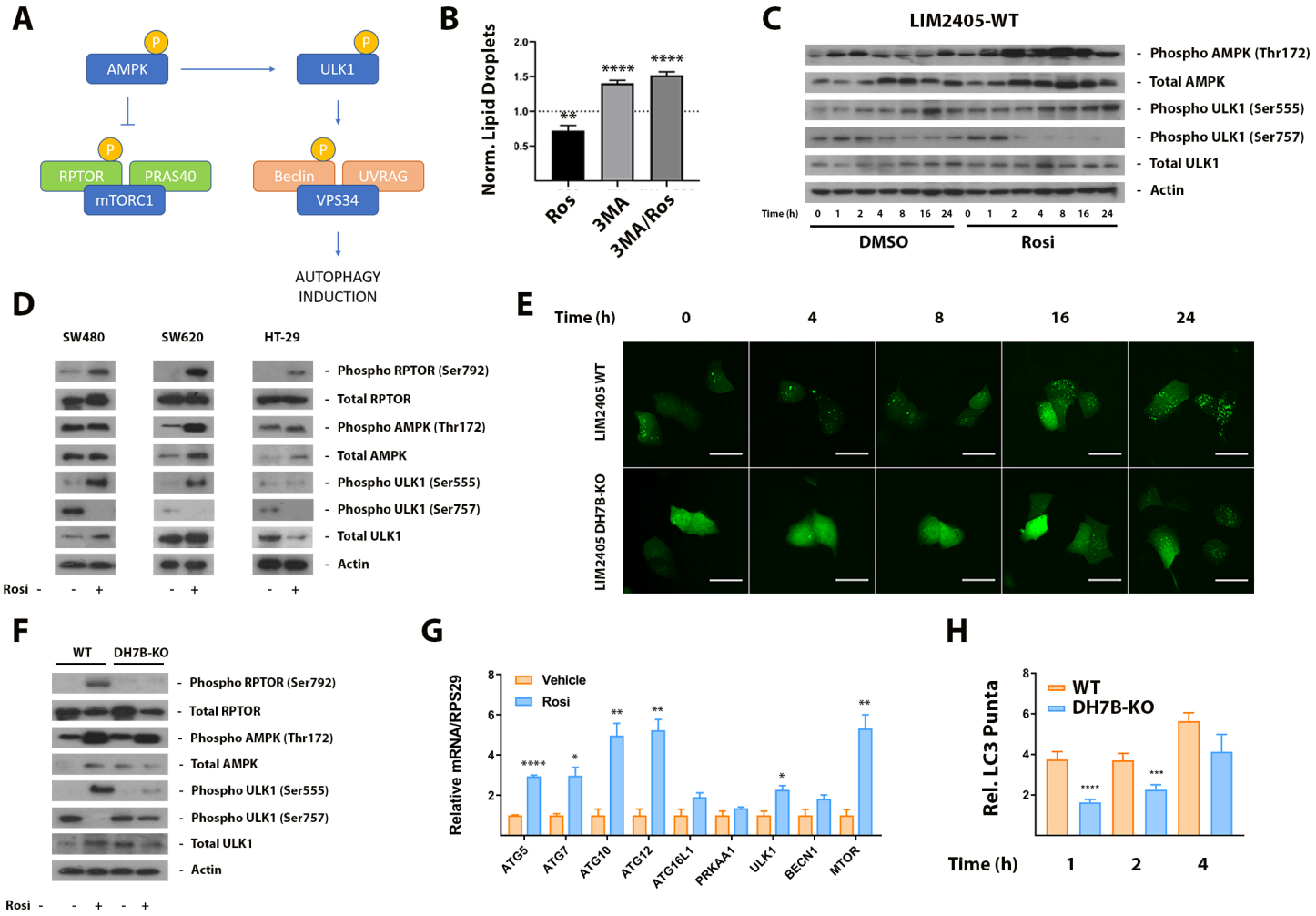

Figure 4.8. Rosiglitazone mediated AMPK signalling networks control intracellular lipid droplets through lipophagy. A. Schematic representation of the AMPK autophagy stimulation pathway. **B.** Quantification of Nile Red positive vesicles in response to either 3-methyadenin, Rosiglitazone or both co-treated compared to a DMSO control. **C.** Time-course analysis of LIM2405 cells treated with either Rosiglitazone or DMSO vehicle using western blot analysis. **D.** Western blot analysis of key autophagy signaling proteins in SW480, SW620 and HT-29 cells in response to either Rosiglitazone or DMSO vehicle control. **E.** Time-course immunofluorescence analysis of LIM2405 cell expressing an eGFP tagged LC3 gene. **F.** Western blot analysis of LIM2405 WT or LIM2405 DHRS7B null cells in response to either Rosiglitazone or DMSO vehicle control. **G.** Realtime qPCR analysis of key autophagy regulatory genes in response to Rosiglitazone treatment compared to DMSO vehicle controls in LIM2405 cells.**H.** Quantification of LC3 'punta' in response to serum starvation in LIM2405 DHRS7B null cells compared to LIM2405 WT cells. All experiments were performed as n=3 regardless if biological replicates were used or not. Vemurafenib treatments were performed at 0.5uM while all other treatments were performed at 5uM unless otherwise stated. All error bars represent S.E.M and two tailed students t-test was used to test for statistical significance, except for 4.8B where a two way ANOVA was used (*p < 0.05, **p < 0.01, ***p < 0.001 & ****p< 0.0001). For lipid droplet counts 300 individual cells were counted and the experiment was repeated 3 times and averages were taken of each replicate.

mTOR target) (Fig. 4.8C). Polyunsaturated free fatty acids have been shown to activate AMPK while monounsaturated free fatty acids play an inhibitory role in AMPK activation. It would seem possible that loss of DH7B and PPL biosynthesis is a key link between fatty acid metabolism and AMPK dependent lipophagy. Western blot analysis of LIM2405 WT and DH7B null LIM2405 cells treated with either a DMSO or 5μM of Rosiglitazone for 16h showed significant changes in pro-autophagic signalling. Although, levels of phosphor-AMPK were unchanged between the WT and DH7B null LIM2405 cells, downstream targets of AMPK were shown to be significantly downregulated. Levels of phospho-ULK1 (Ser555) were and phospho-RPTOR (Ser792) were downregulated in the null cell line while loss of the inhibitor ULK1 (Ser792) was only observed in the WT cells and not in null cells indicating sustained mTOR activity and inhibition of autophagy **(Fig. 4.8D)**. We further investigate the impact of DHRS7B aberration on autophagy through alternative methods utilising autophagy induction by low serum media (LSM) or complete serum starvation (SS). One of the key autophagy nucleation processes involved sequestration of LC3B into the autophagosome membrane. To investigate this process, I used a eGFP tagged LC3A/B construct and transfected it into LIM2405 WT and DH7B null cell lines. Under normal serum rich conditions autophagy is inhibited and remain cytoplasmic in localisation, upon autophagy stimulation LC3A/B is cleaved to the LC3B form and conjugated with PE at the autophagosome membrane where the GFP signal becomes membrane bound to intracellular vesicles. DH7B null LIM2405 cells were transfected with the LC3A/B-eGFP construct and showed reduced levels of LC3 puncta formation compared to wild type controls across all time points except 24h under LSM conditions, indicating delay in autophagy stimulation **(Fig. 4.8E)**. Quantification of LC3B autophagosome accumulation showed similar results under complete SS conditions with wild type LIM2405 cells showing a rapid accumulation of LC3 punta from 1hour onwards approximately 4-fold greater than under normal serum conditions. DH7B null cells were significantly delayed and ineffective in generation of LC3 punta where DH7B null LIM2405 cells only showing similar levels of LC3 punta after 4hours of serum starvations **(Fig. 4.8H)**. Furthermore, Rosiglitazone treatment was shown to induce mRNA levels of autophagy regulatory proteins including several ATG family proteins and other crucial autophagy initiator signalling complexes that included mTOR, AMPK (PRKAA1) and ULK1 **(Fig. 4.8G).**

DH7B was shown to be critical in regulation of AMPK mediated activation of autophagy pathways in response to Rosiglitazone while autophagy was shown to be a key regulator of Rosiglitazone mediated lipid remodelling. Overexpression of an mCherry tagged DHRS7B expression cassette in LIM2405 cells co-stained with Nile red for lipid droplets showed limited vesicle localisation of DHRS7B with lipid bodies under basal conditions **(Fig. 4.9A, left panel)**. Complete SS conditions led to a mark increase in co-localisation of DHRS7B with lipid bodies **(Fig.9A, middle panel)**, while SS in conjunction with chloroquine (an inhibitor of autophagosome/lysosome fusion) showed complete co-localisation of DHRS7B with lipid bodies **(Fig. 4.9A, right panel)**. Western blot analysis of key markers of autophagosome nucleation, ATG12/7 (autophagosome associated product) and LC3B were all shown to be downregulated in DH7B null cells compared to wild type controls under both LSM and SS induced autophagy **(Fig. 4.9C & D)**. While similar observations were seen in AMPK-dependent autophagy signalling pathways in response to LSM or complete SS, showing reduction in phosphorylated AMPK and loss of downstream phosphorylation targets, such as ULK1 (Ser555) and RPTOR (Ser792) **(Fig. 4.9B)**. We further verified this response in the LIM1215 DHRS7B null cell line. Both nucleation markers for autophagosome formation were downregulated in DH7B null LIM1215 cells compared to wild controls in response to Rosiglitazone and LSM while LC3B was not shown in response to complete SS in LIM1215 wild types cells but low levels were observed in DH7B null cells **(Fig. 4.9E)**. Similar results were shown in LIM1215 wild type and DH7B null cells regarding AMPK signalling pathways. Phospho-AMPK was reduced in LIM1215 DH7B null cells compared to wild type controls across all treatments while reduced levels of AMPK targets phosphor-ULK1(Ser555) and RPTOR (Ser792) were observed in DH7B null LIM1215 cells in response to Rosiglitazone and complete SS. Furthermore, the inhibitory phosphor-ULK1 (Ser792) was shown to be present across all treatment with LIM1215 DH7B null cells but was only present in DMSO vehicle and small amounts in complete SS treatments were seen in LIM1215 WT **(Fig. 4.9F)**. These changes in autophagy pathways also were shown to correlate with increase DHRS7B induced upregulation of members of the phospholipase C family **(Fig. 4.9G)**.

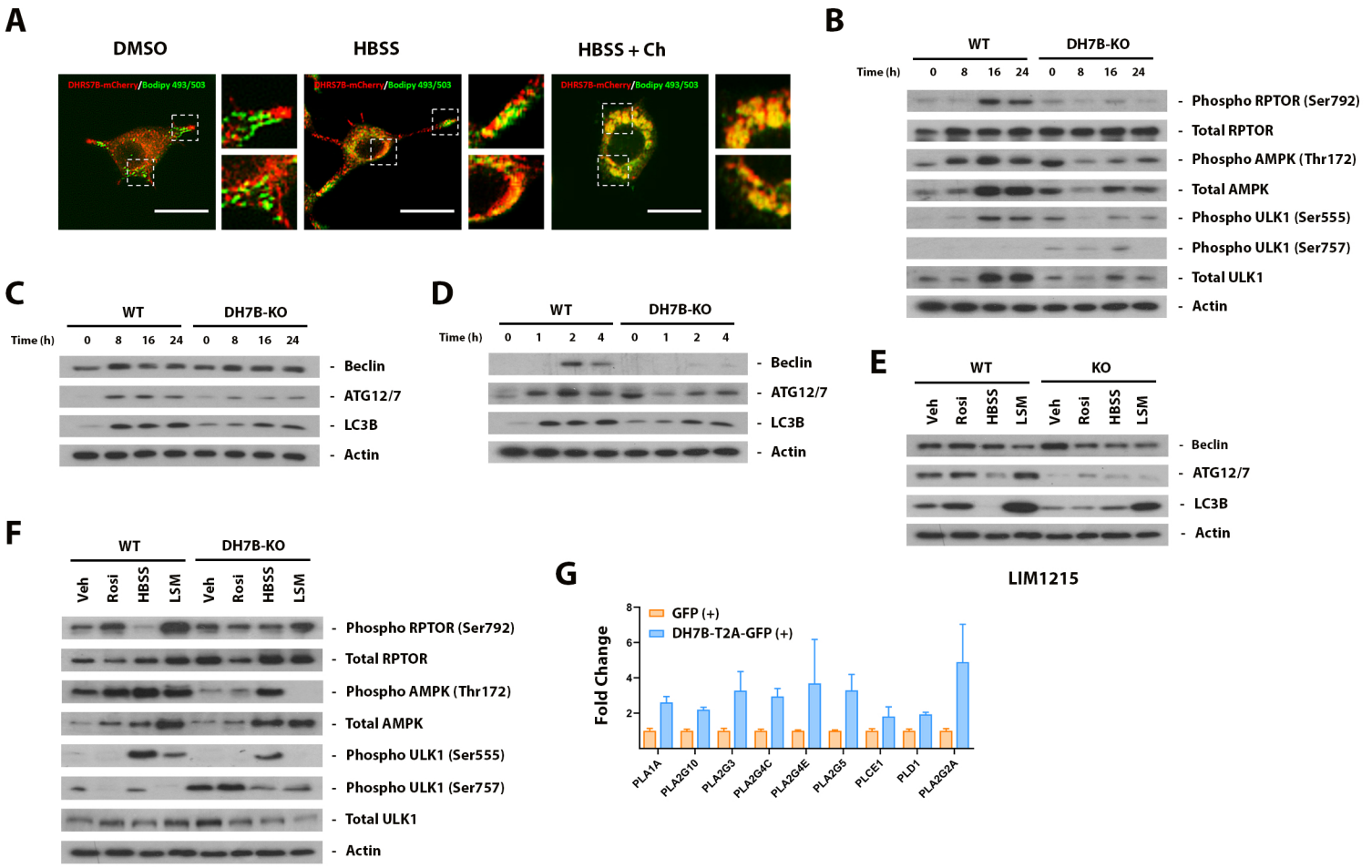

Figure 4.9. DH7B regulates starvation induced lipophagy through impairment of AMPK phosphorylation of ULK1. A. mmunofluorescence analysis of mCherry tagged DHRS7B RKO cells either unstarved or starved of growth factors and with either chloroquine or without. **B.** Time-course western blot analyses of key autophagy signaling proteins in response to low serum media in LIM2405 WT or DHRS7B knockout tumour cells. **C.** Time-course western blot analyses of key autophagy nucleation proteins in response to low serum media in LIM2405 WT or DHRS7B knockout tumour cells. **D.** Time-course western blot analyses of key autophagy nucleation proteins in response to HBSS induced serum starvation in LIM2405 WT or DHRS7B knockout tumour cells. **E.** Western blot analysis of DHRS7B knockout LIM1215 cell compared to LIM1215 WT cells of proteins involved with autophagosome some nucleation. **F.** Western blot analysis of DHRS7B knockout LIM1215 cell compared to LIM1215 WT cells of AMPK autophagy initiation signaling pathway. **G.** Nanostring analysis of gene expression in LIM2405 cells overexpressing either eGFP or DHRS7B-T2A-eGFP construct looking at PUFA specific phospholipases. All experiments were performed as n=3 regardless if biological replicates were used or not. Vemurafenib treatments were performed at 0.5uM while all other treatments were performed at 5uM unless otherwise stated. All error bars represent S.E.M and two tailed students t-test was used to test for statistical significance (*$p < 0.05$, **$p < 0.01$, ***$p < 0.001$ & ****$p< 0.0001$).

4.6. Discussion

Several studies have identified the RAS/RAF signalling pathway as a crucial regulator of cellular energetics in both the context of normal non-transformed cell systems and in tumorigenic cells. BRAF in melanoma is one of the principle mutations that drives this disease and many observations have shown that indicate melanoma cells have altered metabolic states. Oncogenic BRAF has been shown to down regulate mitochondrial turnover and density leading to down regulation of oxidative phosphorylation, while increased levels of glycolysis led to elevated utilization of the pentose pathway and ketoses [279, 280, 291, 292]. The literature has largely ignored the major lipogenic changes that are driven by BRAF mutations which is surprising given the aggressiveness and high proliferation rate that many RAS/RAF mutated cancers display and the ever-increasing roles of fatty acid metabolism and feedback for cell growth and survival. In this chapter I have investigated the interactions between the PPARγ signalling pathway and key lipogenic regulatory pathways, and how they can be used to manipulate tumour metabolic reprogramming to gain cell growth and survival advantages. We have shown that $BRAF^{V600E}$ tumours were able to reprogram cellular energetics through changes in lipogenic pathways leading to an almost global increase in cellular lipid levels. Downregulation of PPARγ-mediated signalling in $BRAF^{V600E}$ tumours was also shown to be a primary contributor to $BRAF^{V600E}$ dependent lipogenic reprogramming. We have highlighted the importance of PPARγ signalling for regulation of lipid homeostasis but also how important PPARγ signalling is for induction of other key lipogenic pathways including SREBF1-mediated lipogenesis and AMPK-stimulated autophagy. One of the major changes observed in $BRAF^{V600E}$ tumour cells was a large alteration in the total pool of PLs and their level of unsaturation. $BRAF^{V600E}$ tumour cells showed very low levels of PUFA PL levels but had large pools of saturated and monounsaturated PL species. Other groups have shown similar observations looking at genomic insights into Vemurafenib resistant $BRAF^{V600E}$ melanoma cells. SREBF1 mediated lipogenesis was identified as a potential target for $BRAF^{V600E}$ targeted therapy leading to increased polyunsaturated PL levels as a key response to Vemurafenib, in both Vemurafenib resistant and sensitive tumour cells [156]. Vemurafenib treatment was shown to inhibit mSREBF1 accumulation while resistant cell lines showed sustained SREBF1 activity even in the presence of

Vemurafenib. Although other research has highlighted that MEK1/ERK1 phosphorylation of SREBF1 at Ser-117 is required for efficient SREBF1 signalling, suggesting that sustained SREBF1 activity may have been a consequence to Vemurafenib resistance rather than the driving force, given that Vemurafenib resistant cells also had sustained MER1/ERK1 activity [293]. We have also shown similar responses to Vemurafenib in non-resistant colorectal $BRAF^{V600E}$ driven tumour cells, while PPARγ agonist treatment had a similar response leading to a pooling of polyunsaturated PL levels and a reduction of saturated PL levels. While sustained SREBF1 activity was likely to be a key driver of sustained lipogenesis in $BRAF^{V600E}$ tumours this could be reversed by Rosiglitazone treatment and PPARγ activation. PPARγ activity is known to be regulated by unsaturated free fatty acid levels which could explain why increased SREBF1 activity was observed in $BRAF^{V600E}$ tumour cells. Furthermore, given that Rosiglitazone leads to decreased mSREBF1 levels through increased AMPK activity provides insight into an interesting feedback mechanism that could maintain fatty acid homeostasis. We have shown that loss of PPARγ signalling in $BRAF^{V600E}$ tumours is an important regulatory mechanism that must be overcome in order to maintain high levels of lipogenic activity driven by sustained SREBF1 activation. This mechanism has been highlighted in adipogenesis models where elevated levels of SREBF1 activity leads to increased levels of PPARγ activity and was hypothesised to be a driving force of adipocyte differentiation [153]. Although they failed to show the effects of increased PPARγ activity on SREBF1 activity and while the similarities between SREBF1 and PPARγ target genes can often make it difficult to make any conclusions on the effects of PPARγ on SREBF1 activity through expression-based analysis alone, some groups have identified PPARγ inhibition of SREBF1 through restriction of LXR access to the SREBF1 promoter [274].

This highlights the importance of membrane lipid metabolic feedback and its role in the maintenance of a healthy metabolic balance in cellular energetics and the identification of non-canonical cholesterol independent SREBF1 pathways highlights the importance of PL regulation of lipogenesis [131, 132]. SREBF1 has been shown to be regulated by intracellular PC levels in metazoans and drosophila while ER PL composition has been shown to be critically important for SREBF1 activity in mice [294-296]. We have shown that $BRAF^{V600E}$ and $KRAS^{G12X}$ tumours to a lesser extent were able to break this lipidomic balance leading to greatly increased cellular lipid levels through downregulation of

peroxisomal PL metabolism leading to increased expression of genes involved in beta oxidation. This change in the balance of fatty acid metabolism present in the peroxisome led to changes in metabolic feedback leading to altered peroxisome function. We showed that you could model this peroxisomal $BRAF^{V600E}$ phenotype in $BRAF^{WT}$ cells through blocking peroxisomal PL biosynthesis by CRISPR/Cas9-mediated ablation of the SDR enzyme DHRS7B. Loss of DHRS7B led to a 2-3-fold increase in intracellular lipid droplet content while mass spectrometry lipidomic analysis showed a similar increase in total lipid levels. Disruption of peroxisomal PL biosynthesis also mimicked the effect of the $BRAF^{V600E}$ mutation on the ratio of intracellular PUFA: SFA levels. Other groups have described similar results looking at peroxisomal deficient or defective models. One group that modelled peroxisomal defects by introducing a mutation in the Pex5 gene, leading to a PTS-1 peroxisomal targeting signal defective model, showed that removal of the PTS-1 dependent protein targeting to the peroxisome, led to significant changes in peroxisomal lipid metabolism and more importantly altered membrane fluidity [297]. Furthermore, mutational analysis of PL biosynthesis pathways in yeast peroxisomes showed a similar reduction in membrane fluidity while modelling of peroxisomal biogenesis defects in Drosophila showed similar results highlighting the importance of peroxisomes in the regeneration of membrane fluidity and maintenance of higher order PUFA PL levels [298, 299]. Ether linked PL biosynthesis and peroxisomal lipid metabolism and their roles in tumour metabolism have been explored in recent years. Investigation of cells with high tumorigenicity compared to parental cells showed increased levels of ether linked lipids that correlated with a 1000-fold increase in colony formation while other groups have shown significant changes in ether linked lipid levels are associated with changes in growth and proliferation [300-302].

The mechanisms in which tumour cells disrupt cellular energetics is incredibly diverse and present an overwhelming hurdle for tumour biologists to overcome in order to effectively treat cancer as a metabolic disease. We have identified a novel and deeply embedded signalling axis that interconnects three major lipogenic pathways, PPARγ, SREBF1 and the AMPK pathways. PPARγ was shown to be the critical regulator and loss of PPARγ signalling in cellular models such as $BRAF^{V600E}$ tumours led to a severe disruption of this axis. Loss of PPARγ signalling led to sustained SREBF1 transcriptional activity while loss of peroxisomal PL synthesis (via loss of DHRS7B expression) mimicked this effect

even in the presence of PPARγ activity. We showed that this change in signalling outcome was largely dependent on AMPK activity which was further shown to be dependent on DHRS7B-controlled peroxisomal feedback. Loss of DHRS7B led to inefficient AMPK activity, loss of lipophagy and sustained SREBF1 transcriptional activity. This is consistent and correlates across species with the yeast homologue Ayr1p having been shown to be important in autophagosome formation, however the signalling mechanism underlying this phenotype is unclear [303]. Furthermore, SREBF1 is a known target of AMPK whereby AMPK regulates the stability of truncated SREBF1 protein levels. AMPK phosphorylates SREBF1 at Ser372 which has been shown to inhibit Golgi translocation and thus further inhibits SREBF1 processing leading to protein stabilisation in the ER and downregulation of SREBF1 target genes [173, 174]. As shown previously, loss of DHRS7B leads to ineffective AMPK activation and leading to sustained SREBF1 transcriptional activity driving lipogenic pathways and inhibiting lipid homeostasis through autophagy resistance. Furthermore, we showed that Rosiglitazone to be a potent activator of AMPK and an inhibitor of mSREBF1 stability, while loss of DHRS7B led to a loss of Rosiglitazone mediated SREBF1 inhibition through loss of AMPK signalling. This accounts for sustained SREBF1-mediated lipogenesis and can account for the hyperlipidemic phenotype. Interestingly, autophagy pathways have been shown to be strongly induced in response to BRAF inhibitors and further sensitizes cells to BRAF targeted therapy [304, 305]. Furthermore, several groups have shown the importance of peroxisomes in autophagy feedback mechanisms. PEX5 depletion has been shown to regulate TSC2 expression levels which in turn regulates autophagy induction through inhibition of mTORC1 [306]. Increased levels of PUFA free FAs have been shown as a potent stimulator of AMPK activity in many different cellular models while saturated FA's such as palmitate has been shown to inhibit AMPK activity [307-309]. This is compelling given the low levels of PUFA PLs in both DHRS7B null cells and $BRAF^{V600E}$ cells.

Chapter 5 – Reverse genomic approaches reveal peroxisomal lipid metabolism as a key regulator of chemoresistance and cancer stemness

5.1. Introduction

Diagnostic biomarkers are an important tool in interventional medicine. Identification of reliable marker genes or metabolites associated with disorganised tumour metabolism provides a tool to distinguish between normal and tumorigenic metabolic states. Tumour metabolism has provided an intriguing link between tumorigenic metabolic networks and classical cancer hallmarks. Furthermore, increasing evidence suggests that metabolic reprogramming is a key process that drives tumour drug resistance and progression under unfavourable cellular environments. Modern NGS techniques have provided a reliable and relativity cheap method for implementation of designer therapeutics. However, there is still much work to be performed in this space with ever increasing cellular mechanism driving key oncogenic process such as chemoresistance and rapid tumour progression. .

In chapter 3 I highlighted the use of a linear GSEA base on whole tumour mRNA transcriptomes to dissect tumour metabolism. Identification of $BRAF^{V600E}$ mutations as a driver of a hyperlipidemic phenotype through downregulation of PPARγ regulated PPL biosynthetic pathways was shown to be a key driver of lipid metabolic reprogramming. Despite utilising these techniques to accurately predict PPARγ signalling and unravelling a complex multi-oganelle signalling network regulating intracellular lipid stores, prediction of metabolic states based solely on snapshot mRNA transcriptomics provided inconsistencies depending on a number of factors. This highlights a challenging problem for accurate prediction of cellular metabolic states and ultimately associated tumour dependencies. Transcriptional based prediction is based upon a key assumption that for example if geneset x is associated with TAG biosynthesis and is upregulated/downregulated then the associated phenotype or intracellular levels of TAG must reciprocate. To a degree this must be true and can be a good starting point in any scientific investigation [249, 310]. However, it fails to account for many aspects of cellular biology such as overlapping signal transduction and the phospho-proteome. For example, AMPK has been shown to inhibit fatty acid biosynthesis through direct phosphorylation of ACC at Ser79 [170]. Furthermore, a key process in regulating intracellular lipid storage is mediated through lipophagy in which it is also regulated through signalling mechanisms

governed by AMPK [311]. While AMPK is also known to phosphorylate and inhibit a key lipogenic transcription factor SREBF1, these are key examples of how lipogenesis can be regulated through non-transcriptional processes. Furthermore, I have shown that PPARγ is an important regulator of lipophagy in colorectal tumour cells. Despite upregulation and validation of many key lipogenic enzymes through PPARγ transcriptional pathways, lipid levels were shown to be ultimately unchanged while lipid compartmentalisation showed reduced levels of lipid droplets though activation of AMPK-mediated lipophagy. .

This highlights a problem where transcriptomics can led to misleading conclusions. Genetic signatures are often based solely on idealised experimental models such as treating cells with high concentrations of agonists to induce transcriptional changes of a particular pathway. The reality is that in normal conditions this creates artificial bias and while this can be helpful in controlled settings looking at aspects such as tumour metabolism it is impractical/unethical to treat patients with high levels of Rosiglitazone prior to diagnostic screening to evaluate the impact of PPARγ signalling in tumorigenesis. Recent advances with computation biology has allowed for screening of large volumes of data through semi-curated biological datasets through use of categorical language [312]. This approach provides solutions to some problems by looking at commonalities between different datasets but still ignores the faults of previous GSEA based approaches. Furthermore, recent advances in parallel/single cell sequencing and CRISPR/Cas9 has proven to be a valuable tool for identification of true target genes through implementation of multi guide libraries [313-316]. Despite this, the use of reserve based genetic approaches to predict tumour metabolism and identify associated susceptibilities is largely unexplored. In this chapter I have investigated a reverse based genomic approach to dissect the lipid metabolome and explore the possibilities of using lipid biomarkers to identify tumour susceptibilities. I identified a high confidence genomic readout through integration of multi-dimensional and layered biological datasets, utilising previously discussed cellular models of PPL biosynthetic pathways. The predictive signature was far more effective for the prediction of phenotypic outcome compared to current GSEA based approaches such as KEGG. PPL associated genetic signatures were used to identify key roles that PUPL's play in chemoresistance through regulation of ER stress responses. Furthermore, given the role that PPARγ played in regulation of

membrane saturation I further investigated PPAR signalling utilising unobtrusive molecular biology approaches to get a better idea for the roles that PPAR's play in tumour metabolism. PPAR active cells where shown to have reduced levels of OxPHOS related genes and were shown to correlate with markers of G2/M phase transitional cells. Furthermore, changes in cellular metabolism and key genes associated with small molecule transport and differentiation was shown to reverse PUPL associated chemoresistance by targeting JNK mediated ER stress responses leading to increase apoptosis induction.

5.2. Tumour mutational load positively correlates with gene set dysregulation but not with phenotypic outcome

In Chapter 3 I discussed methodology to utilise current high throughput large scale transcriptomic analysis in order to predict tumour metabolic states. Normalisation and transformation of large cohorts of patient RNAseq data using t statistics showed its use in complex data analysis across heterogeneous biological datasets. Another notion that was investigated was the idea of gene promiscuity. Removal of promiscuous genes across datasets allowed more standardised data analysis while avoiding issues that low expression genes and tissue specific genes may cause leading to false positives. As discussed previously, Geneset enrichment analysis fails to consider fundamental biological processes including non-transcriptional regulatory networks. All these fundamental biological processes in addition to many others not mentioned complicate data analysis leading to higher incidences of false positives and false negatives. The notion of linear based models in which the assumption that x = y is not always correct, and oversimplification of tumour metabolism can result in poor accuracy in final cellular based models **(Fig. 5.1)**. To further investigate the issues associated with linear based predictive models I looked at a small subset of 9 metabolic pathways previously described in Chapter 3. I used a modified CCLE RNAseq dataset with matched cell line samples for polar metabolomics. Supervised k-means based clustering of the manually curated gene sets identified six distinct lipid associated cancer phenotypes. Cholesterol ester biosynthesis was shown to be upregulated in cluster 1 along with PUFA biosynthesis.

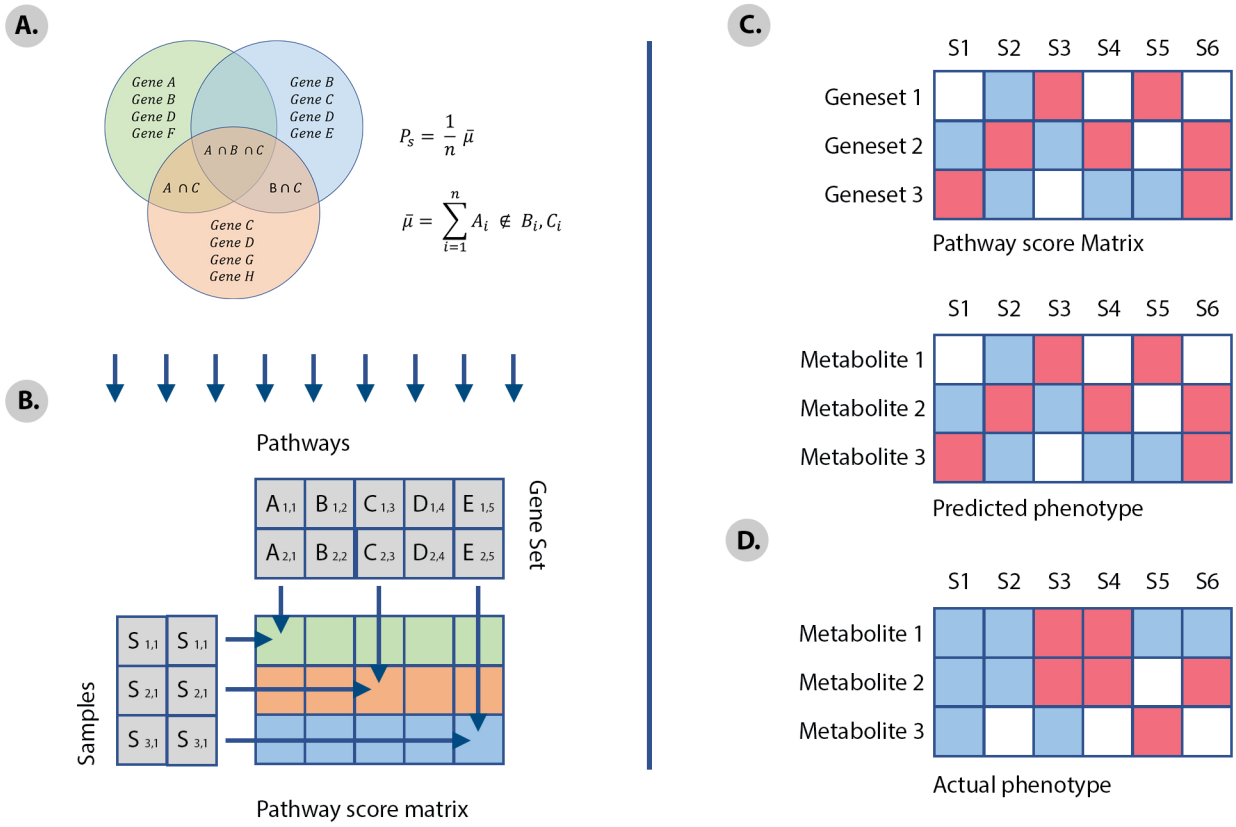

Figure 5.1. Data pipeline for linear based predictor scores and the shortcomings of linear based predictive models. A. Gene set enrichment data analysis based on correction for gene promiscuity where gene set A is the summation of average t-score (Ps) of genes that are not a part of gene set B and C. **B.** Ps is represented as a pathway score matrix of gene set scores segmented by tissue samples looking at the average effects of gene expression signature with a predicted phenotypical output. **C.** Pathway score matrix can be used as a predictor for phenotypic output with the assumption that is patient A has enriched pathway B therefor patient A must over express metabolite B. **D.** Actual phenotypical output however often reads significantly different to predicted phenotype due to the multiple dimensions of complexity in biological systems.

The CE biosynthesis associated geneset scores were downregulated in both cluster 2 and 6. Cluster 3 was associated with upregulate levels of with peroxisomal PL and FA-CoA biosynthesis genesets, while phospholipid metabolism and TAG biosynthesis gene sets were ubiquitously expressed across all cell lines **(Fig. 5.2A)**. To further address the poor correlation that some gene sets showed with phenotypic output we looked at the effects of mutational load on gene set dysregulation. A ranked order list of 9 different lipid metabolic gene sets were measured across 888 tumour cell lines matched with polar metabolomics **(Fig. 5.2B, bottom panel)**. Mutation load was identified in the 90th percentile group of cell lines in 9 different lipid metabolic pathways upregulated compared to cell lines with no differential gene set regulation, except for two metabolic pathways, FA-CoA and PL biosynthesis **(Fig. 5.2B, top panel)**. Furthermore, the average levels of CE, PL and TAG's across the six clusters, identified by supervised clustering based on gene set scores, showed loose association between CE and CE biosynthesis pathway scores, while PL correlated with PL biosynthesis gene set scores. We did identify that the distribution of PL biosynthesis gene set scores, along with TAG biosynthesis gene set scores, to be linear rather than logarithmic indicating little dysregulation across the population **(Fig. 5.2C)**. To further address the association between GSEA based techniques and tumour mutation load I looked at the correlation and association between different metabolic pathway scores and number of tumour mutations. For this analysis I limited the samples to solid tumour derived cancer cells and excluded myeloid/leukemia derived tumour cells. Positive correlation was found to be associated with all tested genesets with ether lipid metabolism and PPARγ signature genesets associated with the highest correlation. **(Fig. 5.2D, E & I)**. I performed the same linear based analysis this time looking at the z-scores calculated for each metabolite across the Depmap metabolomics datasets again limiting the analysis to solid tumour derived cancer cell lines. Both TAG's and CE's showed no correlation between metabolite level and mutation load **(Fig. 5.2F)**. This is not surprising given the vast array of genomic independent mechanism that regulate tumour metabolism. Furthermore, Pearson's correlation coefficients were calculated between geneset scores and metabolite levels. TAG levels correlated strongly with TAG biosynthesis gene set scores while PL biosynthesis gene set scores showed no association with PL levels indicating that GSEA based approaches are not always appropriate **(Fig. 5.2H)**.

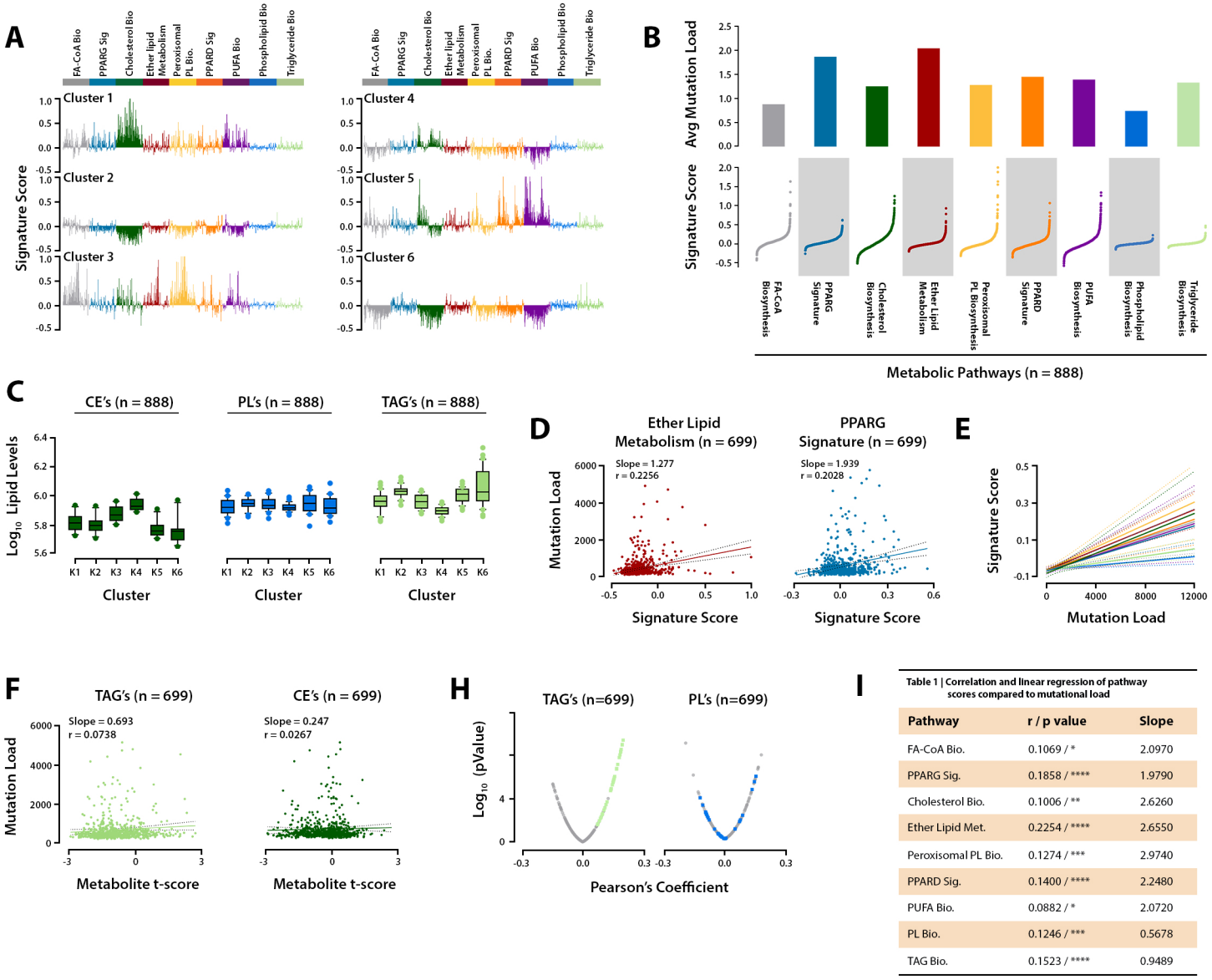

I

Table 1 | Correlation and linear regression of pathway scores compared to mutational load

Pathway	r / p value	Slope
FA-CoA Bio.	0.1069 / *	2.0970
PPARG Sig.	0.1858 / ****	1.9790
Cholesterol Bio.	0.1006 / **	2.6260
Ether Lipid Met.	0.2254 / ****	2.6550
Peroxisomal PL Bio.	0.1274 / ***	2.9740
PPARD Sig.	0.1400 / ****	2.2480
PUFA Bio.	0.0882 / *	2.0720
PL Bio.	0.1246 / ***	0.5678
TAG Bio.	0.1523 / ****	0.9489

Figure 5.2. Linear based prediction models correlate with tumour mutation load but not always with predicted metabolite. A. Linear based gene expression gene set prediction scores were calculated for 9 gene sets in 888 cell lines and were subjected to spearman based supervised clustering identifying 6 gene set signatures with the sample score of each gene set shown as a bar chart. **B.** Average mutation load of the top 10th percentile and middle 10th percentile of tumour samples based on gene set scores, top panel. Ranked gene set scores of 888 cell lines based on gene expression t-statistic base data normalisation, bottom panel. **C.** Average metabolite levels of CE, PL's and TAG's across 6 gene set clusters based on 888 cell lines. **D.** correlation between average gene set scores of ether lipid metabolism (left panel) and PPARG signature (right panel) and the average mutation load of 699 cell lines derived from solid tumour masses neglecting hematopoietic derived cells. **E.** linear regression model based on the correlation levels between 9 gene sets and mutation load in 699 solid tumour derived cell lines. **F.** Correlation between mass spectrometry measured metabolite level and gene set score of TAG's (left panel) and CE (right panel) in 699 solid tumour derived cell lines. **H.** Spearman based correlation between 229 polar metabolites and log10 (pvalue) of TAG biosynthesis (left panel) PL biosynthesis (middle panel) and CE biosynthesis (right panel) in 699 solid tumour derived cell lines. **I.** Table showing the correlation, p value and slope of 9 gene sets compared to average mutation load in 699 solid tumour derived cell lines. Error bars on boxplots represent the 10th and 90th percentile while boxplot represents the median, 25th and 75th percentile. For linear regression analysis the line of best fit represents the slope while the dotted lines represent the 95th confidence interval. All data used in the analysis is available through the DeepMAP project data download portal (https://depmap.org/portal/download/) and all data analysis was performed in MATLAB 2019b.

To better understand the cellular lipid metabolome, I investigated major lipid species across 15 different tumour cells derived from 7 topological tumour tissue types **(Table 2.1)**. The limitations of the CCLE metabolomic dataset is that very limited number of lipid species are identified. Our own methodologies in high throughput non-polar metabolomics allowed for the identification of ~950 lipid species across 22 different lipid classes. Spearman ranked correlation was used to generate a correlation matrix to identify lipidome similarities across cancer cell lines. Correlation analysis of tumour cells based on cellular lipidome showed that tumours do not cluster according to tissue of origin as they would with genomic based approaches **(Fig. 5.3A)**. tSNE clustering was used to identify associated cell lines based on lipidomic readouts. While supervised k means cluster was used in conjunctions to validate the tSNE cluster. k means clustering was projected onto the tSNE cluster but grouping the k means results as colours onto the tSNE cluster showing well defined cluster margins associated with k integer values **(Fig. 5.3B)**. Initially, I looked at the lipidomic profile based on tissue of origin. However, this analysis was limited since I only had multiple biological replicates from breast and colorectal derived tumorigenic cells. Despite this, analysis of the two major forms of intracellular lipid stores showed that tissues that primarily had high levels of CE's had low levels of TAG's and vice versa. For example, ovary and prostate showed elevated CE levels but lower levels of TAG's **(Fig. 5.3C)**. I further addressed mutational based analysis of the 15 most prevalent mutated genes. KRAS and BRAF mutations were largely associated with colorectal cancers while as expected the highest incidence of mutation was seen in TP53. However, no association between common oncogenic mutations and lipid metabolites were observed **(Fig. 5.3D)**. Analysis of the total lipidomic profile of all cells arranged by tissue of origin showed somewhat tissue-specific lipidomic profiles in both breast and colorectal derived tumours **(Fig. 5.3E)**. However, when considering supervised based clustering methods, the cells in the main did not cluster based on tissue of origin and with the exception of TAG levels most clusters showed a fairly high level of error between cell lines, and total lipid class levels of 9 major lipid classes included PL and ether linked PL levels **(Fig. 5.3G)**. Interestingly analysis of lipid species associated with tissue of origin showed some interesting potential biomarkers. Saturated forms of LPE were highly enriched in intestinal colorectal derived tumour cells while monounsaturated forms of SM lipid classes were elevated in breast derived tumour cells **(Fig. 5.3H)**. I also investigated any potential associations

between lipidomic profile and tumour cell growth rates using metadata collected from several sources (*https://web.expasy.org/cellosaurus/*). However, no associations between cell proliferation rate and lipidomic profile were observed and again k-means clustering did not show significant levels of clustering that correlated with cell growth rate **(Fig. 5.3F & G)**. Finally, I looked at the transcriptome of the four lipidomic based clusters searching for similarities that the clustered cells might portray. A transcriptionally associated signature was generated and GSEA was used to look at up/downregulated genes associated with key oncogenic pathways utilising the Hallmarks, and KEGG datasets. 22 commonly dysregulated pathways were identified between the four clusters. Cluster 1 was found to downregulate almost all oncogenic associate pathways, cluster 2 upregulated a large proportion including a hypoxia associate HIF1A signature, EMT associated genes and a NFkB signature. Furthermore, the top 50 upregulated genes identified in each metabolic cluster was determined and represented as a heatmap with the top 5 genes ID's listed according to p-value **(Fig. 5.3I & J)**.

5.3. Implementation of the multi-dimensional reverse genetics-based approach for lipidomic phenotype prediction.

In the previous section I introduced a high throughput lipidomic dataset based on the lipid profiles from 15 human cancer cell lines derived from 7 tumour subtypes with a varied mutation landscape. Analysis showed that tumour topography, growth rate and mutation load largely had little impact on the associations of cell lipid profiles. Therefor I was interested in the lipid-based patterns that regulated cell lipidome clustering. To further address this I developed a simple method is quantification of the ratio between saturated and unsaturated lipid levels through linear based regression models (a Saturation Index. Focusing on TAG metabolites for the majority of this analysis I looked at the total lipid levels, and lipid levels of each TAG associated lipid species across all 15 human cancer cell lines arranged according to the k means cluster performed in the previous section. TAG species levels were largely correlated with total lipid levels **(Fig 5.4A, Top & middle panel)**. Adjusting for total lipid levels, TAG levels by species were shown to largely be homogeneous across all cell lines **(Fig. 5.4A,**

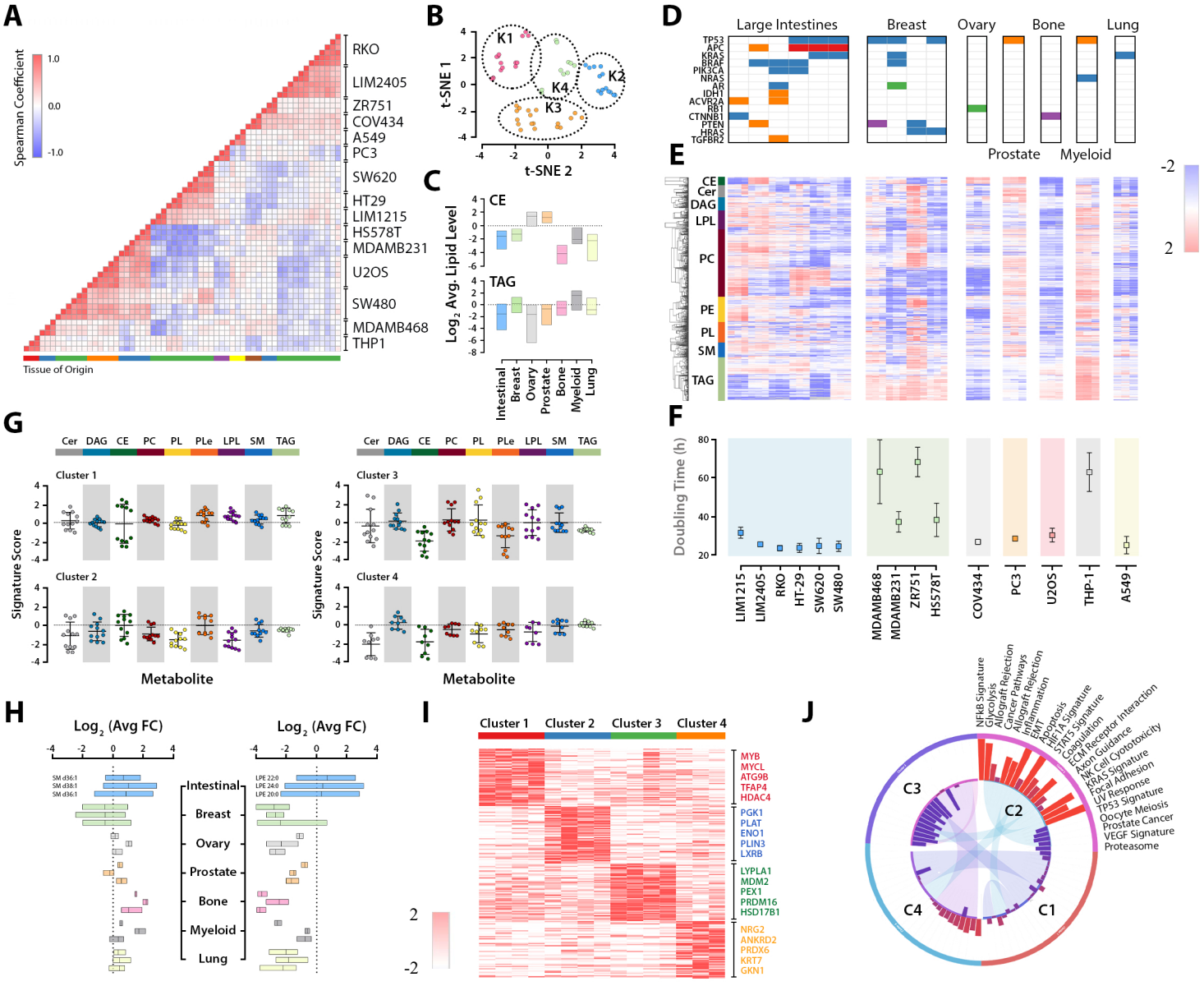

Figure 5.3. The lipidomic landscape of 15 human cancer cell lines. A. Spearman based correlation of nonpolar high throughput metabolomic readouts of 15 human cancer cell lines organised into a similarity matrix. **B.** T-distributed stochastic neighbourhood joining method showing the four clustered based on supervised k means clustering of 15 cancer cell line lipidomic readouts. **C.** Log2 average fold change of CE (Top panel) and TAG (Bottom panel) lipid species identified through nonpolar mass spectrometry organised according to cell tissue of origin. **D.** Mutational analysis of 15 cancer cell lines of organised based on tissue of origin looking at 14 commonly mutated oncogene/tumour suppressor. **E.** Total lipidomic read out measured through nonpolar mass spectrometry of 15 human cancer cell lines organised by tumour cell tissue of origin. **F.** Average doubling time of 15 human cancer cell lines organised by tissue of origin. **G.** Log2 average metabolite level of 9 lipid classes across four identified clusters based on nonpolar lipidomic readouts in 15 human cancer cell lines. **H.** Top three dysregulate lipid species according to tissue of origin in breast cancer (left panel) and colorectal derived cells (Right panel). **I.** Heatmap representation of the top 50 upregulated genes identified through Deseq2 differential gene expression in each metabolic kmeans cluster. **J.** Radial bar chart showing the GSEA scores of each lipid metabolic cluster of 22 commonly dysregulated enriched pathways across 4 k means clusters (outer circle) with imposed chord diagram of the level of total overlap between identified dysregulated pathways measured by GSEA (inner circle). Error bars on boxplots represent the 10th and 90th percentile while boxplot represents the median, 25th and 75th percentile. Nonpolar metabolomics were normalised to total cell number and protein levels and all data analysis including differential expression, supervised and unsupervised machine learning based analysis was performed using Matlab 2019b.

bottom panel). Again, this is unsurprising when you consider that TAG's are the major storage form of intracellular lipids and it would seem likely that TAG levels correlate strongly with total lipids. Furthermore, this indicated that the lipid cluster was largely independent of total lipid. This same positive correlation between lipid species levels was observed in PC's. PC levels showed to strongly correlate with total lipid levels **(Fig. 5.4D, right panel)**. Interestingly, the opposite held true for CE's where a negative association between CE levels and total lipid levels was observed **(Fig. 5.4D, left panel)**. To further address the lipidome pattern associated with the k means cluster I looked at the levels of TAG order by chain length and then ordered by number of unsaturation's. When TAG was ordered according to chain length and unsaturation number the clusters were largely homeostatic in appearance across all four k means clusters **(Fig. 5.4B & C)**. To address this pattern of cell based on the lipid chain length and saturation level I developed a simple linear regression-based model to dissect the ratio of saturated compared to unsaturated intracellular lipid species (Saturation index, section 2.15. SI was calculated across all cell lines tested based on either TAG lipid species or PC lipid species. TAG SI showed a negative correlation between total lipid levels and TAG SI scores where PC SI score showed no correlation with total lipid levels **(Fig. 5.4E)**. I further looked to address the genetic association with SI and total lipid levels. Pearson's correlation coefficients were calculated for total lipid level and SI compared to gene mRNA read counts for the cell lines used in the lipidomic dataset. Positive correlated genes with TAG based SI was compared to genes that were negatively correlated total lipid levels **(Fig. 5.4F, left panel)**. Furthermore, genes that positively correlated with TL levels but negatively correlated with TAG SI were also calculated **(Fig. 5.4F, right panel)** Geneset overlap was calculated between these two groups of correlating genes with total lipid level and TAG SI. TAG SI was shown to positively correlate with genes associated with EMT, NFkB and WNT signalling. While FA oxidation, MYC signalling, mitochondrial biogenesis and respiration were largely associated with high total lipid but low TAG SI, indicating that high TAG SI is associated with later metastatic-associated phenotypes, and provides an interesting prospect for measuring tumour aggressiveness **(Fig. 5.4G, left panel)**. I further addressed the same analysis utilising SI calculations based on PL's. Interestingly, the PL based SI showed an opposing signature with positive correlation between FA metabolism and WNT signalling, while it also showed upregulation in NFkB, HIF1A signalling and

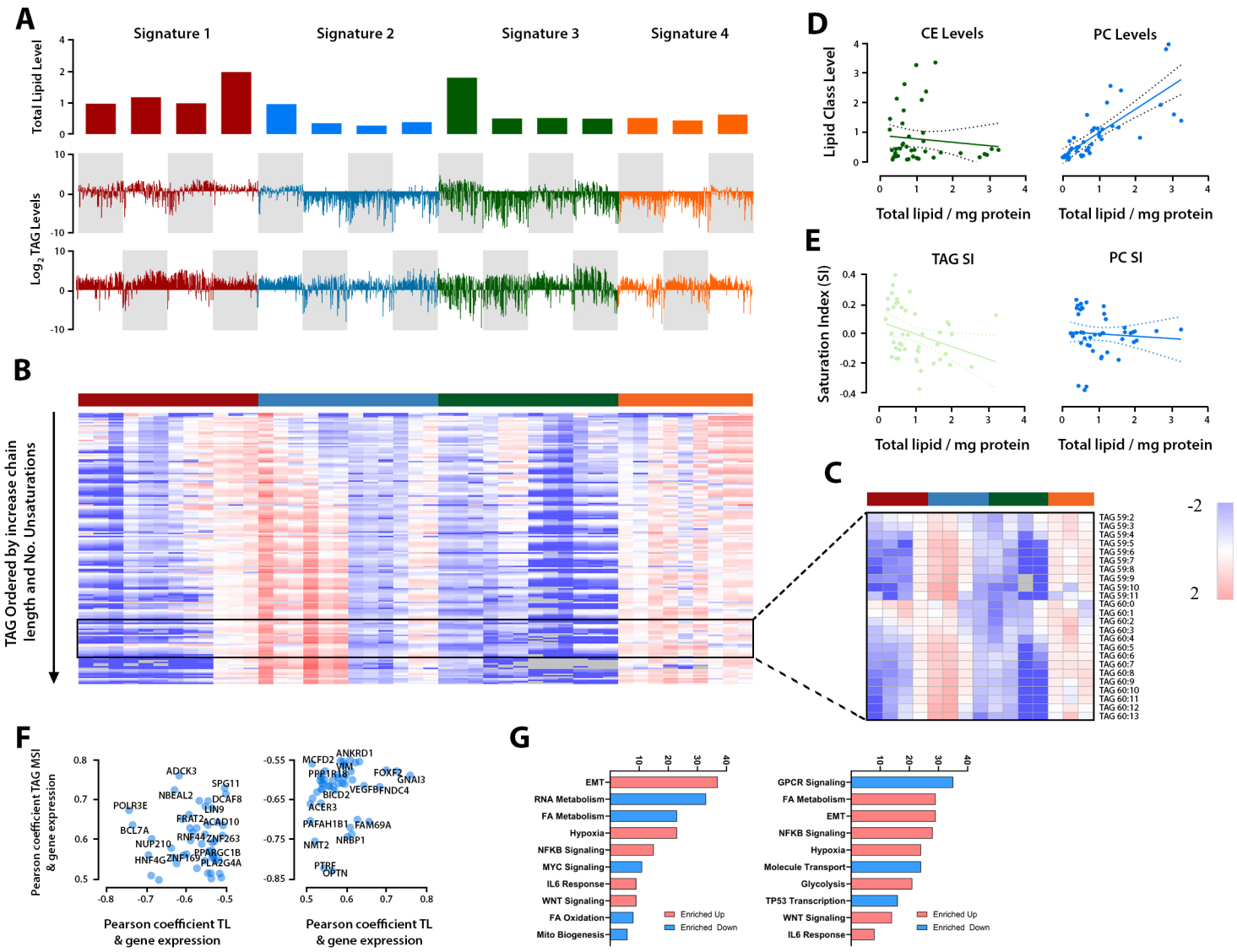

Figure 5.4. Clustering of tumour lipidome is based on lipid saturation patterns and is predictive of a progressive tumour phenotype. A. Relative total lipid level measured by mass spectrometry of 15 human derived cancer cell lines, top panel. Log2 average fold change of TAG species measured by mass spectrometry, middle panel. Log2 average fold change of TAG species normalised to total lipid level, bottom panel. **B.** Heatmap representation of the average fold change of TAG species organised by carbon chain length and number of unsaturation's measured by mass spectrometry. **C.** Zoomed in heatmap representation of panel. b looking at the average fold change of TAG species in 15 human cancer cell lines each represented as an average of three individual replicates. **D.** Pearson's correlation of mass spectrometry measured total lipid levels per mg/protein compared to the average level of CE's, left panel and TAG's, right panel. **E.** Pearson's correlation of mass spectrometry measured total lipid levels per mg/protein compared to the average saturation index score of TAG's, left panel and PL, right panel. **F.** Spearman correlation of top genes positively correlated with total lipid level and genes negatively correlated with TAG saturation index, left panel and genes negatively correlated with total lipid level and genes positively correlated with TAG saturation index, right panel based on RNAseq gene expression. **G.** Gene set enrichment analysis of genes identified through spearman correlation in panel. g utilising KEGG and Hallmarks curated genesets showing the top ten dysregulated pathways based on correlation of total lipid levels with TAG SI, left panel and PL SI, right panel. Nonpolar metabolomics were normalised to total cell number and protein levels and performed in triplicate. All data is represented by the mean and error bars represent the SEM unless otherwise stated. All correlative data analysis was performed using Matlab 2019b.

EMT processes. Finally, downregulation of TP53 signatures was observed in addition to small molecule transport and genes involved in GPCR-based signal transduction **(Fig. 5.4I)**. Given the associations between SI and key oncogenic processes such as tumour metabolism, EMT and key signalling pathways involved in the regulation of these processes, I looked to further address the impact of SI on tumour progression and survival. In order to better investigate SI, the use of CRISPR/Cas9 based technologies was employed. In the previous chapter I looked at targeting peroxisomal PL biosynthesis pathways in the regulation of lipid metabolism in $BRAF^{V600E}$ tumours. I decided to further these approaches to generate a molecular signature that could be used to investigate and probe pre-existing transcriptome-based datasets. A data analysis pipeline was developed whereby a CRISPR-based screening methodology could be used to determine a desired phenotype based on high throughput mass spectrometry analysis. A second dimension can be generated using transcriptomics utilising NGS based technologies. From the implementation of NGS from multiple experiments I can better control for nonspecific changes in the transcriptome and identify high confidence genes that can be further used to correlate and predict metabolic phenotypes in patient datasets **(Fig. 5.5)**. To investigate the possibilities of implementation of complex biological datasets to better predict metabolic phenotype I began by analysing the previously characterised lipidomic readout of 15 human cancer cell lines. In the previous section I identified that cell line lipidomic readouts were largely correlated with SI score as opposed to other metrics including total lipid levels or lipid classes. Grouping PL species based on the number of unsaturation's present in the FA chain showed that SI largely did not correlate with total lipid level and thus also not with total PL level **(Fig. 5.6A & B)**. Cluster 2 was associated with cells carrying high SI scores while cluster 3 showed cells with low SI scores **(Fig. 5.6B, left panel & C)**. This together with the TAG SI score which I had previously showed negatively correlated with total lipid levels, while PL SI scores did not show correlation with total lipid levels **(Fig. 5.4F)**. Transcriptomics of each lipid cluster was performed using the TCGA dataset and was presented previously above **(Fig. 5.3I & J)**. To further investigate that transcriptome-based changes associated with SI scores I used the previously characterised PPL null models targeting the terminal enzyme in this lipid pathway, DHRS7B. DHRS7B was shown in the previous chapter to regulate intracellular polyunsaturated PL levels. DHRS7B null cells showed a reduced SI score and were unable to pool polyunsaturated PL's in

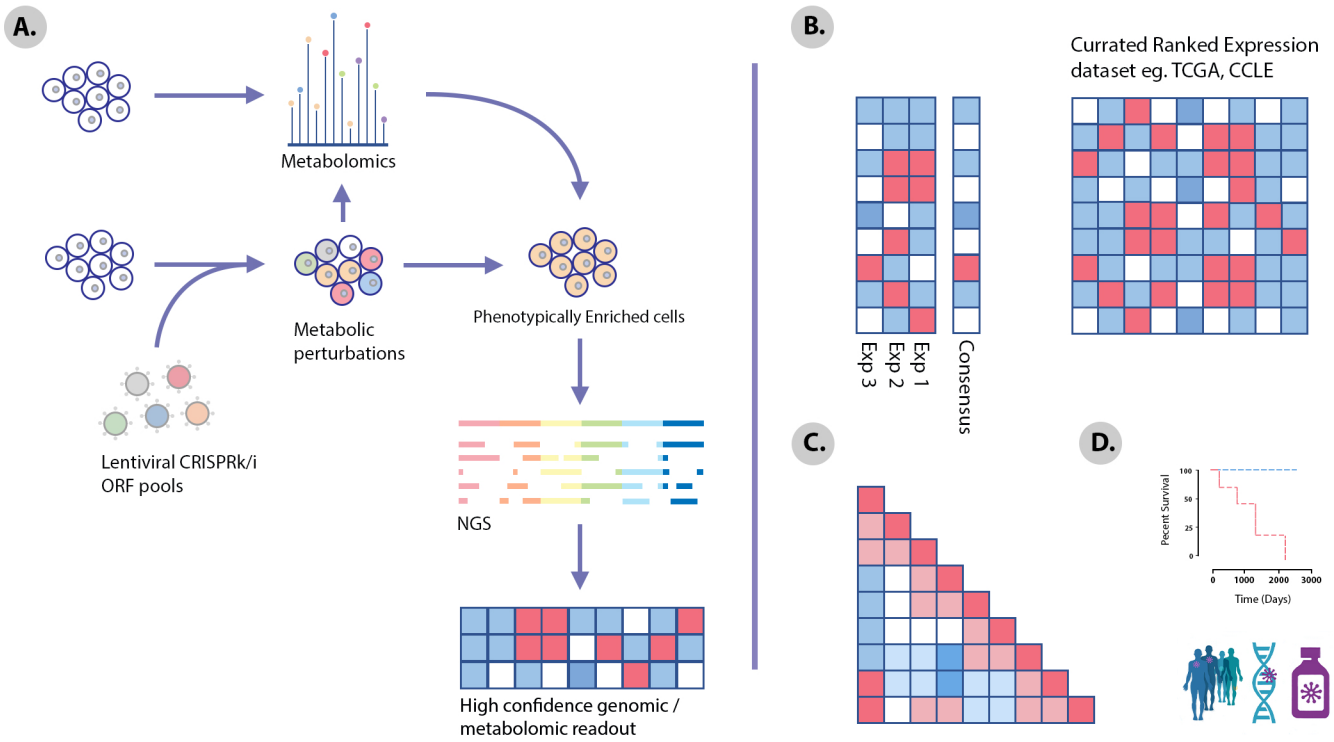

Figure 5.5. Data analysis pipeline of reverse genetics based integrated signature identification. A. Data analysis pipeline of reverse genetics-based strategy for identification of high confidence genes associated with metabolic phenotypes. Screening methods based on CRISPR/Cas9 technology can be performed using library or targeted screening methods. High throughput mass spectrometry is used to identify metabolic phenotypes in cohorts while mass spectrometry-based identification of genes associated with matched phenotypes can be processed for transcriptomic analysis and gene signature identification. **B.** Post transcriptomic analysis utilises multiple experimental models to better identify real gene targets. T-statistics based data analysis pipeline allows more effective identification of genetic signatures-based population distribution rather than raw or normalised read counts. **C.** Spearman based correlation algorithms allow for predictive probability of a sample's likelihood of a predicted phenotype. **D.** Predicted phenotype can be used to identify pathways associated with commonly used oncogenic metrics such as drug therapy prediction and survival analysis. .

response to stimuli **(Fig. 5.6B, right panel)**. Nanostring transcriptomic analysis was performed on two separate CRISPR/Cas9 models using LIM2405 and LIM1215 backgrounds and were compared to untargeted CRISPR/Cas9 control cell lines. Furthermore, DHRS7B overexpression analysis was performed again using Nanostring technologies on RNA extracted from eGFP sorted LIM2405 cells either overexpressing eGFP alone or a DHRS7B-T2A-eGFP construct. Pearson's correlation was used to generate a gene list of top correlated genes with SI scores and all models were investigated for gene set overlap. Significant levels of overlap were observed particularly with high correlated genes and cluster 2 based transcriptomic analysis. Furthermore, significant levels of overlap were seen between both DHRS7B knockout models and the DHRS7B overexpressing LIM2405 cells **(Fig. 5.6F)**. From each of the normalised gene sets a list of 88 genes were identified with two or more of the cell models showing significant and homeostatic changes in mRNA transcription levels **(Fig. 5.6D)**. Spearman ranked correlation of normalised CCLE datasets showed unsupervised clustering of the 888-cell line dataset into 5 major clusters. The first cluster was associated with SI and held all four cell lines that were measure with positive SI scores **(Fig. 5.6G)**. I further investigated the validity of the genetic signature utilising the previously discussed polar metabolomics dataset. 888 cell lines were ranked according to signature score and mutational analysis was performed looking for enriched mutations associated with a high SI probability or a low SI probability. NRAS and JAG2 showed enriched mutation levels in high SI probability cells while ACACB and KEAP1 showed enriched mutations in cells with high probability towards low SI scores **(Fig. 5.6H, bottom panel)**. In addition, unlike traditional gene set enrichment methods, discussed in Fig 5.2, the PUPL signature score was not associated with increased mutational load **(Fig. 5.6H, top panel)**. Furthermore, polar lipidomic analysis of 888 cell lines using the CCLE metabolomic dataset with cell lines ranked by SI score probability and metabolite species subjected to unsupervised Pearson based hierarchical clustering showed that polyunsaturated FA clustered with one another while the same was true for monounsaturated and saturated FA's. Furthermore, polyunsaturated FA's were enriched in high SI probability cell lines while fold change analysis of the top 10^{th} percentile of high verse low SI probability cell liens showed that a large percentage of polyunsaturated PL's were upregulated significantly in high SI probability cells **(Fig. 5.6E & I)**. Finally, gene set enrichment analysis of different cell models targeting PPL

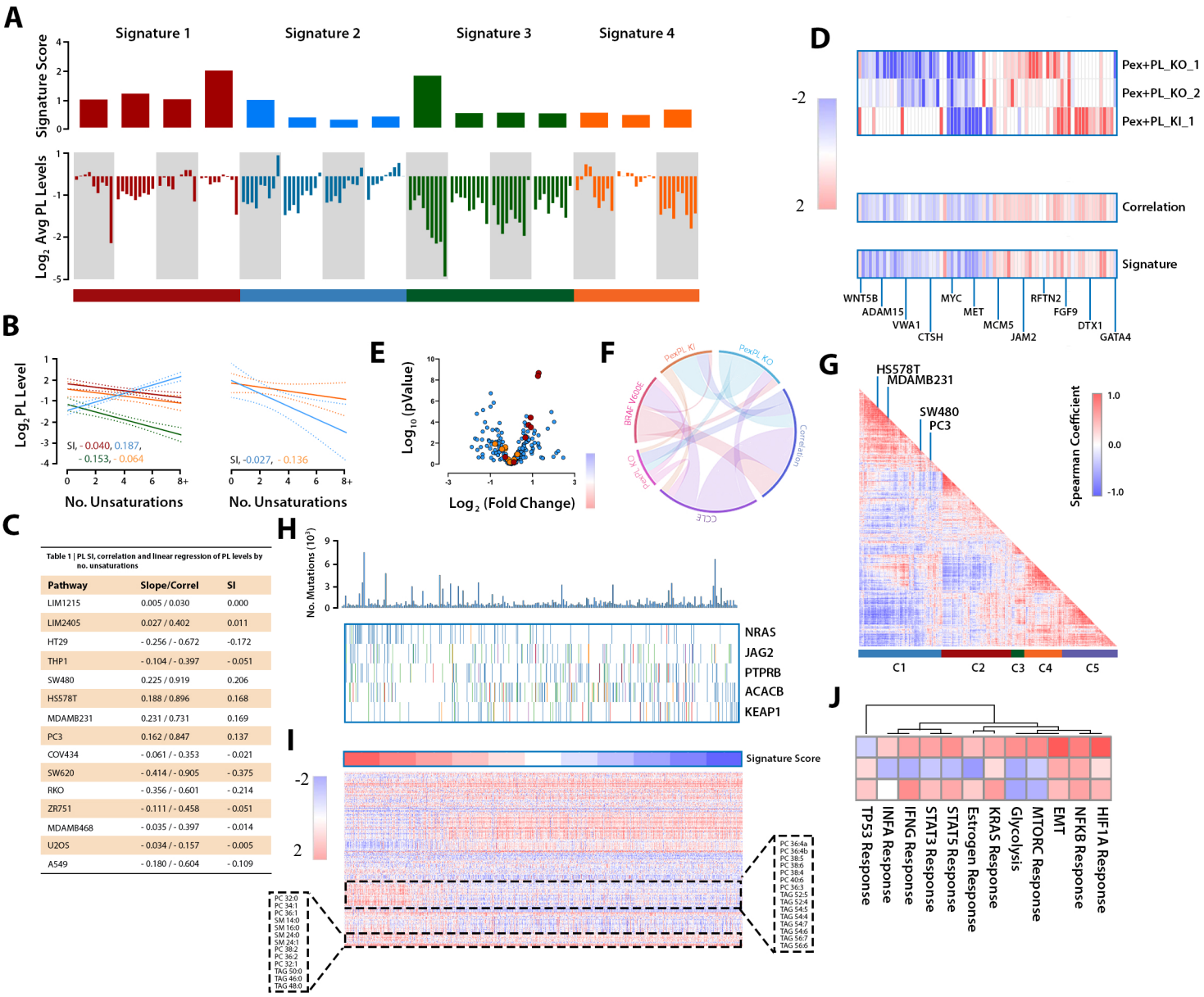

Figure 5.6. Identification of a gene signature associated with membrane associated lipid saturation level. A. Relative total lipid level measured by mass spectrometry of 15 human derived cancer cell lines, top panel. Log2 average fold change of PL species normalised by number of unsaturation's in fatty acid chain, bottom panel. **B.** Linear regression based on Log2 average fold change of PL levels normalised to number of unsaturations in the fatty acid chain in each of the four lipidomic clusters identified previously, left panel and the average linear regression of the two PPL biosynthesis null cell lines used, right panel. Table showing the linear regression, correlation and calculated average SI score of all 15 measrure human derive cancer cell lines. **C.** Table representing the slope and pearson's coefficient value of each cell line used in the analysis with a associated SI score. **D.** Identification of a group of 88 genes identified to be dysregulated in 2 or more experimental models associated with SI score. **E.** Volcano plot of 231 metabolites measure through polar mass spectrometry of the top correlated cell lines based on spearman ranked correlation of the PUPL signature identified in panel. c. **F.** Chord diagram representing the level of overlap between the 6 different cell models used to generate the PUPL signature in panel. c. **G.** Spearman based correlation matrix of 888 cell lines based on the PUPL genetic signature identified in panel c. **H.** Average mutational load of 888 cell lines in ranked order of correlation with PUPL genetic signature, top panel and the 5 heterogeneously mutated genes, NRAS and JAG associated with PUPL and ACACB, KEAP1 associated with SPL, bottom panel. **I.** Heatmap representation of 231 polar metabolites in 888 cell lines organised according to correlation with PUPL signature with rows hierarchical cluster using spearman-based correlation methods. **J.** Gene set enrichment analysis of 12 oncogenic associated signalling pathways based on differential expression analysis of three PPL knockin/out cell models. Nonpolar metabolomics were normalised to total cell number and protein levels and performed in triplicate. All data is represented by the mean and error bars represent the SEM unless otherwise stated. All correlative data analysis and differential expression analysis was performed using Matlab 2019b.

biosynthesis showed significant changes. HIF1A and NFKB responses were associated with all models used while other commonly dysregulated pathways in oncogenic tumours were shown to be differential regulated **(Fig. 5.6J)**.

5.4. Saturation Index regulates tumour chemoresistance through regulation of cancer stemness phenotype.

Given the association between SI and several key signalling pathways associated with a progressive tumour phenotype I investigated the consequence of SI on key prognostic factors including disease progression and responsiveness to common place clinical treatment options. To investigate the clinical relevance of our PUPL associated signature we assessed the correlation between tumours normalised to tissue of origin based on t-statistics in 15 tumour subtypes utilising the TCGA datasets. The 90th and 10th percentile of each tumour subtype were investigated for average patient survival. High correlating tumours indicating a predicted high SI phenotype predicted poor overall clinical survival, with 9 tumour subtypes investigated having a significance of less 0.05 **(Fig. 5.7A)**. One key prognostic factor that has been under investigation in recent years is the association between lipid biosynthesis and drug resistance. I therefore investigated the roles that PUPL may play in drug resistance primarily focusing on colorectal cancer and commonly prescribed chemotherapy drugs. The CCLE dataset clustered according to correlation with a PUPL signature that was cross referenced with cell lines that also were found in the Drug sensitivity dataset, and was further modified to remove oncogenic mutations to TP53 to remove interference with genomic-based drug resistance mechanism **(Fig. 5.6G & H)**. Average drug IC50 fold change of the top 10th and 90th percentile of peroxisomal PL signature correlating tumour cells was plotted against p-value showing an increased level of drug resistance in cell lines correlating with the PUPL signature, including the commonly prescribed chemotherapeutic 5-Fluorouracil (5FU) **(Fig. 5.7B)**. I further validated this observation utilising SI score measured with my high throughput lipidomic dataset in 15 parental cell lines, in addition to our characterised DHRS7B peroxisomal PL biosynthesis knockout/in cell lines. The

average 5FU IC50 was shown to correlate strongly with SI scores with a Pearson's coefficient of 0.78 **(Fig. 5.7C)**. To further address this mechanism, I further looked at the lipidomic landscape in response to 5FU, Oxaliplatin and combinational therapy 5-Fluorouracil/Oxaliplatin (FOX) in both wild type and DHRS7B null cell lines for the LIM1215 and LIM2405 background parental cells. Nile red labelling of lipid bodies was used to quantify lipid body formation and numbers in cells treated with either 5FU, Oxa or FOX. All treatments were shown to significantly increase lipid body number in both DHRS7B wild type and null cell lines in both LIM1215 and LIM2405 as background parental cell lines **(Fig. 5.7F)**. Furthermore, this observation was validated using high through lipidomic analysis in LIM2405 wild type and DHRS7B null cells. Measurement of major lipid storage forms CE, PL and TAG were shown to increase in response to 5FU in both wild type and null cells and while null cells had reduced overall levels, the fold increase was consistent **(Fig. 5.7G)**. Perhaps most importantly, a significant increase in both ether-linked and non-ether linked membrane associated SI score was observed in response to 5FU in LIM2405 wild type cells **(Fig. 5.7D)**. While this observation was also true for most other major forms of unsaturated lipid species, including increased unsaturation, in addition to total levels of DAG's, TAG's and LPL's **(Fig. 5.7J)**. Given the increase in unsaturated lipid levels in response to chemotherapy I further investigated the role of membrane associated fluidity utilising the DHRS7B null cell lines as a model of inhibited peroxisomal PL biosynthesis. As described in the previous chapter DHRS7B null cells are defective in the terminal steps of peroxisomal PL biosynthesis, and these cells are unable to increase cellular stores of n:3-5 unsaturated PL species. I was interested in the responses to 5FU in DHRS7B null cells given the large increase in PUPL levels, and indeed other lipid species. DHRS7B null cells were treated with either DMSO or 5FU for 48hrs and subjected to high through untargeted whole cell lipidomic analysis. 5FU as discussed previously led to a sharp increase in SI score in LIM2405 wild type cells. However, loss of DHRS7B was again shown to block the production of PUPL with only a small increase from -0.1359 to -0.0733 in response to 5FU in DHRS7B null LIM2405 cells with a small increase measured in ether linked PL levels **(Fig. 5.7K)**. This blockade in PUPL biosynthesis corresponded to an approximately 2.5-fold increase in 5FU sensitivity in the two DHRS7B null cell models **(Fig. 5.7L)**. To investigate potential molecular pathways involved in the PUPL-mediated chemo-response mechanism we investigated transcriptional changes in DHRS7B

null cells. The Nanostring cancer progression panel was used to investigate genes associated with key stages of cancer development. 80 differentially expressed genes were identified in LIM2405 null cells while LIM1215 null cells had 180 differentially expressed genes. These results reflected what was previously shown regarding $BRAF^{V600E}$ dependent downregulation of the PPL pathway leading to sustained lipogenesis and therefore loss of DHRS7B in LIM2405 cells had less impact to cellular identity and expression profiles. I identified 25 genes that were co-regulated in both LIM1215 and LIM2405 cell lines. Co-downregulated genes showed a decrease in the expression of stem cell like genes and genes associated with beta catenin transcriptional activity while upregulated genes were primarily associated with NFkB signalling and EMT indicating loss of epithelial identity and cancer stem cell properties **(Fig. 5.7E)**. Furthermore, there were also a significant number of genes that were differentially expressed in LIM1215 cells compared to LIM2405 cells. Increased levels of hypoxia and HIF1A targets involved in cellular oxidative stress such as NOS3 and HMOX1 were upregulated in LIM2405 DHRS7B null cells but were downregulated in LIM1215 cells while LIM1215 DHRS7B null cells upregulated HIF1A targets associated with glycolysis such as PGK, LDHA and PFKFB4 **(Fig. 5.7H)**. Gene set enrichment also showed a significant level of divergence in response to DHRS7B loss in LIM1215 and LIM2405 cells. Most pathway enrichment showed opposing differential expression in many pathways including HIF1A, cancer stem cell and cell cycle, which is likely a result of gene essential differences as a consequence of the oncogenic mutational landscape.

5.5. Transcriptional networks and lipid remodelling in human tumour cell lines by the PPARδ/γ nuclear receptors

In the previous chapter I dissected a complex signalling network regulated through the actions of intracellular PUPL levels and PPAR mediated transcriptional responses and activity. DHRS7B, together with other members of the PPL biosynthetic pathway and PPARγ, were downregulated in $BRAF^{V600E}$ tumours. This loss of PUPL levels drove sustained SREBF1 transcriptional activity and led to a hyper-lipidomic phenotype associated $BRAF^{V600E}$ driven cancers.

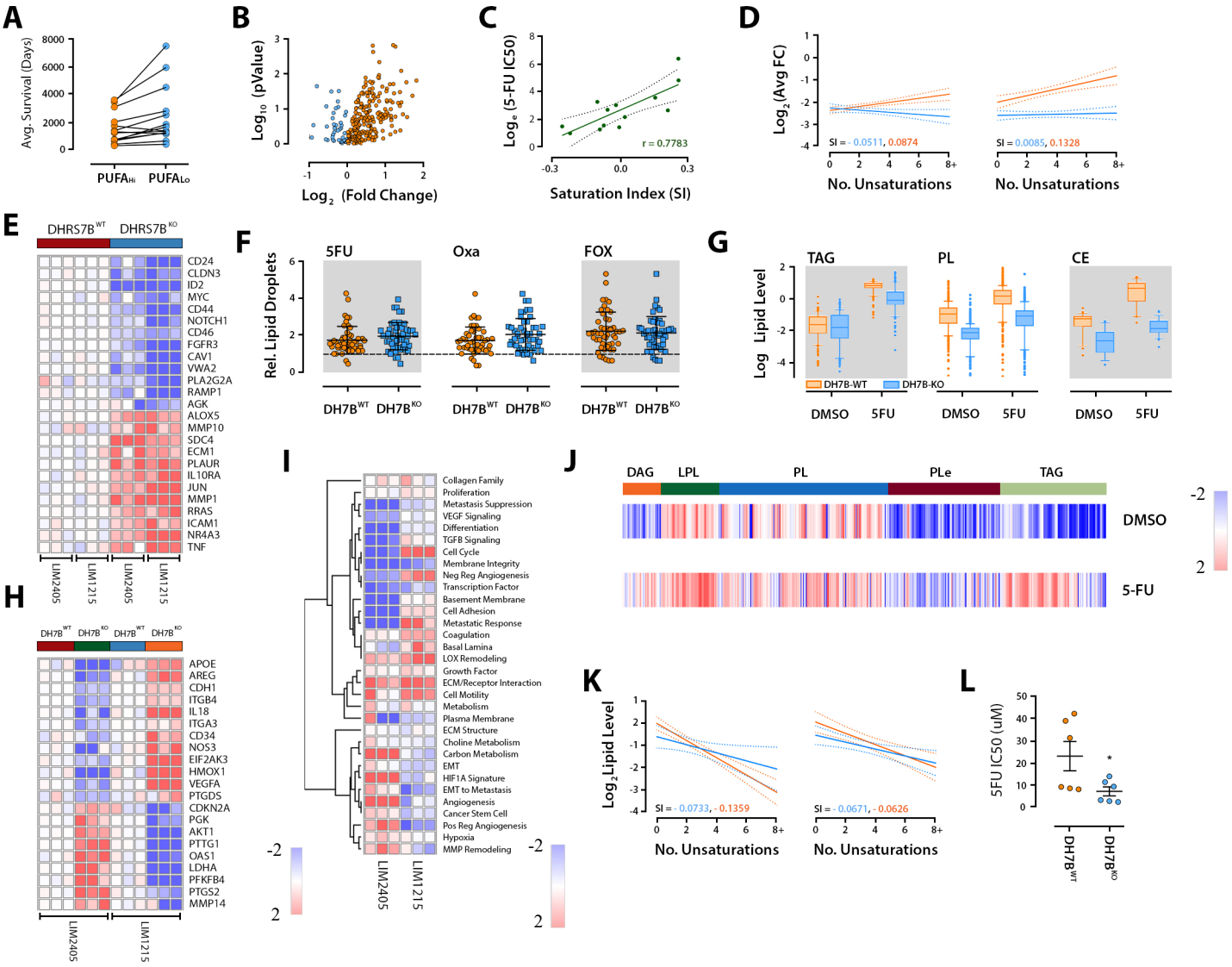

Figure 5.7. A polyunsaturated phospholipid genetic signature is associated with tumour survival and chemo/drug-resistance. A. Patient survival analysis in 15 human cancer subtypes based on previously identified PUPL signature. **B.** Log2 of the fold change of drug sensitivity in top and middle 10th percentile of cell lines associated with PUPL signature. **C.** Linear regression model of average IC50 and SI score of 15 human derived tumour cells. **D.** Linear regression model of PL species average fold change of PL by number of unsaturation in fatty acid chain of LIM2405 cells treated with 5uM of 5FU for 24 hours compared to DMSO vehicle control of non-ether linked PL, left panel and ether linked PL, right panel. **E.** Heatmap representation of the top homogeneously differentially expressed genes in two separate PPL biosynthesis null cell line models measure by Nanostring technology. **F.** Quantification of Nile red immunofluorescence of the average fold change of LIM2405 and LIM1215 wild type and DHRS7B knockout cell line models in response to 5FU, left panel, Oxaliplatin, middle panel and combination therapy FOX, right panel. **G.** Nonpolar mass spectrometry LIM2405 cells treated with either DMSO or 5uM of 5FU for 24hours of TAG's, left panel PL's, middle panel and CE, right panel. **H.** Heatmap representation of the top heterogeneously differentially expressed genes in two separate PPL biosynthesis null cell line models measure by Nanostring technology. **I.** Log2 fold change of gene set enrichment analysis of KEGG based curated gene sets of oncogenic cellular processor/signalling pathways in PPL biosynthesis null LIM1215/ LIM2405 null cell models compared to untargeted control cells. **J.** Heatmap representation of Log2 average fold change of lipid species measure by mass spectrometry ordered according to species, chain length and number of unsaturation's treated with either DMSO 5FU. **K.** Linear regression model of PL species average fold change of PL by number of unsaturation in fatty acid chain of PPL biosynthesis numb LIM2405 cells treated with 5uM of 5FU for 24 hours compared to DMSO vehicle control of non-ether linked PL, left panel and ether linked PL, right panel. **L.** Average IC50 value of PPL biosynthesis LIM1215/LIM2405 null cell treated with 5FU for 48hours compared to untargeted wild type controls. Nonpolar metabolomics were normalised to total cell number and protein levels and performed in triplicate. All data is represented by the mean and error bars represent the SEM unless otherwise stated. All treatments were performed at 5uM and 24 hours unless otherwise stated. All correlative data analysis and differential expression analysis was performed using Matlab 2019b.

Given the importance of PPARγ for the regulation of intracellular lipid metabolic pathways I further investigated the roles of PPAR signalling utilising the previously characterised lipidomic datasets and discussed earlier in this chapter. I initially quantified the transcriptional activity of the PPAR family of transcription factors in the various cell-based models. Lentiviral dual-reporter cassettes with a destabilised (ds) GFP-T2A-Luciferase open reading frame under the control of four consecutive consensus PPRE's downstream of a puromycin selectable marker under the control of a EIF2A promoter was constructed and used to generate a stable PPRE reporter cell lines used in the lipidomic analysis presented in Fig. 5.2. A cut-off of 100 arbitrary luciferase units (approximately 5 times the background) was set to distinguish between cells with induced PPAR activity compared to cells with little or no PPAR activity. Transfected cells were selected with 1-2ug/ml of puromycin for 96 hours and then 20,000 cells were plated in white luminescent 96well tissue culture treated plates and left to adhere overnight in normal cell culture media. The following day the media was changed to a low serum media (2% FBS) to minimise the effects of serum on PPRE activity, and treated with either DMSO, Rosiglitazone of GW501516 (PPARδ agonist) and left for an additional 24 hours followed by cell lysis and luciferase/protein quantification. Seven cell lines were shown to be below the PPRE activity cut-off and were determined to be PPAR inactive cells while an additional 8 cell lines were shown to be above the cutoff and deemed to be PPRE active cell lines **(Fig. 5.8A & C)**. Furthermore, to address the which PPAR family members were active in each cell line, cells were treated with either Rosiglitazone or GW501516 for 24 hours and measured for changes in luciferase activity compared to DMSO vehicle controls. $BRAF^{V600E}$ tumour cell lines, RKO and LIM2405 were shown to be PPAR active but were unresponsive to Rosiglitazone but were GW501516 Responsive while a third $BRAF^{V600E}$ tumour cell HT-29 were not PPRE active. SW480 and SW620 cells were Rosiglitazone responsive but did not respond to GW501516 while LIM1215, U2OS, HS578T and MDAMB231 were both Rosiglitazone and GW501516 responsive **(Fig. 5.8B & C)**. Analysis of the previously characterised lipidomic datasets consisting of 15 human cancer cell lines was used to address the lipid association of PPAR active compared to inactive cells. Cells were cluster according to PPRE activity as either PPAR active or PPAR inactive and then were further clustered according to agonist response. Cluster 1 corresponded to GW501516 responsive PPRE active cells, cluster 2 was Rosiglitazone responsive PPRE active cells,

cluster 3 was Rosiglitazone/GW501516 responsive PPRE active cells and cluster 4 corresponded to PPRE inactive cells. Relative levels normalised to total protein of major lipid species within these clusters showed no major differences in lipidomic profiles with the exception of cluster 4 which was associated with no PPRE activity having increased lipid levels across all lipid classes with the exception of CE's which as discussed previously was negatively correlated with total lipid levels **(Fig. 5.8D)**. Unsupervised Pearson's based hierarchical clustering analysis was performed on each of the four clusters. Cluster 4 showed significant divergence in the lipidomic profile while cluster 2 and 3 showed a very similar lipidomic profile across all cell lines found in this group and the same was observed in cluster 1 which was not similar to cluster 2 and 3 but both RKO and LIM2405 cells had similar lipidomic profiles **(Fig. 5.8E)**. Pearson's correlation of individual lipid species associated with PPARγ mRNA levels compared to PPRE reporter activity in 15 human cancer cell lines showed an interesting correlation with lipid classes. All lipid species compared to PPRE activity and mRNA expression levels showed an overall positive correlation while ether linked PL's were shown to weakly correlated with both PPARγ expression and PPRE reporter activity **(Fig. 5.8F)**. Looking at the top correlated lipid species with both PPARγ expression and PPRE activity showed that this group consisted primarily of ether linked PL with higher ordered numbers of unsaturation **(Fig. 5.8G)**. Similarly, negatively correlating lipid species showed largely monosaturated/saturated ether linked PL's or short chain ether-linked PL species **(Fig. 5.8H)**. I performed the same analysis this time looking at the PPARδ mRNA expression levels. The associations were far less consistent with several lipid classes and species associated strongly with PPARδ expression and PPRE activity consisting of ether-linked PL's, PG, LPL and SM species **(Fig. 5.8I)**. Looking at the top three upregulated lipid species identified in each cluster based on PPRE activity and response showed that PPARγ and PPARδ responsive cells showed increased levels of higher order polyunsaturated ether linked PL's species. PPARδ associated cells showed increased levels of Myelin sheath lipids while PPAR inactive cells showed increased levels of phosphoglycerates **(Fig. 5.8J)**. Finally, differential expression analysis on untreated RNAseq transcriptomes based on clusters associated with PPRE activity and agonist response as discussed previously was used to identify associated alterations in oncogenic pathways associated with PPAR signalling. Gene set enrichment analysis of the transcriptomics of the 15 cell lines based on PPRE

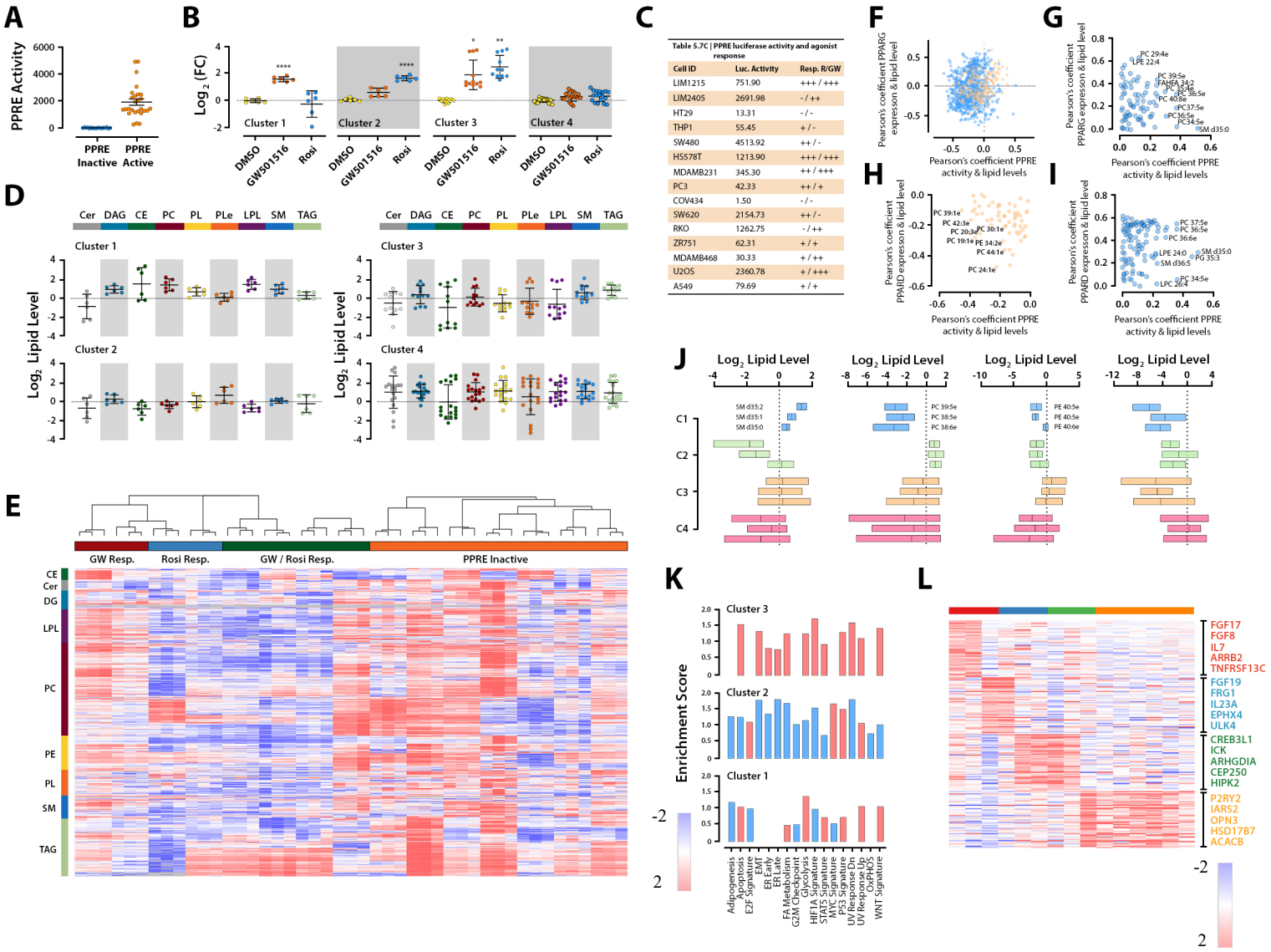

Figure 5.8. Opposing roles of PPARδ/PPARγ activity in human tumour cell reveals a metabolic signature of transcriptional activity. A. PPRE luciferase reporter activity measures in 15 human cancer cell lines. **B.** PPRE luciferase reporter activity measured in cells in response to either DMSO, GW501516 or Rosiglitazone normalised to DMSO vehicle control and clustered according to reporter activity. **C.** Table corresponds to average PPRE luciferase activity and the response to Rosiglitazone and GW501516. -, non-responsive, + 2-3 fold increase, ++ 3-4 fold increase and +++ >5 fold increase in luciferase activity. **D.** Non polar lipidomic analysis of 15 human cancer cells clustered according to PPRE activity, cluster 1 cell that only response to GW501516, cluster 2 are cells that only respond to Rosiglitazone, cluster3 are cells that respond to both Rosiglitazone and GW501516 and cluster 4 are cell that do not have significant PPRE activity (PPAR inactive). **E.** Heatmap representation of non polar lipidomics analysis clustered according to PPRE activity and agonist response. **F.** Pearson correlation of PPARγ mRNA expression level and lipid species level compared to PPRE activity and lipid species level & **G.** zoomed in of lipid species correlation between PPARγ expression level and PPRE activity with a coefficient greater than 0 or **H.** less than zero. **I.** Pearson's correlation of PPARD mRNA expression level and lipid species level with a pearson coefficient greater than 0. **J.** Log2 average fold change of lipid species associated with each cluster depending on PPRE activity and response. **K.** Gene set enrichment analysis of commonly dysregulated oncogenic pathways associated with each cell cluster based on PPRE activity and response. **L.** Heatmap representation of the top 50 genes upregulated in each cell cluster based on PPRE activity and response. All data presented is representative of three independent experiments. Nonpolar metabolomics were normalised to total cell number and protein levels and performed in triplicate. All data is represented by the mean and error bars represent the SEM unless otherwise stated. Two tailed students t-test was used to test for statistical significance ((*p < 0.05, **p < 0.01, ***p < 0.001 & ****p< 0.0001). All treatments were performed at 5uM and 24 hours unless otherwise stated. All correlative data analysis and differential expression analysis was performed using Matlab 2019b.

activity and response showed distinct changes in several oncogenic associated pathways. PPARγ largely showed downregulation of many oncogenic pathways including HIF1A, WNT and OxPHOS while PPARδ associated cell lines showed a largely contradictive profile opposing PPARγ mediated influences **(Fig. 5.8K & L)**. Interestingly, the pathway analysis was shown to also largely mimic the effects of DHRS7B which follows what was previously shown regarding the PPL/PPARγ axis highlighted in the previous chapter **(Fig. 5.8K & Fig. 5.6J)**.

To further address the roles of PPAR signalling in human tumour lipidomic reprogramming I looked to characterise the PPAR responsive cell populations associated in human cancer cell lines using fluorescent activated cell sorting compared to unsorted cell populations. The role of PPAR signalling in human cancer is rather complicated to dissect. Artificial stimulation of PPAR receptors has been an important tool in looking at their functions but amplifies experimental bias but forcing cells into unnatural cellular states. Furthermore, I showed throughout this thesis the pathway cross talk even small quantities of potent agonists such as Rosiglitazone have on cellular signalling networks including autophagy, apoptosis and stress responses. Again, highlights experiment bias within the system. Furthermore, one of the key issues with linear based transcriptome analysis was gene-set overlap. This is highlighted when looking at a group of closely related transcription factors associated with lipid metabolism. ChIPseq analysis of LXRA, PPARδ, PPARγ and SREBF1 highlights the level of overlap between the converging pathways. Transcription factor recruitment to promoter regions of specific genes showed significant levels of redundancy between PPARγ and PPARδ, shown to be co-recruited to over 1000 different gene promoters, while significant levels of redundancy with SREBF1, PPARγ and PPARδ was observed too, with 229 and 85 co-recruitments to gene promoters respectively. LXRA had significantly less redundancy compared to PPARδ, PPARγ and SREBF1 **(Fig. 5.9C)**. Furthermore, this is highlighted by looking at predicted PPAR activity utilising GSEA based methods compared to experimental analysis of PPRE reporter activity in a group of 15 human cancer cell lines. No correlation was observed between PPRE reporter activity and predicted PPAR signature scores **(Fig. 5.9E)**. The reasons become clear when you look at the genes associated with PPARγ signatures, largely consisting of key metabolic enzymes that overlap with several other well characterised transcriptional gene

signatures including SREBF1. Furthermore, given the survival advantages of sustained SREBF1 activity in addition to the negative effects of PPARγ activity on tumour growth and survival it is easy to see were false conclusion can be made. To better understand the cellular mechanism of PPAR activity in the context of tumour metabolism I looked to further investigate PPRE active cell populations compared to unsorted cell populations utilising the previously described lentiviral reporter system. Cells with high PPRE promoter activity were FACS sorted using a destabilised GFP construct separated from the luciferase construct through means of a T2A peptide sequence **(Fig. 5.9A)**. Lentiviruses packaged with the duel reported transfer vector were used to generate stable cells with a PPRE-dsGFP-Luciferase construct. Post cell selection cell populations were either sorted for GFP or re-plated. Finally, cell was left to grow for a further 96hours, and samples were taken for luciferase measurement or lipid and RNA isolation **(Fig. 5.9B)**. Luciferase activity was measured in two of the sorted cell populations. dsGFP sorted and unsorted PPRE reporter cells were plated at 20,000 cells/well in white luminescent 96 well tissue treated culture plates were left to adhere overnight. Cells were transferred onto low serum media (2% FBS) for a further 24 hours and then lysed for luminescence/protein quantification. dsGFP sorted cells showed between a 10-15-fold increase in luciferase activity compared to the unsorted populations **(Fig. 5.9D)**. RNAseq analysis of dsGFP sorted cells compared to unsorted cell populations showed several major changes in the mRNA profile. Interestingly, many of the upregulated and downregulated genes in GFP sorted cell populations compared to unsorted populations were not PPAR target genes. PPARγ associated cells showed decreased expression of oxidative stress associated genes including PRDX2, NOS2 and GPX1 while both groups upregulated various solute and lipid transporters **(Fig. 5.9F & G)**. PPARγ associated sorted cells did not show significant enrichment of genes associated with lipid metabolism however, PPARδ associated sorted cells showed upregulated levels of key lipid metabolic genes such as LPIN1, SCD and well characterised PPAR targets genes including PCK2, LDLR and FABP6 **(Fig. 5.9G)**. Finally looking at the changes in major lipid stores between GFP sorted and unsorted cell populations showed patterns. U2OS, RKO, SW620 and SW480 GFP sorted cell showed significant increases in TAG levels while this correlated with increase in DAG levels in SW620 and SW480 cell but not RKO cells. This was as descried earlier in relation to Rosiglitazone treated colorectal cancer cells. Furthermore, a second major lipid class that showed significant changes was

increased levels shown in ether linked PL's shown in SW480 and LIM2405 cells again similar to previous observations **(Fig. 5.9H & K)** This was shown to correlate with SI as per previously shown when utilising Rosiglitazone treatment. RKO, SW620 and U2OS were all shown to have increase SI scores compared to unsorted cell populations **(Fig. 5.9H & I)**.

5.6. Targeting PPARγ mediated tumour lipid metabolism to reverse PPL induced chemoresistance

As previously shown, PPARγ is a key regulator of peroxisomal PL biosynthesis. PPARγ activation is associated with increased ether lipid production, saturation index stabilisation and downregulates key enzymes through transcriptional regulation. Lipid content in tumour cells has previously been shown to influence chemoresistance (227), so I therefore investigated the effects that PPARγ agonists had on tumour cell chemoresistance. Firstly, I measure the correlation between PPRE reporter activity and 5FU resistance but found no association **(Fig. 5.10A)**. However, the effects of the co-treatment of Rosiglitazone with 5-FU showed a 2.5-fold increase in 5FU cytotoxicity compared to 5FU alone, while this effect was shown only to be effective in DHRS7B WT cells with no significant change in 5FU sensitivity in DHRS7B null cells, indicating that Rosiglitazone was potentially working through the regulation of peroxisomal PL biosynthesis **(Fig. 5.10B)**. One of the key findings from section 5.3 was the association between 5FU and chemo induced lipogenesis. 5FU treatment resulted in a sharp increase in lipid droplet formation that was shown to regulate the levels of PUPL leading to chemoresistance. Rosiglitazone was shown to negatively regulate this phenotype with co-treatment of Rosiglitazone with 5FU or Oxa showing no increase in SI or lipid droplet formation. I therefore investigated the effects of Rosiglitazone co-treatment with 5FU on lipid compartmentalisation and storage via Nile red quantification of intracellular lipid bodies. As previously discussed above, chemo-induced lipogenesis was a key alteration in cellular lipid metabolism in response to chemotherapy. Co-treatment of cells with both Rosiglitazone and 5FU relieved cells of chemo-induced lipogenesis in DHRS7B WT cells and coincided with reduced 5FU resistance, while DHRS7B null cells followed the previously described trend and resulted in a large significant increase in lipid droplet number when co-treated with 5FU and Rosiglitazone **(Fig. 5.10C)**. High throughput untargeted lipidomic analysis verified these observations

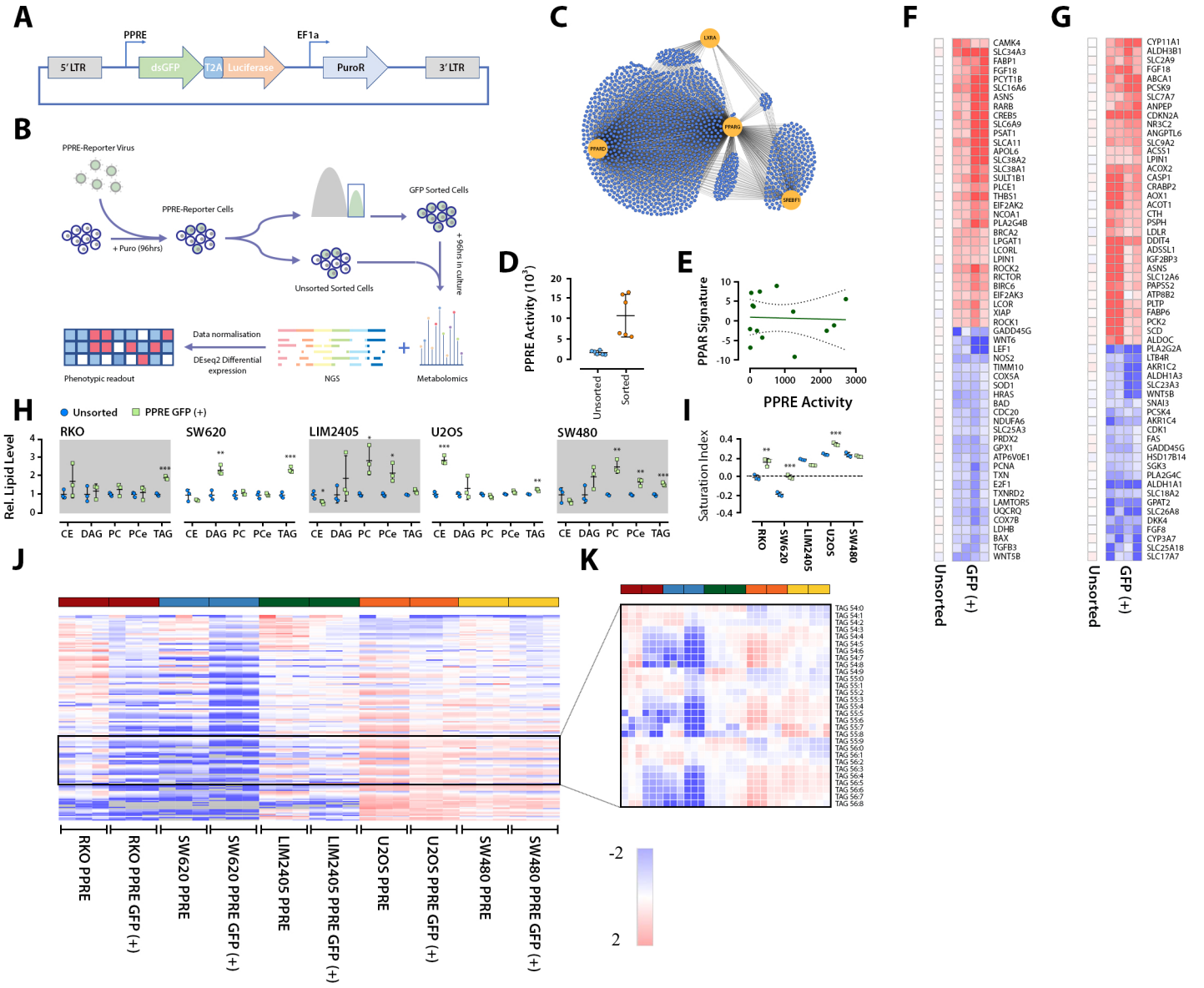

Figure 5.9. Non-invasive dissection of PPAR signalling in human tumours shows subpopulation of cells associated with changes in TAG metabolism and saturationindex. A. Cartoon schematic of the duel reporter lentiviral transfer vector used in this study with a firefly luciferase in addition to destabilised GFP open reading frame under the control of a consensus PPRE motif. **B.** experimental design associated with generating non-invasive methods to study tumour PPAR transcriptional networks by generating PPRE-GFP reporter stable cell lines and measuring phenotypical readouts including high throughput untargeted mass spectrometry and next-generation sequencing of untreated sorted cells and unsorted control cells. **C.** Network diagram representing overlaps in transcriptional networks of 4 closely related transcription factors, PPARγ, PPARD, LXRA and SREBF1. **D.** Luciferase activity in PPAR active U2OS and LIM2405 cells either left unsorted or sorted for GFP positive cells. **E.** Linear regression analysis based on Pearson's algorithms of measured PPRE luciferase activity and predicted PPAR activity based on transcriptomics of manually curated gene sets in 15 human cancer cell lines. **F.** Heatmap representation of RNAseq analysis of the top dysregulted genes associated with cell lines (LIM1215, SW620, RKO & LIM2405) that were responsive to PPARγ activation and **G.** Same as F but for PPARD activation. **H.** Mass spectrometry measure lipid levels of 5 major forms of intracellular lipid species of GFP sorted cells compared to appropriate unsorted control cells. **I.** SI score of PPAR active cell lines in GFP sorted cell populations compared to unsorted control populations. **J.** heatmap representation of high throughput untargeted mass spectrometry of PPAR active GFP sorted unsorted control cell populations of TAG's. **K.** Zoomed in representation of panel **J.** All data is representative of three independent experiments and are representative of the mean and SD unless otherwise stated. Nonpolar metabolomics were normalised to total cell number and protein levels and performed in triplicate. GFP and unsorted cell populations were sorted and left to grow for an addition 96 hours before RNA/lipid extraction while for luciferase activity 20,000 were plated into 96 well plates and left for an addition 48hours. Two tailed students t-test was used to test for statistical significance ((*p < 0.05, **p < 0.01, ***p < 0.001 & ****p< 0.0001).

with DHRS7B WT cells showing large increases in major lipid storage forms in response to chemotherapy while no significant change was observed when co-treated with Rosiglitazone. DHRS7B null cells showed a similar pattern but co-treated groups showed a large increase in all major lipid storage forms confirming the observations made in relation to increased lipid body formation **(Fig. 5.10E)**. Furthermore, as previously described, key to chemo-induced lipogenesis was the formation of PUPL with DHRS7B null cells unable to pool PUPL and this led to a corresponding decrease in chemoresistance. Co-treatment with rosiglitazone in LIM2405 DHRS7B WT cell showed that 5FU alone led to an increase in saturation index score while co-treatment with Rosiglitazone inhibited the cells ability to pool PUPL. This corresponded to DHRS7B null cells where neither 5FU alone or co-treated with Rosiglitazone were able to pool PUPL's and may explain why DHRS7B null cells showed no marked increase in cytotoxicity in response to both Rosiglitazone and 5FU **(Fig. 5.10H)**. One of the key functions of 5FU induced lipogenesis leading to increase in lipid droplet levels is thought to be a protective role against chemo-induced ER stress responses. To further investigate the pathways that are involved in the regulation of PL dependent chemoresistance I used western blotting techniques to investigate the activity of key signalling proteins involved in the regulation of ER stress. LIM1215 cells were treated with 5FU, Oxa(platin) and Rosiglitazone in combination or alone for 24 and 48hrs. I assessed key members of the ER-related stress response pathway and showed that both Rosiglitazone and co-treatment with chemotherapeutic drugs produced a marked increase in ER stress associated markers including increased phosphorylated eIF2A (at Ser63) and a transcriptional target involved in protein chaperone and folding functions, BiP. Furthermore, increased levels of phosphorylated SAPK/JNK1 were observed in response to 5FU alone in addition to Rosiglitazone, and co-treated cells with Rosiglitazone, at both 24 and 48hrs. Active SAPK/JNK is key to driving cell undergoing the UPR toward apoptotic pathways rather than protective and reparative cellular mechanism **(Fig. 5.10D)**. Similar results were observed in other colorectal cancer cell lines with ER stress markers phosphor eIF2a and BiP shown to be increased in chemo drug treated cells while this corresponded to an increase in the terminal apoptotic marker, cleaved PARP, with co-treated groups showing a greater fidelity towards pro-apoptotic responses as a result of UPR activation **(Fig. 5.10G)**. Stabile RKO cells overexpressing either DHRS7B-T2A-eGFP ORF or eGFP were generated through transfection.

Positively transfected cells were selected with GFP through FAS and were further maintained on geneticin allowing for cells with integrated expression cassettes to propagate. RKO-DH7B overexpression cells showed a significant increase in 5FU resistance while GFP alone showed similar IC50 value compared to RKO transfected WT cells **(Fig. 5.10F, left panel)**. LIM2405 5FU resistant cell lines were generated through clonal expansion of 5FU resistant clones. LIM2405 5FUR cell were validated for 5FU resistance by determining the IC50 value of 5FU. LIM2405-5FUR cells were approximately 4-fold more resistant to 5FU cellular cytotoxicity compared to parental LIM2405 cells **(Fig. 5.10F, middle panel)**. Co-treatment of LIM2405R cells with Rosiglitazone lead to a 3-fold increase in 5FU sensitivity showing similar results in wild type and 5FU insensitive cell lines **(Fig. 5.10F, right panel)**. However, the lipidomic profile of these cells were not assessed. To further investigate the direct cellular responses to overexpression of DHRS7B in RKO cell I investigated ER stress pathways by western blot analysis. RKO control-GFP transfected cells showed similar results to other $BRAF^{V600E}$ tumour cell lines with cells being largely unresponsive to Rosiglitazone alone but co-treated cell groups showed increased cleaved PARP that corresponded with increased levels of the UPR in response to co-treatment of cells with Rosiglitazone. Furthermore, an RKO-DHRS7B stably overexpressing cell line were generated through transfections of wild RKO cells with a DH7B-T2A-eGFP cassette with a geneticin selectable marker. RKO-DH7B cells were selected through the GFP marker and were further maintained on geneticin. Overexpression of DH7B in RKO cells was shown to protect cells from UPR with decreased levels of total and phosphorylated-eIF2a, in addition to downstream UPR transcriptional targets such as BiP, while decreased levels of cleaved PARP were observed in 5FU treated cells but returned to basal levels when co-treated with Rosiglitazone **(Fig. 5.10I)**. One key transcription factor acting downstream of the UPR driving cells towards survival is NFkB. Overexpression of DHRS7B in LIM2405 cells showed increased transcriptional levels of many well characterised NFkB target genes including several interleukins, TNF, MMP9 and NKFBIA/Z. Furthermore, other upregulated genes in response to DHRS7B overexpression included key genes involved in stress responses in addition to genes associated with chemoresistance and cancer stem cells **(Fig. 5.10J)**.

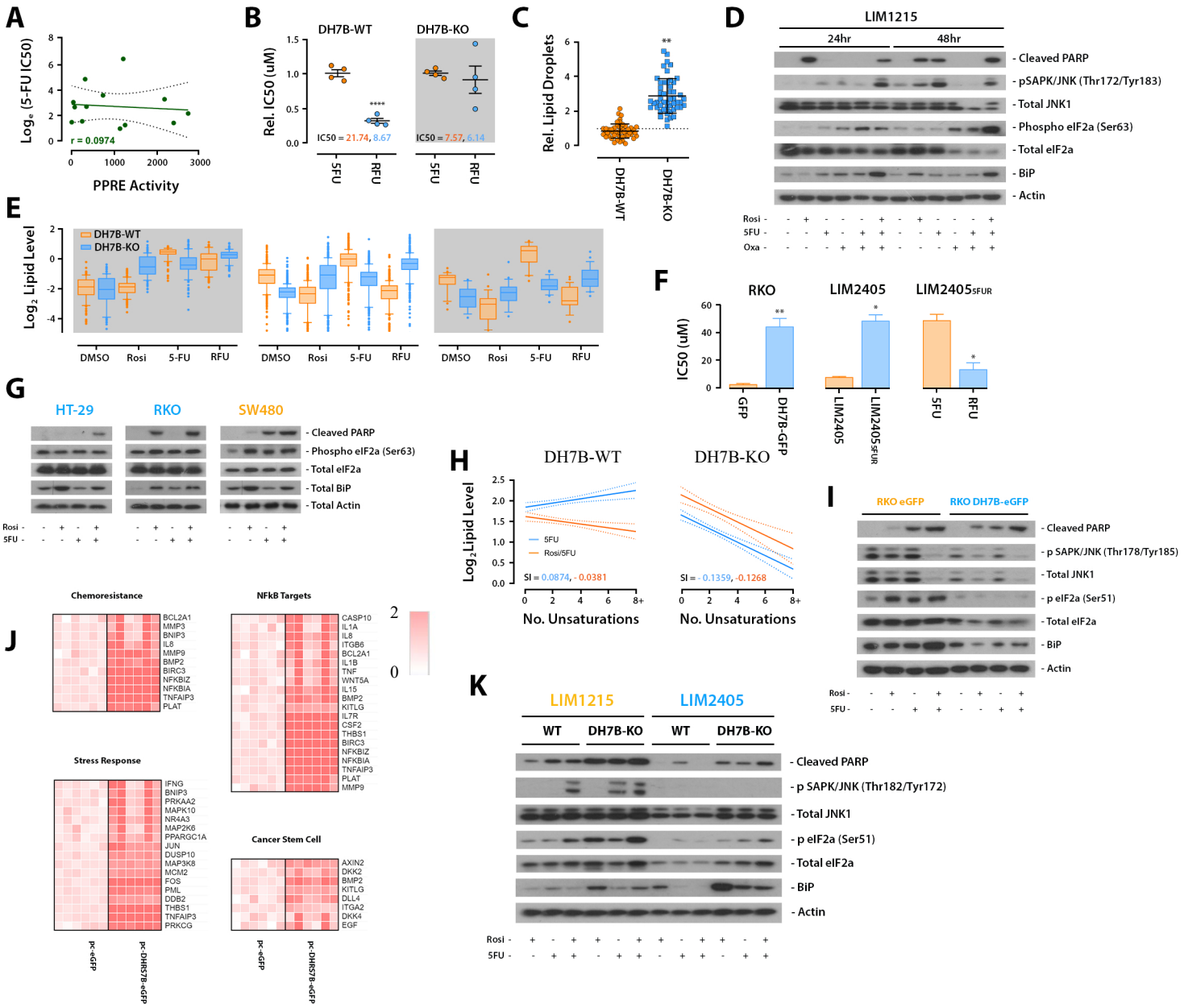

Figure 5.10. Rosiglitazone counteracts peroxisomal phospholipid mediated chemoresistance by driving ER stress induced apoptosis. A. Linear regression analysis using Pearsons based algorithms comparing PPRE-luciferase reporter activity and average IC50 of 5FU. **B.** Average relative IC50 values of LIM2405 and LIM1215 cells treated with increasing concentrations of 5FU and 1uM of Rosiglitazone, left panel and LIM1215/LIM2405 DHRS7B knockout cell models, right panel. **C.** Quantification of Nile red immunofluorescence measuring average lipid droplet fold change per cell in response to 5FU/Rosiglitazone combination treatment in LIM2405 wild type and DHRS7B null cell lines. **D.** Representative western blot analysis of LIM1215 wild type cells treated with 5FU, Oxa, FOX or R/5FU for 24 and 48hours looking a key marker associated with ER stress activation and late stage apoptosis. **E.** Mass spectrometry lipidomic analysis of LIM2405 wild and DHRS7B null cells lines in response to Rosiglitazone or 5FU alone or in combination of TAG's, left panel, PL's. meddle panel and CE's, right panel. Error bars represent the 5th and 95th percentile and box represents the median and the 25th and 75th percentile **F.** 5FU average IC50 values of Stable RKO cell lines overexpressing either eGFP along of DHRS7B-T2A-eGFP constructs, left panel. 5FU average IC50 values of LIM2405 wild compared to 5FU resistant LIM2405 cells, middle panel. Average IC50 values of LIM2405 5FU resistant cells treated with 5FU alone or in combination with a 1uM of Rosiglitazone. **G.** Representative western blot analysis of key markers of ER stress activation and apoptosis in HT29, and SW480 cells treated with either Rosiglitazone or 5FU along or in combination 24 hours post treatment. **H.** Linear regression analysis of Log2 average fold change of PL species organised according to number of unsaturation's per lipid chain in response to 5FU alone or in combination with Rosiglitazone in LIM2405 wild type cells, left panel and LIM2405 DHRS7B null cell, right panel. **I.** Representative analysis of RKO eGFP or RKO DHRS7B-T2A-eGFP stable cells treated with either Rosiglitazone or 5FU along or in combination or key markers associated with ER stress and late stage apoptosis 24 hours post treatment. **J.** Nanostring analysis of GFP sorted LIM2405 cells either over expressing eGFP alone or DHRS7B-T2A-eGFP construct with top upregulated genes sorted according to gene ontology associated with chemoresistance, stress responses, NFkB targets and cancer stem cell associated genes (n=6). **K.** Representative western blot analysis of LIM2405/LIM1215 wild type or DHRS7B null cell lines looking at key genes associated with ER stress activation and late stage apoptosis. All data is representative of three independent experiments and are representative of the mean and SEM unless otherwise stated. All treatments were performed at 5uM and 24 hours unless otherwise stated. All correlative data analysis and differential expression analysis was performed using Matlab 2019b. Two tailed students t-test was used to test for statistical significance ((*p < 0.05, **p < 0.01, ***p < 0.001 & ****p< 0.0001).

To further confirm these observations, I also analysed the changes in ER stress responses in DHRS7B null cells. DHRS7B null cells showed markedly increased levels of key ER stress markers such as phosphorylated-eIF2a and BiP while this also increased the levels of pro-apoptotic regulatory JNK pathway which correlated with cleaved-PARP levels in both LIM1215 and LIM2405 background DH7B null cells **(Fig. 5.10K)**. Transcriptionally, DH7B null cells showed decreased levels of cancer stem cell associated genes while NFkB targets were both up and downregulated, upregulated genes were largely pro-inflammatory/pro-apoptotic associated. PPRE-GFP sorted cell populations also showed significant changes to solute transporters, in addition to reduced NFkB target genes showing that DHRS7B is a key regulator of pro-survival stress responses. PPARγ activation transcriptionally regulates peroxisomal activity through both pro-autophagic responses and transcriptional downregulation of peroxisomal PL biogenesis allowing for pro-apoptotic JNK signalling in response to stress driving cells down pro-apoptotic pathways in response to chemotherapeutics **(Fig. 5.10l)**. In the previous section I described and investigated signalling networks that were governed by PUPL levels within colon tumour cell lines. Membrane associated lipid saturation levels were shown to regulate PPARG signalling outcome through an AMPK dependent signalling mechanism that ultimately led to sustained SREBF1 activity and thus drove sustained lipogenesis. Furthermore, I have shown that PUPL levels are important for metabolic dependent chemoresistance. To further investigate the cellular processes that play a role in the regulation of chemoresistance to 5FU in the context of PPAR signalling and colorectal cancer I again made use of the TCGA datasets for clinically relevant mRNA expression data. Analysis of differential expression of colorectal tumours divided into two sub-group dependent on tumour expression levels of DHRS7B into the top 10^{th} and 90^{th} percentile showed a significant proportion of genes associated with oxidative phosphorylation were upregulated in $DHRS7B^{Hi}$ tumour samples while the opposite was true for PPRE-GFP sorted cells described in previously **(Fig. 5.11B)**. $DHRS7B^{Hi}$ tumours

were shown to also downregulate HIF1A signatures and predominantly opposed the signature observed in the PPRE-GFP sorted cells **(Fig. 5.11A & B)**. Looking at the average expression of OxPHOS associated genes in DHRS7BHi vs DHRS7BLo tumours showed that OxPHOS associated genes were mostly upregulated in DHRS7BHi tumours **(Fig. 5.11C, left panel)**. The opposite held true for PPRE-GFP sorted cells associated with PPARG, with OxPHOS associated genes primarily downregulated while PPARD associated genes showed no significant change in average expression compared to unsorted controls **(Fig. 5.11C, right panel)**. To further validate these observations, I used previously described DHRS7B overexpression and null cell models. Overexpression of DH7B led to upregulation of key transcriptional regulators of mitochondrial biogenesis an OxPHOS that included PPARGC1A, PML and NUR77 **(Fig. 5.11H)**. Furthermore, in the context of oxidative stress, several key targets of HIF1A were shown to be differentially regulated in response to loss of DHRS7B. Metastatic and stress associated genes were mostly upregulated in DHRS7B null cells while changes in key glycolysis genes were shown to be dependent on cellular genotype with $BRAF^{WT}$ cells often showing opposing differential expression compared to $BRAF^{V600E}$ cells **(Fig. 5.11 H-K)**. Interestingly, these changes in oxidative phosphorylation together with subsequent HIF1A responses correlated with changes in cell survival. Colorectal tumours either expressing high levels of OxPHOS associated genes or lowly expressing OxPHOS genes showed no significant change in patient survival. However, looking at colorectal tumours overexpressing both OxPHOS associated genes an DHRS7B showed that DHRS7B correlated with OxPHOS related gene expression in addition to poor patient survival **(Fig. 5.11E)**. Furthermore, analysis of patient-matched tumour samples showed that DHRS7B was overexpressed in most stage IV colorectal tumours compared to adjected normal mucosa controls **(Fig. 5.11D, left panel)**. Conversely, DHRS7B was downregulated in metastatic disease showing a reduction in mRNA expression levels in liver metastasis compared to stage IV tumour controls **(Fig. 5.11D, right panel)**. This in conjunction with DHRS7B transcriptomic analysis indicates DHRS7B is required for cellular stress responses but is a negative regulator of metastatic disease through protection of cells from HIF1A activation.

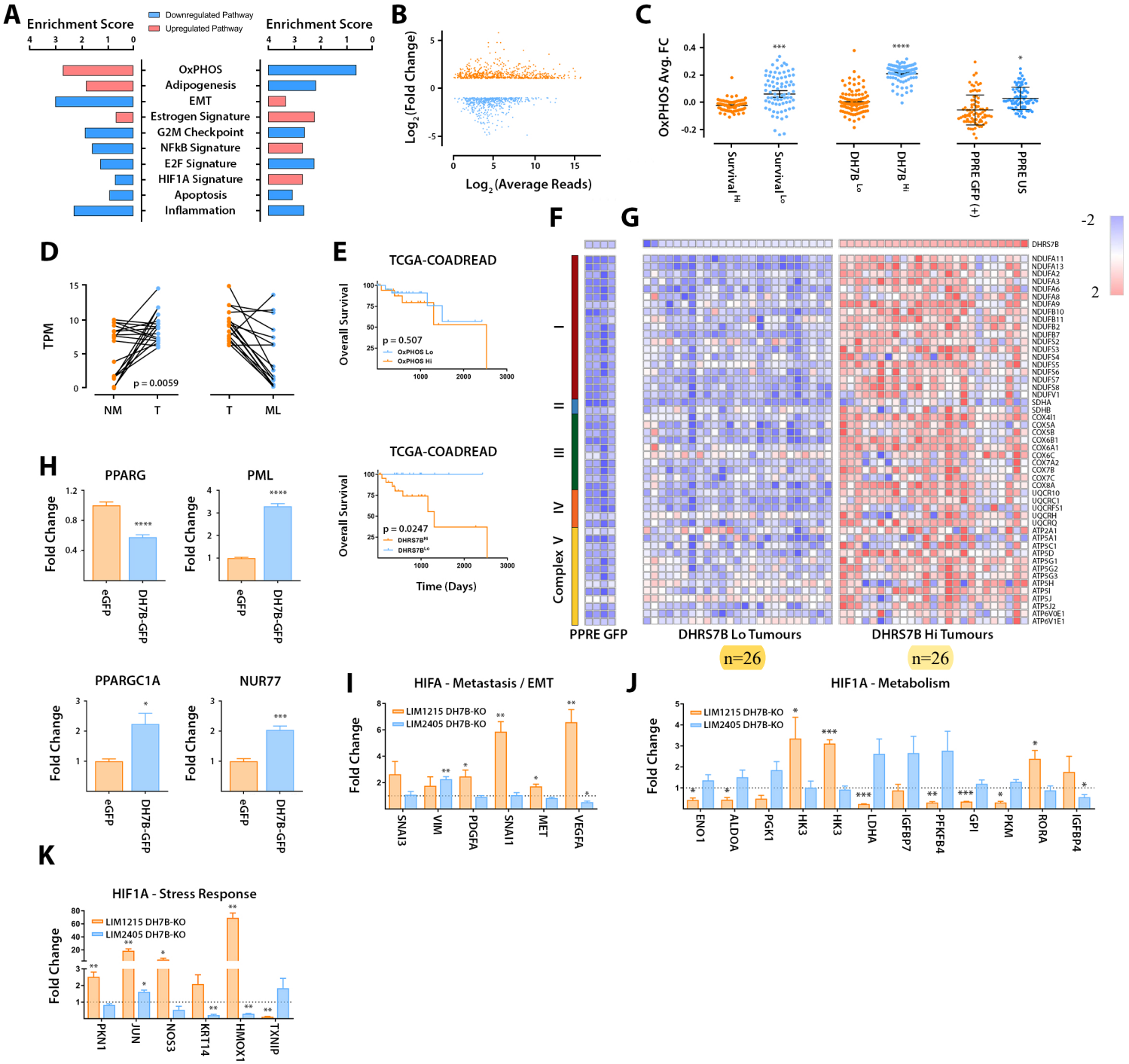

Figure 5.11. DHRS7B and PPARG are associated with oxidative phosphorylation, HIF1A signalling signatures and poor prognosis in colorectal cancer. A. Gene set enrichment analysis of RNAseq transcriptomics of PPARG associated cell, left panel and PPARD associated cells, right panel. **B.** MA plot of differential expression analysis of colorectal tumours with the 90th percentile of DHRS7B compared to the 10th percentile. **C.** Average gene expression of OxPHOS associated genes in high survival and low survival patient groups, left panel. Analysis of OxPHOS associated gene expression of DHRS7B hi expressing tumour compared DHRS7B low expression colorectal tumours, middle panel. RNAseq analysis of OxPHOS associated genes of PPARG associated sorted cell compared to unsorted wild type controls, right panel. **D.** RNAseq analysis of DHRS7B expression levels in patient matched normal and tumour tissue samples, left panel. RNAseq analysis of DHRS7B expression levels in patient matched stage IV colorectal tumours and liver metastasise. **E.** Patient survival levels of tumours overexpressing OxPHOS associated genes, top panel. Patient survival analysis of tumours overexpressing OxPHOS associated genes that also overexpress DHRS7B, bottom panel. **F.** Heatmap representation of OXPHOS associated genes measured by RNAseq analysis of PPARG associated GFP sorted cells compared to unsorted control cells. **G.** Heatmap representation of dysregulated OxPHOS associated genes from panel. g in DHRS7B high verse DHRS7B low expression colorectal tumours. **H.** Nanostring analysis of mRNA expression of key transcription factors involved in mitochondrial turnover and oxidative phosphorylation in LIM2405 GFP or DHRS7B-T2A-eGFP sorted cells. Nanostring analysis of mRNA levels of well characterised HIF1A genes associated with Metastasis, **I.**, Metabolism, **J.** and Stress, **K.** in LIM1215/LIM2405 DHRS7B null cells normalised to untargeted control cells. All data is representative of three independent experiments and are representative of the mean and SEM unless otherwise stated. All treatments were performed at 5uM and 24 hours unless otherwise stated. All correlative data analysis and differential expression analysis was performed using Matlab 2019b.

5.7. Discussion

GSEA based tools are widely implemented and common place in the bioinformatics data pipeline. The idea as an approach interpret often daunting and complex datasets such as NGS based transcriptomics by grouping ranked ordered gene lists by either p value or fold change into enriched pathway scores and easily digestible datasets while reducing the amount of many hours required to process. However, we have shown throughout this chapter and the previous chapters that GSEA is often not a useful tool for prediction of tumour metabolic states, particularly in metabolic disease models such as cancer. In this chapter, I presented a data analysis pipeline based on reverse genetics to better dissect high confidences genetic readouts associated with metabolic phenotypes in human tumours. Other groups have in recent years attempted to outperform classical GSEA based approaches first developed by the Broad institute. For example, high throughput data mining-based approaches such as the Hallmarks data set generates gene sets based on experimental annotations. However, this methodology still targets genes with functional similarities and fails to take into account confidence and promiscuity of gene sets [312]. A more recent methods to target geneset enrichment looked at slightly modified algorithms of standard GSEA. GSEA is similar to standard GSEA by looking at the ranked list of genes based on metrics including pValue or fold change in order to rank genes in the given population sample, NGSEA looks at the ranked orders network based score [317]. While classical GSEA does take into account network size and the proportion of gene overlap the authors claim the NGSEA outperforms standard GSEA significantly. Other datasets such as PID and Biocarta do take into account experimental data analysis targeting primarily growth factor induced transcriptome changes in addition to looking at the effects of oncogenic mutations into various disease models [318]. Interestingly, reverse genetic based approaches are among the earliest developed and while the experimental procedures of targeting these pathways are often rather intrusive, they provide well curated targeted datasets with high confidence.

One of the major problems I identified in chapter 3 was the poor association that some metabolic phenotypes had with targeted functional based GSEA. Part of the issues that hinder accurate prediction of genetic signatures is a numbers game, where small datasets often targeted in small cellular

subpopulations show alterations that are either cell type specific or nonspecific. The notion of FDR was introduced into transcriptomics analysis based on complications introduced into t-tests when looking at very large datasets. For example, looking at the changes across two transcriptomic datasets based on similar or even the same samples, t-test introduce the possibility that 5% of the dataset could be differentially regulated based solely on probability. This makes it hard to distinguish between true positives and false positives [319]. Small datasets are particularly susceptible to false discovery. Using multiple biological replicates can significantly increase the fidelity of accurate prediction of true positives and this is an issue that many genetic signatures do not consider. Furthermore, multiple biological datasets can also somewhat circumvent or diminish the impact of the complexity of biological systems including changes in signalling mechanism across multiple cell-based models accounting for changes in transcriptomics and other cellular process such as epigenetics. In this chapter I highlighted the effects of mutational load on GSEA based approaches to identified dysregulated metabolic pathways in human cancer. GSEA based approaches on ranked order transcriptomic datasets revealed that genetic pattern in human cancer cell lines were either linear and parametric in nature or skewed non-linear logarithmic in nature. Linear based gene sets such as what we observed in TAG biosynthesis was parametric in nature in relation to its population distribution while mutational load had no impact on signature scores. Furthermore, they were shown to often be relatively good predictors of phenotypical outcome such as TAG's biosynthesis where gene set scores correlated highly with TAG metabolite levels. Logarithmic based gene sets often showed little or no correlation and sometimes even negative correlation such as with CE's where high gene set scores was a predictor of low cholesterol levels. Furthermore, logarithmic defined gene set patterns showed positive correlation with tumour mutation load. This notion is not surprising given the principle of individualism is based on small nucleotide polymorphisms. For example, identification of 280, 843 somatic mutations associated with 36 different non-cancerous tissue sites from 547 samples showed significant associations of mutational landscape with age and race. Furthermore, C>T mutations associated with Caucasian sun exposure showed significant levels of pathway enrichment dysregulation which was further associated with chromatin state [320]. Other groups describe non-cancerous copy number aberrations of NOTCH1 associated with human skin leading to oncogenic signature in tumour free

tissues [321]. Furthermore, similar somatic impacts on cellular transcriptomics of normal human tissue has been observed in many tissues including GI tract [322-324] and brain [323, 325]. While the influence of oncogenic signatures has not been extensively investigated, cancer is fundamentally a genetic disease and it is not hard to see why these rules not only apply to normal tissue but tumorigenic tissue as well. Tumour heterogeneity is another concept that follows these principles. The idea that tumours are a mass of identical cells is not only flawed, it is not correct. Even in cell populations in controlled environments such as laboratories genetic changes are observed in monoclonal cell populations. I showed this with dissection of PPAR signalling networks. Cell sorted based on PPAR responsive cells compared to unsorted populations showed significant changes in transcriptomics of genes associated with small molecule transport, cell cycle checkpoints and oxidative phosphorylation. While this is based on transcriptional changes the principle is the same and provides a schematic of a complex interconnect biological system. Single cell sequencing is a more commonly implemented tool in oncology research. It gives the ability to investigate changes in given populations on a transcriptome level. Single cell sequencing to dissect tumour cell populations has been used to investigate tumours including melanomas and gliomas [326, 327]. Furthermore, SCS to dissect transcriptional changes associated with drug resistance in human breast cancer cell lines has also been explored validating the notion of tumour heterogeneity is no only a *in vivo* observation [328]. Furthermore, recent advances in CRISPR technology has allowed scientists to replicate heterogene*ity in* vitro utilising techniques including perturb-seq [314,315]. .

Given the issues associated with using GSEA based prediction on metabolic phenotyping I looked to better predict previously targeting metabolic phenotypes. I identified a genetic signature associated with PUPL levels using a simple method for quantification of the ratio of unsaturated fatty acids compared to saturated PL levels based on simple linear regression model. Correlation analysis of my genetic signature was shown to predict high:low ratio of unsaturation:saturated PL to a high degree. Furthermore, I was able show that that associated genetic signature was associated with chemoresistance while further demonstrating that this association was causative. Previous analysis of membrane saturation in relation to drug resistance was suggestive that saturated PL were important in regulation of cellular stress however the conclusions in regards to PL and drug resistance were largely

speculative rather than causational [329]. Investigation into the long-chain fatty acid receptor, GRP120 showed that chemo induced upregulation of GRP120 led to increased production of *de novo* fatty acid synthesis while also supporting increase expression of peroxisomal ABC fatty acid transporters through actions of NFkB [330]. In addition, ABC fatty acid transporters are currently under investigation in their potential use as a chemosensitizer [331, 332]. I saw similar biological response in our various PPL biosynthesis models. Overexpression DHRS7B led to increase expression of key NFkB target genes while downregulation of peroxisomal PL biosynthesis pathway in $BRAF^{V600E}$ tumour cells also correlated with decreased 5FU resistance compared to $BRAF^{WT}$ cells correlating with SI. Furthermore, other groups has associated fatty acid desaturation as a key marker of cancer stem cells while I showed similar observations in colorectal cancer cells with loss of DHRS7B leading to loss of stem-like phenotype leading to a mesenchymal phenotype [217, 333]. SCD1, the gene that is thought to be a key promoter of lipid desaturation has also been associated with similar tumorigenic features. SCD1 has been associated with chemoresistance and stem-like phenotypes in hepatocellular carcinoma and lung carcinoma in addition to breast, colorectal and prostate [212, 213, 334, 335]. Furthermore, as observed with my PPL models a clear distinction was observed in pushing ER stress responses towards pro-apoptotic JNK signalling activation which was not observed in DHRS7B overexpressing cells and wild type cells under moderate selection. Several other groups have shown the importance of unsaturated FA in protective roles in ER stress responses [161, 336, 337]. While links between chemoresistance and lipid body formation have also been formed I found that loss of PUPL's didn't impact the formation of lipid droplets but did directly impact the ability of cells to survive in chemo-enriched media [227]. Despite the overwhelming evidence to support the roles of polyunsaturated fatty acids levels in tumours as key regulators of stem-like cell phenotype and chemoresistance several studies have shown opposing results. Omega 3 unsaturated fatty acids have been investigated as chemo-sensitising agents in many clinical studies and were meet with varied results (see review, [338]). Other groups showed that co-treatment of COLO320 DM cells with eicosapentaenoic acid (EPA) or steric acid (SA) in conjunction with Oxaliplatin and 5Fluouracil led to the reduction of IC50 values with EPA but not SA in total cell populations but this effect was not evident in stem-like cell populations [339]. Similar results were shown in a study co-treating human cancer cell lines with docosahexaenoic acid and doxorubicin using

two glioblastoma cell lines, A172 and U87MG while two additional lung cancer cell lines, A427 and SK-LU-1 showed no increase in doxorubicin toxicity while *in vivo* analysis of MDAMB231 based xenograft models showed an increase in response to doxorubicin [340, 341]. In the previous chapter I showed that PUPL levels were a crucial regulator of PPARγ signalling while, PPARγ was shown to regulate PPL biosynthesis positively and increase membrane associated PL unsaturation. One of the key features associated with chemotherapeutics at a cellular level is ER stress associated lipogenesis or chemotherapeutic lipogenesis. Although the function of this cellular response is not fully known some groups have attributed the large influx of lipid storage as a protective role against chemotherapeutics driving chemoresistance and cell survival pathways [227, 342, 343]. While the effects of chemo induced lipogenesis and lipid body formation was attributed as the primary driven of chemoresistance, I showed that chemoresistance was largely independent of lipid droplet levels. While discrepancies in chemoresistance of some cell lines used across labs were significant. HT-29 cells were shown to harbour large number of lipid bodies per cell, my results reflected this observation where HT-29 cells had the highest lipid body levels across all the colorectal cancer cells used, I showed that HT-29 cells were very sensitive to 5-FU while groups describing that lipid body formation as a key driver of chemoresistance showed a 100 fold increase in 5-FU resistance to what was measured in our lab and in the Broad institute [227, 344, 345]. DHRS7B null cell lines also exhibited marked increase in chemo-sensitivity. Looking at the saturation index of PL in these cells showed a strong positive correlation with high PUPL ratios with 5-FU resistance and indeed many other cytotoxic drugs. I validated these findings using our lipidomic dataset. There is little in the literature addressing the associations of phospholipid metabolism and tumorigenesis. Looking at high and low risk patients with Hepatocellular carcinomas showed that saturated species of LPL taken from plasma samples were associated with low risk patients. However, the depth of the lipidomic analysis was not great and given the vast number of lipid species and variations there was an overall poor coverage of the human lipidome [346]. Phospholipid phosphatases, important for the generation of DAG's from PA have been extensively associated with tumorigenesis. PLPP4 was demonstrated to be overexpressed in 8 paired lung cancer tumours and correlated strongly with clinicopathological features including tumour grade and prognosis [347]. While mediators of the PPL biosynthesis

pathway upstream of DHRS7B have been shown to regulate tumour progression. GNPAT overexpression in hepatocellular carcinoma through cMYC was associated with poor clinical prognosis and stabilised USP30 leading to stabilisation of lipid metabolism and mitochondrial stability [348]. Furthermore, AGPS knockout studies showed that loss of PPL biosynthesis pathways led to reduced cell viability and decrease tumour growth in breast cancer [302]. While inhibitors of PPL pathway through targeting AGPS have been explored and show promise as an anti-tumour therapeutic [349].

While one of the key features of DHRS7B knockout cell lines was decreased PUPL levels driving chemosensitivity. This was also associated with other anti-oncogenic features. DHRS7B was shown to regulate pro-survival signalling pathways protecting cells from chemo-induced ER-stress and driving chemoresistance. One the other spectrum loss of DHRS7B was associated with increased a HIF1A signature and ultimately increase metastatic potential. Loss of DHRS7B in LIM1215 cells showed increased transcriptional levels of key regulators of EMT including members of the SNAIL family in addition to marker genes associated with EMT such as vimentin. While the phenotypical output was not validated through use of migration assays this does provide an insight into the possible issues with targeting PPL pathway as a therapeutic. Other groups have shown similar results while looking at upstream enzymes of DHRS7B. AGPC knockdown was shown to drive loss of CSC and epithelial phenotypes through downregulation of CD44 and E-Cadherin while this coincided with an increase in TWIST and SNAIL in HEPG2 and U87 cells [350]. Similarly, PPARγ has been shown to regulate facets of EMT and is part of the reason why is association with cancer as a tumour suppressor is conflicting. While its function in the regulation of EMT is contradicting itself. For example, PPARγ agonism was shown to promote EMT through Rho GTPase activation of ERK1/2 [351]. Other groups have described the exact opposite where targeting PPARγ inhibited EMT through SMAD3 antagonism [352]. Clearly the roles that PPARγ plays in regulation of EMT appear to circumstantial. The fact that PPARγ regulated chemoresistance through regulation of PUPL levels makes it an interesting possibility to target chemoresistance. While some of the literature suggests that PPARγ plays a role in regulating EMT and given the result presented here it is likely this is a consequence of downregulation of the PPL pathway. In addition, restoration of PPARγ signalling in ovarian tumours

was shown to have similar effects. Constitutive activation of NFκB regulation of XIAP expression was shown to drive downregulation of PPARγ signalling while combined therapy through PPARγ agonists and XIAP inhibitors was shown to effectively induce cellular apoptosis [353]. Peroxisomal biogenesis pathways have also shown to be involved in EMT. TGF induced downregulation of PEX13 was shown to be important in driving EMT and decreased numbers of peroxisomes [354]. Given the associations made between targeting PL biosynthesis and regulating chemotherapy resistance, DHRS7B is a possible therapeutic target. However, as discussed, the difficulties lie in the associations made between loss of DHRS7B and EMT while utilising PPARγ to regulate this pathway other groups have shown that a metastatic response is possible. Development of DHR7B inhibitors and linvestigating PPARγ signalling in the context of EMT and conjunction with metastatic inhibitors would provide an interesting next step in evaluating the use of PPARγ agonists targeting PPL pathway for cancer therapeutics.

Chapter 6 – General Discussion

6.1. General discussion and conclusions

High throughput computing capabilities are integral for many aspects of modern biology including data processing of complex tasks such as transcript mapping of NGS data that would take many lifetimes to process manually. Computers have the ability to perform relatively simple tasks in rapid succession and process many factors more accurately and efficiently than manual processing. One of the challenges that allude researchers is the ability to accurately model biological system for predictive capabilities and risk association with diseases. Tumour metabolism is a relatively complicated topic that in recent years has shed light on how tumour proliferate uncontrollably and develop mechanism that led to drug desensitisation. Several recent papers have highlighted the importance of lipid metabolism in drug resistance while key oncogenic driver mutations have also been shown to be dependent on the metabolic rearrangements that are consequential to these mutations [156, 227, 280, 283]. However, targeting metabolism is often difficult due to significant levels of pathway redundancies and the inherent similarities between normal and oncogenic transformed cells. Targeted cell therapy against mutant forms of IDH1/2 are among the more common and successful methods targeting oncogenic metabolism. IDH1/2 mutations are commonly found in Glioblastoma and acute myeloid leukemias while mutant forms of IDH1/2 are responsible for abnormal and increased levels of D-2-hydroxygluterate leading to aberrant changes in the cellular epigenetics often resulting in oncogenic transformations [355]. Two mutant specific inhibitors have been developed AG- 120 (Ivosidenib) and AG-221 (Enasidenib). Both of which have been used to treat AML in xenograft mice models in addition to human clinical trials with both having been approved for use to treat AML [356-359]. Despite IDH1/2 accounting for 6-18% of AML and significantly more frequent in gliomas, accounting for ~50% of lower-grade gliomas and more than 80% of recurrent secondary gliomas, IDH1/2 mutants are far less common in other solid tumours [360, 361]. Targeting lipogenesis as a therapeutic has been explored with some success. COX2 inhibitors are currently in use targeting familial adenomatous polyposis (FAP) and have been investigated for potential use in breast cancer [362]. Other investigated targets include ACSS2, ACLY and FASN all targeting *de novo* lipogenesis [69, 72, 232, 363]. More recent research has shown interest targeting

lipid metabolism through lipid transporters such as CD36 [55]. Metabolic reprogramming in other solid tumours including epithelial derived gastrointestinal and breast cancers that were largely described in this thesis are somewhat more complex. Oncogenic mutations can often perturb the metabolic balance in a certain direction while metabolic lipid reprogramming has been described as a key feature observed in many tumorigenic processes such as drug resistance and cancer stem cell-like phenotypes [205, 217]. A recent metanalysis of the TCGA datasets has shown associations between downregulation of oxidative phosphorylation genes as a key process required in primary to metastatic tumour transitions. TCGA datasets were analysed using computational geneset pathway analysis of solid human tumour transcriptomes, in much the same as I have described in chapter 3 [246]. This data was in line with the observations that I showed regarding targeting peroxisomal phospholipid biosynthesis pathways originally in $BRAF^{V600E}$ tumours, in addition utilising this as a model to mimic $BRAF^{V600E}$ induce lipid remodelling. Consequentially, cells lacking peroxisomal phospholipid biosynthesis had high saturation:unsaturated phospholipid ratios leading to sustained SREBF1 transcriptional activity through loss of PPARγ signalling which was shown to negatively regulate mSREBF1 accumulation through stimulation of the AMPK pathway.

BRAF mutant tumours are not the only tumour subtypes that have aberrant metabolic reprogramming. Despite showing that $BRAF^{V600E}$ tumours cells held much higher proportions of lipid droplets, coinciding with increase cellular lipid levels in almost all lipid species except for triglyceride's and Cholesterol ester's, comparison of $BRAF^{V600E}$ tumours cells against additional human cancer cell lines showed that $BRAF^{V600E}$ colorectal cancer cells had significantly reduced lipid levels compared to other tumour cell lines investigated. This indicates the existence of several transcription pathways in which a tumour cells can manipulate and exploit to gain control over cellular metabolism. Metabolic profiling of solid human tumours revealed significant redundancy among grouping of tumours. Tumour subtypes such as pancreatic, liver and kidney tumours showed largely defined groups based on metabolic signatures while most other tumour groups were randomly clustered in a super cluster associated with several different topological tumour subtypes. Colorectal cancer was somewhat more interesting with two major clusters defined by a HIF1A signature identified. Tumour with high SREBF1 signature were

largely defined to a smaller HIF1A active tumour subtype and this coincided with tumours with a low PPARγ subtype. This is a common observation, and SREBF1 has been associated with oncogenic features in colorectal such as drug resistance [156, 161, 376], proliferation and survival [155, 161] and metastasis [158, 159]. Furthermore, SREBF1 is known to have similar pro-oncogenic effects in other tumours including melanoma, glioblastoma and breast [157, 160, 162]. Loss of PPARγ as shown in chapter 4 is a key attribute to sustained SREBF1 activity. Induced PPAR activation led to a reduction of mature forms of SREBF1 to undetectable levels 24 hours post treatment while the same observation was made where Rosiglitazone induced AMPK phosphorylation and autophagy. Furthermore, this process was shown to be critical for Rosiglitazone induced lipophagy where inhibition of autophagy through pre-treatment of colorectal cancer cells with 3MA or chloroquine led to an inhibition of Rosiglitazone mediated lipolysis. In addition, DHRS7B was shown to a be a player in the regulation of this process. Loss of DHRS7B and thus loss of polyunsaturated phospholipid's was shown to be a key driver of SREBF1 sustained activity and was observed in both $BRAF^{V600E}$ and $BRAF^{WT}$ colorectal tumour cells and correlated with autophagy resistance. Loss of DHRS7B led to the inability of AMPK to target downstream effectors and consequentially loss of effective autophagosome formation. This is interesting because AMPK is a known regulator of mSREBF1 transcriptional stability. Phosphorylation of SREBF1 by AMPK at Ser372 is a critical regulator of mSREBF1 transcriptional activity while further phosphorylation events at Ser430 and Thr426 are thought to regulate protein stability [173, 377, 378]. Furthermore, polyunsaturated free fatty acids are also known to regulate SREBF1 transcriptional activity through AMPK dependent mechanism while other groups have described phosphocholine/free polyunsaturated phospholipid regulated SREBF1 non-canonical pathways [296, 379-381]. While the roles of DHRS7B until now have been relatively unclear other than its enzymatic activity in the peroxisomal phospholipid biosynthesis pathway protein homologues in ***S. Cerevisiae*** has shown similar result presented in this thesis [290]. The yeast homologue to DHRS7B, Ayr1p was shown to regulate lipid droplet formation in addition to efficient autophagosome formation although the signalling mechanism were not addressed while another group demonstrated that loss of Ayr1p was associated with increase triglyceride levels however they associated this with Ayr1p associated triglyceride lipase activity [303, 382]. In addition, polyunsaturated phospholipid levels have also been associated with

autophagy induction. Phospholipase groups A and D have been shown be involved in nutrient depletion dependent autophagy mechanism while docosahexaenoic acid was shown to induce AMPK/mTOR dependent autophagy in p53 wild type human tumour cells [383-386]. DHRS7B was shown to a be a key regulator of AMPK regulated tumour lipogenesis and a schematic of the proposed mechanism can be found in **(Fig. 6.1)**.

One of the major shortcomings of the Depmap is limited in the number lipid species identified. Five lipid classes (CE, PL, LPL, SM, TAG) are identified with each class only representing between 5-20 lipid species. This is not surprising given the major aim of this study was to investigate polar metabolomics in many cancer cell lines. My dataset utilising high throughput non-polar lipidomics. To address this issue, lipid enrichment targeting 22 different lipid classes and more than 950 lipid species were identified across all 15 human cancer cell lines. This allowed for a much more thorough view of the lipidomic profile. A recent study looking at transcription factor profiling utilising computational identification of transcriptional networks identified by matched polar, non-polar metabolomics and RNA transcriptomes was developed to analyse a large cohort of human cancer cell lines [255]. Metabolic profiling of 54 tumour cell lines from 8 different tissues of origin matched with transcriptomic analysis was used to generate transcriptional signatures associated with transcription factor networks. Much of the analysis was based on GSEA based approaches and thus was still confined by the limitation of GSEA based network associations. HIF1A signalling was investigates and validated by siRNA-based methods to confirm the associations made in the models [255]. However, HIF1A and glycolytic processes were one of few biological processes that behaved in a linear fashion with transcriptional regulation. Lipid metabolism was largely not discussed in detail nor was it experimentally validated. The limitations of GSEA based approaches in relation to tumour metabolism highlighted in chapter 5 most likely applies to this dataset. One of the key findings of chapter 5 was the association that mutational load played on pathway dysregulation in a phenotypical independent manner. Pathway signature correlated strongly with non-parametrically skewed datasets (logarithmic) while did not always correlate with predicted phenotypic outcome. Furthermore, changes in metabolites from the analysis I performed was largely mutation independent while the genetic signatures

investigated related to phospholipid saturation was independent of mutational load but predicted saturation index accurately across multiple tumour tissues of origin. Other groups have studied patient tumour samples normalised to normal non transformed tissue samples targeting the polar metabolome and showed a largely mutation independent change in metabolism in colorectal cancer. Changes in metabolites in all stages of colorectal cancer was shown to correlate with MYC, MET mRNA expression, in addition to several interleukins indicating a consequential relationship between metabolism and tumorigenesis [387]. MYC expression levels were shown to be dysregulated in both DHRS7B null and overexpressing cell models but was not investigated further, however this paper largely ignored lipid metabolism.

The non-polar lipidomic dataset presented in chapter 5 showed no significant pattern displaying mutational dependence or tissue of origin affecting the lipidomic profile. However, several lipid classes were highly upregulated more frequently in some topological tumour subtypes compared to other. For example, breast cancer cell lines showed upregulation of several sphingomyelin lipid species that were not observed in other tumours from different tissues of origin. While myelin sheath lipids are primarily associated with neuronal tissue, they are found in several other tissue types including breast cancer cell lines while analysis looking at the levels of lipids compared to normal untransformed cells has shown that upregulation of sphingomyelin is a common attribute in breast tumours. While use of sphingomyelin as a biomarker in brain tumours has been explored, the roles that sphingomyelin play in tumour metabolism is controversial with conflicting evidence [388-391]. Furthermore, in the context of colorectal cancer several lysophosphoethanolamine species were significantly upregulated compared to other tumours from different tissues of origin. This has also been described previously, with lysophosphoethanolamine associated with cell survival in nutrient starvation conditions [392]. While the TCGA and CCLE datasets provide a useful tool for transcriptomics and tumour metabolism, recent advances in next-generation sequencing technology has made single-cell sequencing a relatively routine application available for researchers. Much of this technology has been used to identify cell populations in mouse tumour or xenograft models primarily focusing on immune cell populations and tumour associated fibroblasts. A recent paper has used this technology to dissect tumour metabolism across

multiple cells types. Overexpression of the TCA cycle and OxPHOS was observed in several malignancies while other metabolic associated pathways such as fatty acid metabolism and amino acid metabolism were overexpressed in a small percentage of malignancies [393]. Despite this, computational approaches looking at tumour metabolism continue to primarily focus on data mining-based approaches, while this is highly efficient the associations made through these applications remain circumstantial. Tumour metabolism is an ever-increasing research topic as the roles it plays in so many aspects of tumour biology are critical for successful therapeutic intervention. It remains clear that tumour metabolism remains convoluted and more work is required to gather a better understanding of the mechanisms at play and for a better understanding of crucial processes in tumours such as drug resistance and metastasis.

One of the key processes regarding tumorigenesis is late stage epithelial to mesenchymal transition associated with metastatic disease. $BRAF^{V600E}$ and CRISPR/Cas9 generated DHRS7B null cell models also showed a more mesenchymal cellular phenotype compared to wild type controls, while this coincided with dysregulated HIF1A signalling and high levels of OxPHOS associated gene expression that correlated with DHRS7B expression in a clinical setting. Transcriptomic analysis of PPARγ responsive GFP sorted cell populations compared to unsorted control populations revealed that PPARγ active cells downregulated ~33% of OxPHOS complex genes. Furthermore, co-treatment of tumour cells with the chemotherapeutic 5FU and Rosiglitazone led to a 2-4-fold increase in 5FU sensitivity. PPARγ and its roles in tumorigenesis has had a complex and conflicting history despite showing great efficacy for anti-proliferative effects in many solid tumours [107, 151]. Early studies in both *in vivo* and *in vitro* showed contrasting results in the context of gastrointestinal cancers. Some groups showed that PPARγ was anti-oncogenic leading to G1 cell cycle arrest while other groups showed that ligand dependent activation of PPARγ in $APC^{Min/+}$ mice led to enhancement of polyp formation [144, 145, 364, 365]. However, considering the results presented in this thesis it is likely that while PPARγ influences cell proliferation it also coincides with increased metastatic potential making its use as a therapeutic potentially more complex. The roles of PPARγ in relation to cell motility has been documented in the intestinal mucosa with PPARγ associated with terminal differentiation and epithelial

motility [366]. Furthermore, much of the anti-oncogenic response attributed to PPARγ is through inhibition of GSK-3B dependent activation of NFkB signalling [151]. NFkB has been associated with chemoresistance in many solid tumours including intestinal, ovarian and pancreatic while PPARγ together with several other nuclear receptors are known inhibitors of NFkB [353, 367-370] Interestingly, I also described a small population of $BRAF^{V600E}$ tumours that were PPARγ signalling deficient but still had high expression levels of DHRS7B and were associated with increased expression of OxPHOS related genes and were subsequently associated with poor prognosis. Overexpression of DHRS7B in $BRAF^{V600E}$ tumour cells led to a 10-fold increase in 5FU resistance. Furthermore, overexpression of DHRS7B in $BRAF^{V600E}$ tumour cells also coincided with increased expression of well characterised NFkB target genes.

Despite the contradictory history that PPARγ signalling has with human tumorigenesis use of PPARγ agonists has been targeted as a therapeutic possibility with varying levels of success. Rosiglitazone together with other Thiazolidinedione's targeting the PPAR's are used to treat a variety of human diseases including type II diabetes [371]. Furthermore, natural ligands of PPAR including prostaglandins are known to have anti-tumorigenic effects. However, much of the confusion surrounding PPARγ can be attributed at least in some part towards pathway cross talk with other PPAR members. For example, all PPAR's are known to respond to polyunsaturated FA, and this is an issue given the differences in the responses observed across family members. PPARγ as mentioned previously is associated with terminal differentiation and cell cycle arrest while other groups have described that PPARδ plays a cooperative role in the proliferative WNT/β-catenin signalling pathway both in normal colon mucosa and in CTNNB1 driven colorectal cancers [137, 138]. The role of phospholipid metabolism as a key player in regulation of PPARγ signalling was described throughout much of this thesis. The peroxisomal phospholipid biosynthesis pathway was shown to regulate many of the processes regarding fatty acid metabolism and PPARγ signalling in tumours. PPARγ mediated sensitisation of tumour cells to chemotherapeutics was shown largely to be related to DHRS7B activity. Loss of DHRS7B in colorectal cancer cells showed IC50 values almost identical to wild type cells co-treated with Rosiglitazone and 5FU while DHRS7B null colorectal cancer cells showed no increase in

5FU sensitivity when co-treated with Rosiglitazone. 5FU was shown to positively regulate saturated membrane lipids. Loss of DHRS7B leading to the inability of phospholipid desaturation correlated with a marked increase in 5FU sensitivity. Rosiglitazone had a similar effect by limiting the availability of polyunsaturated phospholipid's in response to 5FU and again was meet with a correlative increase in 5FU resistance. The association of polyunsaturated phospholipid's with drug resistance has been identified in relation of $BRAF^{V600E}$ melanomas [156]. Sustained SREBF1 activity in response to prolonged exposure to Vemurafenib in resistant melanoma cell lines was a key alteration observed while this correlated with increase polyunsaturated phospholipid levels [156]. However, the status of PPARγ expression or activity was not addressed but SREBF1 was shown to be a key driver of colorectal $BRAF^{V600E}$ hyperlipidaemia. Other groups have associated membrane lipid saturation to protection against oxidative stress while our results suggested that loss of DHRS7B led to increased HIF1A transcriptional activity in addition to increased stress responses in the form of UPR [329]. Furthermore, other key enzymes regulating the production of phospholipid's including LPCAT2 was shown to regulate lipid droplet levels while this correlated with chemoresistance and ER stress protection in response to chemotherapeutics in colorectal cancer [227]. In addition, LXR mediated expression of LPCAT3 was shown to have a similar effect on ER stress under inflammatory conditions leading to phospholipid desaturation protecting cells from ER stress activation and apoptosis [372]. Other groups have also explored the importance of phospholipid desaturation on regulation of ER stress responses and apoptosis protections [161, 336, 337]. Conversely, forcible saturation of phospholipid ER composition through palmitate treatment in hepatic cells promoted increased ER stress levels [373]. PPARγ has been implicated in agonist induced ER stress activation in pancreatic beta cells while cooperation of C/EBP and NFkB signalling activated through repression of PPARγ signalling has also been attributed to ER stress activation in response to chronic inflammation [374, 375]. Furthermore, SREBF1 mediated lipid synthesis was shown to be a key regulator of ER stress associated lipogenesis and played a key protective role in ER stress associated cell survival in U87 human glioblastoma cells [161]. Given the roles showed here that PPARγ plays in the regulation of SREBF1, PPARγ induced ER stress is likely attributed to regulation of phospholipid biosynthesis through sustained inhibition of SREBF1 transcriptional activity.

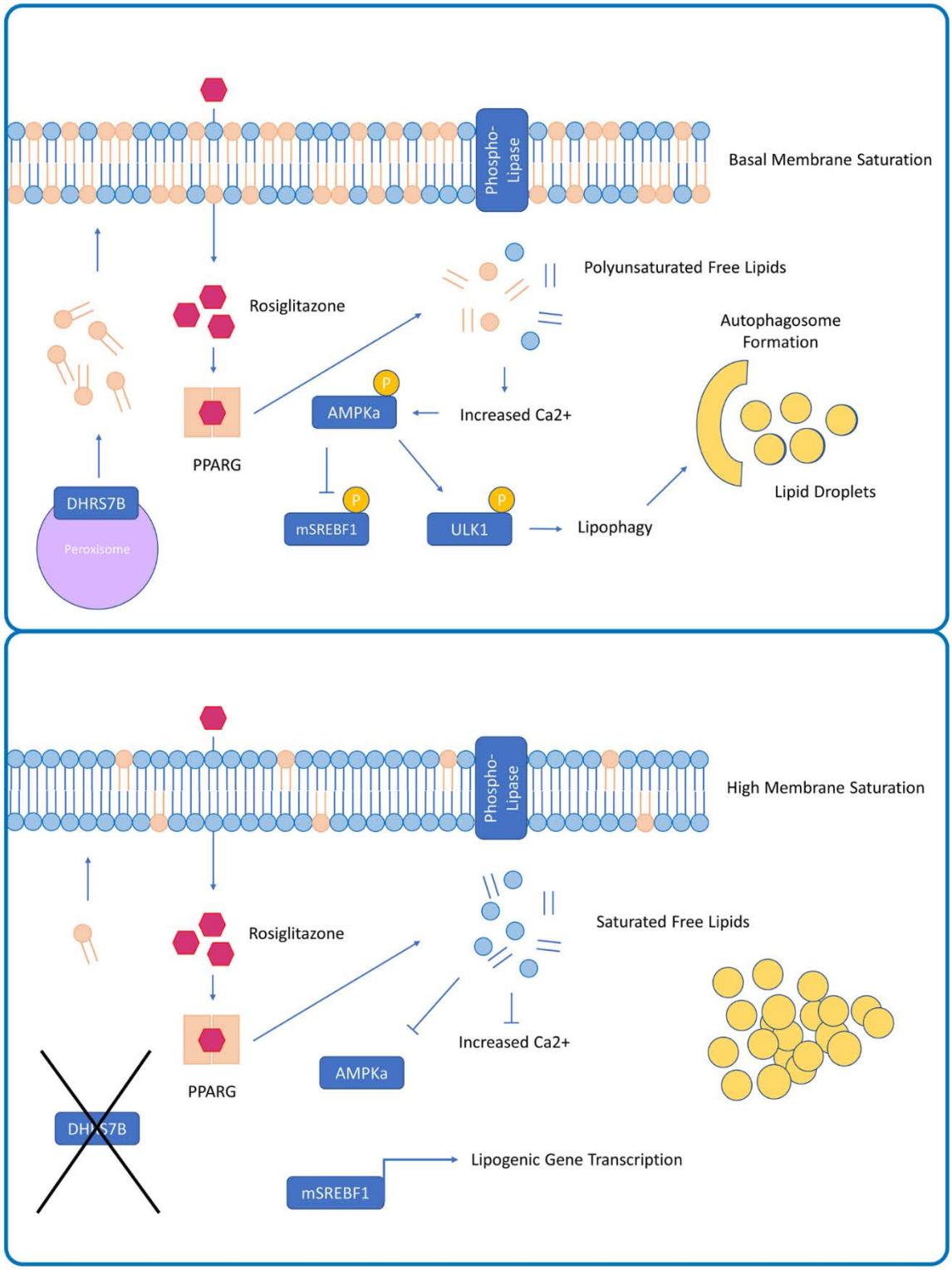

Figure 6.1. Pathway schematic of the research presented. Top panel. PPARγ mediated regulation of lipid droplets through phospholipid membrane associated lipid remodelling targets AMPK activating that drives lipophagy and negative regulation of lipogenic transcription through inhibition of mSREBF1. **Bottom panel**. Loss of DHRS7B activity replicates $BRAF^{V600E}$ mutants, where low levels of PUFA phospholipids led to decreased AMPK activity. Loss of polyunsaturated phospholipid dependent activation of AMPK leads to sustained SREBF1 transcriptional activity prolonged lipogenesis and decreased PPARγ activity.

6.2. Conclusion and future directions

Therapeutic targeting lipid metabolism in the context of tumour biology is difficult and the complex level of contradicting information available reinforces how much there is left to learn about this topic. Large scale transcriptomic datasets provide a useful tool to analyse the metabolic state of tumours. In this thesis I developed a different approach utilising well developed GSEA based approaches looking at tumour metabolism. From this data analysis pipeline, I was able to further investigate the lipid metabolome of colorectal cancer identifying a risk factor associated with loss of PPARγ signalling and the peroxisomal phospholipid biosynthesis pathway in $BRAF^{V600E}$ driven tumours. The subsequent loss of peroxisomal phospholipid biosynthesis was a key feature driving the hyperlipidemic phenotype observed in $BRAF^{V600E}$ tumour cells. CRISPR/Cas9 DHRS7B knockouts were resistant to PPARγ mediated autophagy initiation in addition to SREBF1 inhibition. This study provided an insight into a complex signalling and feedback mechanism driving lipogenesis in tumour cells while PPARG was shown to a be a critical regulator of this pathway. Loss of PPARG signalling such as what I observed in $BRAF^{V600E}$ tumours showed complete unregulated lipogenesis pathways while AMPK mediated autophagy stimulation was required for effective lipolysis and was shown to be regulated by PPARγ. Furthermore, loss of DHRS7B and thus polyunsaturated phospholipids was shown to be crucial in AMPK signalling and autophagy stimulation. Decreased polyunsaturated phospholipid levels associated with $BRAF^{V600E}$ tumours or CRISPR/Cas9 DHRS7B null cell models showed autophagy resistance and were more susceptible to starvation induced apoptosis in addition to stress induced apoptosis from cytotoxic drug therapy. Conversely, loss of effective AMPK stimulation was shown to led to sustained SREBF1 activity driving the unregulated $BRAF^{V600E}$ lipogenic phenotype. This coincided with increased metastatic potential but also correlated with increased sensitivity towards cytotoxic drugs while overexpression of DHRS7B led to decreased sensitivity towards chemotherapeutics.

The nature of all the experiments performed in this study were all *in vitro*. Future *in vivo* studies will be crucial to further investigate these results in the context of more biological complex and relevant

systems. The development of both DHRS7B tissue/cell specific null mice lines utilising CRISPR or Cre recombinase-based technologies will better address the biological functions of DHRS7B and more importantly verify the findings made *in vitro*. 3D cell culture application could also be utilised to further investigate this signalling pathway given the associations made with DHRS7B overexpression and NFkB activation, it would be interesting to assess the effects of DHRS7B on the tumour microenvironment particularly on macrophage polarisation. Furthermore, given the efficiency of targeting PPARG in regulating PL dependent drug resistance presented here, development of DHRS7B inhibitors would be required to further assess the possibilities of exploiting this pathway for use in a clinical setting. In relation to further pathway analysis, it remains unclear whether the responses of polyunsaturated phospholipids towards AMPK are a result from direct actions or indirect signalling mechanism. Further analysis including AMPK binding assays or signalling pathway screening could be used to address this short coming. Furthermore, CRISPR/Cas9 implementation using current knockout models with library-based screening methods targeting phospholipases could be used to investigate the roles of membrane signalling feedback through the action of phospholipase type C mechanism.

In Chapter 5 I looked to better address our understanding of the lipid metabolome through implementation of high throughput lipidomic screening using 15 human cancer derived cell lines. From this data along with RNAseq transcriptomic analysis I was able to predict the levels of membrane associated saturation. This was shown to correlate with chemoresistance while I verified this association using already characterised DHRS7B null cell models. PPARγ activation was shown to desensitize cells that were resistant to 5FU through regulation of membrane associated lipid saturation levels. While this was associated with metabolic reprogramming. PPARγ active cells were shown to downregulate OxPHOS associated genes while the opposite was true regarding DHRS7B. Consequentially, loss of DHRS7B led to increased HIF1A associated transcriptional activity and increased metastatic potential. This was clinically relevant in colorectal cancer where DHRS7B is shown to be upregulated in most stage IV colorectal cancers using matched adjacent patient controls. In contrast to this DHRS7B was shown to be downregulated in metastatic liver tumours compared to stage IV colorectal tumours. The major downfall of this chapter was purely biological replicates and over representation of certain

topological tumour derived cell types. Breast and colorectal cancer derived cells were the only two cells to have multiple biological replicates for similar tissues with four breast cancer cell lines and six colorectal cancer cell lines tested. The rest of the dataset was made up of single cell lines. Furthermore, this was true with the transcriptional assay where PPAR responsive cell transcriptomes were analysed compared to unsorted cell populations. This was performed entirely in colorectal derived cancer cell lines. To get a better and more accurate overview of transcriptional regulation of lipogenesis in human tumours we need to address large amounts of biological data. High throughput analysis of the lipidomic profile generating a large dataset will increase the flexibility of the dataset. Furthermore, I addressed the issue regarding transcriptomic analysis of lipogenic transcription factors. High throughput ChIP analysis showed significant levels of overlap between promoter occupancy of transcription factors such as the PPAR's, SREBF1 and LXRA. Development of similar lentiviral-based PPRE reporter cell lines in more cell types in addition to targeting more lipogenic transcription factors would add more complexity and versatility to the dataset presented while development of duel reporter cell lines would allow to further analyse cross-talk between pathways including PPARγ and SREBF1 reporter in this thesis. Furthermore, recent implementation of CRISPR/Cas9 and single cell sequencing technology allowing for the development of data analysis such as Perturb-seq, a single cell sequencing based method targeting small group of target genes with matched gRNA and single cell RNA libraries allowing for analysis of transcriptional perturbation across multiple gene knockout models using CRISPR/Cas9. Perturb-seq would be a useful tool in addressing the similarities of converging pathways allowing for fast efficient and cost effect data analysis targeting multiple pathways including PPARγ and SREBF1 in the same experiment without the requirement to general multiple cell lines.

References

1. Stehelin, D., et al., *DNA related to the transforming gene(s) of avian sarcoma viruses is present in normal avian DNA.* Nature, 1976. **260**(5547): p. 170-173.
2. Parker, R.C., H.E. Varmus, and J.M. Bishop, *Expression of v-src and chicken c-src in rat cells demonstrates qualitative differences between pp60v-src and pp60c-src.* Cell, 1984. **37**(1): p. 131-9.
3. Iba, H., et al., *Rous sarcoma virus variants that carry the cellular src gene instead of the viral src gene cannot transform chicken embryo fibroblasts.* Proc Natl Acad Sci U S A, 1984. **81**(14): p. 4424-8.
4. Harvey, J.J., *An unidentified virus which causes the rapid production of tumours in mice.* Nature, 1964. **204**: p. 1104-5.
5. Kirsten, W.H. and L.A. Mayer, *Morphologic responses to a murine erythroblastosis virus.* J Natl Cancer Inst, 1967. **39**(2): p. 311-35.
6. Tsuchida, N., T. Ryder, and E. Ohtsubo, *Nucleotide sequence of the oncogene encoding the p21 transforming protein of Kirsten murine sarcoma virus.* Science, 1982. **217**(4563): p. 937-9.
7. Dhar, R., et al., *Nucleotide sequence of the p21 transforming protein of Harvey murine sarcoma virus.* Science, 1982. **217**(4563): p. 934-6.
8. Levine, A.J. and M. Oren, *The first 30 years of p53: growing ever more complex.* Nature Reviews Cancer, 2009. **9**: p. 749.
9. Cavenee, W.K., et al., *Expression of recessive alleles by chromosomal mechanisms in retinoblastoma.* Nature, 1983. **305**(5937): p. 779-784.
10. Friend, S.H., et al., *A human DNA segment with properties of the gene that predisposes to retinoblastoma and osteosarcoma.* Nature, 1986. **323**(6089): p. 643-6.
11. Duesberg, P.H., K. Bister, and P.K. Vogt, *The RNA of avian acute leukemia virus MC29.* Proceedings of the National Academy of Sciences of the United States of America, 1977. **74**(10): p. 4320-4324.
12. Bister, K. and P.H. Duesberg, *Structure and specific sequences of avian erythroblastosis virus RNA: evidence for multiple classes of transforming genes among avian tumor viruses.* Proc Natl Acad Sci U S A, 1979. **76**(10): p. 5023-7.
13. Li, D.M. and H. Sun, *TEP1, encoded by a candidate tumor suppressor locus, is a novel protein tyrosine phosphatase regulated by transforming growth factor beta.* Cancer Res, 1997. **57**(11): p. 2124-9.
14. Nishisho, I., et al., *Mutations of chromosome 5q21 genes in FAP and colorectal cancer patients.* Science, 1991. **253**(5020): p. 665-669.
15. Wang, Z., et al., *β-catenin mutation is correlated with a favorable prognosis in patients with hepatocellular carcinoma.* Molecular and clinical oncology, 2015. **3**(4): p. 936-940.
16. Arend, R.C., et al., *The Wnt/beta-catenin pathway in ovarian cancer: a review.* Gynecol Oncol, 2013. **131**(3): p. 772-9.
17. Schubbert, S., K. Shannon, and G. Bollag, *Hyperactive Ras in developmental disorders and cancer.* Nature Reviews Cancer, 2007. **7**: p. 295.
18. Samatar, A.A. and P.I. Poulikakos, *Targeting RAS–ERK signalling in cancer: promises and challenges.* Nature Reviews Drug Discovery, 2014. **13**: p. 928.
19. Rowan, A.J., et al., *APC mutations in sporadic colorectal tumors: A mutational "hotspot" and interdependence of the "two hits".* Proc Natl Acad Sci U S A, 2000. **97**(7): p. 3352-7.
20. Anastas, J.N. and R.T. Moon, *WNT signalling pathways as therapeutic targets in cancer.* Nature Reviews Cancer, 2012. **13**: p. 11.

21. Willert, K., et al., *Casein kinase 2 associates with and phosphorylates dishevelled.* Embo j, 1997. **16**(11): p. 3089-96.
22. Rothbacher, U., et al., *Dishevelled phosphorylation, subcellular localization and multimerization regulate its role in early embryogenesis.* Embo j, 2000. **19**(5): p. 1010-22.
23. Walther, A., et al., *Genetic prognostic and predictive markers in colorectal cancer.* Nature Reviews Cancer, 2009. **9**(7): p. 489-499.
24. Perugorria, M.J., et al., *Wnt–β-catenin signalling in liver development, health and disease.* Nature Reviews Gastroenterology & Hepatology, 2019. **16**(2): p. 121-136.
25. Gao, C., et al., *Exon 3 mutations of CTNNB1 drive tumorigenesis: a review.* Oncotarget, 2017. **9**(4).
26. Bass, A.J., et al., *Genomic sequencing of colorectal adenocarcinomas identifies a recurrent VTI1A-TCF7L2 fusion.* Nat Genet, 2011. **43**(10): p. 964-968.
27. Davidsen, J., et al., *The VTI1A-TCF4 colon cancer fusion protein is a dominant negative regulator of Wnt signaling and is transcriptionally regulated by intestinal homeodomain factor CDX2.* PLoS One, 2018. **13**(7): p. e0200215.
28. Buday, L. and J. Downward, *Epidermal growth factor regulates p21ras through the formation of a complex of receptor, Grb2 adapter protein, and Sos nucleotide exchange factor.* Cell, 1993. **73**(3): p. 611-20.
29. Huang, D.C., C.J. Marshall, and J.F. Hancock, *Plasma membrane-targeted ras GTPase-activating protein is a potent suppressor of p21ras function.* Mol Cell Biol, 1993. **13**(4): p. 2420-31.
30. Staal, F.J.T., T.C. Luis, and M.M. Tiemessen, *WNT signalling in the immune system: WNT is spreading its wings.* Nature Reviews Immunology, 2015. **15**: p. 329.
31. Chong, H., J. Lee, and K.L. Guan, *Positive and negative regulation of Raf kinase activity and function by phosphorylation.* Embo j, 2001. **20**(14): p. 3716-27.
32. Weber, C.K., et al., *Active Ras induces heterodimerization of cRaf and BRaf.* Cancer Res, 2001. **61**(9): p. 3595-8.
33. King, A.J., et al., *The protein kinase Pak3 positively regulates Raf-1 activity through phosphorylation of serine 338.* Nature, 1998. **396**(6707): p. 180-3.
34. Fabian, J.R., I.O. Daar, and D.K. Morrison, *Critical tyrosine residues regulate the enzymatic and biological activity of Raf-1 kinase.* Mol Cell Biol, 1993. **13**(11): p. 7170-9.
35. Guan, K.L., et al., *Negative regulation of the serine/threonine kinase B-Raf by Akt.* J Biol Chem, 2000. **275**(35): p. 27354-9.
36. Sprenkle, A.B., et al., *Identification of Raf-1 Ser621 kinase activity from NIH 3T3 cells as AMP-activated protein kinase.* FEBS Lett, 1997. **403**(3): p. 254-8.
37. Yu, H.A., et al., *Prognostic impact of KRAS mutation subtypes in 677 patients with metastatic lung adenocarcinomas.* J Thorac Oncol, 2015. **10**(3): p. 431-7.
38. Armaghany, T., et al., *Genetic Alterations in Colorectal Cancer.* Gastrointestinal Cancer Research : GCR, 2012. **5**(1): p. 19-27.
39. Waters, A.M. and C.J. Der, *KRAS: The Critical Driver and Therapeutic Target for Pancreatic Cancer.* Cold Spring Harbor perspectives in medicine, 2018. **8**(9): p. a031435.
40. Beukers, W., A. Hercegovac, and E.C. Zwarthoff, *HRAS mutations in bladder cancer at an early age and the possible association with the Costello Syndrome.* Eur J Hum Genet, 2014. **22**(6): p. 837-9.
41. Ascierto, P.A., et al., *The role of BRAF V600 mutation in melanoma.* Journal of translational medicine, 2012. **10**: p. 85-85.
42. D'Abaco, G.M., R.H. Whitehead, and A.W. Burgess, *Synergy between Apc min and an activated ras mutation is sufficient to induce colon carcinomas.* Mol Cell Biol, 1996. **16**(3): p. 884-91.
43. Harada, N., et al., *Hepatocarcinogenesis in mice with beta-catenin and Ha-ras gene mutations.* Cancer Res, 2004. **64**(1): p. 48-54.

44. Kim, S.E. and K.Y. Choi, *EGF receptor is involved in WNT3a-mediated proliferation and motility of NIH3T3 cells via ERK pathway activation.* Cell Signal, 2007. **19**(7): p. 1554-64.
45. Park, K.S., et al., *APC inhibits ERK pathway activation and cellular proliferation induced by RAS.* J Cell Sci, 2006. **119**(Pt 5): p. 819-27.
46. Biteau, B. and H. Jasper, *EGF signaling regulates the proliferation of intestinal stem cells in Drosophila.* Development, 2011. **138**(6): p. 1045-1055.
47. Caballero-Franco, C., et al., *Tuning of protein kinase circuitry by p38alpha is vital for epithelial tissue homeostasis.* J Biol Chem, 2013. **288**(33): p. 23788-97.
48. Lee, S.K., et al., *beta-Catenin-RAS interaction serves as a molecular switch for RAS degradation via GSK3beta.* EMBO Rep, 2018. **19**(12).
49. Biechele, T.L., et al., *Wnt/beta-catenin signaling and AXIN1 regulate apoptosis triggered by inhibition of the mutant kinase BRAFV600E in human melanoma.* Sci Signal, 2012. **5**(206): p. ra3.
50. Tong, K., et al., *Degree of Tissue Differentiation Dictates Susceptibility to BRAF-Driven Colorectal Cancer.* Cell Rep, 2017. **21**(13): p. 3833-3845.
51. Vander Heiden, M.G., L.C. Cantley, and C.B. Thompson, *Understanding the Warburg effect: the metabolic requirements of cell proliferation.* Science, 2009. **324**(5930): p. 1029-33.
52. Shim, H., et al., *c-Myc transactivation of LDH-A: implications for tumor metabolism and growth.* Proc Natl Acad Sci U S A, 1997. **94**(13): p. 6658-63.
53. Guo, D., et al., *EGFR signaling through an Akt-SREBP-1-dependent, rapamycin-resistant pathway sensitizes glioblastomas to antilipogenic therapy.* Sci Signal, 2009. **2**(101): p. ra82.
54. Horton, J.D., J.L. Goldstein, and M.S. Brown, *SREBPs: activators of the complete program of cholesterol and fatty acid synthesis in the liver.* J Clin Invest, 2002. **109**(9): p. 1125-31.
55. Watt, M.J., et al., *Suppressing fatty acid uptake has therapeutic effects in preclinical models of prostate cancer.* Science Translational Medicine, 2019. **11**(478): p. eaau5758.
56. Manning, B.D. and A. Toker, *AKT/PKB Signaling: Navigating the Network.* Cell, 2017. **169**(3): p. 381-405.
57. Liberti, M.V. and J.W. Locasale, *The Warburg Effect: How Does it Benefit Cancer Cells?* Trends in Biochemical Sciences. **41**(3): p. 211-218.
58. Shaw, R.J., et al., *The tumor suppressor LKB1 kinase directly activates AMP-activated kinase and regulates apoptosis in response to energy stress.* Proc Natl Acad Sci U S A, 2004. **101**(10): p. 3329-35.
59. Lum, J.J., et al., *Growth factor regulation of autophagy and cell survival in the absence of apoptosis.* Cell, 2005. **120**(2): p. 237-48.
60. Kim, H., et al., *The DUSP26 phosphatase activator adenylate kinase 2 regulates FADD phosphorylation and cell growth.* Nature Communications, 2014. **5**: p. 3351.
61. Fujisawa, K., et al., *Modulation of anti-cancer drug sensitivity through the regulation of mitochondrial activity by adenylate kinase 4.* Journal of Experimental & Clinical Cancer Research, 2016. **35**(1): p. 48.
62. Jan, Y.H., et al., *Adenylate kinase-4 is a marker of poor clinical outcomes that promotes metastasis of lung cancer by downregulating the transcription factor ATF3.* Cancer Res, 2012. **72**(19): p. 5119-29.
63. Hezel, A.F. and N. Bardeesy, *LKB1; linking cell structure and tumor suppression.* Oncogene, 0000. **27**(55): p. 6908-6919.
64. Balaban, S., et al., *Obesity and cancer progression: is there a role of fatty acid metabolism?* Biomed Res Int, 2015. **2015**: p. 274585.
65. Medes, G., A. Thomas, and S. Weinhouse, *Metabolism of Neoplastic Tissue. IV. A Study of Lipid Synthesis in Neoplastic Tissue Slices in Vitro.* Cancer Research, 1953. **13**(1): p. 27-29.

66. Menendez, J.A. and R. Lupu, *Fatty acid synthase and the lipogenic phenotype in cancer pathogenesis.* Nat Rev Cancer, 2007. **7**(10): p. 763-777.
67. Kolukula, V.K., et al., *SLC25A1, or CIC, is a novel transcriptional target of mutant p53 and a negative tumor prognostic marker.* Oncotarget, 2014. **5**(5): p. 1212-1225.
68. Catalina-Rodriguez, O., et al., *The mitochondrial citrate transporter, CIC, is essential for mitochondrial homeostasis.* Oncotarget, 2012. **3**(10): p. 1220-1235.
69. Hatzivassiliou, G., et al., *ATP citrate lyase inhibition can suppress tumor cell growth.* Cancer Cell, 2005. **8**(4): p. 311-21.
70. Hanai, J., et al., *Inhibition of lung cancer growth: ATP citrate lyase knockdown and statin treatment leads to dual blockade of mitogen-activated protein kinase (MAPK) and phosphatidylinositol-3-kinase (PI3K)/AKT pathways.* J Cell Physiol, 2012. **227**(4): p. 1709-20.
71. Bauer, D.E., et al., *ATP citrate lyase is an important component of cell growth and transformation.* Oncogene, 2005. **24**(41): p. 6314-22.
72. Qian, X., et al., *ATP citrate lyase expression is associated with advanced stage and prognosis in gastric adenocarcinoma.* International Journal of Clinical and Experimental Medicine, 2015. **8**(5): p. 7855-7860.
73. Brusselmans, K., et al., *RNA interference-mediated silencing of the acetyl-CoA-carboxylase-alpha gene induces growth inhibition and apoptosis of prostate cancer cells.* Cancer Res, 2005. **65**(15): p. 6719-25.
74. Chajes, V., et al., *Acetyl-CoA carboxylase alpha is essential to breast cancer cell survival.* Cancer Res, 2006. **66**(10): p. 5287-94.
75. Beckers, A., et al., *Chemical inhibition of acetyl-CoA carboxylase induces growth arrest and cytotoxicity selectively in cancer cells.* Cancer Res, 2007. **67**(17): p. 8180-7.
76. Zhou, W., et al., *Malonyl-CoA decarboxylase inhibition is selectively cytotoxic to human breast cancer cells.* Oncogene, 2009. **28**(33): p. 2979-87.
77. Monaco, M.E., et al., *Expression of Long-chain Fatty Acyl-CoA Synthetase 4 in Breast and Prostate Cancers Is Associated with Sex Steroid Hormone Receptor Negativity.* Translational Oncology, 2010. **3**(2): p. 91-98.
78. Cao, Y., et al., *Intracellular unesterified arachidonic acid signals apoptosis.* Proceedings of the National Academy of Sciences of the United States of America, 2000. **97**(21): p. 11280-11285.
79. Mashima, T., et al., *p53-defective tumors with a functional apoptosome-mediated pathway: a new therapeutic target.* J Natl Cancer Inst, 2005. **97**(10): p. 765-77.
80. Kearney, K.E., T.G. Pretlow, and T.P. Pretlow, *Increased expression of fatty acid synthase in human aberrant crypt foci: possible target for colorectal cancer prevention.* Int J Cancer, 2009. **125**(1): p. 249-52.
81. Zaytseva, Y.Y., et al., *Increased expression of fatty acid synthase provides a survival advantage to colorectal cancer cells via upregulation of cellular respiration.* Oncotarget, 2015. **6**(22): p. 18891-904.
82. Chang, L., et al., *Loss of fatty acid synthase suppresses the malignant phenotype of colorectal cancer cells by down-regulating energy metabolism and mTOR signaling pathway.* J Cancer Res Clin Oncol, 2016. **142**(1): p. 59-72.
83. Zaytseva, Y.Y., et al., *Inhibition of fatty acid synthase attenuates CD44-associated signaling and reduces metastasis in colorectal cancer.* Cancer Res, 2012. **72**(6): p. 1504-17.
84. Zaytseva, Y.Y., et al., *Cancer cell-associated fatty acid synthase activates endothelial cells and promotes angiogenesis in colorectal cancer.* Carcinogenesis, 2014. **35**(6): p. 1341-51.
85. Camarero, N., et al., *Ketogenic HMGCS2 Is a c-Myc target gene expressed in differentiated cells of human colonic epithelium and down-regulated in colon cancer.* Mol Cancer Res, 2006. **4**(9): p. 645-53.

86. Helenius, T.O., et al., *Keratin 8 absence down-regulates colonocyte HMGCS2 and modulates colonic ketogenesis and energy metabolism.* Molecular Biology of the Cell, 2015. **26**(12): p. 2298-2310.
87. Bengtsson, E., et al., *HMG-CoA reductase expression in primary colorectal cancer correlates with favourable clinicopathological characteristics and an improved clinical outcome.* Diagn Pathol, 2014. **9**: p. 78.
88. Clendening, J.W., et al., *Dysregulation of the mevalonate pathway promotes transformation.* Proc Natl Acad Sci U S A, 2010. **107**(34): p. 15051-6.
89. Bethke, L., et al., *Polymorphisms in the cytochrome P450 genes CYP1A2, CYP1B1, CYP3A4, CYP3A5, CYP11A1, CYP17A1, CYP19A1 and colorectal cancer risk.* BMC Cancer, 2007. **7**: p. 123-123.
90. Terry, K., et al., *Genetic variation in CYP11A1 and StAR in relation to endometrial cancer risk.* Gynecologic oncology, 2010. **117**(2): p. 255-259.
91. Bayrer, J.R., et al., *Silencing LRH-1 in colon cancer cell lines impairs proliferation and alters gene expression programs.* Proc Natl Acad Sci U S A, 2015. **112**(8): p. 2467-72.
92. Issemann, I. and S. Green, *Activation of a member of the steroid hormone receptor superfamily by peroxisome proliferators.* Nature, 1990. **347**(6294): p. 645-50.
93. Sumanasekera, W.K., et al., *Heat shock protein-90 (Hsp90) acts as a repressor of peroxisome proliferator-activated receptor-alpha (PPARalpha) and PPARbeta activity.* Biochemistry, 2003. **42**(36): p. 10726-35.
94. Umemoto, T. and Y. Fujiki, *Ligand-dependent nucleo-cytoplasmic shuttling of peroxisome proliferator-activated receptors, PPARalpha and PPARgamma.* Genes Cells, 2012. **17**(7): p. 576-96.
95. Chandra, V., et al., *Structure of the intact PPAR-gamma-RXR- nuclear receptor complex on DNA.* Nature, 2008. **456**(7220): p. 350-6.
96. Nagy, L., et al., *Nuclear receptor repression mediated by a complex containing SMRT, mSin3A, and histone deacetylase.* Cell, 1997. **89**(3): p. 373-80.
97. Miyata, K.S., et al., *Receptor-interacting protein 140 interacts with and inhibits transactivation by, peroxisome proliferator-activated receptor alpha and liver-X-receptor alpha.* Mol Cell Endocrinol, 1998. **146**(1-2): p. 69-76.
98. Debevec, D., et al., *Receptor interacting protein 140 regulates expression of uncoupling protein 1 in adipocytes through specific peroxisome proliferator activated receptor isoforms and estrogen-related receptor alpha.* Molecular endocrinology (Baltimore, Md.), 2007. **21**(7): p. 1581-1592.
99. Barger, P.M., et al., *p38 mitogen-activated protein kinase activates peroxisome proliferator-activated receptor alpha: a potential role in the cardiac metabolic stress response.* J Biol Chem, 2001. **276**(48): p. 44495-501.
100. Schild, R.L., et al., *The kinase p38 regulates peroxisome proliferator activated receptor-gamma in human trophoblasts.* Placenta, 2006. **27**(2-3): p. 191-9.
101. Shalev, A., et al., *The peroxisome proliferator-activated receptor alpha is a phosphoprotein: regulation by insulin.* Endocrinology, 1996. **137**(10): p. 4499-502.
102. Vanden Heuvel, J.P., et al., *Comprehensive analysis of gene expression in rat and human hepatoma cells exposed to the peroxisome proliferator WY14,643.* Toxicol Appl Pharmacol, 2003. **188**(3): p. 185-98.
103. Adams, M., et al., *Transcriptional activation by peroxisome proliferator-activated receptor gamma is inhibited by phosphorylation at a consensus mitogen-activated protein kinase site.* J Biol Chem, 1997. **272**(8): p. 5128-32.
104. Camp, H.S., S.R. Tafuri, and T. Leff, *c-Jun N-terminal kinase phosphorylates peroxisome proliferator-activated receptor-gamma1 and negatively regulates its transcriptional activity.* Endocrinology, 1999. **140**(1): p. 392-7.
105. Shao, D., et al., *Interdomain communication regulating ligand binding by PPAR-gamma.* Nature, 1998. **396**(6709): p. 377-80.

106. Camp, H.S. and S.R. Tafuri, *Regulation of peroxisome proliferator-activated receptor gamma activity by mitogen-activated protein kinase.* J Biol Chem, 1997. **272**(16): p. 10811-6.
107. Bolden, A., et al., *The PPAR Gamma Agonist Troglitazone Regulates Erk 1/2 Phosphorylation via a PPARγ-Independent, MEK-Dependent Pathway in Human Prostate Cancer Cells.* PPAR research, 2012. **2012**: p. 929052-929052.
108. Krogsdam, A.M., et al., *Nuclear receptor corepressor-dependent repression of peroxisome-proliferator-activated receptor delta-mediated transactivation.* Biochem J, 2002. **363**(Pt 1): p. 157-65.
109. Hansen, J.B., et al., *Peroxisome proliferator-activated receptor delta (PPARdelta)-mediated regulation of preadipocyte proliferation and gene expression is dependent on cAMP signaling.* J Biol Chem, 2001. **276**(5): p. 3175-82.
110. Han, L., et al., *SIRT1 is regulated by a PPAR{gamma}-SIRT1 negative feedback loop associated with senescence.* Nucleic Acids Res, 2010. **38**(21): p. 7458-71.
111. Qiang, L., et al., *Brown remodeling of white adipose tissue by SirT1-dependent deacetylation of Ppargamma.* Cell, 2012. **150**(3): p. 620-32.
112. Hauser, S., et al., *Degradation of the Peroxisome Proliferator-activated Receptor γ Is Linked to Ligand-dependent Activation.* Journal of Biological Chemistry, 2000. **275**(24): p. 18527-18533.
113. Lee, J.M., et al., *The E3 ubiquitin ligase TRIM25 regulates adipocyte differentiation via proteasome-mediated degradation of PPARγ.* Experimental & Molecular Medicine, 2018. **50**(10): p. 135.
114. Li, J.J., et al., *Ubiquitin Ligase NEDD4 Regulates PPARγ Stability and Adipocyte Differentiation in 3T3-L1 Cells.* Scientific Reports, 2016. **6**: p. 38550.
115. Blanquart, C., et al., *Peroxisome Proliferator-activated Receptor α (PPARα) Turnover by the Ubiquitin-Proteasome System Controls the Ligand-induced Expression Level of Its Target Genes.* Journal of Biological Chemistry, 2002. **277**(40): p. 37254-37259.
116. Fei, J., C. Cook, and N. Santanam, *omega-6 lipids regulate PPAR turnover via reciprocal switch between PGC-1 alpha and ubiquitination.* Atherosclerosis, 2012. **222**(2): p. 395-401.
117. Daynes, R.A. and D.C. Jones, *Emerging roles of PPARS in inflammation and immunity.* Nature Reviews Immunology, 2002. **2**(10): p. 748-759.
118. Rawson, R.B., et al., *Failure to cleave sterol regulatory element-binding proteins (SREBPs) causes cholesterol auxotrophy in Chinese hamster ovary cells with genetic absence of SREBP cleavage-activating protein.* J Biol Chem, 1999. **274**(40): p. 28549-56.
119. Kuan, Y.C., et al., *Heat Shock Protein 90 Modulates Lipid Homeostasis by Regulating the Stability and Function of Sterol Regulatory Element-binding Protein (SREBP) and SREBP Cleavage-activating Protein.* J Biol Chem, 2017. **292**(7): p. 3016-3028.
120. Sun, L.P., et al., *Insig required for sterol-mediated inhibition of Scap/SREBP binding to COPII proteins in vitro.* J Biol Chem, 2005. **280**(28): p. 26483-90.
121. Zhang, Y., et al., *Direct Demonstration That Loop1 of Scap Binds to Loop7: A CRUCIAL EVENT IN CHOLESTEROL HOMEOSTASIS.* J Biol Chem, 2016. **291**(24): p. 12888-96.
122. Cheng, C., et al., *Glucose-Mediated N-glycosylation of SCAP Is Essential for SREBP-1 Activation and Tumor Growth.* Cancer Cell, 2015. **28**(5): p. 569-581.
123. Yang, T., et al., *Crucial step in cholesterol homeostasis: sterols promote binding of SCAP to INSIG-1, a membrane protein that facilitates retention of SREBPs in ER.* Cell, 2002. **110**(4): p. 489-500.
124. Yabe, D., M.S. Brown, and J.L. Goldstein, *Insig-2, a second endoplasmic reticulum protein that binds SCAP and blocks export of sterol regulatory element-binding proteins.* Proc Natl Acad Sci U S A, 2002. **99**(20): p. 12753-8.

125. Radhakrishnan, A., et al., *Sterol-regulated transport of SREBPs from endoplasmic reticulum to Golgi: oxysterols block transport by binding to Insig.* Proc Natl Acad Sci U S A, 2007. **104**(16): p. 6511-8.
126. Lee, J.H., et al., *Ring finger protein20 regulates hepatic lipid metabolism through protein kinase A-dependent sterol regulatory element binding protein1c degradation.* Hepatology (Baltimore, Md.), 2014. **60**(3): p. 844-857.
127. Lee, J.P., et al., *The TRC8 Ubiquitin Ligase Is Sterol Regulated and Interacts with Lipid and Protein Biosynthetic Pathways.* Molecular Cancer Research, 2010. **8**(1): p. 93-106.
128. Jo, Y., et al., *Sterol-induced degradation of HMG CoA reductase depends on interplay of two Insigs and two ubiquitin ligases, gp78 and Trc8.* Proc Natl Acad Sci U S A, 2011. **108**(51): p. 20503-8.
129. Rawson, R.B., et al., *Complementation cloning of S2P, a gene encoding a putative metalloprotease required for intramembrane cleavage of SREBPs.* Mol Cell, 1997. **1**(1): p. 47-57.
130. Sakai, J., et al., *Cleavage of sterol regulatory element-binding proteins (SREBPs) at site-1 requires interaction with SREBP cleavage-activating protein. Evidence from in vivo competition studies.* J Biol Chem, 1998. **273**(10): p. 5785-93.
131. Lee, J.N., et al., *Unsaturated fatty acids inhibit proteasomal degradation of Insig-1 at a postubiquitination step.* J Biol Chem, 2008. **283**(48): p. 33772-83.
132. Lee, J.N., et al., *Identification of Ubxd8 protein as a sensor for unsaturated fatty acids and regulator of triglyceride synthesis.* Proc Natl Acad Sci U S A, 2010. **107**(50): p. 21424-9.
133. Baker, B.G., et al., *Lack of expression of the proteins GMPR2 and PPARalpha are associated with the basal phenotype and patient outcome in breast cancer.* Breast Cancer Res Treat, 2013. **137**(1): p. 127-37.
134. Li, T., et al., *Fenofibrate induces apoptosis of triple-negative breast cancer cells via activation of NF-kappaB pathway.* BMC Cancer, 2014. **14**: p. 96.
135. Zak, Z., P. Gelebart, and R. Lai, *Fenofibrate induces effective apoptosis in mantle cell lymphoma by inhibiting the TNFalpha/NF-kappaB signaling axis.* Leukemia, 2010. **24**(8): p. 1476-86.
136. Ito, K., et al., *A PML-PPAR-delta pathway for fatty acid oxidation regulates hematopoietic stem cell maintenance.* Nat Med, 2012. **18**(9): p. 1350-8.
137. Beyaz, S., et al., *High-fat diet enhances stemness and tumorigenicity of intestinal progenitors.* Nature, 2016. **531**(7592): p. 53-8.
138. Mihaylova, M.M., et al., *Fasting Activates Fatty Acid Oxidation to Enhance Intestinal Stem Cell Function during Homeostasis and Aging.* Cell Stem Cell, 2018. **22**(5): p. 769-778.e4.
139. Harman, F.S., et al., *Peroxisome proliferator-activated receptor-delta attenuates colon carcinogenesis.* Nat Med, 2004. **10**(5): p. 481-3.
140. Reed, K.R., et al., *PPARdelta status and Apc-mediated tumourigenesis in the mouse intestine.* Oncogene, 2004. **23**(55): p. 8992-6.
141. Wang, D., et al., *Peroxisome proliferator-activated receptor delta promotes colonic inflammation and tumor growth.* Proc Natl Acad Sci U S A, 2014. **111**(19): p. 7084-9.
142. Shimano, H. and R. Sato, *SREBP-regulated lipid metabolism: convergent physiology — divergent pathophysiology.* Nature Reviews Endocrinology, 2017. **13**: p. 710.
143. He, T.C., et al., *PPARdelta is an APC-regulated target of nonsteroidal anti-inflammatory drugs.* Cell, 1999. **99**(3): p. 335-45.
144. Saez, E., et al., *Activators of the nuclear receptor PPARgamma enhance colon polyp formation.* Nat Med, 1998. **4**(9): p. 1058-61.
145. Lefebvre, A.M., et al., *Activation of the peroxisome proliferator-activated receptor gamma promotes the development of colon tumors in C57BL/6J-APCMin/+ mice.* Nat Med, 1998. **4**(9): p. 1053-7.

146. Jansson, E.Å., et al., *The Wnt/β-catenin signaling pathway targets PPARγ activity in colon cancer cells.* Proceedings of the National Academy of Sciences of the United States of America, 2005. **102**(5): p. 1460-1465.
147. Liu, J., et al., *Functional Interaction between Peroxisome Proliferator-Activated Receptor γ and β-Catenin.* Molecular and Cellular Biology, 2006. **26**(15): p. 5827-5837.
148. L. Vermeulen., et al., *Single-cell cloning of colo cancer stem cells reveals a multi-lineage differentiation capacity.* Proc Natl Acad Sci U S A, 2008. **105(36)**: p. 13427-32.
149. Li, Y. and W. Li, *BRAF mutation is associated with poor clinicopathological outcomes in colorectal cancer: A meta-analysis.* Saudi journal of gastroenterology : official journal of the Saudi Gastroenterology Association, 2017. **23**(3): p. 144-149.
150. Fujisawa, T., et al., *Peroxisome proliferator-activated receptor gamma (PPARgamma) suppresses colonic epithelial cell turnover and colon carcinogenesis through inhibition of the beta-catenin/T cell factor (TCF) pathway.* J Pharmacol Sci, 2008. **106**(4): p. 627-38.
151. Ban, J.O., et al., *Suppression of NF-kappaB and GSK-3beta is involved in colon cancer cell growth inhibition by the PPAR agonist troglitazone.* Chem Biol Interact, 2010. **188**(1): p. 75-85.
152. Ogino, S., et al., *Colorectal cancer expression of peroxisome proliferator-activated receptor gamma (PPARG, PPARgamma) is associated with good prognosis.* Gastroenterology, 2009. **136**(4): p. 1242-50.
153. Kim, J.B., et al., *ADD1/SREBP1 activates PPARgamma through the production of endogenous ligand.* Proc Natl Acad Sci U S A, 1998. **95**(8): p. 4333-7.
154. Konig, B., et al., *Activation of PPARalpha and PPARgamma reduces triacylglycerol synthesis in rat hepatoma cells by reduction of nuclear SREBP-1.* Eur J Pharmacol, 2009. **605**(1-3): p. 23-30.
155. Wen, Y.-A., et al., *Downregulation of SREBP inhibits tumor growth and initiation by altering cellular metabolism in colon cancer.* Cell Death & Disease, 2018. **9**(3): p. 265.
156. Talebi, A., et al., *Sustained SREBP-1-dependent lipogenesis as a key mediator of resistance to BRAF-targeted therapy.* Nature Communications, 2018. **9**(1): p. 2500.
157. Wu, S. and A.M. Näär, *SREBP1-dependent de novo fatty acid synthesis gene expression is elevated in malignant melanoma and represents a cellular survival trait.* Scientific Reports, 2019. **9**(1): p. 10369.
158. Gao, Y., et al., *SREBP1 promotes the invasion of colorectal cancer accompanied upregulation of MMP7 expression and NF-κB pathway activation.* BMC cancer, 2019. **19**(1): p. 685-685.
159. Zhai, D., et al., *Sterol regulatory element-binding protein 1 cooperates with c-Myc to promote epithelial-mesenchymal transition in colorectal cancer.* Oncol Lett, 2018. **15**(4): p. 5959-5965.
160. Perone, Y., et al., *SREBP1 drives Keratin-80-dependent cytoskeletal changes and invasive behavior in endocrine-resistant ERα breast cancer.* Nature Communications, 2019. **10**(1): p. 2115.
161. Griffiths, B., et al., *Sterol regulatory element binding protein-dependent regulation of lipid synthesis supports cell survival and tumor growth.* Cancer & metabolism, 2013. **1**(1): p. 3-3.
162. Lewis, C.A., et al., *SREBP maintains lipid biosynthesis and viability of cancer cells under lipid- and oxygen-deprived conditions and defines a gene signature associated with poor survival in glioblastoma multiforme.* Oncogene, 2015. **34**(40): p. 5128-5140.
163. Woods, A., et al., *Identification of phosphorylation sites in AMP-activated protein kinase (AMPK) for upstream AMPK kinases and study of their roles by site-directed mutagenesis.* J Biol Chem, 2003. **278**(31): p. 28434-42.
164. Zhang, C.-S., et al., *Fructose-1,6-bisphosphate and aldolase mediate glucose sensing by AMPK.* Nature, 2017. **548**: p. 112.

165. Dogliotti, G., et al., *Membrane-binding and activation of LKB1 by phosphatidic acid is essential for development and tumour suppression.* Nature Communications, 2017. **8**: p. 15747.
166. Shaw, R.J., et al., *The kinase LKB1 mediates glucose homeostasis in liver and therapeutic effects of metformin.* Science, 2005. **310**(5754): p. 1642-6.
167. Anderson, K.A., et al., *Hypothalamic CaMKK2 contributes to the regulation of energy balance.* Cell Metab, 2008. **7**(5): p. 377-88.
168. Mihaylova, M.M. and R.J. Shaw, *The AMPK signalling pathway coordinates cell growth, autophagy and metabolism.* Nat Cell Biol, 2011. **13**(9): p. 1016-23.
169. Munday, M.R., et al., *Identification by amino acid sequencing of three major regulatory phosphorylation sites on rat acetyl-CoA carboxylase.* Eur J Biochem, 1988. **175**(2): p. 331-8.
170. Ha, J., et al., *Critical phosphorylation sites for acetyl-CoA carboxylase activity.* J Biol Chem, 1994. **269**(35): p. 22162-8.
171. Fullerton, M.D., et al., *Single phosphorylation sites in Acc1 and Acc2 regulate lipid homeostasis and the insulin-sensitizing effects of metformin.* Nat Med, 2013. **19**(12): p. 1649-54.
172. Carling, D., V.A. Zammit, and D.G. Hardie, *A common bicyclic protein kinase cascade inactivates the regulatory enzymes of fatty acid and cholesterol biosynthesis.* FEBS Lett, 1987. **223**(2): p. 217-22.
173. Li, Y., et al., *AMPK phosphorylates and inhibits SREBP activity to attenuate hepatic steatosis and atherosclerosis in diet-induced insulin-resistant mice.* Cell Metab, 2011. **13**(4): p. 376-388.
174. Porstmann, T., et al., *SREBP activity is regulated by mTORC1 and contributes to Akt-dependent cell growth.* Cell Metab, 2008. **8**(3): p. 224-36.
175. Kawaguchi, T., et al., *Mechanism for fatty acid "sparing" effect on glucose-induced transcription: regulation of carbohydrate-responsive element-binding protein by AMP-activated protein kinase.* J Biol Chem, 2002. **277**(6): p. 3829-35.
176. Lamia, K.A., et al., *AMPK regulates the circadian clock by cryptochrome phosphorylation and degradation.* Science, 2009. **326**(5951): p. 437-40.
177. Hong, Y.H., et al., *AMP-activated protein kinase regulates HNF4alpha transcriptional activity by inhibiting dimer formation and decreasing protein stability.* J Biol Chem, 2003. **278**(30): p. 27495-501.
178. Kim, E., et al., *Metformin inhibits nuclear receptor TR4-mediated hepatic stearoyl-CoA desaturase 1 gene expression with altered insulin sensitivity.* Diabetes, 2011. **60**(5): p. 1493-1503.
179. Jager, S., et al., *AMP-activated protein kinase (AMPK) action in skeletal muscle via direct phosphorylation of PGC-1alpha.* Proc Natl Acad Sci U S A, 2007. **104**(29): p. 12017-22.
180. Wu, L., et al., *AMP-Activated Protein Kinase (AMPK) Regulates Energy Metabolism through Modulating Thermogenesis in Adipose Tissue.* Front Physiol, 2018. **9**: p. 122.
181. Herzig, S. and R.J. Shaw, *AMPK: guardian of metabolism and mitochondrial homeostasis.* Nature Reviews Molecular Cell Biology, 2017. **19**: p. 121.
182. Doherty, J. and E.H. Baehrecke, *Life, death and autophagy.* Nature Cell Biology, 2018. **20**(10): p. 1110-1117.
183. Kim, J., et al., *AMPK and mTOR regulate autophagy through direct phosphorylation of Ulk1.* Nat Cell Biol, 2011. **13**(2): p. 132-41.
184. Hara, K., et al., *Raptor, a binding partner of target of rapamycin (TOR), mediates TOR action.* Cell, 2002. **110**(2): p. 177-89.
185. Gwinn, D.M., et al., *AMPK phosphorylation of raptor mediates a metabolic checkpoint.* Mol Cell, 2008. **30**(2): p. 214-26.
186. Inoki, K., T. Zhu, and K.L. Guan, *TSC2 mediates cellular energy response to control cell growth and survival.* Cell, 2003. **115**(5): p. 577-90.

187. Alers, S., et al., *Atg13 and FIP200 act independently of Ulk1 and Ulk2 in autophagy induction.* Autophagy, 2011. **7**(12): p. 1423-33.
188. Joo, J.H., et al., *Hsp90-Cdc37 chaperone complex regulates Ulk1- and Atg13-mediated mitophagy.* Mol Cell, 2011. **43**(4): p. 572-85.
189. Itakura, E., et al., *Beclin 1 forms two distinct phosphatidylinositol 3-kinase complexes with mammalian Atg14 and UVRAG.* Mol Biol Cell, 2008. **19**(12): p. 5360-72.
190. Sun, Q., et al., *Identification of Barkor as a mammalian autophagy-specific factor for Beclin 1 and class III phosphatidylinositol 3-kinase.* Proc Natl Acad Sci U S A, 2008. **105**(49): p. 19211-6.
191. Park, J.M., et al., *The ULK1 complex mediates MTORC1 signaling to the autophagy initiation machinery via binding and phosphorylating ATG14.* Autophagy, 2016. **12**(3): p. 547-64.
192. Zhong, Y., et al., *Distinct regulation of autophagic activity by Atg14L and Rubicon associated with Beclin 1-phosphatidylinositol-3-kinase complex.* Nat Cell Biol, 2009. **11**(4): p. 468-76.
193. Hanahan, D. and R.A. Weinberg, *The hallmarks of cancer.* Cell, 2000. **100**(1): p. 57-70.
194. Hanahan, D. and R.A. Weinberg, *Hallmarks of cancer: the next generation.* Cell, 2011. **144**(5): p. 646-74.
195. Bonnet, D. and J.E. Dick, *Human acute myeloid leukemia is organized as a hierarchy that originates from a primitive hematopoietic cell.* Nat Med, 1997. **3**(7): p. 730-7.
196. Regenbrecht, C., H. Lehrach, and J. Adjaye, *Stemming Cancer: Functional Genomics of Cancer Stem Cells in Solid Tumors*. Vol. 4. 2008. 319-28.
197. Sancho, P., D. Barneda, and C. Heeschen, *Hallmarks of cancer stem cell metabolism.* Br J Cancer, 2016. **114**(12): p. 1305-12.
198. Cha, Y., et al., *Metabolic control of primed human pluripotent stem cell fate and function by the miR-200c–SIRT2 axis.* Nature Cell Biology, 2017. **19**(5): p. 445-456.
199. Dong, C., et al., *Loss of FBP1 by Snail-mediated repression provides metabolic advantages in basal-like breast cancer.* Cancer Cell, 2013. **23**(3): p. 316-31.
200. Banerjee, A., et al., *The effects of restricted glycolysis on stem-cell like characteristics of breast cancer cells.* Oncotarget, 2018. **9**(33): p. 23274-23288.
201. Zhou, Y., et al., *Metabolic alterations in highly tumorigenic glioblastoma cells: preference for hypoxia and high dependency on glycolysis.* J Biol Chem, 2011. **286**(37): p. 32843-53.
202. Emmink, B.L., et al., *The secretome of colon cancer stem cells contains drug-metabolizing enzymes.* J Proteomics, 2013. **91**: p. 84-96.
203. Folmes, C.D., et al., *Nuclear reprogramming with c-Myc potentiates glycolytic capacity of derived induced pluripotent stem cells.* J Cardiovasc Transl Res, 2013. **6**(1): p. 10-21.
204. Poli, V., et al., *MYC-driven epigenetic reprogramming favors the onset of tumorigenesis by inducing a stem cell-like state.* Nature Communications, 2018. **9**(1): p. 1024.
205. Pasto, A., et al., *Cancer stem cells from epithelial ovarian cancer patients privilege oxidative phosphorylation, and resist glucose deprivation.* Oncotarget, 2014. **5**(12): p. 4305-19.
206. Ye, X.Q., et al., *Mitochondrial and energy metabolism-related properties as novel indicators of lung cancer stem cells.* Int J Cancer, 2011. **129**(4): p. 820-31.
207. De Luca, A., et al., *Mitochondrial biogenesis is required for the anchorage-independent survival and propagation of stem-like cancer cells.* Oncotarget, 2015. **6**(17): p. 14777-95.
208. Janiszewska, M., et al., *Imp2 controls oxidative phosphorylation and is crucial for preserving glioblastoma cancer stem cells.* Genes Dev, 2012. **26**(17): p. 1926-44.
209. Ye, H., et al., *Leukemic Stem Cells Evade Chemotherapy by Metabolic Adaptation to an Adipose Tissue Niche.* Cell Stem Cell, 2016. **19**(1): p. 23-37.

210. Chen, C.L., et al., *NANOG Metabolically Reprograms Tumor-Initiating Stem-like Cells through Tumorigenic Changes in Oxidative Phosphorylation and Fatty Acid Metabolism.* Cell Metab, 2016. **23**(1): p. 206-19.
211. Tirinato, L., et al., *Lipid droplets: a new player in colorectal cancer stem cells unveiled by spectroscopic imaging.* Stem Cells, 2015. **33**(1): p. 35-44.
212. Noto, A., et al., *Stearoyl-CoA-desaturase 1 regulates lung cancer stemness via stabilization and nuclear localization of YAP/TAZ.* Oncogene, 2017. **36**(32): p. 4573-4584.
213. Noto, A., et al., *Stearoyl-CoA desaturase-1 is a key factor for lung cancer-initiating cells.* Cell Death Dis, 2013. **4**: p. e947.
214. Liu, S., et al., *FOXP3 inhibits cancer stem cell self-renewal via transcriptional repression of COX2 in colorectal cancer cells.* Oncotarget, 2017. **8**(27): p. 44694-44704.
215. Nieman, K.M., et al., *Adipocytes promote ovarian cancer metastasis and provide energy for rapid tumor growth.* Nat Med, 2011. **17**(11): p. 1498-503.
216. Vasudevan, A., et al., *Omega-3 fatty acid is a potential preventive agent for recurrent colon cancer.* Cancer prevention research (Philadelphia, Pa.), 2014. **7**(11): p. 1138-1148.
217. Li, J., et al., *Lipid Desaturation Is a Metabolic Marker and Therapeutic Target of Ovarian Cancer Stem Cells.* Cell Stem Cell, 2017. **20**(3): p. 303-314.e5.
218. Wang, X., et al., *MYC-Regulated Mevalonate Metabolism Maintains Brain Tumor-Initiating Cells.* Cancer Res, 2017. **77**(18): p. 4947-4960.
219. Sorrentino, G., et al., *Metabolic control of YAP and TAZ by the mevalonate pathway.* Nat Cell Biol, 2014. **16**(4): p. 357-66.
220. Lin, M., et al., *Downregulation of CPT2 promotes tumorigenesis and chemoresistance to cisplatin in hepatocellular carcinoma.* OncoTargets and therapy, 2018. **11**: p. 3101-3110.
221. Fujiwara, N., et al., *CPT2 downregulation adapts HCC to lipid-rich environment and promotes carcinogenesis via acylcarnitine accumulation in obesity.* Gut, 2018. **67**(8): p. 1493.
222. Montero, J., et al., *Mitochondrial cholesterol contributes to chemotherapy resistance in hepatocellular carcinoma.* Cancer Res, 2008. **68**(13): p. 5246-56.
223. Yao, C.H., et al., *Identifying off-target effects of etomoxir reveals that carnitine palmitoyltransferase I is essential for cancer cell proliferation independent of beta-oxidation.* PLoS Biol, 2018. **16**(3): p. e2003782.
224. Iwamoto, H., et al., *Cancer Lipid Metabolism Confers Antiangiogenic Drug Resistance.* Cell Metab, 2018. **28**(1): p. 104-117.e5.
225. Qiu, B., et al., *HIF2alpha-Dependent Lipid Storage Promotes Endoplasmic Reticulum Homeostasis in Clear-Cell Renal Cell Carcinoma.* Cancer Discov, 2015. **5**(6): p. 652-67.
226. Rysman, E., et al., *De novo lipogenesis protects cancer cells from free radicals and chemotherapeutics by promoting membrane lipid saturation.* Cancer Res, 2010. **70**(20): p. 8117-26.
227. Cotte, A.K., et al., *Lysophosphatidylcholine acyltransferase 2-mediated lipid droplet production supports colorectal cancer chemoresistance.* Nat Commun, 2018. **9**(1): p. 322.
228. Kurtova, A.V., et al., *Blocking PGE2-induced tumour repopulation abrogates bladder cancer chemoresistance.* Nature, 2015. **517**(7533): p. 209-13.
229. Toloczko-Iwaniuk, N., et al., *Celecoxib in Cancer Therapy and Prevention - Review.* Curr Drug Targets, 2019. **20**(3): p. 302-315.
230. Wang, D. and R.N. Dubois, *The role of COX-2 in intestinal inflammation and colorectal cancer.* Oncogene, 2010. **29**(6): p. 781-8.
231. Xu, L., et al., *COX-2 inhibition potentiates antiangiogenic cancer therapy and prevents metastasis in preclinical models.* Sci Transl Med, 2014. **6**(242): p. 242ra84.

232. Schcolnik-Cabrera, A., et al., *Orlistat as a FASN inhibitor and multitargeted agent for cancer therapy.* Expert Opin Investig Drugs, 2018. **27**(5): p. 475-489.
233. Zaidi, N., J.V. Swinnen, and K. Smans, *ATP-Citrate Lyase: A Key Player in Cancer Metabolism.* Cancer Research, 2012. **72**(15): p. 3709.
234. Guan, M., et al., *Nelfinavir induces liposarcoma apoptosis through inhibition of regulated intramembrane proteolysis of SREBP-1 and ATF6.* Clin Cancer Res, 2011. **17**(7): p. 1796-806.
235. Guan, M., et al., *Nelfinavir and nelfinavir analogs block site-2 protease cleavage to inhibit castration-resistant prostate cancer.* Sci Rep, 2015. **5**: p. 9698.
236. Beloribi-Djefaflia, S., S. Vasseur, and F. Guillaumond, *Lipid metabolic reprogramming in cancer cells.* Oncogenesis, 2016. **5**: p. e189.
237. Han, X. and R.W. Gross, *Electrospray ionization mass spectroscopic analysis of human erythrocyte plasma membrane phospholipids.* Proceedings of the National Academy of Sciences of the United States of America, 1994. **91**(22): p. 10635-10639.
238. Han, X. and R.W. Gross, *Global analyses of cellular lipidomes directly from crude extracts of biological samples by ESI mass spectrometry: a bridge to lipidomics.* J Lipid Res, 2003. **44**(6): p. 1071-9.
239. Lee, S.H., et al., *Targeted lipidomics using electron capture atmospheric pressure chemical ionization mass spectrometry.* Rapid Communications in Mass Spectrometry, 2003. **17**(19): p. 2168-2176.
240. Cheng, H., et al., *Specificity and potential mechanism of sulfatide deficiency in Alzheimer's disease: an electrospray ionization mass spectrometric study.* Cell Mol Biol (Noisy-le-grand), 2003. **49**(5): p. 809-18.
241. Shalem, O., et al., *Genome-Scale CRISPR-Cas9 Knockout Screening in Human Cells.* Science, 2014. **343**(6166): p. 84-87.
242. Anders, S. and W. Huber, *Differential expression analysis for sequence count data.* Genome Biology, 2010. **11**(10): p. R106.
243. Li, H., et al., *The landscape of cancer cell line metabolism*. Vol. 25. 2019. 850-860.
244. Wang, T., et al., *Genetic screens in human cells using the CRISPR-Cas9 system.* Science, 2014. **343**(6166): p. 80-4.
245. Warburg, O., *The Metabolism of Carcinoma Cells.* The Journal of Cancer Research, 1925. **9**(1): p. 148-163.
246. Gaude, E. and C. Frezza, *Tissue-specific and convergent metabolic transformation of cancer correlates with metastatic potential and patient survival.* Nature Communications, 2016. **7**(1): p. 13041.
247. Hu, J., et al., *Heterogeneity of tumor-induced gene expression changes in the human metabolic network.* Nat Biotechnol, 2013. **31**(6): p. 522-9.
248. Subramanian, A., et al., *GSEA-P: a desktop application for Gene Set Enrichment Analysis.* Bioinformatics, 2007. **23**(23): p. 3251-3.
249. Subramanian, A., et al., *Gene set enrichment analysis: A knowledge-based approach for interpreting genome-wide expression profiles.* Proceedings of the National Academy of Sciences, 2005. **102**(43): p. 15545-15550.
250. Love, M.I., W. Huber, and S. Anders, *Moderated estimation of fold change and dispersion for RNA-seq data with DESeq2.* Genome Biology, 2014. **15**(12): p. 550.
251. Evans, C., J. Hardin, and D.M. Stoebel, *Selecting between-sample RNA-Seq normalization methods from the perspective of their assumptions.* Briefings in bioinformatics, 2018. **19**(5): p. 776-792.
252. Li, P., et al., *Comparing the normalization methods for the differential analysis of Illumina high-throughput RNA-Seq data.* BMC Bioinformatics, 2015. **16**(1): p. 347.
253. Alkhateeb, A. and L. Rueda, *Zseq: An Approach for Preprocessing Next-Generation Sequencing Data.* Journal of computational biology : a journal of computational molecular cell biology, 2017. **24**(8): p. 746-755.

254. Colantuoni, C., et al., *SNOMAD (Standardization and NOrmalization of MicroArray Data): web-accessible gene expression data analysis.* Bioinformatics, 2002. **18**(11): p. 1540-1541.
255. Ortmayr, K., S. Dubuis, and M. Zampieri, *Metabolic profiling of cancer cells reveals genome-wide crosstalk between transcriptional regulators and metabolism.* Nature Communications, 2019. **10**(1): p. 1841.
256. Ghandi, M., et al., *Next-generation characterization of the Cancer Cell Line Encyclopedia.* Nature, 2019. **569**(7757): p. 503-508.
257. van der Maaten, L.J.P.H., G.E., *Visualizing High-Dimensional Data Using t-SNE.* Hournal of Machine Learning Research, 2008. **9**(Nov): p. 2579-2605.
258. Reznik, E. and C. Sander, *Extensive decoupling of metabolic genes in cancer.* PLoS Comput Biol, 2015. **11**(5): p. e1004176.
259. Gross, A.M., J.F. Kreisberg, and T. Ideker, *Analysis of Matched Tumor and Normal Profiles Reveals Common Transcriptional and Epigenetic Signals Shared across Cancer Types.* PLoS One, 2015. **10**(11): p. e0142618.
260. Reznik, E., et al., *A Landscape of Metabolic Variation across Tumor Types.* Cell Syst, 2018. **6**(3): p. 301-313.e3.
261. Miska, J., et al., *HIF-1alpha Is a Metabolic Switch between Glycolytic-Driven Migration and Oxidative Phosphorylation-Driven Immunosuppression of Tregs in Glioblastoma.* Cell Rep, 2019. **27**(1): p. 226-237.e4.
262. Jia, D., et al., *Elucidating cancer metabolic plasticity by coupling gene regulation with metabolic pathways.* Proceedings of the National Academy of Sciences, 2019. **116**(9): p. 3909-3918.
263. Shukla, S.K., et al., *MUC1 and HIF-1alpha Signaling Crosstalk Induces Anabolic Glucose Metabolism to Impart Gemcitabine Resistance to Pancreatic Cancer.* Cancer Cell, 2017. **32**(1): p. 71-87.e7.
264. Zhou, L., et al., *HOXA9 inhibits HIF-1α-mediated glycolysis through interacting with CRIP2 to repress cutaneous squamous cell carcinoma development.* Nature Communications, 2018. **9**(1): p. 1480.
265. Dabral, S., et al., *A RASSF1A-HIF1α loop drives Warburg effect in cancer and pulmonary hypertension.* Nature Communications, 2019. **10**(1): p. 2130.
266. Sinkala, M., N. Mulder, and D. Patrick Martin, *Metabolic gene alterations impact the clinical aggressiveness and drug responses of 32 human cancers.* Communications Biology, 2019. **2**(1): p. 414.
267. Krishnan, J., et al., *Activation of a HIF1alpha-PPARgamma axis underlies the integration of glycolytic and lipid anabolic pathways in pathologic cardiac hypertrophy.* Cell Metab, 2009. **9**(6): p. 512-24.
268. Zhao, Y.Z., et al., *Hypoxia induces peroxisome proliferator-activated receptor gamma expression via HIF-1-dependent mechanisms in HepG2 cell line.* Arch Biochem Biophys, 2014. **543**: p. 40-7.
269. Hu, E., et al., *Inhibition of adipogenesis through MAP kinase-mediated phosphorylation of PPARgamma.* Science, 1996. **274**(5295): p. 2100-3.
270. Duvel, K., et al., *Activation of a metabolic gene regulatory network downstream of mTOR complex 1.* Mol Cell, 2010. **39**(2): p. 171-83.
271. Furuta, E., et al., *Fatty acid synthase gene is up-regulated by hypoxia via activation of Akt and sterol regulatory element binding protein-1.* Cancer Res, 2008. **68**(4): p. 1003-11.
272. Lee, H.J., et al., *BNIP3 induction by hypoxia stimulates FASN-dependent free fatty acid production enhancing therapeutic potential of umbilical cord blood-derived human mesenchymal stem cells.* Redox Biol, 2017. **13**: p. 426-443.
273. Nishiyama, Y., et al., *HIF-1alpha induction suppresses excessive lipid accumulation in alcoholic fatty liver in mice.* J Hepatol, 2012. **56**(2): p. 441-7.
274. Yoshikawa, T., et al., *Cross-talk between peroxisome proliferator-activated receptor (PPAR) alpha and liver X receptor (LXR) in nutritional regulation of fatty acid metabolism. I. PPARs suppress sterol regulatory element binding protein-1c*

promoter through inhibition of LXR signaling. Mol Endocrinol, 2003. **17**(7): p. 1240-54.
275. Kaplan, J.M., et al., *Phosphorylation of extracellular signal-regulated kinase (ERK)-1/2 Is associated with the downregulation of peroxisome proliferator-activated receptor (PPAR)-gamma during polymicrobial sepsis.* Mol Med, 2010. **16**(11-12): p. 491-7.
276. Karoulia, Z., E. Gavathiotis, and P.I. Poulikakos, *New perspectives for targeting RAF kinase in human cancer.* Nature Reviews Cancer, 2017. **17**: p. 676.
277. Pisanu, M.E., et al., *Inhibition of Stearoyl-CoA desaturase 1 reverts BRAF and MEK inhibition-induced selection of cancer stem cells in BRAF-mutated melanoma.* Journal of Experimental & Clinical Cancer Research, 2018. **37**(1): p. 318.
278. Zhao, L., et al., *HMG-CoA synthase 1 is a synthetic lethal partner of BRAF(V600E) in human cancers.* J Biol Chem, 2017. **292**(24): p. 10142-10152.
279. Kang, H.B., et al., *Metabolic Rewiring by Oncogenic BRAF V600E Links Ketogenesis Pathway to BRAF-MEK1 Signaling.* Mol Cell, 2015. **59**(3): p. 345-358.
280. Haq, R., et al., *Oncogenic BRAF regulates oxidative metabolism via PGC1alpha and MITF.* Cancer Cell, 2013. **23**(3): p. 302-15.
281. Sakai, E., et al., *Combined Mutation of Apc, Kras, and Tgfbr2 Effectively Drives Metastasis of Intestinal Cancer.* Cancer Res, 2018. **78**(5): p. 1334-1346.
282. Kuipers, E.J., et al., *Colorectal cancer.* Nature Reviews Disease Primers, 2015. **1**: p. 15065.
283. Hutton, J.E., et al., *Oncogenic KRAS and BRAF Drive Metabolic Reprogramming in Colorectal Cancer.* Molecular & Cellular Proteomics : MCP, 2016. **15**(9): p. 2924-2938.
284. Vallee, A., et al., *Opposite Interplay Between the Canonical WNT/beta-Catenin Pathway and PPAR Gamma: A Potential Therapeutic Target in Gliomas.* Neurosci Bull, 2018. **34**(3): p. 573-588.
285. Vallée, A. and Y. Lecarpentier, *Crosstalk Between Peroxisome Proliferator-Activated Receptor Gamma and the Canonical WNT/β-Catenin Pathway in Chronic Inflammation and Oxidative Stress During Carcinogenesis.* Frontiers in immunology, 2018. **9**: p. 745-745.
286. Lecarpentier, Y., et al., *Interactions between PPAR Gamma and the Canonical Wnt/Beta-Catenin Pathway in Type 2 Diabetes and Colon Cancer.* PPAR research, 2017. **2017**: p. 5879090-5879090.
287. Sabatino, L., et al., *PPARG Epigenetic Deregulation and Its Role in Colorectal Tumorigenesis.* PPAR Res, 2012. **2012**: p. 687492.
288. Lodhi, I.J. and C.F. Semenkovich, *Peroxisomes: a nexus for lipid metabolism and cellular signaling.* Cell metabolism, 2014. **19**(3): p. 380-392.
289. Lodhi, Irfan J., et al., *Inhibiting Adipose Tissue Lipogenesis Reprograms Thermogenesis and PPARγ Activation to Decrease Diet-Induced Obesity.* Cell Metabolism, 2012. **16**(2): p. 189-201.
290. Lodhi, I.J., et al., *Inhibiting adipose tissue lipogenesis reprograms thermogenesis and PPARgamma activation to decrease diet-induced obesity.* Cell Metab, 2012. **16**(2): p. 189-201.
291. Hutton, J.E., et al., *Oncogenic KRAS and BRAF Drive Metabolic Reprogramming in Colorectal Cancer.* Mol Cell Proteomics, 2016. **15**(9): p. 2924-38.
292. Nagarajah, J., et al., *Correlation of BRAFV600E Mutation and Glucose Metabolism in Thyroid Cancer Patients: An (1)(8)F-FDG PET Study.* J Nucl Med, 2015. **56**(5): p. 662-7.
293. Roth, G., et al., *MAP kinases Erk1/2 phosphorylate sterol regulatory element-binding protein (SREBP)-1a at serine 117 in vitro.* J Biol Chem, 2000. **275**(43): p. 33302-7.
294. Lim, H.Y., et al., *Phospholipid homeostasis regulates lipid metabolism and cardiac function through SREBP signaling in Drosophila.* Genes Dev, 2011. **25**(2): p. 189-200.

295. Rong, X., et al., *ER phospholipid composition modulates lipogenesis during feeding and in obesity.* J Clin Invest, 2017. **127**(10): p. 3640-3651.
296. Walker, A.K., et al., *A conserved SREBP-1/phosphatidylcholine feedback circuit regulates lipogenesis in metazoans.* Cell, 2011. **147**(4): p. 840-52.
297. Nagura, M., et al., *Alterations of fatty acid metabolism and membrane fluidity in peroxisome-defective mutant ZP102 cells.* Lipids, 2004. **39**(1): p. 43-50.
298. Flis, V.V., et al., *Phosphatidylcholine Supply to Peroxisomes of the Yeast Saccharomyces cerevisiae.* PloS one, 2015. **10**(8): p. e0135084-e0135084.
299. Chen, H., Z. Liu, and X. Huang, *Drosophila models of peroxisomal biogenesis disorder: peroxins are required for spermatogenesis and very-long-chain fatty acid metabolism.* Hum Mol Genet, 2010. **19**(3): p. 494-505.
300. Roos, D.S. and P.W. Choppin, *Tumorigenicity of cell lines with altered lipid composition.* Proc Natl Acad Sci U S A, 1984. **81**(23): p. 7622-6.
301. Howard, B.V., H.P. Morris, and J.M. Bailey, *Ether-lipids, -glycerol phosphate dehydrogenase, and growth rate in tumors and cultured cells.* Cancer Res, 1972. **32**(7): p. 1533-8.
302. Benjamin, D.I., et al., *Ether lipid generating enzyme AGPS alters the balance of structural and signaling lipids to fuel cancer pathogenicity.* Proc Natl Acad Sci U S A, 2013. **110**(37): p. 14912-7.
303. Shpilka, T., et al., *Lipid droplets and their component triglycerides and steryl esters regulate autophagosome biogenesis.* The EMBO Journal, 2015. **34**(16): p. 2117-2131.
304. Li, S., et al., *Transcriptional regulation of autophagy-lysosomal function in BRAF-driven melanoma progression and chemoresistance.* Nature Communications, 2019. **10**(1): p. 1693.
305. Wang, W., et al., *Targeting Autophagy Sensitizes BRAF-Mutant Thyroid Cancer to Vemurafenib.* The Journal of Clinical Endocrinology & Metabolism, 2016. **102**(2): p. 634-643.
306. Eun, S.Y., et al., *PEX5 regulates autophagy via the mTORC1-TFEB axis during starvation.* Experimental & Molecular Medicine, 2018. **50**(4): p. 4.
307. Watt, M.J., et al., *Fatty acids stimulate AMP-activated protein kinase and enhance fatty acid oxidation in L6 myotubes.* The Journal of physiology, 2006. **574**(Pt 1): p. 139-147.
308. Xue, B., et al., *Omega-3 polyunsaturated fatty acids antagonize macrophage inflammation via activation of AMPK/SIRT1 pathway.* PLoS One, 2012. **7**(10): p. e45990.
309. Weikel, Karen A., et al., *Knockdown of GSK3β increases basal autophagy and AMPK signalling in nutrient-laden human aortic endothelial cells.* Bioscience Reports, 2016. **36**(5): p. e00382.
310. Mootha, V.K., et al., *PGC-1α-responsive genes involved in oxidative phosphorylation are coordinately downregulated in human diabetes.* Nature Genetics, 2003. **34**(3): p. 267-273.
311. Kaushik, S. and A.M. Cuervo, *AMPK-dependent phosphorylation of lipid droplet protein PLIN2 triggers its degradation by CMA.* Autophagy, 2016. **12**(2): p. 432-8.
312. Liberzon, A., et al., *The Molecular Signatures Database (MSigDB) hallmark gene set collection.* Cell Syst, 2015. **1**(6): p. 417-425.
313. Gapp, B.V., et al., *Parallel reverse genetic screening in mutant human cells using transcriptomics.* Molecular systems biology, 2016. **12**(8): p. 879-879.
314. Jaitin, D.A., et al., *Dissecting Immune Circuits by Linking CRISPR-Pooled Screens with Single-Cell RNA-Seq.* Cell, 2016. **167**(7): p. 1883-1896.e15.
315. Adamson, B., et al., *A Multiplexed Single-Cell CRISPR Screening Platform Enables Systematic Dissection of the Unfolded Protein Response.* Cell, 2016. **167**(7): p. 1867-1882.e21.
316. Yost, K.E., et al., *Clonal replacement of tumor-specific T cells following PD-1 blockade.* Nature Medicine, 2019. **25**(8): p. 1251-1259.

317. Han, H., S. Lee, and I. Lee, *NGSEA: Network-Based Gene Set Enrichment Analysis for Interpreting Gene Expression Phenotypes with Functional Gene Sets.* Molecules and cells, 2019. **42**(8): p. 579-588.
318. Nishimura, D., *BioCarta.* Biotech Software & Internet Report, 2001. **2**(3): p. 117-120.
319. Benjamini, Y. and Y. Hochberg, *Controlling the False Discovery Rate: A Practical and Powerful Approach to Multiple Testing.* Journal of the Royal Statistical Society. Series B (Methodological), 1995. **57**(1): p. 289-300.
320. García-Nieto, P.E., A.J. Morrison, and H.B. Fraser, *The somatic mutation landscape of the human body.* bioRxiv, 2019: p. 668624.
321. Martincorena, I., et al., *High burden and pervasive positive selection of somatic mutations in normal human skin.* Science, 2015. **348**(6237): p. 880-886.
322. Lee-Six, H., et al., *The landscape of somatic mutation in normal colorectal epithelial cells.* bioRxiv, 2018: p. 416800.
323. Yokoyama, A., et al., *Age-related remodelling of oesophageal epithelia by mutated cancer drivers.* Nature, 2019. **565**(7739): p. 312-317.
324. Martincorena, I., et al., *Somatic mutant clones colonize the human esophagus with age.* Science, 2018. **362**(6417): p. 911-917.
325. Bae, T., et al., *Different mutational rates and mechanisms in human cells at pregastrulation and neurogenesis.* Science, 2018. **359**(6375): p. 550-555.
326. Tirosh, I., et al., *Dissecting the multicellular ecosystem of metastatic melanoma by single-cell RNA-seq.* Science, 2016. **352**(6282): p. 189-196.
327. Patel, A.P., et al., *Single-cell RNA-seq highlights intratumoral heterogeneity in primary glioblastoma.* Science, 2014. **344**(6190): p. 1396-1401.
328. Lee, M.-C.W., et al., *Single-cell analyses of transcriptional heterogeneity during drug tolerance transition in cancer cells by RNA sequencing.* Proceedings of the National Academy of Sciences, 2014. **111**(44): p. E4726-E4735.
329. Rysman, E., et al., *De novo Lipogenesis Protects Cancer Cells from Free Radicals and Chemotherapeutics by Promoting Membrane Lipid Saturation.* Cancer Research, 2010. **70**(20): p. 8117-8126.
330. Wang, X., et al., *Fatty acid receptor GPR120 promotes breast cancer chemoresistance by upregulating ABC transporters expression and fatty acid synthesis.* EBioMedicine, 2019. **40**: p. 251-262.
331. Cui, H., et al., *ABC Transporter Inhibitors in Reversing Multidrug Resistance to Chemotherapy.* Curr Drug Targets, 2015. **16**(12): p. 1356-71.
332. Gottesman, M.M., T. Fojo, and S.E. Bates, *Multidrug resistance in cancer: role of ATP–dependent transporters.* Nature Reviews Cancer, 2002. **2**(1): p. 48-58.
333. Roodhart, J.M., et al., *Mesenchymal stem cells induce resistance to chemotherapy through the release of platinum-induced fatty acids.* Cancer Cell, 2011. **20**(3): p. 370-83.
334. Kim, S.-J., et al., *Stearoyl CoA desaturase (SCD) facilitates proliferation of prostate cancer cells through enhancement of androgen receptor transactivation.* Molecules and cells, 2011. **31**(4): p. 371-377.
335. Cruz-Gil, S., et al., *Targeting the lipid metabolic axis ACSL/SCD in colorectal cancer progression by therapeutic miRNAs: miR-19b-1 role.* J Lipid Res, 2018. **59**(1): p. 14-24.
336. Young, R.M., et al., *Dysregulated mTORC1 renders cells critically dependent on desaturated lipids for survival under tumor-like stress.* Genes Dev, 2013. **27**(10): p. 1115-31.
337. Wang, H., G. Kouri, and C.B. Wollheim, *ER stress and SREBP-1 activation are implicated in β-cell glucolipotoxicity.* Journal of Cell Science, 2005. **118**(17): p. 3905-3915.
338. Corsetto, P.A., et al., *ω-3 Long Chain Polyunsaturated Fatty Acids as Sensitizing Agents and Multidrug Resistance Revertants in Cancer Therapy.* International journal of molecular sciences, 2017. **18**(12): p. 2770.

339. De Carlo, F., et al., *Omega-3 eicosapentaenoic acid decreases CD133 colon cancer stem-like cell marker expression while increasing sensitivity to chemotherapy.* PLoS One, 2013. **8**(7): p. e69760.
340. Rudra, P.K. and H.E. Krokan, *Cell-specific enhancement of doxorubicin toxicity in human tumour cells by docosahexaenoic acid.* Anticancer Res, 2001. **21**(1a): p. 29-38.
341. Hardman, W.E., et al., *Three percent dietary fish oil concentrate increased efficacy of doxorubicin against MDA-MB 231 breast cancer xenografts.* Clin Cancer Res, 2001. **7**(7): p. 2041-9.
342. Yan, M., et al., *15-Hydroxyprostaglandin dehydrogenase inactivation as a mechanism of resistance to celecoxib chemoprevention of colon tumors.* Proc Natl Acad Sci U S A, 2009. **106**(23): p. 9409-13.
343. Cotte, A.K., et al., *LPCAT2 controls chemoresistance in colorectal cancer.* Molecular & cellular oncology, 2018. **5**(3): p. e1448245-e1448245.
344. Iorio, F., et al., *A Landscape of Pharmacogenomic Interactions in Cancer.* Cell, 2016. **166**(3): p. 740-754.
345. Garnett, M.J., et al., *Systematic identification of genomic markers of drug sensitivity in cancer cells.* Nature, 2012. **483**(7391): p. 570-575.
346. Cotte, A.K., et al., *Phospholipid profiles and hepatocellular carcinoma risk and prognosis in cirrhotic patients.* Oncotarget, 2019. **10**(22): p. 2161-2172.
347. Zhang, X., et al., *Phospholipid Phosphatase 4 promotes proliferation and tumorigenesis, and activates Ca(2+)-permeable Cationic Channel in lung carcinoma cells.* Mol Cancer, 2017. **16**(1): p. 147.
348. Gu, L., et al., *Amplification of Glyceronephosphate O-Acyltransferase and Recruitment of USP30 Stabilize DRP1 to Promote Hepatocarcinogenesis.* Cancer Res, 2018. **78**(20): p. 5808-5819.
349. Piano, V., et al., *Discovery of Inhibitors for the Ether Lipid-Generating Enzyme AGPS as Anti-Cancer Agents.* ACS chemical biology, 2015. **10**(11): p. 2589-2597.
350. Zhu, Y., et al., *Role and mechanism of the alkylglycerone phosphate synthase in suppressing the invasion potential of human glioma and hepatic carcinoma cells in vitro.* Oncol Rep, 2014. **32**(1): p. 431-6.
351. Chen, L., et al., *Peroxisome proliferator-activated receptor gamma promotes epithelial to mesenchymal transformation by Rho GTPase-dependent activation of ERK1/2.* J Biol Chem, 2006. **281**(34): p. 24575-87.
352. Reka, A.K., et al., *Peroxisome proliferator-activated receptor-gamma activation inhibits tumor metastasis by antagonizing Smad3-mediated epithelial-mesenchymal transition.* Mol Cancer Ther, 2010. **9**(12): p. 3221-32.
353. Leung, D.T.H., et al., *Combined PPARgamma Activation and XIAP Inhibition as a Potential Therapeutic Strategy for Ovarian Granulosa Cell Tumors.* Mol Cancer Ther, 2019. **18**(2): p. 364-375.
354. Oruqaj, G., et al., *Compromised peroxisomes in idiopathic pulmonary fibrosis, a vicious cycle inducing a higher fibrotic response via TGF-beta signaling.* Proc Natl Acad Sci U S A, 2015. **112**(16): p. E2048-57.
355. Luengo, A., D.Y. Gui, and M.G. Vander Heiden, *Targeting Metabolism for Cancer Therapy.* Cell Chem Biol, 2017. **24**(9): p. 1161-1180.
356. Yen, K., et al., *AG-221, a First-in-Class Therapy Targeting Acute Myeloid Leukemia Harboring Oncogenic IDH2 Mutations.* Cancer Discov, 2017. **7**(5): p. 478-493.
357. Janin, M., et al., *Serum 2-hydroxyglutarate production in IDH1- and IDH2-mutated de novo acute myeloid leukemia: a study by the Acute Leukemia French Association group.* J Clin Oncol, 2014. **32**(4): p. 297-305.
358. Kim, E.S., *Enasidenib: First Global Approval.* Drugs, 2017. **77**(15): p. 1705-1711.
359. Dhillon, S., *Ivosidenib: First Global Approval.* Drugs, 2018. **78**(14): p. 1509-1516.
360. Huang, L.E., *Friend or foe—IDH1 mutations in glioma 10 years on.* Carcinogenesis, 2019.

361. Dang, L., S. Jin, and S.M. Su, *IDH mutations in glioma and acute myeloid leukemia.* Trends Mol Med, 2010. **16**(9): p. 387-97.
362. Chow, L.W., W.T. Loo, and M. Toi, *Current directions for COX-2 inhibition in breast cancer.* Biomed Pharmacother, 2005. **59 Suppl 2**: p. S281-4.
363. Comerford, S.A., et al., *Acetate dependence of tumors.* Cell, 2014. **159**(7): p. 1591-602.
364. Sarraf, P., et al., *Differentiation and reversal of malignant changes in colon cancer through PPARgamma.* Nat Med, 1998. **4**(9): p. 1046-52.
365. Chen, Y.X., et al., *15d-PGJ2 inhibits cell growth and induces apoptosis of MCG-803 human gastric cancer cell line.* World J Gastroenterol, 2003. **9**(10): p. 2149-53.
366. Chen, L., et al., *RS5444, a novel PPARgamma agonist, regulates aspects of the differentiated phenotype in nontransformed intestinal epithelial cells.* Mol Cell Endocrinol, 2006. **251**(1-2): p. 17-32.
367. Yu, C., et al., *Oncogenic TRIM31 confers gemcitabine resistance in pancreatic cancer via activating the NF-kappaB signaling pathway.* Theranostics, 2018. **8**(12): p. 3224-3236.
368. Wang, D., et al., *Colorectal cancer cell-derived CCL20 recruits regulatory T cells to promote chemoresistance via FOXO1/CEBPB/NF-κB signaling.* Journal for ImmunoTherapy of Cancer, 2019. **7**(1): p. 215.
369. Remels, A.H., et al., *PPARgamma inhibits NF-kappaB-dependent transcriptional activation in skeletal muscle.* Am J Physiol Endocrinol Metab, 2009. **297**(1): p. E174-83.
370. Hou, Y., F. Moreau, and K. Chadee, *PPARgamma is an E3 ligase that induces the degradation of NFkappaB/p65.* Nat Commun, 2012. **3**: p. 1300.
371. Zhou, K., et al., *Pharmacogenomics in diabetes mellitus: insights into drug action and drug discovery.* Nature Reviews Endocrinology, 2016. **12**(6): p. 337-346.
372. Rong, X., et al., *LXRs regulate ER stress and inflammation through dynamic modulation of membrane phospholipid composition.* Cell metabolism, 2013. **18**(5): p. 685-697.
373. Leamy, A.K., et al., *Enhanced synthesis of saturated phospholipids is associated with ER stress and lipotoxicity in palmitate treated hepatic cells.* J Lipid Res, 2014. **55**(7): p. 1478-88.
374. Weber, S.M., et al., *PPARgamma ligands induce ER stress in pancreatic beta-cells: ER stress activation results in attenuation of cytokine signaling.* Am J Physiol Endocrinol Metab, 2004. **287**(6): p. E1171-7.
375. Park, S.H., et al., *Endoplasmic reticulum stress-activated C/EBP homologous protein enhances nuclear factor-kappaB signals via repression of peroxisome proliferator-activated receptor gamma.* J Biol Chem, 2010. **285**(46): p. 35330-9.
376. Shen, W., et al., *Targeting SREBP1 chemosensitizes colorectal cancer cells to gemcitabine by caspase-7 upregulation.* Bioengineered, 2019. **10**(1): p. 459-468.
377. Punga, T., M.T. Bengoechea-Alonso, and J. Ericsson, *Phosphorylation and ubiquitination of the transcription factor sterol regulatory element-binding protein-1 in response to DNA binding.* J Biol Chem, 2006. **281**(35): p. 25278-86.
378. Bengoechea-Alonso, M.T. and J. Ericsson, *A phosphorylation cascade controls the degradation of active SREBP1.* J Biol Chem, 2009. **284**(9): p. 5885-95.
379. Tajima-Shirasaki, N., et al., *Eicosapentaenoic acid down-regulates expression of the selenoprotein P gene by inhibiting SREBP-1c protein independently of the AMP-activated protein kinase pathway in H4IIEC3 hepatocytes.* J Biol Chem, 2017. **292**(26): p. 10791-10800.
380. Thewke, D.P., S.R. Panini, and M. Sinensky, *Oleate potentiates oxysterol inhibition of transcription from sterol regulatory element-1-regulated promoters and maturation of sterol regulatory element-binding proteins.* J Biol Chem, 1998. **273**(33): p. 21402-7.

381. Worgall, T.S., et al., *Polyunsaturated fatty acids decrease expression of promoters with sterol regulatory elements by decreasing levels of mature sterol regulatory element-binding protein.* J Biol Chem, 1998. **273**(40): p. 25537-40.
382. Ploier, B., et al., *Screening for hydrolytic enzymes reveals Ayr1p as a novel triacylglycerol lipase in Saccharomyces cerevisiae.* J Biol Chem, 2013. **288**(50): p. 36061-72.
383. Cai, M., et al., *Phospholipase D1-regulated autophagy supplies free fatty acids to counter nutrient stress in cancer cells.* Cell Death & Disease, 2016. **7**(11): p. e2448-e2448.
384. Jing, K., et al., *Docosahexaenoic acid induces autophagy through p53/AMPK/mTOR signaling and promotes apoptosis in human cancer cells harboring wild-type p53.* Autophagy, 2011. **7**(11): p. 1348-58.
385. Qi, H.Y., et al., *A cytosolic phospholipase A2-initiated lipid mediator pathway induces autophagy in macrophages.* J Immunol, 2011. **187**(10): p. 5286-92.
386. Niso-Santano, M., et al., *Unsaturated fatty acids induce non-canonical autophagy.* The EMBO journal, 2015. **34**(8): p. 1025-1041.
387. Satoh, K., et al., *Global metabolic reprogramming of colorectal cancer occurs at adenoma stage and is induced by MYC.* Proceedings of the National Academy of Sciences, 2017. **114**(37): p. E7697-E7706.
388. Zavialova, M.G., et al., *Is myelin basic protein a potential biomarker of brain cancer?* European Journal of Mass Spectrometry, 2017. **23**(4): p. 192-196.
389. Nagahashi, M., et al., *High levels of sphingolipids in human breast cancer.* J Surg Res, 2016. **204**(2): p. 435-444.
390. Zheng, K., et al., *Sphingomyelin synthase 2 promotes an aggressive breast cancer phenotype by disrupting the homoeostasis of ceramide and sphingomyelin.* Cell Death & Disease, 2019. **10**(3): p. 157.
391. Moro, K., et al., *Ceramide species are elevated in human breast cancer and are associated with less aggressiveness.* Oncotarget, 2018. **9**(28): p. 19874-19890.
392. Osawa, T., et al., *Phosphoethanolamine Accumulation Protects Cancer Cells under Glutamine Starvation through Downregulation of PCYT2.* Cell Rep, 2019. **29**(1): p. 89-103.e7.
393. Xiao, Z., Z. Dai, and J.W. Locasale, *Metabolic landscape of the tumor microenvironment at single cell resolution.* Nature Communications, 2019. **10**(1): p. 3763.
394. Mootha, V.K., et al, *PGC-1a-responsive genes involved in oxidative phosphorylation are coordinately downregulated in human diabetes*. Nature Genetics, 2003. **34**:p.267
395. Birsoy, K., et al, An essential role of the mitochondrial electron transport chain in cell proliferation is to enable aspartate synthesis. Cell, 2015. **162**(3):p540
396. Miska, J., et al, *HIF-1a is a metabolic switch between glycolytic-driven migration and oxidative phosphorylation-driven immunosuppression of Tregs in glioblastoma.* Cell Reports, 2019. **2**(27):p.226.
397. Livak, K. J., & Schmittgen, T., D, Analysis of relative gene expression data using real-time quantitative PCR and the 2(-DeltaDelta C(T)) Method. Methods, 2001. Dec 25(4): p402-8.
398. Schneider, C. A., Rasband, W. S. & Eliceiri, K. W., *NIH Image to ImageJ: 25 years of image analysis.* Nature Methods, 2012. **9**:p671-75
399. Kim, D., et al. G*raph-based genome alignment and genotyping with HISAT2 and HISAT-genotype,* Nature Biotechnology. 2019. **37**:p907-15

Appendix A. Publications

Hydroxysteroid dehydrogenase HSD1L is localised to the pituitary–gonadal axis of primates

A Daniel Bird[1,*,†], Spencer Greatorex[1,†], David Reser[2], Gareth G Lavery[3,4] and Timothy J Cole[1]

[1]Department of Biochemistry and Molecular Biology, Monash University, Melbourne, Victoria, Australia
[2]Department of Physiology, Monash University, Melbourne, Victoria, Australia
[3]Institute of Metabolism and Systems Research, 2nd Floor IBR Tower, University of Birmingham, Birmingham, UK
[4]Centre for Endocrinology, Diabetes and Metabolism, Birmingham Health Partners, Birmingham, UK
*(A D Bird is now at the Centre for Endocrinology and Metabolism, Hudson Institute of Medical Research, Monash Medical Centre, Clayton, Victoria, Australia)
[†](A D Bird and S Greatorex contributed equally to this work)

Correspondence should be addressed to T J Cole
Email
tim.cole@monash.edu

Abstract

Steroid hormones play clinically important and specific regulatory roles in the development, growth, metabolism, reproduction and brain function in human. The type 1 and 2 11-beta hydroxysteroid dehydrogenase enzymes (11β-HSD1 and 2) have key roles in the pre-receptor modification of glucocorticoids allowing aldosterone regulation of blood pressure, control of systemic fluid and electrolyte homeostasis and modulation of integrated metabolism and brain function. Although the activity and function of 11β-HSDs is thought to be understood, there exists an open reading frame for a distinct 11βHSD-like gene; *HSD11B1L,* which is present in human, non-human primate, sheep, pig and many other higher organisms, whereas an orthologue is absent in the genomes of mouse, rat and rabbit. We have now characterised this novel *HSD11B1L* gene as encoded by 9 exons and analysis of EST library transcripts indicated the use of two alternate ATG start sites in exons 2 and 3, and alternate splicing in exon 9. Relatively strong *HSD11B1L* gene expression was detected in human, non-human primate and sheep tissue samples from the brain, ovary and testis. Analysis in non-human primates and sheep by immunohistochemistry localised HSD11B1L protein to the cytoplasm of ovarian granulosa cells, testis Leydig cells, and gonadatroph cells in the anterior pituitary. Intracellular localisation analysis in transfected human HEK293 cells showed HSD1L protein within the endoplasmic reticulum and sequence analysis suggests that similar to 11βHSD1 it is membrane bound. The endogenous substrate of this third HSD enzyme remains elusive with localisation and expression data suggesting a reproductive hormone as a likely substrate.

Key Words
- hydroxysteroid dehydrogenases
- pituitary
- gonads
- ovary
- testis

Endocrine Connections (2017) **6**, 489–499

Introduction

The short-chain alcohol dehydrogenase/reductase enzymes 11βHSD1 and 11βHSD2 play important intracellular roles in mammals, regulating tissue availability of physiologically relevant glucocorticoid (1, 2). They are members of the large short-chain dehydrogenase/reductase (SDR) family of enzymes that are NAD^+ or $NADP^+$ dependent oxidoreductases, typically 250–350 amino acids in length (3). SDR enzymes have a wide range of substrates including steroids, aromatic compounds and xenobiotics. The human genome

http://www.endocrineconnections.org
DOI: 10.1530/EC-17-0119

encodes up to 63 different SDR enzymes with many uncharacterised for substrate and function *in vivo* (4). All SDR family members share a residue homology of only 20–40%. They have two conserved motifs, a 'GXXXGXG' nucleotide cofactor ($NAD^+/NADP^+$) binding domain and an 'YXXXK' catalytic active site domain (4).

11βHSD1 and 11βHSD2 carry out largely opposing roles in the preceptor modification of corticosteroids. 11βHSD1, encoded by the *HSD11B1* gene and located on chromosome 1q32–41 in humans, is a bidirectional enzyme but normally acts as an oxidoreductase *in vivo* to drive formation of the active glucocorticoid cortisol. Located in the endoplasmic reticulum (ER) membrane, it requires NADPH provided by the enzyme hexose-6-phosphate dehydrogenase (H6PDH) for activity. 11βHSD1 is expressed widely in metabolic tissues such as liver, muscle, adipose and kidney, and also in many specific regions of the brain (5). In contrast, 11βHSD2, encoded by the *HSD11B2* gene and located on chromosome 16q22.1 in humans, is a unidirectional dehydrogenase producing the inactive 11-keto metabolite cortisone from cortisol (5). 11βHSD2 has a more restricted expression pattern, and is detected predominantly in aldosterone target tissues where it prevents inappropriate activation of the mineralocorticoid receptor (MR) by glucocorticoids by efficiently converting cortisol to inactive cortisone (6, 7).

Inappropriate 11βHSD1 expression and activity is implicated in human disease such as obesity, insulin resistance and metabolic syndrome. Several 11βHSD1 selective inhibitors have been developed by the pharmaceutical industry and are currently being tested in Phase II trials to treat type-2 diabetes and obesity (8, 9).

A search of the annotated human genome for other potential SDR family members detected an 11βHSD1-like gene termed *HSD11B1L* on human chromosome 19p13.3. *HSD11B1L* is composed of 9 exons, stretching over 7.5 kb and analysis of EST library transcripts indicates the use of two alternate ATG start sites in exons 2 and 3, and alternative RNA splicing in exon 9. HSD11B1L has also been referred to as SCDR10B, and an SDR enzyme family member, and showed that it was highly expressed in the brain, with evidence that the when expressed *in vitro* the enzyme possesses very weak dehydrogenase activity in inactivate glucocorticoid (10). Surprisingly phylogenetic analysis of this gene in other mammalian genomes revealed that it is completely absent from all rodent genomes and also the rabbit genome (11). From an increasingly more detailed annotation of mammalian genomes the number of primate-specific or primate-restricted genes is growing (12, 13, 14). The lack of paralogues in the common laboratory rodent models makes characterisation of these new genes much more difficult and loss-of-functional analysis almost impossible. We have therefore extended our understanding of *HSD11B1L* expression, and tissue and cell localisation by analysis in the non-human primate marmoset and in the sheep. We reveal strong levels of expression in the pituitary gland and the ovary, with moderate-to-low expression in other organs, including the testis. Immunohistochemistry using a polyclonal antibody to human HSD1L localised protein to gonadotroph cells in the anterior pituitary and the granulosa cells of the ovary.

Materials and methods

Animals, tissue samples and cell lines

Collection of non-human primate, sheep and mouse tissues were approved in advance by the Monash University Animal Ethics Committee, and conformed to the Australian National Health and Medical Research Council Guide for Care and Use of Laboratory Animals, which strongly encourages use of archived and scavenged tissues. Tissue samples were collected from adult and foetal sheep, the non-human primate marmoset and macaque, and from mice, then they were snap frozen for RNA isolation or fixed in 4% paraformaldehyde (PFA) overnight at 4°C for histology and analysis by immunohistochemistry. Human HEK293 cells were maintained in culture in DMEM/high glucose medium with 2 mM glutamine, 10% FCS.

Bioinformatics and protein structure modelling

Sequence alignment of human HSD11B1L and 11βHSD1 were performed using the Clustral Omega (EMBL-EBI, http://www.ebi.ac.uk/Tool/msa/clustalo) software package. Amino acid sequences were obtained from the NCBI database for human HSD11B1L (NM_198706) and 11βHSD1 (NP_005516.1). Signal peptide prediction for human HSD11B1L was determined with the SignalIP4.1 software package (http://www.cbs.dtu.dk/services/SignalIP/). Three-dimensional modelling was performed using the Phyre2 software package to predict the 3D structure of human HSD11B1L (286 amino acid form) and was compared to the solved 3D structure of human 11βHSD1 that was obtained from the protein database (http://www.rcsb.org/pdb/), 11βHSD1 identifier 1XU9.

http://www.endocrineconnections.org
DOI: 10.1530/EC-17-0119

RNA extraction, cDNA synthesis and analysis by qPCR and droplet-digital PCR

Total RNA was isolated from tissue samples using TRIzol reagent (Invitrogen) as per the manufacturer's instructions. cDNA was then synthesised from total RNA using the QuantiTect reverse transcriptase kit (Qiagen) as per the manufacturer's instructions. Expression levels of mRNA in adult sheep and human tissue or cell samples were analysed using a Rotor-Gene 3000 PCR (Qiagen), with each biological replicate assayed in triplicate using SYBR Green qPCR SuperMix (Invitrogen). Rps29 and 18S-rRNA levels were used as a normalising RNA control. Dissociation curves were performed for each qPCR experiment to ensure that a single PCR product had been amplified per primer set and PCR products were also sequenced to verify fragment identity. Differential expression was determined using the comparative delta-delta CT method (15). Foetal sheep gene expression levels were analysed using the QX-200 droplet-digital PCR system (Biorad). For all PCR-based analyses, primers corresponding to mRNAs of interest were designed to overlap exon–exon boundaries and therefore prevent amplification of genomic DNA.

Immunohistochemistry and immunofluorescence

Marmoset, macaque and sheep tissue samples were immersion-fixed in 4% paraformaldehyde overnight at 4°C, then processed and embedded into paraffin. Paraffin sections with a thickness of 5 µm were cut and mounted on slides, blocked with an appropriate animal serum (5%), then immunostained with donkey anti-HSD1L (sc-1004, Santa Cruz) primary antibodies overnight at 4°C. Supplementary Table 1 (see section on supplementary data given at the end of this article) provides details of all antibodies used in this study. Primary antibodies were then detected by subsequent application of biotinylated secondary antibodies, Streptavidin-HRP (Invitrogen), and DAB (3,3′-diaminobenzidine) solution (Dakocytomation, Glostrup, Denmark). All immunohistochemistry images were obtained using the Olympus brightfield microscopy. For immunofluorescence, 5 µm thick paraffin sections were cut and mounted on slides blocked with an appropriate animal serum (5%), then immunostained with primary antibodies (donkey anti-HSD1L; rabbit anti-FoxL2, LH and Cyclin D2 antibodies) overnight at 4°C. Sections were washed and stained with fluorescent secondary antibodies (goat anti-donkey 488 and donkey anti-rabbit 555, Life Technologies). Sections were counterstained with Hoechst 33342 (Sigma), then mounted in fluorescent mounting medium (Dako). All fluorescent images were taken using an Olympus fluorescent microscope (IX71) and images were prepared using ImageJ software.

Intracellular localisation

HEK293 cells were grown at 37°C and 5% CO_2 in DMEM High Glucose: F12 supplemented with 10% FBS, 2 mM glutamine and 1% penicillin–streptomycin. Once confluent, cells were detached using trypsin and resuspended in pre-warmed media to a cell density of 2×10^5 cells/mL, then plated out in a 6-well dish with 1 mL per well. Cells were left overnight to re-attach and reach approximately 80–90% confluency, then washed and treated with 1 µg of either pc-DNA6B-HSD11B1L, pcDNA6B-HSD11B1L/mCherry or control pcDNA6B (No insert) DNA in 8 µL of lipofectamine 2000 diluted in 500 µL of serum-free media, then incubated overnight. Cells were then fixed in 2% PFA, permeabilised using 1% SDS and then immunostained with primary antibodies (rabbit anti-GRP78 and a mouse anti-HSD1L monoclonal antibody produced in the laboratory to a hHSD1L peptide), then washed and detected with secondary antibodies (anti-rabbit IgG alexa-488 and anti-mouse IgG2a alexa-555 (Life Technologies)). Cells were then counterstained with Heochst 33342 and mounted using DAKO fluorescent mounting media. All cells were imaged using the Olympus IX71 fluorescent microscope.

Statistical analysis

GraphPad Prism software was used to analyse the results of all experiments. The statistical significance from qPCR analyses was determined using a two-tailed unpaired Student's *t*-test. For all analyses, the statistical significance was set at $P<0.05$, with all error bars depicting standard error of the mean (S.E.M.).

Results

Analysis of the putative human SDR enzyme encoded by the HSD11B1L gene

A bioinformatics search of the annotated human genome for members of the SDR enzyme superfamily related to *11βHSD1* identified an 11βHSD1-like annotated gene on human chromosome 19p13.3 termed *HSD11B1L*. This gene was composed of 9 exons, covering 7.5 kb of genomic

http://www.endocrineconnections.org
DOI: 10.1530/EC-17-0119

DNA and analysis of EST library transcripts indicated the use of two alternate ATG translation start sites in exons 2 and 3, respectively. Furthermore, alternate RNA splicing in exon 9 generated two isoforms, an A and B form that encode variable C-terminal ends (Fig. 1A). One publication exists on the analysis of this gene, referred to as SCDR10B, an SDR enzyme family member, which suggested the human gene was highly expressed in the brain and weakly expressed in other organs (10). Analysis was, however, very limited, and also suggested that the enzyme may have a very weak substrate dehydrogenase activity for the steroid cortisol *in vitro*. Phylogenetic analysis of this gene in other genomes revealed that it is completely absent from all rodent genomes and is also absent in the rabbit genome (11). It has an orthologue in all primate, cow, ovine and dog genomes, and two similar genes exist in the zebrafish genome. The syntenic region of human chromosome 19p13.3 in the mouse genome (located on chromosome 17) has the same surrounding cluster of genes (SAFB2, SAFB, RPL36, LONP1) but remarkably is completely missing an annotated *HSD11B1L* gene between SAFB and RPL36. Comparison of the amino acid sequence of the encoded protein for the *HSD11B1L* gene to human 11βHSD1 and 11βHSD2 showed a striking level of homology and the strong conservation of the $NAD^+/NADP^+$ nucleotide binding and dehydrogenase/reductase catalytic site domains. HSD11B1L is most similar in sequence to human 11βHSD1 (Fig. 1B) with an approximate 40% amino acid identity and a strong conservation of the key catalytic enzyme domain and cofactor binding site (Fig. 1B). These analyses imply that *HSD11B1L* represents a species-restricted member of the SDR superfamily that is absent in all rodent genomes, and in humans, it may play a critical role in modulating availability of an as yet unidentified substrate *in vivo*. The sequence of the 286 amino acid HSD1L9A isoform was used with the 'Pymol' molecular modelling programme (PyMOL Molecular Graphics System, Version 1.8 Schrödinger, LLC) to compare a predicted 3D structure of human HSD1L to the known structures of human 11βHSD1 and predicted structure of 11βHSD2 (Fig. 2A, B and C). Predicted α-helices and the β-sheet 'Rossmann' fold, a common feature of all SDR enzymes (4), were very similar to the determined structure of murine 11βHSD1 (16) and somewhat similar to that for predicted 11βHSD2 structure (Fig. 2A, B and C, shown in magenta and red). Positioning of residues important at the catalytic site was also very similar between 11βHSD1 and HSD1L9A (Fig. 2, panels B and C, shown in dark blue). HSD1L also contained a putative ER localisation signal sequence at the N-terminus (Fig. 2C in light blue). Charged amino acids at Tyr-178 and Lys-182 were found in the predicted catalytic domain (Fig. 2D, arrow 1), orientated in such a way that their side chains pointed towards the predicted cofactor binding motif (Fig. 2D, arrow 2). Analysis of HSD1L hydrophobicity using a surface map (Fig. 2E red residues) showed that the charged amino acids pointed towards a hydrophobic pocket (Fig. 2E arrow).

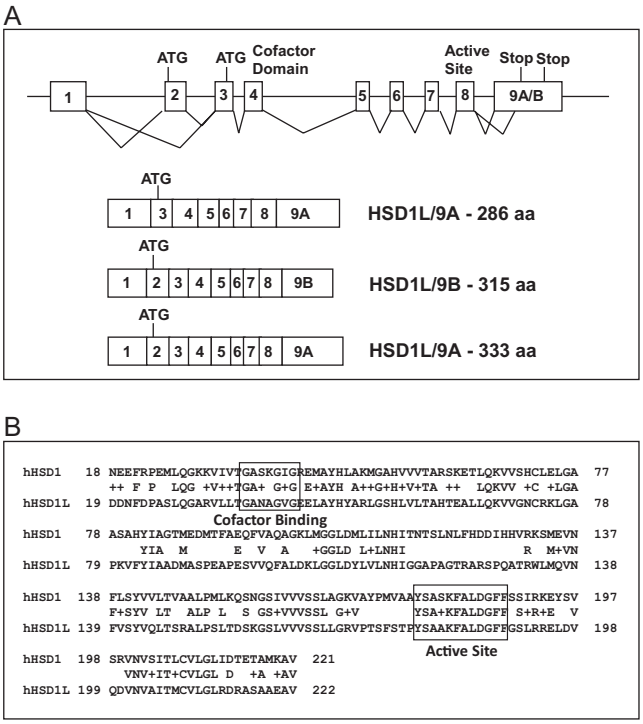

Figure 1
The exon/intron structure of the human *HSD11B1L* gene and the amino acid sequence comparison of human 11βHSD1 and HSD1L. (A) The exon/intron structure of the human *HSD11B1L* gene on chromosome 19p33.3. Positions of two alternate ATG start sites, the cofactor binding domain and active site are indicated above exons. Alternate splicing of exons is able to generate three major protein isoforms of 286, 315 and 333 amino acids. (B) Amino acid sequence comparison of human 11βHSD1 and HSD1L showing the known positions of the NAD/NADP binding and active sites for 11βHSD1 and HSD1L (boxed). Conserved and similar (+) residues across the two sequences are also indicated.

HSD11B1L mRNA is expressed in the pituitary, ovary, lung and gastrointestinal tract

Previous studies indicated that human HSD11B1L mRNAs were strongly expressed in the brain and weakly in other organs (10). We assessed human *HSD11B1L* expression in total RNA from various human tissues and cells by RT-PCR (Fig. 3A). Using PCR primers from exons 6 and 8

http://www.endocrineconnections.org
DOI: 10.1530/EC-17-0119

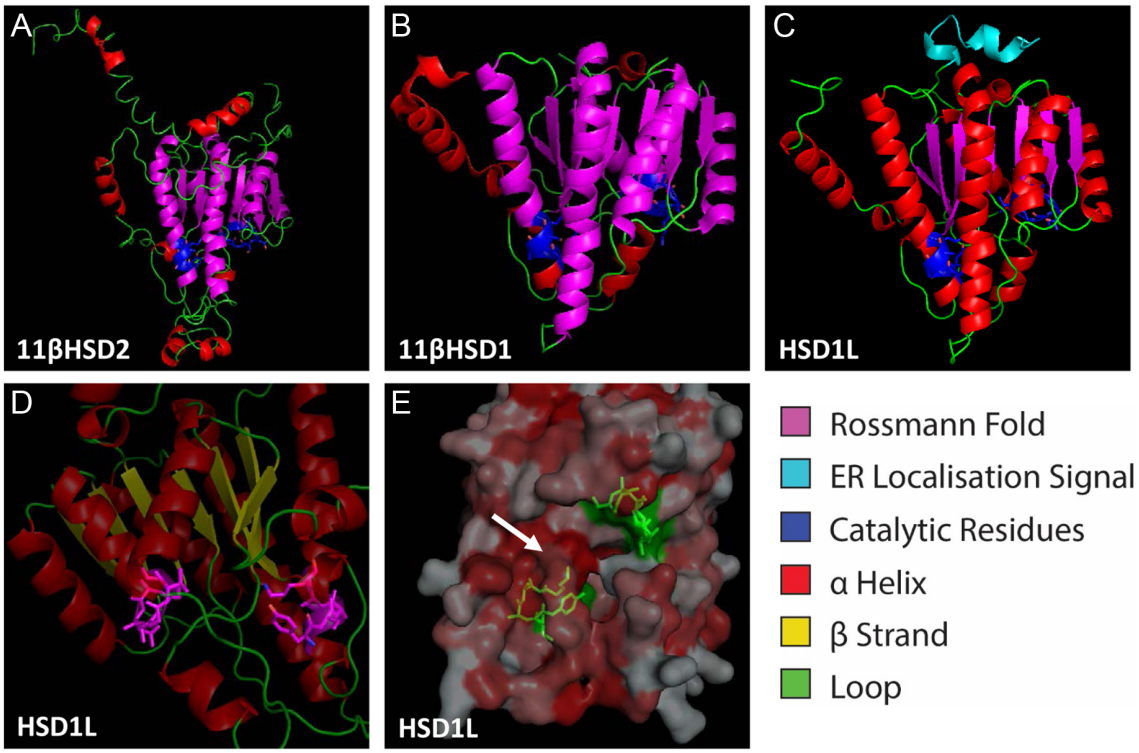

Figure 2
Structural modeling of the open reading frame of the human *HSD11B1L* gene with its closest homologues 11βHSD1 and 11βHSD2. The three-dimensional structure of 11β-HSD1 (IXU9), 11β-HSD2 (NM_000196) and HSD1L (NM_198706). All imaging was performed using the programme 'Pymol' and coloured as described unless stated otherwise. Predicted structures of 11βHSD2 and 11βHSD1L were produced using the Phyre2 software suite. (A) The predicted 3D structure of 11βHSD2 produced using Phyre2 at >90% confidence in 74% of residues. (B) Depicts the solved structure of 11βHSD1. (C) The predicted 3D structure of HSD1L produced using Phyre2 at >90% confidence in 74% of residues. (D) Shows the predicted substrate binding site of 11βHSD1L with both catalytic residues represented as stick diagrams. (E) Shows a hydrophobicity surface structure of the predicted HSD1L structure. Red regions indicate hydrophobic areas whereas white indicated hydrophilic regions. Both the catalytic and cofactor binding domains are shown in green and the respective side chains are represented as stick diagrams.

of the *hHSD1L* gene we detected moderate expression in total RNA from whole brain in agreement with previous reports (10). We detected stronger bands for HSD11B1L transcripts in the ovary, testis and lung, and weaker expression in total RNA from human kidney (Fig. 3A). We then compared mRNA levels of hHSD1L to h11βHSD1 and h11βHSD2 in total RNA from human colon. 11βHSD2 mRNA levels were as expected very high, with hHSD1L and 11βHSD1 almost undetectable (Fig. 3B). A similar analysis in total RNA from human brain and ovary showed similar levels of expression in the ovary, and similar mRNA levels for 11βHSD1 and hHSD1L in the brain (Fig. 3C). To allow a broader assessment of the expression of HSD1L in the mammalian body, we measured mRNA levels in total RNA from various organs of the sheep. Total RNA was prepared from the major organs of the foetal sheep (female, day 150, just prior to birth) and mRNA levels compared for HSD1L, 11βHSD1 and 11βHSD2 using droplet-digital qPCR (Fig. 4A). Highest levels of HSD1L mRNA were detected in ovary, pituitary, colon and lung, with lower levels detected in other organs analysed. In the adult female sheep, much higher levels of HSD1L mRNA were detected in pituitary and ovary compared to the lung (Fig. 4C).

Localisation of HSD1L protein in the ovary

The cellular localisation of HSD1L was assessed in the ovary and testis of the non-human primate marmoset by immunohistochemistry using a commercial anti-human HSD1L polyclonal antibody. Strong immunostaining for HSD1L was detected in developing follicles of the ovary at all stages of ovarian follicle development (Fig. 5A and D). Also shown are negative controls with no primary antibody (panel B) and an immunizing peptide, pre-incubation control (panel C). The mouse ovary, that should not express a HSD1L protein, was used as an additional negative control for immunostaining and showed no specific staining in the mouse ovary above

http://www.endocrineconnections.org
DOI: 10.1530/EC-17-0119

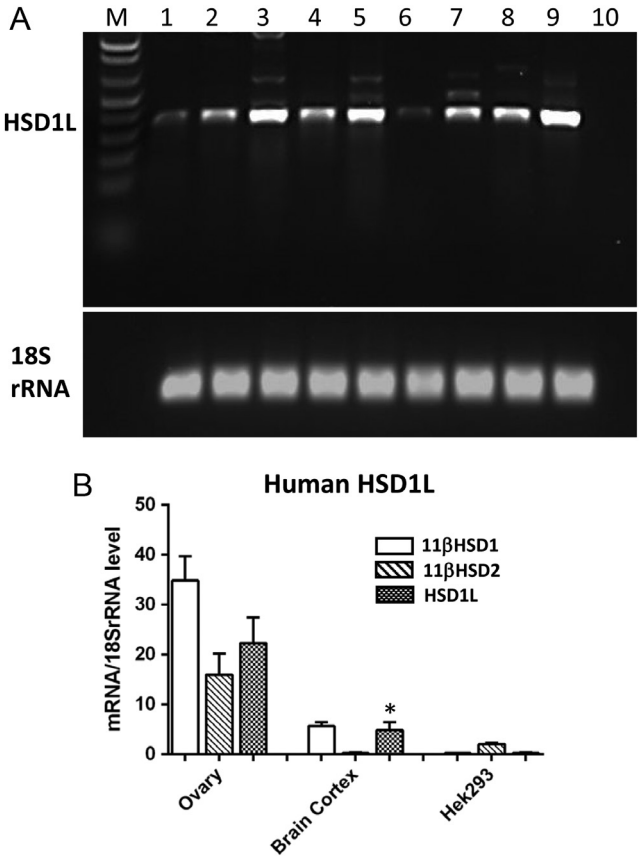

Figure 3
Detection of HSD11B1L mRNA in total RNA from human tissues and cell lines. (A) Detection of HSD11B1L mRNA by RT-PCR in cDNA from human kidney (lane 1), lung (lane 2), ovary (lanes 3 and 5), testis (lanes 4 and 6) and whole brain (lanes 7–9). (B) Relative mRNA levels of 11βHSD1, 11βHSD2 and HSD1L determined by qPCR in total RNA from human ovary, brain and the HEK293 cell line ($n=3$). RNA levels of HSD1L compared to 11βHSD2 in brain cortex, *$P<0.05$.

background (Fig. 5E and F). Staining within the marmoset ovary was specific for the granulosa cell layer of the follicle and interestingly also for the oocyte within the follicle (arrow, Fig. 5D). An identical staining pattern was also observed in the ovary from the adult sheep (data not shown). Immunohistochemistry with sections of the marmoset testis was also analysed and detected staining in cells resembling Leydig cells (Fig. 5, panel G and negative control, panel H). To positively identify the cell type specifically labelled in the marmoset ovary, we performed double-immunofluorescence for HSD1L with two known granulosa cell markers, cyclin D2 and FoxL2 (Fig. 6). Immunostaining for HSD1L was co-localised in granulosa cells with both cyclin D2 (Fig. 6A, B and C) and FoxL2 (Fig. 6D, E and F), clearly identifying HSD1L expression specifically to the cytoplasm of ovarian granulosa cells.

Localisation of HSD1L protein within the anterior pituitary

The cellular localisation of HSD1L in the pituitary was also assessed by immunohistochemistry in the marmoset. Immunostaining was detected in a small subset of cells and only in anterior pituitary (Fig. 7). No staining was detected in regions of the posterior pituitary (data not shown). In the anterior pituitary, strong cytoplasmic staining was observed in scattered cells throughout the anterior lobe (Fig. 7A and D). To identify the particular cell type stained for HSD1L double-immunofluorescence was performed with antibody markers specific for pituitary somatotrophs (growth hormone), lactotrophs (prolactin), gonadotrophs (luteinizing hormone (LH)) and corticotrophs (melanocyte-stimulating hormone) (Fig. 7E,

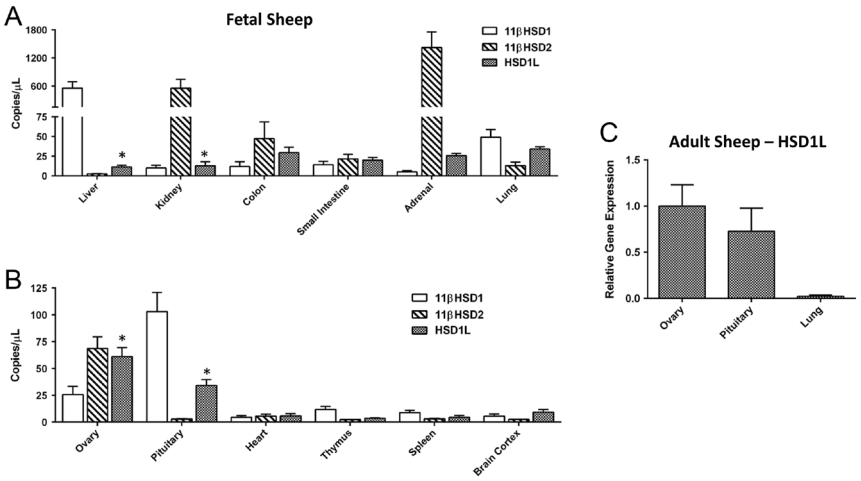

Figure 4
Levels of Sheep 11βHSD1, 11βHSD2 and HSD1L mRNA in total RNA isolated from female foetal (156 day old) and female adult sheep tissues determined by drop-digital PCR ($n=3$). Values shown are absolute relative transcripts/10 ng total RNA for (A) foetal liver, kidney, colon, small intestine, adrenal and lung. (B) Foetal ovary, pituitary, heart, thymus, spleen and brain cortex. (C) Adult ovary, pituitary and lung. Error bars are S.E.M., $n=3$. RNA levels of HSD1L compared to 11βHSD1 in liver, *$P<0.01$, RNA levels of HSD1L compared to 11βHSD2 in kidney and adrenal, *$P<0.01$, RNA levels of HSD1L compared to 11βHSD1 in ovary, *$P<0.05$, and RNA levels of HSD1L compared to 11βHSD1 and 11βHSD2 in pituitary, *$P<0.01$.

http://www.endocrineconnections.org
DOI: 10.1530/EC-17-0119

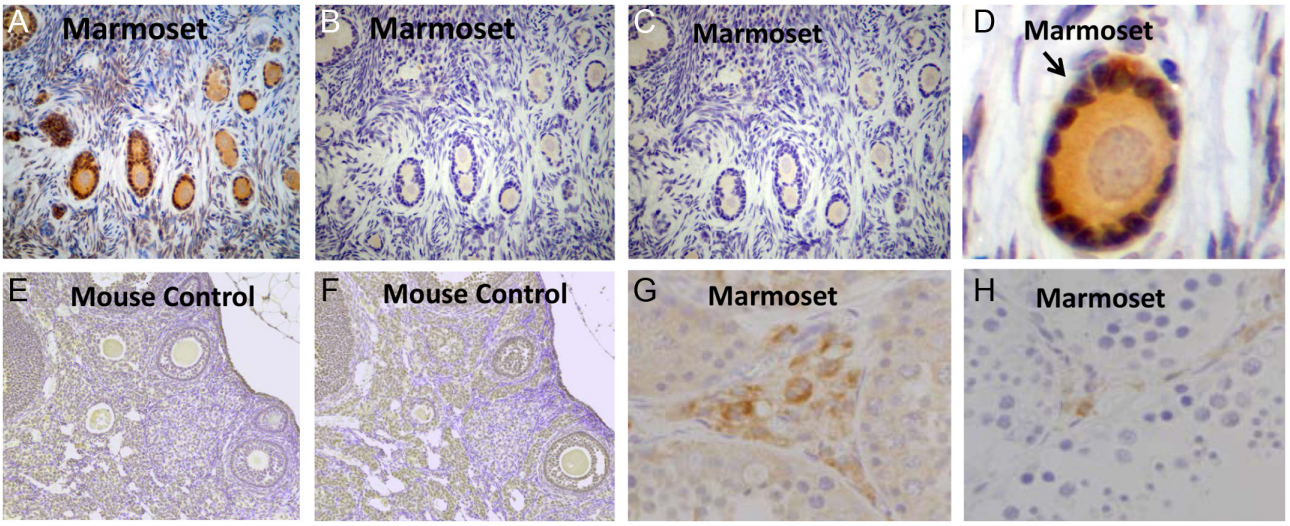

Figure 5
Localisation of HSD1L by immunohistochemistry in the ovary and testis from the non-human primate adult marmoset. (A) HSD1L in marmoset ovary (N16 HSD1L peptide polyclonal antibody) ×10. (B) Marmoset ovary no primary antibody control. (C) Marmoset ovary immunising peptide pre-incubation-negative control. (D) HSD1L in Marmoset ovary (N16 HSD1L peptide polyclonal antibody) ×40. (E) Mouse ovary (N16 HSD1L peptide polyclonal antibody) ×10. (F) C Marmoset ovary no primary antibody negative control. (G) HSD1L in Marmoset testis (N16 HSD1L peptide polyclonal antibody) ×10. (H) Marmoset testis no primary antibody control.

F, G and H). There was no co-localisation of HSD1L (green colour) with markers for somatotrophs, corticotrophs or lactotrophs (red colour), but remarkably there was close to 100% co-localization of HSD1L with LH (panel H, merged yellow colour), marking these HSD1L-specific cells as pituitary gonadotrophs.

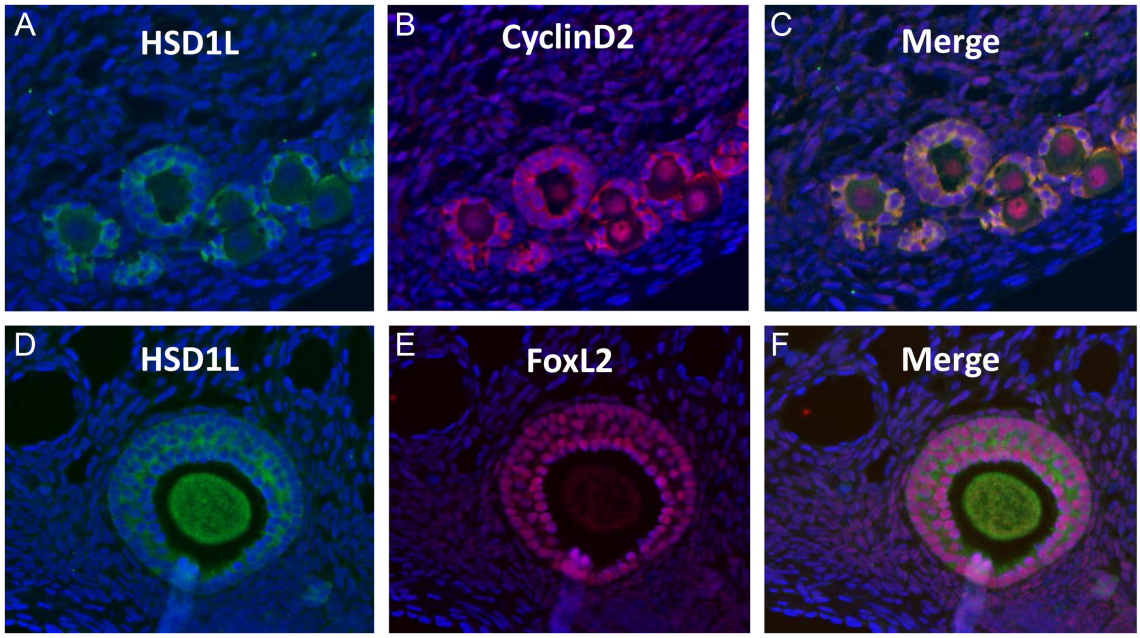

Figure 6
Localisation of HSD11B1L protein to granulosa cells of the adult marmoset ovary by double-immunofluorescence. (A, B and C) Double-Immunofluorescence for HSD1L (green) and cyclinD2 (red) in the adult marmoset ovary. CyclinD2 was used a marker of follicle granulosa cells and shows co-localisation with HSD1L to the cytoplasm of granulosa cells (C; yellow, Merge). (D, E and F) Double-immunofluorescence for HSD1L (green) and FoxL2 (red) in the adult marmoset ovary. FoxL2 was used a nuclear marker of follicle granulosa cells. HSD1L and FoxL2 were strongly co-localised to the cytoplasm and nucleus, respectively of follicle granulosa cells (F; Merge). Scale bars: A, B, C, D, E and F: 80 µm.

http://www.endocrineconnections.org
DOI: 10.1530/EC-17-0119

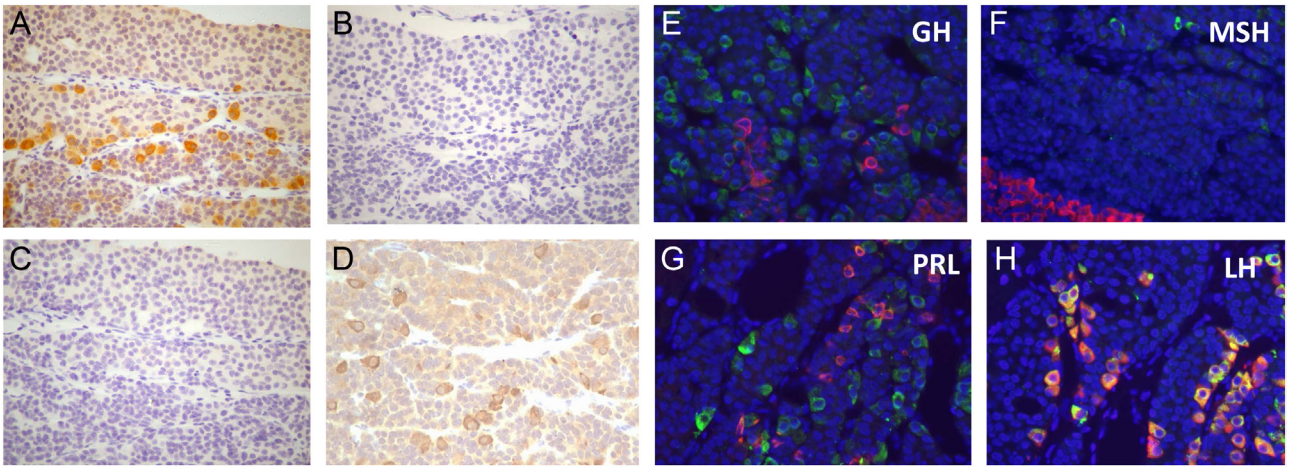

Figure 7
Localisation of HSD11B1L by immunohistochemistry and double-immunofluorescence in the anterior pituitary of non-human primate adult marmoset. (A, B, C and D) Immunohistochemistry for HSD1L (DAB, brown stain) in the adult marmoset anterior pituitary. (A) HSD1L N16 primary antibody (SC-244840) 20×. (B) no primary antibody (N16-SC) control. (C) Immunising peptide (SC-244840) pre-incubation (before primary antibody) control. (D) 11βHSD1L N16 primary antibody 40×. (E, F, G and H) Double-immunofluorescence for HSD1L (green fluorescence) with either growth hormone (panel E, GH – red), αMSH (panel F, MSH – red), prolactin (panel G, PRL – red) or Luteinizing hormone (panel H, LH – red). Co-localisation is shown as yellow fluorescence.

HSD1L protein is localised to the cytoplasmic endoplasmic reticulum

The level of conservation between HSD11B1 and HSD11B1L on a protein level is exceptionally high particularly in amino acid sequences that form the secondary structure involved in the Rossmann fold. Further levels of conservation are observed at the N-terminal end of HSD11B1L showing a string of hydrophobic amino acids that suggested the possibility of a localisation signal and/or transmembrane domain. Analysis of the HSD1L amino acid sequence using

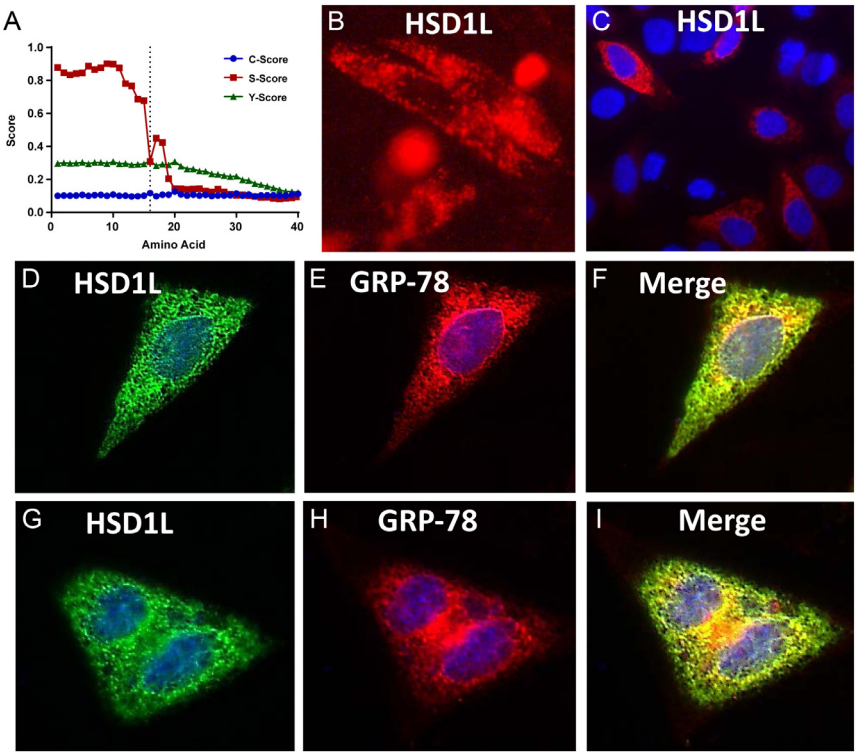

Figure 8
Intracellular localisation of HSD1L to the endoplasmic reticulum in transfected human HEK293 cells. (A) Predicted signal peptide score for the first 40 amino acids of human HSD1L (286 isoform) using SignalIP4.1 software. C-Score (raw cleavage site score): S-Score (signal peptide score), Y-Score (combined cleavage site score). (B) Fluorescent image of C-terminal DS-red-tagged human HSD11B1L9A transfected in HEK293 cells. (C) Full length human HSD11B1L transfected into HEK293 cells and then immunostained with an in-house mouse monoclonal anti-human HSD11B1L antibody and also anti-IgG alexa555 to stain nuclei. (D and G) Indirect immunofluorescence (green) for the known ER-localised protein GRP78. (E and H) Indirect immunofluorescence (red) for transfected human HSD1L in HEK293 cells using the mouse monoclonal anti-human HSD11B1L antibody. (F and I) Merged double-immunofluorescence (yellow) for transfected HSD1L (red) and endogenous GRP78 (green) in HEK293 cells.

http://www.endocrineconnections.org
DOI: 10.1530/EC-17-0119

SignalIP 4.1 revealed a predicted N-terminal hydrophobic ER localisation signal with a cleavage site predicted to reside between residues 15 and 16 of the protein (Fig. 8A). To further investigate the potential intracellular localisation of HSD1L to the ER, transfection experiments were performed in human HEK293 cells. Transfection of cells with HSD1L tagged with mCherry at the C-terminus showed a cytoplasmic localisation reminiscent of localisation to the ER (Fig. 8B). Indirect immunofluorescence of untagged HSD1L transfected into HEK293 cells using an anti-human HSD1L antibody showed a similar pattern of localisation (Fig. 8C). Finally, indirect immunofluorescence was performed for HSD1L and the ER marker GRP-78 in HEK393 cells transfected with HSD1L, and showed specific co-localisation of HSD1L to the cytoplasmic ER (Fig. 8, panels F and I, merged yellow fluorescence).

Discussion

The protein HSD1L has been identified as a member of the SDR superfamily of oxidoreductase enzymes with a high level of homology at the amino acid level to the very well characterised glucocorticoid steroid metabolising enzymes 11βHSD1 and 11βHSD2. We have further characterised HSD1L as a species-restricted member of the SDR superfamily strikingly absent from the majority of rodent genomes. We have compared the mRNA expression patterns of all three HSD-like SDR family members and identified cell type specific localization of HSD1L protein in a subset of specific tissues. Protein localization was cell type specific and was primarily localised to well characterised endocrine cells including gonadotrophs within the anterior pituitary and the steroid producing granulosa cells surrounding ovarian follicles. Further analysis in HSD1L transfected HEK293 cells showed that like the other family members, HSD1L is indeed an ER cytoplasmic localised protein. Recently published evidence have shown that HSD1L is unlikely to be involved in interconversion of cortisol and cortisone, nor metabolism of 11-keto or 11-hydroxy-testosterone (17), but given the high levels of sequence homology and tissue localisation, a steroid-based substrate is a likely target and will be the focus of future studies.

The presence of a third potential 11βHSD enzyme in the sheep kidney was proposed in 1997 by Gomez-Sanchez and coworkers (18) and was referred to as 11β-HSD3 (18). Gomez-Sanchez and coworkers (18) isolated intact kidney microsomes and showed the presence of unidirectional conversion of cortisone/corticosterone that was NADP+ dependent with a K_m for corticosterone of 1.3 nM (18), a 100-fold increase in activity compared to 11βHSD1 in liver and other papers at the time that had described kinetics of 11βHSD1 from purified rat liver microsomes (19). However, this study was lacking in viable controls for the experiment with no confirmation that cortisol to cortisone reduction was not a result of 11βHSD2 activity given the well characterised high levels of 11βHSD2 in the sheep kidney. This is especially true for 11βHSD1 with specificity for cortisone both *in vitro* and *in vivo* relatively low, with some groups providing data to suggest that 11βHSD1 has a higher affinity for cortisol over cortisone (19, 20, 21). Other studies have shown that the specificity of 11βHSD1 towards cortisone is the result of co-expression of Hexose-6-Phosphate Dehydrogenase (H6PD) with 11βHSD1 in the ER (22). The co-expression and localisation of HSD1L with H6PD has so far not been explored. A recent study has characterised a novel and potentially third 11βHSD activity in human liver nuclei that had lower K_m values for corticosterone, was NADP+ dependent and blocked by HSD1 inhibitors (23). This is however very unlikely to be HSD1L as we have shown that human HSD1L is not nuclear localised and has a very low level of expression in the sheep liver.

A more recent study by Ohno and coworkers (24) described HSD1L in the pig as a third HSD11B isozyme expressed in the neonatal pig testis (24). They showed by semi-quantitative PCR that a HSD1L mRNA was expressed in the neonatal pig testis and brain at lower levels compared to 11βHSD1 and 11βHSD2. The HSD1L activity in the testis was not inhibited by glycyrrhetinic acid, a strong inhibitor of 11βHSD1. These results are in agreement with our study that shows high expression of HSD1L in the brain and testis of non-human primates and sheep, with localised expression of marmoset HSD1L to testicular Leydig cells. Both 11βHSD1 and 11βHSD2 have been characterised in the Leydig cells surrounding the seminiferous tubules in the testis of rats and opens up the question of the additional role of HSD1L that may play in the functioning of Leydig cell (25).

The results published by Huang and coworkers (10), further defined the expression and role of human HSD1L, termed SCDR10B, a member of the SDR enzyme family (10). They defined the intron/exon structure of the human HSD1L gene, showed strong expression in brain RNA by northern blot analysis and a very weak expression in other organs were analysed. Using expressed and purified HSD1L protein they demonstrated *in vitro* a very weak 11β-HSD dehydrogenase activity. Interestingly immunohistochemistry using an in-house polyclonal

http://www.endocrineconnections.org
DOI: 10.1530/EC-17-0119

antibody to human HSD1L indicated elevated expression in lung cancer biopsies and in various areas of the brain such as the hippocampus. We have found some evidence of elevated mRNA levels of human HSD1L in various cancer cell lines (unpublished results), but these results need to be explored in more detail to define a potential role for this enzyme in cancer cell proliferation. We have confirmed high expression of HSD1L in total RNA of the brain and show strong specific expression in the pituitary gland where HSD1L is localised specifically to gonadotrophs within the anterior pituitary. There are lower levels of expression in other regions of the non-human primate and sheep brain, yet the specific cell types expressing HSD1L are yet to be defined. In comparison to 11βHSD1 and 11βHSD2 in the foetal sheep, we also detect similar yet lower levels of HSD1L mRNA in the kidney, lung, adrenal and gastrointestinal tract.

Expression of HSD1L both at the mRNA and protein level in tissues of the hypothalamic–pituitary–gonadal (HPG) axis is striking and suggests a potential role for the enzyme in regulating aspects of reproduction. Expression of HSD1L in the anterior pituitary was shown to co-localise to gonadotroph cells through double labelling with LH, a well characterised cell marker of gonadotrophs. A major role of gonadotrophs in females is the cyclic release of LH and FSH, which in turn stimulates receptors on the surface of granulosa cells surrounding ovarian follicles. We intend to explore HSD1L-mediated regulation of LH and FSH production and release from pituitary gonadotrophs. This process is very important in the maintenance of reproductive homeostasis in both females and males and the expression of HSD1L in both ovarian granulosa cells and gonadotrophs provides evidence for a novel regulatory loop potentially regulated by HSD1L. This observation is also important with respect to its substrate given the importance role of granulosa cells for steroid production. Granulosa cells have been shown to upregulate important genes involved in steroid production including p450 aromatases, StAR and 17β-HSD in response to LH and FSH (26, 27). Increased levels of LH and FSH mediate stimulation of granulosa cells to increase serum levels of testosterone that are important substrates for aromatase enzymes present within theca cells responsible for the conversion of androgens to estradiol (28). Interestingly, the androgen receptor has been shown to be selectively expressed in rat granulosa cells acting as a mediator of positive feedback mechanisms (29). Furthermore, 11βHSD1 has been shown to bind and metabolise several androgenic derivatives (30, 31). This substrate promiscuity of 11βHSD1 may provide potential clues to the substrate of HSD1L given the high levels of sequence homology at a protein level. 11βHSDs are also able to metabolise 11-oxy androgens, such as 11-keto- and 11-hydroxy-testosterone (32, 33). A very recent study has investigated the steroids as substrates for HSD1L in zebrafish but showed absence of 11-ketosteroid reduction in zebrafish, with both human HSD1L (11βHSD3) and the two zebrafish homologues were unable to convert cortisone or 11-keto-testosterone to their 11 hydroxy metabolites (17). The identity of the physiological substrate for HSD1L/11βHSD3 is therefore elusive and may be an as yet uncharacterised reproductive steroid metabolite.

In summary, we have further characterised a novel species-restricted SDR hydroxysteroid dehydrogenase enzyme called HSD1L that is localised primarily to tissues of the pituitary–gonadal axis. The *in vivo* substrate for this enzyme is as yet unknown and given its level of expression in pituitary gonadatropes and the ovary, may serve as a modulator of reproductive function.

Supplementary data
This is linked to the online version of the paper at http://dx.doi.org/10.1530/EC-17-0119.

Declaration of interest
The authors declare that there is no conflict of interest that could be perceived as prejudicing the impartiality of the research reported.

Funding
This research did not receive any specific grant from any outside funding agency in the public, commercial or not-for-profit sector. Spencer Greatorex was funded by a Monash University MBio PhD scholarship. This work was partly funded by the Monash University Outside-Study Programme.

Acknowledgements
The authors would like to thank Judy Ng and Dr Robert De Matteo for technical assistance.

References

1 Kallberg Y, Oppermann U, Jornvall H & Persson B. Short-chain dehydrogenase/reductase (SDR) relationships: a large family with eight clusters common to human, animal, and plant genomes. *Protein Sciences* 2002 **11** 636–641. (doi:10.1110/ps.26902)
2 Persson B, Kallberg Y, Bray JE, Bruford E, Dellaporta SL, Favia AD, Duarte RG, Jornvall H, Kavanagh KL, Kedishvili N, *et al*. The SDR (short-chain dehydrogenase/reductase and related enzymes) nomenclature initiative. *Chemico-Biological Interactions* 2009 **178** 94–98. (doi:10.1016/j.cbi.2008.10.040)
3 Jornvall H, Hedlund J, Bergman T, Kallberg Y, Cederlund E & Persson B. Origin and evolution of medium chain alcohol dehydrogenases. *Chemico-Biological Interactions* 2013 **202** 91–96. (doi:10.1016/j.cbi.2012.11.008)
4 Kallberg Y, Oppermann U, Jornvall H & Persson B. Short-chain dehydrogenases/reductases (SDRs). *European Journal of Biochemistry* 2002 **269** 4409–4417. (doi:10.1046/j.1432-1033.2002.03130.x)

http://www.endocrineconnections.org
DOI: 10.1530/EC-17-0119

5 Chapman K, Holmes M & Seckl J. 11beta-Hydroxysteroid dehydrogenases: intracellular gate-keepers of tissue glucocorticoid action. *Physiological Reviews* 2013 **93** 1139–1206. (doi:10.1152/physrev.00020.2012)

6 Agarwal AK, Rogerson FM, Mune T & White PC. Gene structure and chromosomal localization of the human HSD11K gene encoding the kidney (type 2) isozyme of 11 beta-hydroxysteroid dehydrogenase. *Genomics* 1995 **29** 195–199. (doi:10.1006/geno.1995.1231)

7 Krozowski Z, Li KX, Koyama K, Smith RE, Obeyesekere VR, Stein-Oakley A, Sasano H, Coulter C, Cole T & Sheppard KE. The type I and type II 11beta-hydroxysteroid dehydrogenase enzymes. *Journal of Steroid Biochemistry and Molecular Biology* 1999 **69** 391–401. (doi:10.1016/S0960-0760(99)00074-6)

8 Morgan SA, McCabe EL, Gathercole L, Hassan-Smith ZK, Larner DP, Bujalska IJ, Stewart PM, Tomlinson JW & Lavery GG. 11β-HSD1 is the major regulator of the tissue-specific effects of circulating glucocorticoid excess. *PNAS* 2014 **111** E2482–E2491. (doi:10.1073/pnas.1323681111)

9 Gathercole LL, Lavery GG, Morgan SA, Cooper MS, Sinclair AJ, Tomlinson JW & Stewart PM. 11beta-Hydroxysteroid dehydrogenase 1: translational and therapeutic aspects. *Endocrine Reviews* 2013 **34** 525–555. (doi:10.1073/pnas.1323681111)

10 Huang C, Wan B, Gao B, Hexige S & Yu L. Isolation and characterization of novel human short-chain dehydrogenase/reductase SCDR10B which is highly expressed in the brain and acts as hydroxysteroid dehydrogenase. *Acta Biochimica Polonica* 2009 **56** 279–289. (doi:10.1016/j.bbagrm.2008.09.005)

11 Baker ME. Evolution of 11beta-hydroxysteroid dehydrogenase-type 1 and 11beta-hydroxysteroid dehydrogenase-type 3. *FEBS Letters* 2010 **584** 2279–2284. (doi:10.1016/j.febslet.2010.03.036)

12 Sousa JF, Torrieri R, Silva RR, Pereira CG, Valente V, Torrieri E, Peronni KC, Martins W, Muto N, Francisco G, *et al*. Novel primate-specific genes, RMEL 1, 2 and 3, with highly restricted expression in melanoma, assessed by new data mining tool. *PLoS ONE* 2010 **5** e13510. (doi:10.1371/journal.pone.0013510)

13 Takamatsu K, Maekawa K, Togashi T, Choi DK, Suzuki Y, Taylor TD, Toyoda A, Sugano S, Fujiyama A, Hattori M, *et al*. 2002 Identification of two novel primate-specific genes in DSCR. *DNA Research* 2009 **9** 89–97. (doi:10.1093/dnares/9.3.89)

14 Tay SK, Blythe J & Lipovich L. Global discovery of primate-specific genes in the human genome. *PNAS* 2009 **106** 12019–12024. (doi:10.1073/pnas.0904569106)

15 Pfaffl MW. A new mathematical model for relative quantification in real-time RT-PCR. *Nucleic Acids Research* 2001 **29** e45. (doi:10.1093/nar/29.9.e45)

16 Zhang J, Osslund TD, Plant MH, Clogston CL, Nybo RE, Xiong F, Delaney JM & Jordan SR. Crystal structure of murine 11 beta-hydroxysteroid dehydrogenase 1: an important therapeutic target for diabetes. *Biochemistry* 2005 **44** 6948–6957. (doi:10.1021/bi047599q)

17 Tsachaki M, Meyer A, Weger B, Kratschmar DV, Tokarz J, Adamski J, Belting HG, Affolter M, Dickmeis T & Odermatt A. Absence of 11-keto reduction of cortisone and 11-ketotestosterone in the model organism zebrafish. *Journal of Endocrinology* 2017 **232** 323–335. (doi:10.1530/JOE-16-0495)

18 Gomez-Sanchez EP, Ganjam V, Chen YJ, Cox DL, Zhou MY, Thanigaraj S & Gomez-Sanchez CE. The sheep kidney contains a novel unidirectional, high affinity NADP(+)-dependent 11 beta-hydroxysteroid dehydrogenase (11 beta-HSD-3). *Steroids* 1997 **62** 444–450. (doi:10.1016/S0039-128X(97)00011-1)

19 Lakshmi V & Monder C. Purification and characterization of the corticosteroid 11 beta-dehydrogenase component of the rat liver 11 beta-hydroxysteroid dehydrogenase complex. *Endocrinology* 1988 **123** 2390–2398. (doi:10.1210/endo-123-5-2390)

20 Condon J, Ricketts ML, Whorwood CB & Stewart PM. Ontogeny and sexual dimorphic expression of mouse type 2 11beta-hydroxysteroid dehydrogenase. *Molecular and Cellular Endocrinology* 1997 **127** 121–128. (doi:10.1016/S0303-7207(97)04000-8)

21 Hult M, Jornvall H & Oppermann UC. Selective inhibition of human type 1 11beta-hydroxysteroid dehydrogenase by synthetic steroids and xenobiotics. *FEBS Letters* 1998 **441** 25–28. (doi:10.1016/S0014-5793(98)01515-4)

22 Bujalska IJ, Draper N, Michailidou Z, Tomlinson JW, White PC, Chapman KE, Walker EA & Stewart PM. Hexose-6-phosphate dehydrogenase confers oxo-reductase activity upon 11 beta-hydroxysteroid dehydrogenase type 1. *Journal of Molecular Endocrinology* 2005 **34** 675–684. (doi:10.1677/jme.1.01718)

23 Robinzon B & Prough RA. A novel NADP(+)-dependent dehydrogenase activity for 7alpha/beta- and 11beta-hydroxysteroids in human liver nuclei: a third 11beta-hydroxysteroid dehydrogenase. *Archives of Biochemistry and Biophysics* 2009 **486** 170–176. (doi:10.1016/j.abb.2009.04.010)

24 Ohno S, Nakagawara S, Honda Y & Nakajin S. Evidence for expression of 11beta-hydroxysteroid dehydrogenase type3 (HSD11B3/HSD11B1L) in neonatal pig testis. *Molecular and Cellular Biochemistry* 2013 **381** 145–156. (doi:10.1007/s11010-013-1697-4)

25 Zhou HY, Chen XX, Lin H, Fei AL & Ge RS. 11beta-Hydroxysteroid dehydrogenase types 1 and 2 in postnatal development of rat testis: gene expression, localization and regulation by luteinizing hormone and androgens. *Asian Journal of Andrology* 2014 **16** 811–816. (doi:10.4103/1008-682X.132471)

26 Minegishi T, Tsuchiya M, Hirakawa T, Abe K, Inoue K, Mizutani T & Miyamoto K. Expression of steroidogenic acute regulatory protein (StAR) in rat granulosa cells. *Life Science* 2000 **67** 1015–1024. (doi:10.1016/S0024-3205(00)00696-2)

27 Richards JS, Jonassen JA, Rolfes AI, Kersey K & Reichert LE Jr. Adenosine 3′,5′-monophosphate, luteinizing hormone receptor, and progesterone during granulosa cell differentiation: effects of estradiol and follicle-stimulating hormone. *Endocrinology* 1979 **104** 765–773. (doi:10.1210/endo-104-3-765)

28 Erickson GF & Hsueh AJ. Stimulation of aromatase activity by follicle stimulating hormone in rat granulosa cells in vivo and in vitro. *Endocrinology* 1978 **102** 1275–1282. (doi:10.1210/endo-102-4-1275)

29 Tetsuka M & Hillier SG. Androgen receptor gene expression in rat granulosa cells: the role of follicle-stimulating hormone and steroid hormones. *Endocrinology* 1996 **137** 4392–4397. (doi:10.1210/endo.137.10.8828500)

30 Odermatt A & Klusonova P. 11beta-Hydroxysteroid dehydrogenase 1: regeneration of active glucocorticoids is only part of the story. *Journal of Steroid Biochemistry and Molecular Biology* 2015 **151** 85–92. (doi:10.1016/j.jsbmb.2014.08.011)

31 Odermatt A & Kratschmar DV. Tissue-specific modulation of mineralocorticoid receptor function by 11beta-hydroxysteroid dehydrogenases: an overview. *Molecular and Cellular Endocrinology* 2012 **350** 168–186. (doi:10.1016/j.mce.2011.07.020)

32 Storbeck KH, Bloem LM, Africander D, Schloms L, Swart P & Swart AC. 11beta-Hydroxydihydrotestosterone and 11-ketodihydrotestosterone, novel C19 steroids with androgenic activity: a putative role in castration resistant prostate cancer? *Molecular and Cellular Endocrinology* 2013 **377** 135–146. (doi:10.1016/j.mce.2013.07.006)

33 Swart AC, Schloms L, Storbeck KH, Bloem LM, Toit T, Quanson JL, Rainey WE & Swart P. 11beta-Hydroxyandrostenedione, the product of androstenedione metabolism in the adrenal, is metabolized in LNCaP cells by 5alpha-reductase yielding 11beta-hydroxy-5alpha-androstanedione. *Journal of Steroid Biochemistry and Molecular Biology* 2013 **138** 132–142. (doi:10.1016/j.jsbmb.2013.04.010)

Received in final form 1 August 2017
Accepted 7 August 2017

http://www.endocrineconnections.org
DOI: 10.1530/EC-17-0119